Tunable Nanomaterials for Controlled Drug Release in Smart Devices

Ashleigh Anderson

BSc

Faculty of Computing and Engineering

of Ulster University

Thesis submitted for the degree of

Doctor of Philosophy

March 2018

I confirm that the word count of this thesis is less than 100,000 words

Contents

List of Figures

List of Tables

Acknowledgements

Firstly, my sincere thanks and gratitude goes to my supervisor Prof James Davis, who has provided an immense amount of support and guidance throughout the PhD. This project would not have been worth its due effort without his enthusiasm, wit and passion for the subject. His supervision stands next to none and I am very grateful for the endeavours and opportunities that he has offered during the PhD and throughout my undergraduate studies.

Many thanks to all the staff and academics who have provided support or technical assistance throughout the duration of my PhD including: Prof Pagona Papakonstaninou, Adrian Boyd, Damian McDonald, Christine McDonald, Jim McLaughlin and Ann Blair. My thanks and appreciation for all your support and assistance.

Special thanks goes to Team Biomole -past and present. To Anna, Sean, Jolene, Aaron, Jordan, Catherine and Charnete, thank you for all your support and laughs, it has been a pleasure to work with you all. To Anna, for taking the journey with me – both during the PhD and in our many adventures.

I would also like to thank my friends and family who have been supportive and encouraging in so many ways. To Mum, Jayne, Lucy and Remy, for your endless support and love. Last but certainly not least, a huge thank you to Michael, you may now have your laptop back in one piece.

Copyright / Credit Notices

Within this thesis material (like text, figures, or tables) from the author's publications is reprinted. The copyright / credit notices are listed at this place in common for all the related chapters, paragraphs or sections. The material might have been modified slightly, however these copyright / credit notices still apply.

doi.org/10.1016/j.elecom.2015.08.008

Acknowledgement is given to the original source of publication for:

> **Anderson, A.** and Davis, J., 2015. Next generation transdermal drug delivery – An electrochemical approach to pH manipulation for controlled release within smart patch technologies. *IFMBE Proceedings: World Congress on Medical Physics and Biomedical Engineering*, June 7-12, 2015, Toronto, Canada. 51, pp. 919-922.

The final publication is available at Springer via
doi:10.1007/978-3-319-19387-8_224

Acknowledgement is given to the original source of publication for:

> Morelli, F., **Anderson, A.,** McLister, A., Fearon, J.J., and Davis, J., 2017. Electrochemically driven reagent release from an electronic suture. *Electrochemistry Communications*, 81, pp.70-73.

The final publication is available at Science Direct via
doi:10.1016/j.elecom.2017.05.020

Acknowledgement is given to the original source of publication for:

> Martin, A., McConville, A., **Anderson, A.**, McLister, A., and Davis, J., 2017 Microneedle Manufacture: Assessing Hazards and Control Measures. *Safety* 2017, 3, 25.

The final publication is available at MDPI via
doi:10.3390/safety3040025

Acknowledgement is given to the original source of publication for:

Book Chapter: Design of Functionalised Materials for Use in Micro-Nanoscale Drug Delivery Devices and Smart Patches. Nanostructures for Drug Delivery, Nanostructures in Therapeutic Medicine Series. Editor(s): Grumezescu & Andronescu. April, 2017. *Elsevier*, ISBN 9780323461436.

The final publication is available at Elsevier via

eBook ISBN: 9780323461498

Abstract

The majority of conventional controlled release technologies tend to be based around encapsulant systems in which a polymeric binder or gel typically responds to changes in the local environment in which the delivery device has been placed. The contents are often released when the particle, capsule, film or droplet is exposed to the appropriate physico-chemical trigger (typically a change in pH) with the time-release-dose delivery characteristics controlled through manipulation of the encapsulant formulation. The adaptation of this core strategy for use in the next generation of transdermal microdevices or smart patch is explored. The core rationale of this work relates to the development of microneedle patches and other delivery architectures, which upon activation by an appropriate electrochemical trigger, leads to the release of a drug.

The methodology adopted herein focused on the use of cellulose acetate phthalate (CAP) as pH sensitive barrier films structured for use within a number of microscale (patch, implant, microneedle and microdroplet) devices. The barrier film was used as a means of entrapping a model drug with the controlled release of the latter achieved through the exploitation of the hydrogen evolution reaction. The application of an electrode potential resulted in an increase in the local pH thereby inducing the controlled dissolution of the barrier film and facilitating the release of the drug.

A variety of approaches have been investigated leading from the use of standalone CAP films through to its direct incorporation as a component in the electrode material itself. The design and characterisation of the carbon composite material from a film to the development of conductive microneedles and electronic sutures is described. The ability to electrochemically manipulate the structural integrity of the composite structures and the ability to affect the controlled release of model drugs is critically appraised.

Abbreviations

ACFW	Anodised Carbon Fibre Electrode
Ag	Silver
AgCl	Silver Chloride
Au	Gold
BE	Binding Energy
BR	Britton Robinson
BSE	Primary Back-Scattered Electrons
CAP-C	Carbon- Cellulose Acetate Phthalate
CAP	Cellulose Acetate Phthalate
CE	Counter Electrode
CF	Carbon Fibre
CF-CAP	Carbon Fibre-Cellulose Acetate Phthalate
CFW	Unmodified Carbon Fibre Electrode
CMC	Carboxy-Methyl Cellulose
CNT	Carbon Nanotube
CV	Cyclic Voltammetry
DCM	Dichloromethane
Dex	Dexamethasone
DPH	Donepezil Hydrochloride
E	Electrode Potential
EE	Ethinyl Estradiol
EVA	Ethylene-Vinyl Acetate
FDA	Food and Drug Administration
GC	Glassy Carbon
GI	Gastrointestinal Tract
GO	Graphene Oxide
HA	Hyaluronic Acid
HEA	Hemispherical Electron Energy Analyzer

HET	Heterogeneous Electron Transfer
HER	Hydrogen Evolution Reaction
HPC	Hydroxypropyl Cellulose
HPMC	Hydroxy-Propyl-Methyl-Cellulose
HRT	Hormone Replacement Therapy
IBD	Inflammatory Bowel Disease
IR	Electrical Resistance of the Bulk Solution
ISO	International Organization for Standardisation
KCl	Potassium Chloride
keV	Kiloelectron Volt
MEMs	Microelectromechanical Systems
MNPs	Magnetic Nanoparticles
MNs	Microneedles
mV	Millivolts
MX	Meloxicam
$NaNO_2$	Sodium Nitrite
NaOH	Sodium Hydroxide
NGMN	Norelgestromin
NICE	National Institute for Health and Care Excellence
NMDA	N-methyl-D-aspartate
NSAIDs	Non-Steroidal Anti-Inflammatory Drugs
PCL	Polycaprolactone
Pd	Palladium
PGA	Poly (Glycolic acid)
PLA	Poly (Lactic Acid)
PLGA	Poly (lactic-co-glycolic acid)
PMVE / MA	Poly (Methyl Vinyl Ether / Maleic Acid)
PVA	Polyvinyl Alcohol
PVP	Poly (vinylpyrrolidone)
RAM™	Random Assemblies of Microdiscs

RE	Reference Electrode
SC	Stratum Corneum
SCMC	Sodium Carboxymethyl Cellulose
SEM	Scanning Electron Microscope
SGN	Spiral Ganglion Neurons
SNHL	Sensorineural Hearing Loss
SPE	Screen Printed Electrodes
SPIONs	Superparamagnetic Iron Oxide Nanoparticles
SWV	Square Wave Voltammetry
TBO	Toluidine Blue O
UC	Ulcerative Colitis
UK	United Kingdom
USA	United States of America
UV-Vis	Ultraviolet-visible
V	Volts
WE	Working Electrode
XPS	X-Ray Photoelectron Spectroscopy

Notes on Access to Contents

"I hereby declare that with effect from the date on which the thesis is deposited in Research Student Administration of Ulster University, I permit

1. the Librarian of the University to allow the thesis to be copied in whole or in part without reference to me on the understanding that such authority applies to the provision of single copies made for study purposes or for inclusion within the stock of another library.

2. the thesis to be made available through the Ulster Institutional Repository and/or EThOS under the terms of the Ulster eTheses Deposit Agreement which I have signed.

IT IS A CONDITION OF USE OF THIS THESIS THAT ANYONE WHO CONSULTS IT MUST RECOGNISE THAT THE COPYRIGHT RESTS WITH THE AUTHOR AND THAT NO QUOTATION FROM THE THESIS AND NO INFORMATION DERIVED FROM IT MAY BE PUBLISHED UNLESS THE SOURCE IS PROPERLY ACKNOWLEDGED".

Chapter 1

Introduction and Summary of the Literature

Abstract

In recent years, there has been an emergence of novel smart devices that possess the ability to monitor a patient's health without the presence of clinical staff. At present, there is a wealth of research being targeted at the development of these technologies. A concise summary of the current and emerging research directed at the release of therapeutic agents from microscale devices is presented and a critical overview of the potential applicability evaluated. While conventional controlled release mechanisms are considered, the focus is on the provision of a detailed review of the current electrochemical developments for controlled release and serves a framework for the research being undertaken in this project.

Part of the literature described in this chapter has been published in Anderson, A. and Davis, J. (2015), Electrochemical Actuators: Controlled Drug Release Strategies for use in Micro Devices. *Electroanalysis*, 27: 872–878.

Design of Functionalised Materials for Use in Micro-Nanoscale Drug Delivery Devices and Smart Patches. Nanostructures for Drug Delivery, Nanostructures in Therapeutic Medicine Series. Editor(s): Grumezescu & Andronescu. February 2017. *Elsevier*, ISBN 9780323461436.

1.1 Introduction

The concept of a 'smart' device that could routinely monitor a patient's health with minimal clinical intervention has garnered considerable interest in recent years and, has evolved from significant advances in sensing and communication technologies. A new generation of connected health systems offering discrete and prompt analysis of vital signs within smart phones and other wearable technology are already available and could be considered as opening up new opportunities in personalised healthcare. It can be anticipated that, as these systems mature, they will have a considerable impact on the future outlook of preventative screening measures within healthcare practices (Agboola *et al.*, 2013; Valle, Tramalloni and Bragazzi, 2015). In recent years, there has been an ambition to drive research towards the integration of electrical and chemical sensors for the detection of a particular disease or injury biomarker (Kumar *et al.*, 2016; Bollella *et al.*, 2017). In their present incarnation, such devices offer a limited range of sensing capabilities, but this could be considered the first stepping stone on the journey to more integrated devices, which could provide a much more detailed biochemical picture of the wearer's health.

The rationale of the current formats rely on a "detect-alert" sequence, which notifies either the patient or a central clinic (Chan *et al.*, 2012). In other situations, where perhaps urgent action is required, a more sophisticated substitution would be the development of a system that could act autonomously in response to information received from the sensing module and, where appropriate, deliver a drug therapy in an appropriate manner. While the current approaches to sensing are well established, the development of "detect-respond" systems that can control the release of a drug is still in its relative infancy but is an area in which considerable effort is now being expended.

Project Aim

The aim of the project undertaken was therefore to take up this challenge and investigate the design of new electrochemical approaches that can facilitate detect and respond delivery mechanisms which could eventually be employed within smart patch and microscale architectures.

The focus of the present thesis is directed towards electrochemical approaches to drug delivery given the compatibility with modern electronics which should, in principle, provide opportunities for the delivery devices to become much smaller and less obtrusive with greater dose control and much more rapid response times. Through the development of functional materials whose properties can be controlled, it is possible to create advanced systems that could deliver a drug, antidote or treatment upon activation by an electrochemical trigger. These "smart" materials could ultimately be incorporated into a micro device or smart patch that would be capable of acting autonomously to deliver a drug therapy. A schematic of the idealised smart device / release mechanism is demonstrated in **Figure 1.1.1**, where drug release is achieved upon the detection of an appropriate biomarker.

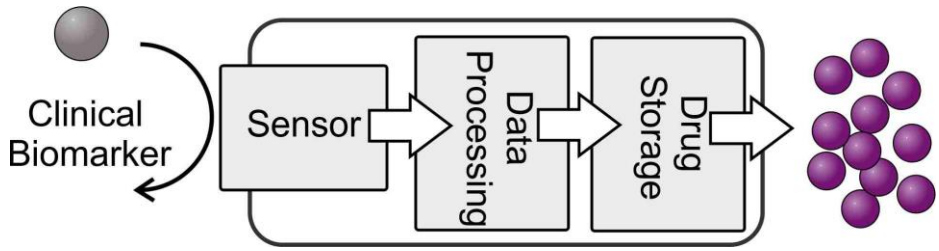

Figure 1.1.1 Combined sensor -actuator device

A critical overview of present drug delivery strategies is considered along with the issues surrounding their application. The evolution of new electrochemical approaches to the controlled drug delivery are considered and the underpinning rationale for the present project is placed in context.

Conventional Drug Delivery Strategies

At present, effective drug delivery can be achieved through several conventional approaches including: oral delivery (Choonara *et al.*, 2014), injection (Prausnitz and Langer, 2008), inhaler (Illum, 2012; Casettari and Illum, 2014), and transdermal absorption (Margetts and Sawyer, 2007a; Maurya *et al.*, 2014), which have allowed the successful treatment of a vast range of clinical conditions. Some of the more common approaches are highlighted in **Table 1.1.1.**

Table 1.1.1 Conventional drug delivery approaches and associated barriers

Route of delivery	Advancements to delivery	Barriers to delivery	References
Oral	Simplicity of use, ease of treatment termination, dose accuracy.	GI tract, acidity in stomach can led to drug degradation, adherence regime.	(Choonara et al. 2014; Sattar et al. 2014; Thanki et al. 2013)
Ocular	Eyes drops provide convenient delivery, high patient acceptance.	Ineffective delivery to the posterior segment, tear washout.	(Kompella et al. 2013; Yasin et al. 2014; Cima et al. 2014)
Nasal	Ease of use, direct route to the blood stream, bypasses gastrointestinal degeneration.	Dosage control, nasal mucosal irritation.	(Casettari & Illum 2014; Illum 2012; Kozlovskaya et al. 2014)
Transdermal	Ease of use, can be worn for long periods of time, less invasive.	Poor permeability, location irritation.	(Arora et al. 2008; Indermun et al. 2014; Paudel et al. 2010)

Oral Delivery

Oral delivery possesses many attractive attributes including; ease of use, control over dosage, design control over delivery system and the overall costings of manufacture are relatively inexpensive. In some cases, particularly where prompt delivery is needed, oral delivery would not be considered the most appropriate form of delivery,

particularly when the drug component could be degraded following interaction with gastrointestinal enzymes, resulting in low oral bioavailability (Choonara *et al.*, 2014). Other negative side effects can present themselves when larger than desired dosages are administrated to ensure dosage is not lost, therefore selective delivery would ensure that only the desired amount of drug dosage would be delivered, thus eliminating the adverse effects. At present, research is being directed at the reduction of negative side effects, particularly with the prevalence of chronic disease, in particular Crohn's and Ulcerative Colitis (UC), where there is a pressing need to develop a more effective way of delivering drugs to the colon (Van den Mooter and Kinget, 1995; Philip and Philip, 2010).

The use of encapsulated systems within oral drug delivery is well understood and extensively documented (Maroni, Zema, *et al.*, 2013; Thanki *et al.*, 2013; Choonara *et al.*, 2014; Sattar, Sayed and Lane, 2014). Slow release coatings are commonly used in oral delivery where, upon ingestion, the encapsulated system travels through the gastrointestinal (GI) tract, where the enteric coating surrounding the drug is breached by intestinal fluid. The period of time for release depends on the residence time of the encapsulated system in the GI tract. Gelatin capsules which offer instantaneous release are unsuitable for delivery to the GI tract, whereas slow release coatings can allow targeted delivery to the colon where uniform absorption can occur throughout the GI tract. Slow release systems can offer progressive control over the release profile, more significantly these coatings can be modified with the addition of enteric coatings, for example cellulous acetate phthalate (CAP). CAP is a commonly used pH sensitive polymer used to protect an entrapped agent in the stomach when presented with acidic conditions and then releases the entrapped components when exposed to more alkaline conditions within the intestinal tract. The use of CAP is the principal system investigated in this thesis. The work involved will focus on exploiting the inherent properties of CAP within new devices. The features of CAP will be outlined in Section 1.2.2 and further explored in Chapters 4,5,6, and 7, where the properties of a CAP film will be researched and its application within a polymer composite film for electrochemical drug delivery will be investigated.

Injection Methods

Drug administration via needle (typically subcutaneous injection) can alleviate some of the issues that limit oral efficacy but can also possesses a number of inherent drawbacks – particularly the degree of invasiveness which can engender an inevitable reluctance on the part of the patient to self-administer. There are also numerous concerns over health and safety in terms of use and disposal (Majumdar *et al.*, 2015). In cases such as diabetes management where patients are required to self-administer insulin, this negative association can lead to further non-compliance and regression of the patient's health. Inadequate adherence by patients as a result of unwillingness to inject, or error in routine can adversely affect the dosage and concentration of a drug therapy. Therefore, it is possible that through insufficient adherence, health practitioners could easily assume that the treatment has been ineffective, resulting in a change in treatment or increase in dosage which can lead to further complications. Delivery via hypodermic needle can overcome many of the issues associated with oral delivery, such as providing the possibility of much more accurate control over dosage. However, there are significant issues surrounding the appropriateness and invasiveness of an injection and it has been estimated that as much as 10% of the population suffer from a phobia related to needles (Sokolowski, Giovannitti and Boynes, 2010).

Transdermal Methods

Over the years, transdermal drug delivery systems have been proffered as prime candidates for effective drug delivery. The development of transdermal patches and microneedle systems have allowed conventional drug delivery to be surpassed by a much more convenient route to delivery that has the capacity to reduce negative side effects that can be associated with traditional forms of drug delivery. At present, most of the commercially available transdermal patches are passive systems, which do not offer the ability to control the release of the drug. Undoubtedly, the most commercially available transdermal patches are nicotine patches which were approved by the Food and Drug Administration (FDA) in 1992. Since they were released, the success of nicotine replacement therapy patches have been widely documented (Rose *et al.*, 1985; Stead *et al.*, 2012). The success of nicotine patches

can be due to several factors which facilitate the cessation of smoking, including: discreetness of size and placement of patch, variation in nicotine strength, ease of use and handling. While the nicotine patch may be considered the first of its generation within patch systems, there are also many more recent advantages within transdermal patch technology. A summary of current transdermal delivery systems has been complied in **Table 1.1.2**.

Table 1.1.2 Transdermal patch systems currently on the market

Product Name	Active ingredient	Indication
BuTrans® Transdermal Patch	Buprenorphine	Analgesia
Catapres-TTS® Transdermal Therapeutic System	Clonidine	High Blood Pressure (hypertension)
Evorel® Transdermal Patch	Estradiol	Hormone Replacement Therapy (HRT)
EVRA® Transdermal Patch	Norelgestromin (NGMN) and Ethinyl estradiol (EE)	Female Contraception
Exelon® Transdermal Patch	Rivastigmine	Alzheimer's Disease
Fencino® Transdermal Patch	Fentanyl	Analgesia
Neupro® Transdermal Patch	Rotigotine	Parkinson's Disease
Nicorette® InvisiPatch	Nicotine	Nicotine Replacement Therapy
Nitro-Dur® Transdermal Patch	Glyceryl trinitrate	Prophylaxis of Angina
Transderm Scop® Transdermal Patch	Scopolamine	Motion Sickness

The advancements and increasing popularity of fentanyl transdermal patches for chronic pain management has been widely documented (Margetts and Sawyer, 2007b; Lane, 2013), but occurrences of abuse have been extensively reported (Moon and Chun, 2011; Mounteney *et al.*, 2015). Specific case studies have reported the extraction and intravenous injection of fatal doses of fentanyl (Tharp, Winecker and Winston, 2004). It is important to be aware of the fact that the potency of fentanyl is around 100-200 times that of morphine, depending on the variety evaluated (Stanley, 2014). To combat this, research groups such as Cai et al. 2015, have recently made efforts to develop a nanostructured patch containing a tamper resistance fentanyl reservoir (Cai, Engqvist and Bredenberg, 2015). Their approach employed geopolymers, a type of ceramic (typically composed of nanoparticulate Silica or Kaolin networks), where the fentanyl is embedded. The physical properties of the nanoparticles can be controlled to regulate the release profiles as required. The movement of drug molecules from most transdermal systems is by passive diffusion, this reduces the chances of success during the extraction processes necessary for acquiring sufficient quantities for abuse (Jämstorp *et al.*, 2010). When considering the widespread issues of delivery system tampering, could the emergence of smart devices reduce the potential for misuse? The answer will depend on the technologies involved and how the drug is sequestered within the system and, may involve a degree of tethering which can only be broken by the action of an electronic signal. In general, transdermal systems proffer several advantages for ease of treatment over conventional drug delivery strategies and the associated advantages and disadvantages of these systems have been highlighted in **Table 1.1.3**.

Table 1.1.3 Advantages and disadvantages of transdermal delivery

Advantages
Less invasive then hypodermic needles
Ease of use
Reduce frequency of dosing
No negative gastrointestinal side effects
Reduction of dosage peaks and troughs
Removal of patch will terminate treatment
Disadvantages
Barrier presented by the skin
Opioid transdermal drug delivery systems can be subject to abuse
Skin sensitivity
Limited availability of pharmacological agents that can be delivered this way
Drug permeability
Issue of power

Transdermal patches represent another emerging mode of drug delivery in the treatment or management of mild to moderate Alzheimer's disease. Treatment regime adherence is a recurring issue for individuals being prescribed psychiatric and non-psychiatric medication. Cholinesterase inhibitors are typically used by 40-70% of people being treated for Alzheimer's (Alzheimer's Society, 2010), where the most common cholinesterase inhibitor used is Rivastigmine. Alzheimer's patients who are prescribed rivastigmine often see improvements in memory/concentration, enhanced communication, restored confidence and independence to continue with daily activities (Adler, Mueller and Articus, 2014) . Currently, Rivastigmine is the only drug of its kind available as a transdermal delivery system for the treatment of Alzheimer's disease (Isaac and Holvey, 2012). The need for further drug formulations to be incorporated into these kinds of delivery systems is evident, this will not only provide a niche method of delivery but will increase the availability of treatment therapies in a transdermal form.

Further innovations of transdermal technologies include the development of microneedles for pain free drug administration. Over the years, transdermal microneedles (MNs) have been heralded as the solution in overcoming the limitations of traditional transdermal devices. One of the primary barriers against

effective delivery from the transdermal delivery system is the outermost layer (10-15 μm) of the stratum corneum (SC), which can prevent the efficient delivery of a drug therapy and limits the range of drugs that can be transported by the transdermal system. Microneedle tips are generally much sharper than hypodermic needles and can be used with ease to pierce the SC. Thus, allowing the transport of drug molecules from the delivery system and through micro channels created by the MNs, bypassing nerves and blood vessels.

The development and interest in MN systems has increasingly grown over the years, and a number of preclinical studies have shown that MNs have performed favourably in applications such as: gene delivery (Dul *et al.*, 2017), insulin delivery (Zhang *et al.*, 2018), allergen delivery (Kim *et al.*, 2018), bio-signal monitoring (Ren *et al.*, 2017) and blood sampling (Lee *et al.*, 2018). A number of research groups have developed a range of microneedles, whose structures vary from in-plane (Paik *et al.*, 2004), where the MN is aligned parallel to the base plate, to out-of-plane where the MN is perpendicular to the base plate (Donnelly *et al.*, 2010; Mansoor *et al.*, 2013). The desired pathway of drug release can also influence the structure of MN arrays which can be further subcategorised as either solid MNs (Gupta *et al.*, 2011), hollow MNs (Lhernould, 2013), dissolving MNs (Ita, 2017a) and swelling MNs (Donnelly *et al.*, 2014). MN systems can be easily categorized by the range of materials that have been used to manufacture the technology and include: silicon (Ji *et al.*, 2006; Yan *et al.*, 2013; Vinayakumar *et al.*, 2014), glass (McAllister *et al.*, 2003; Martanto, Moore, Couse, *et al.*, 2006; Martanto, Moore, Kashlan, *et al.*, 2006), sugar (Martin *et al.*, 2012; Loizidou *et al.*, 2015), hydrogel (Donnelly *et al.*, 2012, 2013, 2014), polymer (Park, Allen and Prausnitz, 2005; Lee, Han and Park, 2013; Ruggiero *et al.*, 2018), metal and palladium composites (Kim and Lee, 2006; Badran, Kuntsche and Fahr, 2009; McConville and Davis, 2016). Regardless of the powerful drive to develop and implement MN platforms, there are still very few MN products available on the market, this can be largely attributed to the trouble with scale up of fabrication of such systems.

1.2 Barriers to Delivery

The route to effective drug delivery can be limited by many challenges namely: response time and physical barriers to delivery. As previously mentioned in **Section 1.1**, transdermal systems can address and overcome many of the drawbacks associated with traditional methods of drug delivery. In many scenarios, it is common place for a health care professional or the patient themselves to administer treatments, which may have to be repeated over a period of days or weeks. While in the short term, such actions can be completed with ease, it can become much more inconvenient when managing a chronic condition where treatment can be prolonged or last a lifetime. The transdermal approach can provide many opportunities to improve patient compliance and co-operation by providing sustained release for a longer period of time without the need of intervention from clinical staff (Prausnitz and Langer, 2008).

One of the main obstacles that can affect the success of a transdermal delivery system is transport of the treatment across the skin barrier. As a result, there are a limited number of drugs that have made the successful transition from traditional delivery into transdermal systems. The skin consists of three major layers: the epidermis, dermis and the hypodermis as shown in **Figure 1.2.1.** It can often be difficult to transport drugs across the skin barrier due to the low permeability of the skin tissue. The stratum corneum (SC) is the first protective layer of the skin which shields the underlying layers from mechanical and chemical stress and acts a barrier to prevent water loss due to its hydrophobic nature. The thickness of the SC layer measures around 10-20 µm in depth, this range varies at different anatomical sites and is comprised of around 25 layers of dead squamous cells which further restricts drug diffusion (Russell, Wiedersberg and Delgado-Charro, 2008; Escobar-Chávez *et al.*, 2011).

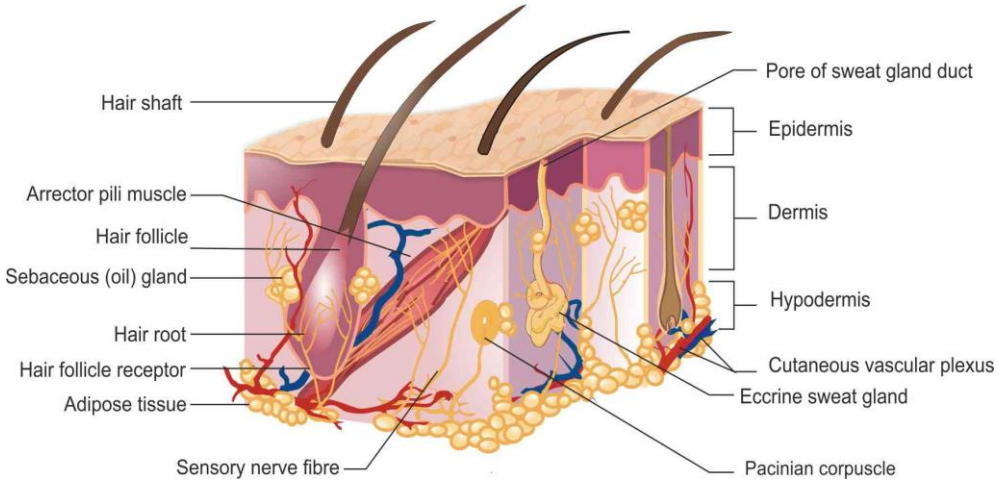

Figure 1.2.1 Schematic demonstrating the layers of the skin. Adapted from (Tate, 2011).

Despite the considerable permeability barrier presented by the stratum corneum, delivery through the skin still presents an attractive alternative to traditional drug delivery methods. The drug permeability of transdermal systems can be significantly improved via the addition of microneedles which can overcome the issues surrounding the skin barrier. The dimensions of an ideal microneedle system can range from 400 µm to 1500 µm thus allowing the delivery systems to easily bypass the protective layers of the stratum corneum and deliver the drug to a highly vascularized site. Patient discomfort that is often associated with traditional approaches to drug delivery, such as hypodermic injection, can be minimised due to the size of the microneedles, where upon administration there should be little to no nervous stimulation or skin trauma (Indermun *et al.*, 2014). While the developments of transdermal systems have come a long way since their inception, there is also significant room for further improvement with regards to dosage control and controlled release. The further development of transdermal systems will also see the addition of complex electronic systems into the device itself, where considerations surrounding power requirements and the finished product size will have to be considered for future 'smart' delivery systems to achieve their full potential. Microneedles systems will be further investigated in Chapter 6, where the development of an electrochemically controlled composite microneedle system is presented.

Issues in Delivery Technique: Compliance

Each method must be carefully considered when determining the most effective route for the delivery of a particular drug - taking into account the physico-chemical characteristics of the latter but also its intended target. Some of the issues that can arise include: poor response time, inadequate drug concentration, degradation. These can often be compounded by other factors such as: delivery invasiveness and errors in drug delivery site and variations in drug uptake due to premature release. As noted in previous sections, the treatment of chronic illnesses can be particularly troublesome where frequent dosing at constant concentrations is required to ensure optimal and successful drug action (Tiwari *et al.*, 2012). This aspect introduces yet another challenge to successful drug delivery: the patient.

The 'human factor' and non-compliance (or adherence) is a substantial issue when it comes to ensuring the effectiveness of a drug therapy. All too often treatment failures have been observed in patients with low drug concentration due to incomplete dosage resulting from the frequency of application rather than issues inherent to prescribed delivery method (Dailey, Kim and Lian, 2001; Tarrants *et al.*, 2010). Inadequate adherence by patients to a treatment regime as a result of apathy in the administration of oral medicines, a fear or reluctance to inject subcutaneously or simple errors in routine can all adversely affect the dosage and concentration of a drug therapy. It is possible to envisage that through insufficient adherence, health practitioners could easily assume that the treatment has been ineffective. The course of action which follows could lead to a change in the patient's treatment – side effects associated with an increase in dosage can lead to further complications. This can significantly increase healthcare costs as a result of incorrect treatment regime adherence (NICE, 2007). There is overwhelming evidence corroborating the fact that patient compliance is a key issue which can interfere with treatment outcomes.

A qualitative review conducted by the National University of Singapore (Jin *et al.*, 2008) evaluated the issues surrounding patient compliance to specific treatments and the factors which can cause deviations from the prescribed regime. While compliance with short term therapies was estimated at between 70% and 80%, it was found that, generally, the rate of compliance for long-term therapies typically fell to between 40% and 50%. In other compliance studies it has been estimated that the rate of compliance for the management of diabetes through the administration of insulin via hypodermic needle is around 20% (Bloom Cerkoney and Hart, 1980).

It is important to consider patient compliance when considering outpatient care and the administration of drug treatments, therefore, for this kind of system, the most desirable outcome would be to completely remove patient intervention from the equation. The administration process is key when considering the overall success of a drug therapy and failure to maintain routine adherence can often compromise the effectiveness of the treatment. The removal of responsibility from the patient, as shown in the smart system concept in **Figure 1.1.1**, would avoid delays in clinical assessment and treatment outcome. It could also be predicted that through passive sensing, greater control over drug release and faster response time could ultimately be achieved.

1.2.1 Existing Technologies

Controlled Release Polymer Technologies

Traditionally, oral capsules have been coated with thin films of water soluble polymer to mask taste and odour, to protect products from moisture degradation and provide increased mechanical resistance during handling. These films remain intact only for a short time period and drug release is generally achieved soon after ingestion, making water soluble polymer films ideal for when drug release is required immediately. Specific polymers that make ideal candidates for immediate release

coatings are cellulose ethers and can include: hydroxypropyl methylcellulose, polyvinyl acetate or polyvinylpyrrolidon. Following from this, polymers can also be designed to be saliva resistant and only degrade when they reach the acidic environment of the stomach, an example is a methacrylic copolymer named Eudragit® E (Evonik Röhm GmbH, Darmstadt, Germany). More recent advances in oral delivery have seen the addition of more sophisticated coatings which can protect the drug dosages from external stimuli and environments to achieve controlled drug release and optimum therapeutic outcome (Muheem *et al.*, 2016; Lin *et al.*, 2017; Ting *et al.*, 2018).

Controlled release systems have been of tremendous value to clinicians where they can enhance drug therapy through a variety of modes. These can include: protecting the drug from degradation, improving patient compliance, provide control over release mechanism and can, ideally, reduce the negative side effects that can come with aggressive treatment regimes. Polymers used within controlled drug release applications can be categorized into the following sections: Diffusion controlled (non-biodegradable), Chemically controlled (biodegradable) and Smart Polymers which are controlled by external factors (i.e. conducting polymers which will be discussed further in **Section 1.4.2**).

Diffusion controlled systems are based on exogenous synthetic materials that are considered non-biodegradable. In such instances, there is no immediate burst release, and the rate of release depends on the physical properties of the polymer i.e. the thickness and permeability, the area of release and the drug solubility. The most commonly used non-biodegradable polymers that have been approved by the Food and Drug Administration (FDA) for safe use in the body are: crosslinked polyvinyl alcohol (PVA), ethylene vinyl acetate (EVA) and silicone (Yang and Pierstorff, 2012). PVA is often used a tunable membrane at the release area, due to its permeability to selective lipophilic drugs, also the thickness of the PVA membrane can be adjusted to achieve desired release rates. EVA on the other hand is often used as a protective membrane encompassing the drug core and preventing early release.

Finally, silicone possesses both permeable and impermeable qualities subject to the grade used. Non-biodegradable polymers continue to be developed for controlled release systems in drug delivery and include block co-polymers (vesicles and coatings) and parylene (films and coatings) (Kamaly, Yameen, Wu and Omid C Farokhzad, 2016).

When comparing polymers used in controlled drug the release applications, it is evident that the most commonly used systems are biodegradable polymers. These polymers are more suited to *in vivo* drug release due to their biocompatible nature of their degradation products and their ability to be either metabolised or excreted from the body. Biodegradable polymers can be categorized as natural polymers or synthetic polymers. Examples of well-defined biodegradable synthetic polymers are detailed in **Table 1.2.1**. Synthetic biodegradable polymers include Polyesters, Polyorthoesters, Polyanhydride and Polyamides. The most commonly used are: Poly(lactic acid) PLA, Poly(lactic-co-gylcolic acid) PLGA and Poly(caprolactone). Commonly occurring natural biodegradable polymers are detailed in **Table 1.2.2**.

In biodegradable systems, the rate of release is often determined by the degradation rate of the polymer. When degradation rates are analysed, they can often be categorised into two different types of degradation: surface and bulk. When the polymer membrane is gradually eroded from the surface of the system, the inside of the material does not degrade until the surrounding polymer matrix has worn away, this is known as surface degradation, this kind of degradation occurs in polyesters such as PLA and PLGA. Bulk degradation on the other hand, occurs throughout the whole system and occurs in poly(ortho ester) and polyanhydrides. Surface and bulk erosion both cause auto-acceleration where the degradation products advance the erosion process. This means there is a preliminary surge and final release during the delivery process with biodegradable drug release mechanisms. Furthermore, there are continuing efforts being developed to reduce surge effects and achieve zero-order kinetics of drug release (Fu and Kao, 2010; Gokhale, 2014).

Table 1.2.1 Commonly used biodegradable synthetic polymers for controlled release

Polymer	Biodegradation	Examples	References
Poly(esters)	Hydrolysis or enzyme mediated degradation	Poly(lactic acid) PLA	(B. Liu *et al.*, 2016; Tyler *et al.*, 2016; Scaffaro *et al.*, 2017)
		Poly(glycolic acid) PGA	(Hurrell and Cameron, 2002; Braunecker *et al.*, 2004)
		Poly(lactic-co-gylcolic acid) PLGA	(Gasmi *et al.*, 2016; Rodríguez *et al.*, 2016; Terukina *et al.*, 2017)
		Poly(caprolactone) PCL	(Hyun, 2015; Genina *et al.*, 2016; Sun *et al.*, 2016)
Poly(ortho ester)	Hydrolysis	Dioxolane – based diketene acetals	(Yang *et al.*, 2003; Nguyen *et al.*, 2008; Einmahl *et al.*, 2016)
Polyanhydride	Hydrolysis	Poly(sebacic anhydride)	(Yin *et al.*, 2013; Bagherifam *et al.*, 2015; Ponnurangam *et al.*, 2015)
		Poly(adipic anhydride)	(Albertsson, Carlfors and Sturesson, 1996)
Polyamide	Hydrolysis or enzyme mediated degradation	Poly-γ-Glutamic Acid	(Akagi *et al.*, 2005; Zhang *et al.*, 2013)
		Poly (l-lysine)	(Askarian *et al.*, 2016; Ren *et al.*, 2016)

Table 1.2.2 Naturally occurring biodegradable polymers

	Example	Reference
Protein Based Polymers	Gelatin	(Fan and Wang, 2016; Mahor *et al.*, 2016)
	Collagen	(Voicu, Geanaliu-nicolae and Pîrvan, 2016; Anandhakumar *et al.*, 2017)
	Albumin	(Woods *et al.*, 2015; Wang *et al.*, 2016)
	Casein	(Luo, Pan and Zhong, 2015; Penalva *et al.*, 2015)
Polysaccharide Based Polymers	Cellulose	(Svagan *et al.*, 2016; Y. Liu *et al.*, 2016)
	Chitosan	(L. Liu *et al.*, 2016; Constantin *et al.*, 2017)
	Hyaluronic Acid (HA)	(Agnello *et al.*, 2016; Dosio *et al.*, 2016)
	Alginate	(Bhutani *et al.*, 2016; Fan *et al.*, 2016; Silva *et al.*, 2016)

Polysaccharide based polymers have been previously used in tissue engineering and drug delivery applications. One particular limiting factor that should be taken into consideration is their batch to batch variability and their variations of MW, in this case, synthetic polymers prove more suitable candidates due to their reproducibility (Kamaly, Yameen, Wu and Omid C. Farokhzad, 2016).

1.3 Evolution of Smart Drug Delivery Devices

In many cases, the conventional approaches to drug delivery work well, but as highlighted in the previous sections there are also many occasions where there is a need for more effective control over the drug therapy. The latter may be due to issues of drug release or patient compliance. Both serve as motivation for developing smarter drug delivery technologies and devices that can autonomously respond in a predesigned way to specific instructions (i.e. from a smart phone, watch or tablet) or to changes in a particular biomarker profile. A variety of electrochemical approaches have been examined to determine if they can offer greater control over drug release and critical evaluations of these emerging systems are explored in the following sections.

1.4 Electrochemical Approaches to Drug Release

Electrochemically controlled drug release systems are still in the early stages of their development, but a considerable number of systems have emerged in recent years and can be attributed to the growing interest in smart devices and the acknowledgement that electrochemical strategies are notably suited for application in microelectromechanical (MEMs) devices. An abundance of electrochemical approaches have been exploited in controlled release applications and include: conducting polymers (Svirskis, Travas-Sejdic, *et al.*, 2010a; Alizadeh and Shamaeli, 2014), carbon nanotube composite structures (Riggio *et al.*, 2009; Luo, Matranga, Tan, Alba and Xinyan T Cui, 2011; Prakash *et al.*, 2011), redox gels (Dong, Wang and Du, 2006; Jin *et al.*, 2012; Narayanan *et al.*, 2012; Liakos *et al.*, 2013), and pump

systems (Ai *et al.*, 2010; Li *et al.*, 2010; Shin *et al.*, 2011; Sheybani, Gensler and Meng, 2013). The electrochemical transitions and chemical structures which permit their adaption to drug release are assessed in the following subsections.

1.4.1 Microelectromechanical Systems (MEMs) Devices

Electrochemically adapted materials and electrochemically controlled drug delivery systems are being increasingly employed as the prime candidates for the development of microdevice release systems. Such systems prevail over stimuli-responsive delivery methods as they can be easily miniaturised to be incorporated into MEMs devices that can control the delivery of a drug in a more precise manner. These microsystems have been shown to effectively deliver a drug in a highly controlled manner and electrochemically initiated release has been achieved through a microchip system as shown in **Figure 1.4.1**. As discussed in the previous sections, patient compliance can be considered a major issue when it comes to assessing the therapeutic outcome of a drug therapy, especially for treatments that require daily injections or multiples dosages. In cases such as this, implantable microdevices can significantly improve therapeutic outcomes by removing the potential for missed doses (Kleiner, Wright and Wang, 2014). At present, implantable micro delivery systems are being developed using sophisticated microfabrication technologies. Microfabricated drug delivery systems have been designed to be equipped with precisely measured geometry lending to the distribution of drug components in a highly favorable and regulated manner.

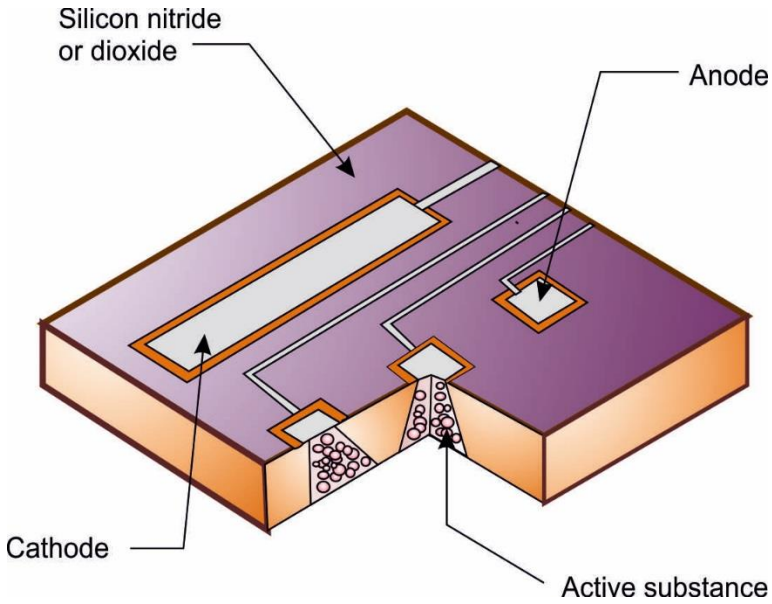

Figure 1.4.1 A Solid-state microchip drug delivery system. Adapted from (John T. Santini, Cima and Langer, 1999).

The micro device shown in **Figure 1.4.1** is a sloid-state microchip system that can deliver individual or multiple reagent release from the micro scale reservoirs located within the microchip (J T Santini, Cima and Langer, 1999). The delivery reservoir is sealed with a gold anode membrane, which remains intact until the imposition of an electrochemical trigger, resulting in the controlled electrochemical dissolution of the gold thereby releasing its contents. The application of an electrochemical potential (+1.04 V for several seconds) at the gold film anode triggers the oxidation of the gold and subsequent degradation of the film, allowing the entrapped drug molecules to move from the reservoir to the desired delivery site in a regulated manner. Further development of microchip delivery systems that could be implanted into the desired tissue have great potential to lead research in the next generation of 'smart' drug delivery devices.

MEMs drug delivery systems offer a substantial profile of benefits, however the invasiveness of implantable drug delivery systems is evident (Kleiner, Wright and Wang, 2014). Of course, with any implantable device, a minor surgical procedure is necessary, this may cause distress among some patients. One of the major advantages of micro implantable systems is that patient discomfort can be minimized,

this however raises questions regarding the quantity of drug agents that can be stored within the device during treatment before this supply is exhausted. Other concerns with micro systems relates to issues of power – is there a need for a battery or can it be done wirelessly. If a physical power source is required – this raises issues over size, life and potential toxicity. The battery inside the system can occupy a large volume which therefore limits the amount of space that can be used for drug storage.

MEMs systems have also been developed for use in a wide range of other applications including: controlled release systems (Pirmoradi *et al.*, 2011), lab-on-a-chip systems (Jung *et al.*, 2015) and microfluidic devices (Yoon *et al.*, 2014). In some cases, it is essential that some drugs such as hormones, will have an enhanced therapeutic outcome if they are delivered in a manner that closely mimics how they would be produced naturally in the body. Through the development and pursuit of micro fabrication technologies, the current prospects of drug delivery have been able to make significant steps forward from traditional techniques. The miniaturisation of drug delivery devices has allowed new kinds of drug therapies, such as micro diffusion pumps (Meng and Hoang, 2012), to be successfully scaled down into more conveniently implantable delivery systems (Gensler, Sheybani, P. Y. Li, *et al.*, 2012; Kleiner, Wright and Wang, 2014). It should be noted however, that the intention of this literature review is not to consider the fabrication of the microsystems themselves but rather to explore and assess the controlled release strategies that they employ and the methodologies that could, in principle, be modified to the ever-decreasing device formats.

Micro device design considerations with regards to material properties are key when it comes to promoting interactions between a biological system and the interface of the device. During material selection, analysis of physiochemical parameters will ensure that the device will respond in a manner that does not initiate an immune response from implantation, factors to be considered include: hydrophilicity, protein adhesion, electrical properties and electrochemical parameters. Careful selection of

materials based on these considerations is enabling the further development of novel delivery systems that have the potential to become the new normal within treatment regimes.

1.4.2 Conducting Polymers

Historically, conducting polymers have been used in a wide variety of biomedical and sensing applications. They have attracted increasing interest in the field of drug delivery due to their electronic and optical properties, high conductivity and tuneable qualities allowing the polymer to be made porous, biodegradable or biocompatible (Priya James *et al.*, 2014; Kamaly, Yameen, Wu and Omid C Farokhzad, 2016).

The ability to have control over the redox state of polymers to allow for physical swelling or dissolution, via the capture or expulsion of anions (detailed in **Figure 1.4.2**) provides an opportunity for drug loading or entrapment. Typical examples can include the use of the following: neurotrophin (Richardson *et al.*, 2009; Wise and Gillespie, 2012), dexamethasone (Leprince *et al.*, 2010; Bohl *et al.*, 2012), risperidone (Svirskis, Wright, *et al.*, 2010) and several N-methyl-D-aspartate (NMDA) receptor inhibitors (Stauffer *et al.*, 2011). The polymer poly(phenylene-vinylene) (Tang *et al.*, 2009), has been previously established as effective candidate in controlled release applications (Wadhwa, Lagenaur and Cui, 2006). Perhaps the most studied conductive polymer within electrochemical applications is the conjugated polymer polypyrrole (George *et al.*, 2006; Svirskis, Wright, *et al.*, 2010). The stimuli responsive properties of polypyrrole lend it to be an excellent candidate for drug release applications, particularly within *in vivo* and *in vitro* biomedical applications due to its biocompatible nature (Wang *et al.*, 2004; George *et al.*, 2005).

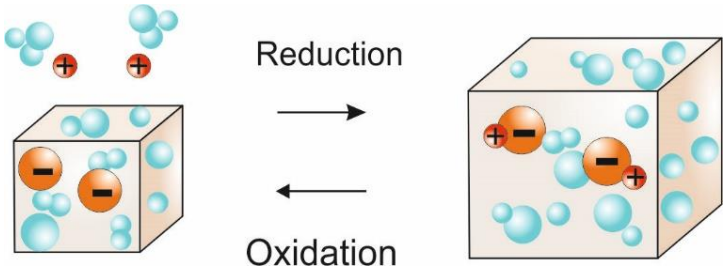

Figure 1.4.2 A Polypyrrole system prepared with immobilized anions that swell and incorporate cations upon reduction; cations can then be expelled on oxidation. Adapted from (Svirskis, Travas-Sejdic, *et al.*, 2010b).

It also possesses advantageous chemical attributes and good conductivity in biological environments. The monomers of polypyrrole undergo oxidative polymerisation as shown in **Figure 1.4.3** , where oxidation forms radical cations, and oligomers are formed via a head to tail coupling reaction resulting in a linear polymer chain (Svirskis, Travas-Sejdic, *et al.*, 2010a). Oxidation can be achieved by either chemical or electrochemical synthesis via the application of an oxidative potential through an appropriate electrode substrate.

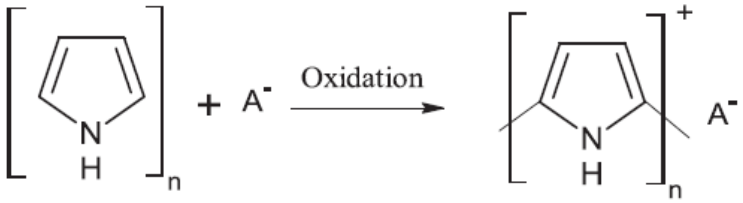

Figure 1.4.3 Oxidative polymerisation of polypyrrole

Electrochemical oxidation is often preferred over chemical oxidation in the preparation of intrinsically conducting polymer based drug delivery systems as they offer precise control of the electrical properties and the scaling of the polymer, which can be achieved by adjusting the rate and the quantity of charge that is circulated. Hard templates are involved in both chemical and electrochemical polymerization. With chemical polymerization, a hard template is submerged in a suspension containing an oxidant, monomers and a dopant. On the other hand, electrochemical

oxidation involves a conductive electrode or a hard template with a conductive face where the polymer grows.

Some of the first tunable polymer systems were drug loaded polymer films with the drug loaded as counter ions. The latter can then be released after a reducing potential is applied to the conductive film. Electrochemically controlled drug release has been reported in a number of biomedical applications where traditional techniques can ultimately fail. Conductive polymer coatings have been used in conjunction with neural prostheses to minimise the formation of an astro-glial sheath around implanted microelectronic devices, which can cause the electrode arrays to fail. Wadhwa et al (2006), observed that by releasing the synthetic glucocorticoid anti-inflammatory drug Dexamethasone (Dex), they could reduce inflammation around the implantation site and therefore reduce the risk of the neural arrays failing. Drug release was achieved using cyclic voltammetry where the voltage was swept from -0.8 to +1.4 V at a polypyrrole coated gold electrode that was loaded with an ionic form of dexamethasone.

The approach to using polymer films as drug releasing actuators may be straightforward, however they have found success in many other biomedical applications including the treatment of Sensorineural Hearing Loss (SNHL). SNHL occurs when the spiral ganglion neurons (SGNs) encounter damage, deterioration or when there is a loss of hair cells that send electrical signals, which have been converted from sound, to the brain (Wise and Gillespie, 2012). A detailed diagram of a normal cochlea (A) and a deaf cochlea (B) are shown in **Figure 1.4.4**, there is a noticeable lack of hair cells in image B, where a cochlea implant electrode has been positioned. Similar to the study with the polypyrrole coated neural prostheses, controlled deposition at the electrode surface of the cochlea implant can be achieved, again furthering the advantages and ease of using conducting polymers from drug release application. This is of key importance when a high degree of deposition precision is required during the manufacture of microfabricated systems at the nano-scale.

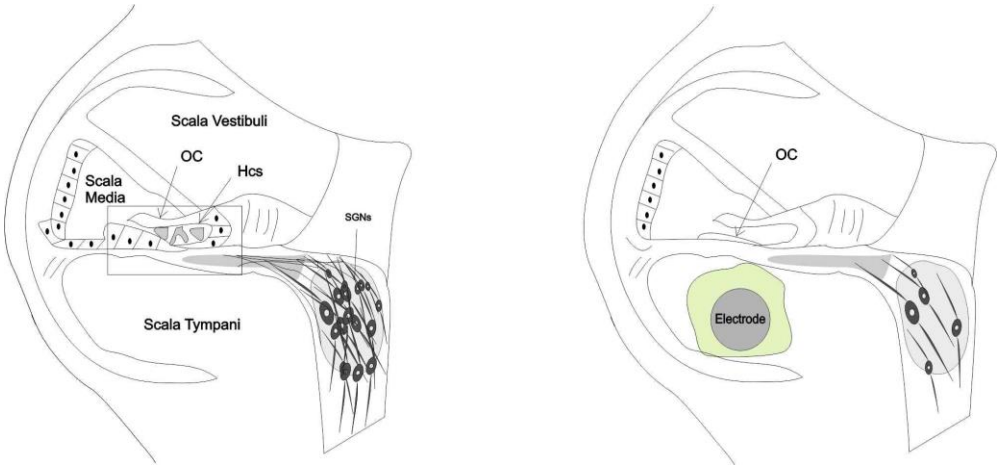

Figure 1.4.4 (A) Normal cochlea (B) Deaf cochlea electrode array can be implanted to electrically activate SGN. Adapted from (Wise and Gillespie, 2012).

It has been shown in existing research that the delivery of neurothrophin from implanted cochlea electrodes can protect the SGNs from damage and help to deliver electrical stimulation to the cochlea. Richardson et al. previously demonstrated the successful delivery of neurothrophin to cochlea neurons from drug eluting polypyrrole coated electrodes (Richardson *et al.*, 2009). The study showed that the polypyrrole modified electrodes were able to aid in the protection and preservation of SGNs, without affecting the function of the cochlear implant. Drug delivery that can be achieved from the device itself is particularly important in this case due to the restricted accessibility of the anatomy within the inner ear, where successful prolonged drug delivery is hard to achieve. Drug loaded polymeric coatings allow full precise control over the release of the drug, along with other benefits over direct injection into the site which may cause fluid leakage resulting in variations and inconsistencies in drug dosage.

One drawback of drug loaded polymer films is that they are limited by their volume, as the film itself is the primary drug carrier, therefore limiting the quantity of the drug molecules that can be loaded within the film. Due to this, applications that can often require high dosages over a long timeframe may not be as feasible. In recent years, there has been an emergence in the use of composites within drug release

applications, which have been favoured due to their larger drug loading capabilities within controlled release systems (Costache *et al.*, 2010; Elliott Donaghue and Shoichet, 2015; Yassine *et al.*, 2016). This has led to a change in the way that polymers can be utilised and manipulated. As an alternative to being used as a 'sponge' that can be electrochemically controlled to release a drug, much more efficient and controllable polymer systems are being exploited as valve mechanisms. This mechanism functions to trap molecules in a drug reservoir until an appropriate electrical signal is triggered. Once the signal is received, the release of the trapped molecules is activated. In previous work, dexamethasone has been electrochemically released from carbon nanotubes (CNT) that have been capped with polypyrrole (Luo, Matranga, Tan, Alba and Xinyan T. Cui, 2011). The controlled release of the dexamethasone was achieved through the electrochemical reduction (-0.5 V) of the pyrrole caps, allowing the movement of the entrapped drug out of the CNT. The CNT can be further manipulated through electrochemical oxidation (+0.5 V) which allows the polymer cap to be closed again when the desired level of drug release has been achieved as demonstrated in **Figure 1.4.5**. Similar methodologies have also been employed in the research of chemotherapy treatments (Prakash *et al.*, 2011; Vashist *et al.*, 2011).

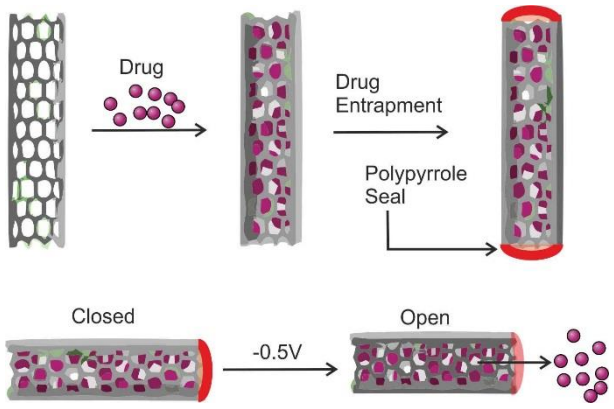

Figure 1.4.5 Electrochemically controlled release of drugs from loaded nanotubes. Adapted from (Luo, Matranga, Tan, Alba and Xinyan T. Cui, 2011).

By using similar approaches to the CNT application, the ability to tailor the properties of conductive polymer films have been demonstrated in the development of

transdermal microneedle systems. As discussed earlier, transdermal systems typically operate on passive transfer, where the drug molecules are delivered from a reservoir and pass across the skin. However, it is apparent that more sophisticated transdermal systems are being developed from smart stimuli responsive polymers. An example of this kind of transdermal technology has been developed by Valdes-Ramirez and co-workers (2012). The basic system is highlighted in **Figure 1.4.6**. In this case, polypyrrole is utilised as the electronic gate. A laser patterned membrane - possessing small micron sized holes is combined with a polypyrrole thin film to seal the drug reservoir. In this particular case, the polypyrrole film acts as a barrier restricting the drug molecules within the reservoir, the film is then deposited onto porous polycarbonate film which has been sputtered with gold. The patch is micromachined to create a surface of hollow microneedles and attached to the polypyrrole/polycarbonate composite layer. Controlled release of the drug molecules occurs when a suitable redox potential is applied to the conductive polycarbonate layer, thereby causing a change in the redox state of the polypyrrole film and allowing the movement of drug molecules to pass up through the film (Valdés-Ramírez, Joshua R. Windmiller, *et al.*, 2012).

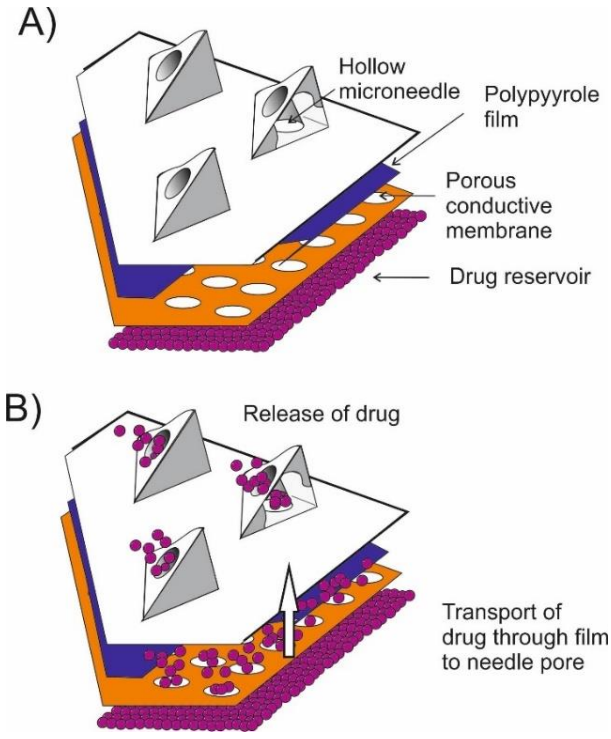

Figure 1.4.6 Microneedle patch with polypyrrole release film. (A) Before release (-1.1 V) and (B) After release (+0.5 V). Adapted from (Valdés-Ramírez, Joshua R Windmiller, *et al.*, 2012).

While the transdermal system contains needles that are at the microscale, the reservoir where the drugs are stored is not however limited to the same scale. The increased capacity allows the device to be used for more sustained release applications where perhaps the patch may need to be worn for a prolonged length of time. Another important observation with this kind of system is that it can be equipped with multiple individually addressable reservoirs which will allows multi reagent release to be achieved from a single patch.

The conception of "artificial muscle" stemmed from early work on the electrochemical behaviour of conducting polymers, in particular polypyrrole (Low *et al.*, 2000). However, in more recent research focused on drug delivery, the "artificial muscle" utilised a chemo mechanical actuator based on a hydrogel combined with a redox polymer equipped with electrochemical abilities. Under the appropriate conditions, the polymer blend exhibits swelling properties when an electrochemical potential is applied, similar to the approach described above, thus resulting in the polymer creating open and close transitions behaving in a manner desirable to controllable valves (Low *et al.*, 2000).

1.4.3 Manipulation of Redox Hydrogels

Alginates are naturally occurring biodegradable polymers found in brown marine alae. They have been extensively used in a number of areas including thickeners in the food industry, binders in the pharmaceutical industry and as drug loaded hydrogels in drug delivery applications (Almeida and Almeida, 2004; Dong, Wang and Du, 2006). Upon hydration, alginates form a viscous gel which can be chemically altered to change its mechanical and physical properties to perform favourably in many biomedical applications. Alginate gels form a hydrogel matrix when they come into contact with cations such as calcium ions and have been used previously in controlled release applications (Liakos *et al.*, 2013), wound dressings (Liakos *et al.*, 2014), and tissue engineering (Venkatesan *et al.*, 2014).

Crosslinking through interaction with metal ions such as Mg^{2+} and Ca^{2+} have long been exploited (Jin *et al.*, 2012) but, from an electrochemical perspective, neither system offers an opportunity for electrochemical control. However, electrochemical control can be achieved if Fe^{2+} is added to the gel as the crosslinking agent rather than calcium. The alginate/ferrous mixture can then be loaded with a therapeutic agent. The presence of ferrous ion (Fe^{2+}) has little effect on dissolved alginate but its electrochemical oxidation to the ferric state (Fe^{3+}) induces crosslinking (**Figure 1.4.7**) and offers the possibility of controlling the nucleation of the hydrogel, its spatial location and the material entrapped within the 3D polysaccharide network.

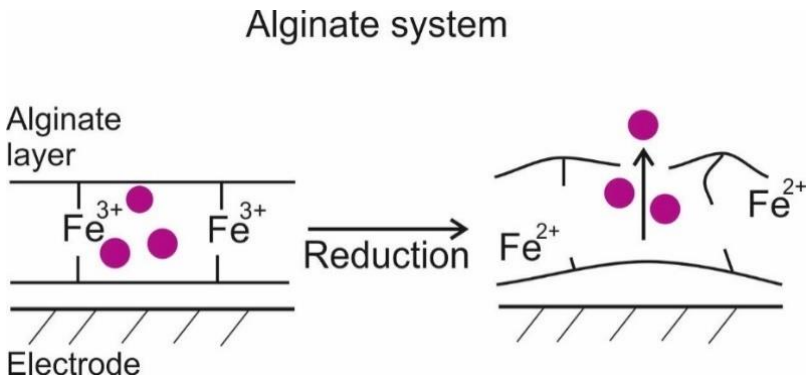

Figure 1.4.7 Electrochemical reduction of the ferric ions resulting in the disruption and dissolution of alginate layers

The ferric ions (Fe^{3+}) are characteristically viewed as hard metal cations, which attach preferentially to the negatively charged carboxyl groups within the alginate - effectively binding much more strongly compared to Fe^{2+}. On the other hand, the ferrous (Fe^{2+}) ions bind preferentially to the neutral ligands and are considered “soft” metal cations. When a reducing potential is applied to the crosslinked ferric component, gel disruption and dissolution will commence, resulting in the release of entrapped drug molecules. These crosslinked hydrogels systems have the potential to be utilised as alternatives to the polypyrrole microneedle systems described in the previous section. Thereby, proposing a new method for achieving a controllable, site specific drug delivery.

1.4.4 Control of Local pH

One of the major concerns when delivering drugs to the colon is designing a drug formulation that remains stable during transit until it reaches the site of delivery. Drug delivery can be particularly problematic when we take into consideration the variation in pH/microbe composition present, which can cause drug degradation or perhaps premature release. Traditionally, drug delivery to a specific part of the gut has been achieved using pH sensitive films that respond by releasing the drug therapy in response to the local pH. The pH within the stomach can vary, during fasting the pH usually falls between pH 1 and 2. After eating, the pH tends to increase to around pH 6.6 or higher due to the movement of chime from the stomach to the small intestine (Evans *et al.*, 1988; Philip and Philip, 2010). During thin film manufacture, the pH resistance of a film can be accurately modified to protect the therapeutic agent until it reaches the delivery site. Upon delivery however, there is little control over the release mechanism. As discussed previously in **Section 1.1**, enteric coatings have been widely used in oral tablet formulation (Maroni, Del Curto, *et al.*, 2013), where the drug content remains intact until the capsule reaches a site of higher pH causing rupturing of the film and consequent release of the drug. Another approach, similar to the method described, uses biodegradable polymeric coatings which protect the drug during transit through environments of elevated pH, until it comes into contact with microbial enzymes located in the colon which trigger film degradation. This ultimately leads to the rupturing of the polymer back bone and the delivery of the drug (Karrout *et al.*, 2009; Amidon, Brown and Dave, 2015).

1.4.5 Electrochemical Pump Systems

The methodologies described within the previous sections have largely focused on the diffusional movement of the drug from a reservoir to the delivery site – in most cases these approaches would not be appropriate when it comes to delivery to more complex or restricted anatomy (Ai *et al.*, 2010). In order to achieve more

substantial and sustained movement of the drug, several methodologies have been developed to prompt the controlled movement of the drug during the release process. Electrochemical investigations have established a sophisticated method for the manipulation of the local pH involving electrolysis (Cheng and Chang, 2011; Anderson and Davis, 2015). An associated limitation of the method is gaseous evolution, however, this product can be exploited for use in other scenarios to achieve drug release from pump systems (Sheybani, Gensler and Meng, 2013).

The two approaches to this pump-like mechanism have been outlined in **Figure 1.4.8A** and **1.4.8B.** In the simplest case (A), the application of a suitable current induces water electrolysis at the electrodes which are in contact with the electrolyte which cause gaseous evolution. The formation of gas within the chamber increases the local pressure and forces the liquid containing the dissolved drug out of the delivery port. A more sophisticated approach (B) involves the use of bellows to prevent the degradation of the drug as a consequence of reaction at the electrode or changes in pH brought about by the electrolysis processes. The gas evolution within the parylene bellows (C) causes expansion which again forces the drug loaded solution to exit the port (Sheybani, Gensler and Meng, 2013). This relatively straight forward approach has been applied to treat various conditions of the eye which require discrete continuous delivery as a result of the intricate anatomy of the delivery site, therefore proving electrochemical systems indeed prevail over conventional delivery techniques (Li *et al.*, 2008; Uday B Kompella *et al.*, 2013; Cima *et al.*, 2014; Yasin *et al.*, 2014). Frequently, drug delivery to the eye is achieved through eye drops or direct injection, yet they do not have the benefit of a highly precise and controllable delivery mechanism.

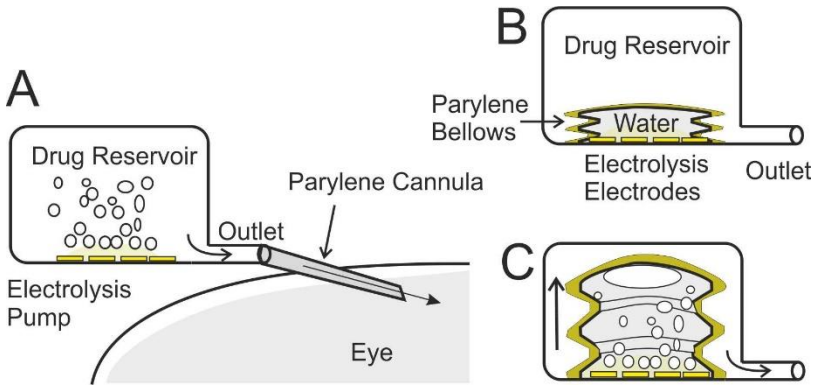

Figure 1.4.8 Electrolysis pumps exploiting gaseous evolution to displace the drug from the device. Adapted from (Sheybani, Gensler and Meng, 2013).

An implantable electrochemical micro device would proffer several advantages over the conventional approaches to drug delivery to the eye, which could allow sustained delivery from a micro sized system. While the bellows system have been successful in their application, a further improvement would feature the use of electroosmotic pumping (Ai *et al.*, 2010). Drug release is achieved in a relatively simple manner from electroosmotic systems, which have no moving parts, by placing a porous layer such as alumina or silica, between two electrodes and allowing the drug to flow from the reservoir (Chen *et al.*, 2010).

Luft and colleagues were one of the first research groups to employ this approach for the development of one of the first electroosmotic insulin pumps in 1978 (Luft, Kuehl and Richter, 1978). Since its inception, their approach has been used in several bioanalytical systems and microfluidic platforms (Bourouina, Bossebuf and Grandchamp, 1997; Pikal, 2001; Litster *et al.*, 2007; Wang *et al.*, 2009). Over time there have been concerns with the operational voltages, where water electrolysis can occur, leading to gaseous evolution. The subsequent production of oxygen and hydrogen, can become trapped within the membrane layer, resulting in partial electrode insulation and irregular flow patterns (Litster *et al.*, 2007; Ai *et al.*, 2010).

1.4.6 Covalently Immobilised Drugs

The methodologies that have been discussed above have generally involved the drug molecules being free – albeit enclosed within the drug reservoir. The methodology employing covalently immobilised drugs aligns with the electrochemical cleavage of drugs covalently bound to the electrode surface. By covalently attaching the drug molecules to the electrode surface it is possible to minimise the likelihood of gradual leakage. Minimising leakage is a key issue if the long-term storage of an active component is necessary. An innovative approach for the treatment of Inflammatory Bowel Disease (IBD) has utilised covalently immobilised drugs linked to the gel framework within a hydrogel via azoaromatic linkages. Within the hydrogel there is an azo cross-linking agent along with a pH sensitive monomer, which ensure protection of the drug during digestion in the stomach and from degradation in the small intestine. The reductive action of the azoreductases found in the colon, cause the breakage of the azo linkages resulting in drug release. The unfortunate side effects of the degradation of azo-polymeric matrices is the production of toxic by-products, rendering them unfit for long-term treatment therapies (Shantha, Ravichandran and Rao, 1995; Yamaoka *et al.*, 2000; Stubbe *et al.*, 2001).

Following this research, an alternative method to the hydrogel system has been developed that is more equipped for use with systems at the micro – nano scale. The technique involves covalent azo linkage, between drugs that possess diazonium salt functionalities, directly to carbon substrates. Drug release can then be achieved through the electrochemical reduction of the azo functional groups at the surface of the carbon, as opposed to relying on enzyme induced degradation to release the drug (Wildgoose *et al.*, 2005). Further Investigation is still required to determine the toxicological consequences of the method; however, it does present a relatively uncomplicated means for functionalisation of carbon nanostructures such as carbon nanotubes and graphene nanoflakes.

1.4.7 Wound Healing Sutures

In recent years there has been growing interest in the development of drug-eluting sutures for a variety of clinical applications. Traditionally, surgical sutures have been used to close wounds and facilitate the healing of wounds by holding tissue together to limit exposure to possible infections. As sutures are placed within the immediate wound site, this makes them a prime candidate for drug delivery. There are a wide variety of suture materials available for clinical use. The two main types are absorbable and non-absorbable. Absorbable sutures lose around 50% of their tensile strength within 60 days of being in contact with tissue, on the other hand non-absorbable suture can maintain their tensile strength beyond 60 days (Dennis, Sethu, Nayak, Mohan, Y. Morsi, *et al.*, 2016).

Historically, suture materials have been derived from several sources including: gold and silver wires, silk, horse hair and plant fibres – including linen and cotton. Sutures derived from naturally occurring materials can be easily broken down by proteolytic enzymes, thus allowing them to be absorbed within 70 days (Benicewicz and Hopper, 1991; Dennis, Sethu, Nayak, Mohan, Y. Morsi, *et al.*, 2016). More recently, synthetic biomaterials such as polydioxanone and poly(lactic-co-glycolic acid) have been used as suture materials (Lee *et al.*, 2013). Degradation of synthetic absorbable sutures occurs via hydrolysis, whereby the polymers chains of the suture material are broken down when water molecules permeate into the polymer. On the other hand, non-absorbable sutures are mostly resistant to degradation within tissue as they are unaffected by hydrolysis and resistant to enzymatic action and consequently must be physically removed after wound healing.

Despite the wide range of suture materials available, there is no one suture material that would be suitable for all types of surgical applications. Many factors must be considered when choosing an ideal suture material, which can depend on the tension

across the wound, the depth of tissue at the wound site, expected duration of wound healing, and if it is likely that there will be an inflammatory response. The mechanical properties of sutures can be tailored to meet the functional requirements of the wound site and can be achieved by braiding or coating the surface of the suture material. The principle feature of a surgical suture is its tensile strength. The tensile strength of the suture material depends on whether the suture is monofilament or multifilament. Multifilament sutures tend to exhibit more desirable mechanical properties with superior flexibility over the monofilament varieties.

In recent years, there has been considerable growth in the development of the next generation of sutures that possess additional modifications such as the addition of antimicrobial agents such as silver nanoparticles or triclosan which have been shown to reduce infection rates and promote wound healing. Historically, silver nanoparticles have been shown as ideal candidates for the coating of polymeric materials for the enhancement of their antimicrobial profile. The antibacterial effect of the nanoparticles initiates the generation of reactive oxygen species which directly affects the cell membrane of infectious microorganisms while also reducing the rate of bacterial adhesion to the surface of the suture (Chaloupka, Malam and Seifalian, 2010; Dennis, Sethu, Nayak, Mohan, Y. Y. Morsi, *et al.*, 2016a). The advantages proffered with the addition of silver nanoparticles are particularly important given the increasing concerns over antimicrobial resistance. In addition to the coating of sutures with antimicrobial agents, the loading of drug agents has been shown to reduce infections and promote wound healing. Drug coating can be achieved through dip coating (Joseph *et al.*, 2017), radiation grafting (Gupta, Jain and Singh, 2008), or by electrospinning (Chen *et al.*, 2012). One of the main challenges faced during the manufacture of drug eluting sutures is to obtain the necessary drug concentration without affecting the mechanical properties of the suture, this can be achieved by controlled release mechanisms.

Controlled release mechanisms that can be incorporated into electronic sutures that are capable of sensing and wound monitoring have garnered immense interest in recent years (Kim *et al.*, 2012a; Dennis, Sethu, Nayak, Mohan, Y. Y. Morsi, *et al.*, 2016b). While still in their infancy, electronic sutures have the potential to monitor, sense and mimic biological responses in the body. The ability to monitor the local temperature and pH from within a wound site could provide early diagnostics that could potentially alert the patient to infection. This type of suture will be further explored in Chapter 7, where electrochemically driven drug release can be controlled through a suture, and the further investigation of the potential for such electronic sutures within biomedical applications will be investigated.

1.4.8 Summary

Advances in conventional drug delivery using oral, topical and injectable drugs have allowed the treatment of an extensive range of diseases. However, even with these improvements, many boundaries still need to be confronted. The effectiveness of traditional drug delivery can often be highly variable at treating chronic illnesses which are dose dependent and require frequent, precise and targeted drug delivery. The development of electrochemical strategies for controlled release would enable the further progression of drug delivery technologies resulting in improved patient outcome.

1.5 Electrochemical Enteric Coatings – New Directions

Conventional drug delivery systems still have fundamental issues over release time, drug suitability and delivery environment. The addition of enteric coatings can offer a more effective approach to delivery by controlling the release of the drug contents. With these coatings, the barrier film is designed to protect the drug molecules in the low pH environments and is then ruptured or eroded when it

encounters higher pH environments found in the duodenum. In order to function as an effective enteric coating, the polymers contain many carboxylic acid groups with a pKa value of 3-5 (Lehmann, 1994) . The most widely used enteric polymers are cellulose acetate phthalate, polyvinyl acetate phthalate, hydroxypropyl methylcellulose phthalate, Eudragit® L and Eudragit® S. Slow release polymers are suitable for drug release applications, but the work within this project will focus on the development a controlled release system utilizing cellulose acetate phthalate (CAP) adapted for a range of electrochemical purposes. CAP is an ideal candidate for enteric coatings as it contains many carboxylic acid groups (**Figure 1.5.1**) and has a pKa of around 5.28 (Rando *et al.*, 2006). This means that when it is exposed to the lower pH conditions of the stomach, the carboxylic acid groups will not be fully dissociated and therefore the CAP will be resistant to dissolution.

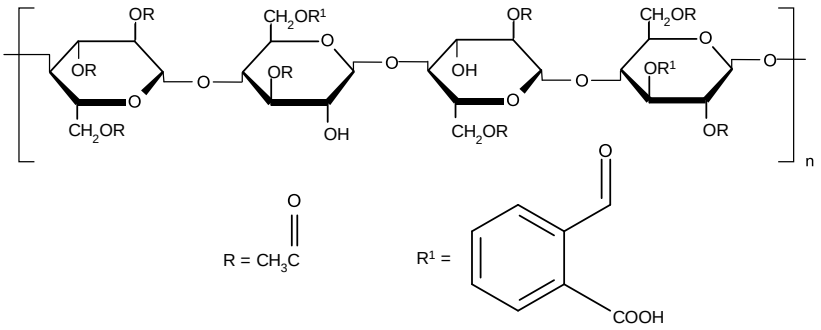

Figure 1.5.1 Chemical structure of cellulose acetate phthalate

An alternative approach has been developed as part of the work described in this thesis. The rationale has been to exploit the CAP enteric coating as a means of retaining a model drug but exploit the electrochemical manipulation of pH to induce the breakdown of the protective film and release the drug. Its objective is to enable a more refined release profile. The base system used throughout is based on conductive carbon composites which have been patterned into films or microneedles. Irrespective of formation, the presence of the carbon particles allows control over the local pH through controlling the potential applied at the interface. It was anticipated that holding the potential at the negative end of the potential

window (i.e. -2 V, 60 seconds) would result in the reduction of protons leading to an increase in the pH. As the pH rises to the alkaline region – it was expected that the dissolution of the CAP film should occur resulting in pores that allow the transfer of the drug molecules. As the change in pH would only be in the immediate vicinity of the holes in the membrane and thus won't affect the surrounding tissue. (Grozovski *et al.*, 2017). As polyesters are unstable in alkaline solutions we can then control the release of the drug at a predetermined time and rate, which can be initiated by the carbon components.

1.5.1 Project Objectives

The project objectives are:

1. To develop a microscale pH measurement system to monitor the pH manipulation capabilities of the functional materials.
2. To develop new functional materials capable of electrochemically controlled release.
3. Characterise drug release profiles.
4. Investigate the manipulation of local pH using electrolytic methods.
5. To develop microneedle patch systems that can deliver a drug agent electrochemically.
6. Optimise the design and assess the efficacy of prototype drug release systems

Ultimately, the rationale would be to provide the preliminary ground work for the development of a micro device that could control the release of a drug. It is envisaged that the drug could be stored within a micro reservoir or could be potentially embedded into the system itself. The opening of the reservoir or the release of the entrapped drug molecules could be achieved by applying an electrochemical potential upon receiving an appropriate biomarker response, inducing a change in configuration of the smart membrane and therein release the drug in a controlled manner.

Chapter 2

Materials and Experimental Methodologies

Abstract

A concise overview of the experimental materials, techniques and system parameters used throughout the project are presented in this chapter. Technical details of the underpinning theory behind each experimental technique is discussed, as is the way in which data is presented and analysed. Specific details of each experimental technique are further examined within the Experimental Procedure sections within each chapter.

2.1 Materials and Instrumentation

Unless stated otherwise, all reagents used during experimental procedures were purchased from Sigma-Aldrich (UK) and were of the highest grade available. Electrochemical measurements were conducted at 22 °C ± 2 °C in stock solutions prepared in Britton-Robinson buffer (acetic, boric and phosphoric acids – each at a concentration of 0.04 M) and then, through the addition of concentrated sodium hydroxide, the pH was adjusted to the appropriate value. All buffer solutions have a specified amount of potassium chloride (0.1 M) added in order to provide sufficient electrolyte and, in cases where a silver wire is used as the reference, define the reference potential. Solutions were prepared in deionised water from an Elgastat (Elga, UK) water system and refrigerated when not in use.

Electrochemical analysis was performed utilising a μAutolab Type III computer operated potentiostat (Eco-Chemie, Utrecht, The Netherlands) and a three electrode configuration was employed unless stated otherwise In some instances, a two electrode configuration was used whereby a silver/silver chloride coated wire was used as a combined counter/reference electrode. Throughout the experimental investigations, several materials were employed as the working electrode and included: glassy carbon, carbon fibre, palladium, gold, and carbon/cellulose acetate phthalate composites. In most cases, a platinum wire was employed as the counter electrode and a commercial Ag|AgCl (3 M KCl) half cell reference electrode (BAS Technicol, UK) completed the cell assembly. Further details of electrochemical configuration and measurements are described in each chapter.

2.2 Electrochemical Instrumentation

Electrochemistry is the study of the chemical process that causes electron transfer between electrodes and reactant species in a solution. Electrochemical analysis can be used to provide both qualitive and quantitative data, as well as ascertaining the thermodynamics and transfer kinetics of a particular reaction.

Analytical electrochemistry is often employed for the detection or analysis of specific biomarkers, where investigation begins with the oxidation or the reduction of the analyte of interest at suitable potentials. It is often common practice from an electrochemical stand point, to modify the working electrode by either chemical or physicals means. Modification is often undertaken to ensure specificity in multifaceted biological media due to the number of species that are considered electrochemical interferences. In this work, a number of electrode surface modification techniques have been employed and will be detailed within the relevant sections. Overall, electrochemistry proffers many advantages over traditional laboratory analysis, it has considerably lower cost of instrumentation compared to spectroscopic instrumentation, proffers many options for the choice of electrode materials and enables control over system design lending to its widespread applicability for incorporation into a large number of applications including: biomedical, industrial and environment fields of research.

2.3 Electrochemical Cells

When undergoing electrochemical investigation, the most commonly used set up is a three electrode system as shown in **Figure 2.3.1**. A three electrode system consists of a working electrode (WE), where the reaction of interest takes place, a reference electrode (RE) which provides a stable and well-known potential and a counter electrode (CE) which controls the flow of current through the working electrode and not the reference. In some experiments including within this work, a two electrode system was employed, whereby a combined counter/reference electrode is utilised. Details of cell setup will be further described in the relevant experimental subsection. The instrumentation that maintains the potential of the working electrode with respect to the reference is a potentiostat.

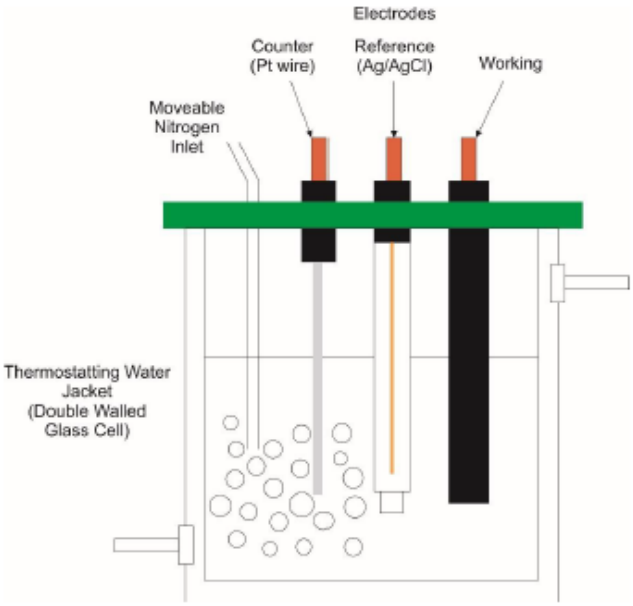

Figure 2.3.1 Diagram of a typical electrochemical system utilising a three electrode setup and a nitrogen inlet

2.3.1 Reference Electrodes

The purpose of a reference electrode is to provide a fixed and stable potential which serves to regulate the potential at the working electrode. The reference electrode's potential is independent of the current density and is generally unaffected by the sample solution of interest, but only in cases where the half cells contain their own reference solution. Throughout this project, a conventional silver-silver chloride (Ag | AgCl) half-cell reference electrode was employed during electrochemical investigations and the electrode fabrication is shown in **Figure 2.3.2**. The silver/silver chloride reference electrode consists of a silver wire (Ag) coated with a layer of silver chloride, typically immersed in a glass cylinder system which contains a solution of 3 M KCl in order to define the potential. Located at the bottom of the Ag/AgCl reference electrode is a porous frit which allows the gradual outflow of KCl to induce electrical conduction within the sample solution.

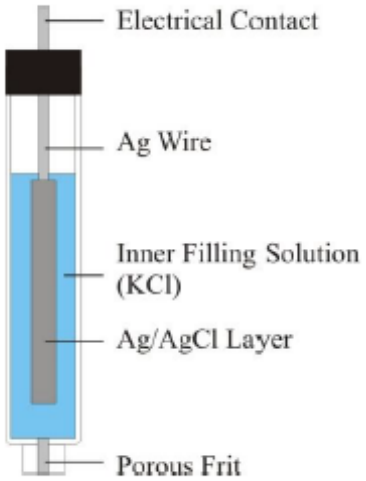

$Cl^-_{(aq)} \mid AgCl_{(s)}, Ag_{(s)}$

$AgCl_{(s)} + e \Leftrightarrow Ag_{(s)} + Cl^-_{(aq)} \quad E^0 = +0.222\ V$

Figure 2.3.2 Commercial reference electrode and corresponding electrode process

The chemical reaction taking place within the cell can undergo two processes namely oxidation and reduction. The difference in potential between the two processes is the emf of the cell. The electrochemical activity that takes place inside the half cell can be defined by the Nernst equation:

$$A + ne^- \leftrightarrow B$$

$$E = E^o - \frac{RT}{nF}\ln\frac{[B]}{[A]}$$

$$AgCl_{(S)} + e \leftrightarrow Ag_{(s)} + Cl^-_{(aq)} \qquad E^0 = +0.222\ V$$

…Eq.2.1

Where:
E is the electrode potential (Volts);

E^o is the standard electrode potential for the redox couple (Volts);

R is the gas constant (8.314 $JK^{-1}\ mol^{-1}$);

T is temperature (Kelvin);

n is the number of electrons transferred to the electrode during reaction;

F is Faraday constant (96485 $C\ mol^{-1}$)

[*A*] and [*B*] are activities of the oxidised and reduced species.

As mentioned above, some experiments utilised a chloridised silver wire, further details of specific set up can be found in the electrochemical configuration section of each chapter. The chloridised silver wire was prepared by oxidising the wire at +1 V for a defined length of time in the presence of KCl (process detailed below) by following an already established technique (Huang and Dasgupta, 1997).

$$Ag_{(s)} \rightarrow Ag^{+}{}_{(aq)} + e$$
$$Ag^{+}{}_{(aq)} + Cl^{-}{}_{(aq)} \rightarrow AgCl_{(s)}$$

…Eq.2.3

This process causes the initial stripping of silver, resulting in the rapid deposition of a silver chloride layer which behaves in a similar way to that of a standard commercial Ag |AgCl reference electrode. In contrast with the commercial system, the Ag|AgCl wire does not incorporate its own internal chloride solution. Therefore, during investigations where a silver wire reference was used, it was necessary to add a known concentration of chloride (0.1 M KCl) to the test solutions to maintain a constant reference potential.

2.3.2 Working Electrodes

During electrochemical investigations, the reaction of interest takes place at the working electrode. A potential is applied between the working electrode and the reference through a computer controlled potentiostat. Due to the constant potential at the reference electrode, it can be determined that any changes in the electrode potential are as a result of changes at the working electrode.

$$E = (\emptyset_M - \emptyset_S)_{working} - (\emptyset_M - \emptyset_S)_{reference}$$

…Eq.2.4

Where:
E = Electrode Potential
$\emptyset_M$ = Electrical
$\emptyset_S$ = Solution

In some cases where a two electrode system was used during investigations, Equation 2.3 would no longer be appropriate as the current may now pass through the reference, thus altering $(\emptyset M - \emptyset S)_{reference}$. To determine the electrode potential for a two electrode system, the equation would now be replaced with:

$$E = (\emptyset_M - \emptyset_S)_{working} + IR - (\emptyset_M - \emptyset_S)_{reference}$$

…Eq.2.5

Where:
IR = electrical resistance of the bulk solution between RE and CE

Within this set up, any variations in the potential (E) would result in unspecified changes in IR along with $(\emptyset M - \emptyset S)\, working$. In this case, the current flowing through the working electrode is no longer regulated. However, in situations where the working electrode is a microelectrode, this does not apply. The current that passes through these electrodes is very small due to their micron dimensions. Small currents will therefore have little effect on the electrolytic change within the reference and the IR will be small enough to disregard (Compton and Banks, 2011).

Throughout experimental procedures, several substrates where chosen as working electrodes, depending on their suitability to the applications. The materials investigated included: carbon, palladium and carbon composites due to their inert chemical properties. Choice of electrode material can be dependent on how well the electrode will exhibit fast electron transfer kinetics, as well as performing in a manner that will yield reproducible results. The sensing area of each working electrode is defined within each results chapter, this was achieved by using a laminate assemble with a specified window, this approach is used to accurately interpret voltammetry

results. Specific details of their composition, pre-treatment and electrode assembly are detailed within the electrode design section within each chapter.

2.3.3 Counter Electrodes

Within a three-electrode system, the auxiliary electrode, or the counter electrode as it's more commonly referred to, serves to prevent the surge of large currents from flowing through the reference electrode and triggering changes in its potential. A counter electrode should not interfere with the reaction at the working electrode, therefore they are usually made from inert materials which are inherently conductive. Due to these desirable characteristics, common materials chosen as counter electrodes are platinum, carbon, steel and nickel. It is important to take into consideration the size of a counter electrode, as to reduce the amount of current density gathered at this electrode it must be as large as possible (Pletcher, 2009). Unless stated otherwise, a platinum wire was chosen as a counter electrode throughout experiments due to its inert nature and high conductivity.

2.3.4 Buffer Solution

The background solution of a standard electrode electrochemical chemical cell is comprised of one or more analytes which are dissolved in a conductive electrolyte solution therefore allowing current to flow through the cell thus allowing electrochemical measurements to be undertaken. The conductive electrolyte solution should be inert so that specific measurements can be directed at the analyte of interest. Variations in pH at the electrode surface can also be minimised by used buffer solutions, this can be particularly influential if the electrode process undergoes the production or depletion of H^+ (or OH^-) (Pletcher, 2009). Throughout the duration

of experimental procedures, Britton-Robinson buffer was used, and its composition is detailed in Section 2.1 above.

The Nernst equation shown (shown below) an be rearranged to determine the change in potential (E) as a consequence of taking the log change in the concentration of hydrogen ion (1 pH unit). Therefore, if a process behaves in a Nernstian manner, where a change of 1 pH unit occurs, the potential shift would be 59.1 mV under standard conditions (i.e. 25 ˚C, and where n=1) This electrochemical principle is the underpinning theory behind electrochemical pH sensing concepts (Compton and Banks, 2011).

$$E = E^o + \frac{2.303RT}{nF}\log[H^+] + \log\frac{[B]}{[A]}$$

$$E = E^o + \frac{RT}{nF}\,2.303\,pH$$

$$E = E^o + \frac{8.314 \times 298.15}{96485}\,2.303\,pH$$

$$E = E^o + 0.0591\,\mathrm{V}\,pH$$

…Eq.2.2

2.4 Mass Transport

The types of molecular movement are described below, their importance in analytical electrochemistry is key as molecules can be chemically altered during the measurement process at the electrode-solution interface. The three main types of molecular movement in solution are: diffusion, migration and convection.

2.4.1 Diffusion

When molecules move from areas of high concentration to areas of low concentration the motion is known as diffusion. Diffusion can occur at an electrode surface when a chemical change is initiated for example, when a reaction at the electrode triggers the transitional change of the original material to the product. When in solution, the concentration of the original material is less concentrated at the electrode surface than the concentration of that in the bulk of the solution, while the opposite of this applies to the product. Therefore, when a reaction takes place at the electrode, diffusion drives the starting material toward the electrode sensing area, and the resulting product will then diffuse out into the bulk solution (Pletcher, 1982). The product can be defined quantitatively by Fick's laws of diffusion. Fick's first law (Equation 2.5) expresses that the rate of diffusion, goes from an area of high concentration to an area of low concentration and is directly proportional to the steepness of the concentration gradient.

$$\text{Flux} = -D\,\frac{dc}{dx}$$

…Eq.2.6

Where:

D = diffusion coefficient in cm^2/s

dc / dx = the concentration gradient at distance x

Fick's second law of diffusion describes how diffusion causes the concentration to change with time and is shown in **Equation 2.7**. The equation dictates that the concentration is now a function of both distance and time (Pletcher, 2009).

$$\frac{\partial c}{\partial t} = D\,\frac{\partial^2 c}{\partial x^2}$$

…Eq.2.7

4.4.2 Migration

Migration is the transport of charged molecules due to electrostatic-attraction and electrostatic-repulsion. The transport of these charged molecules across a potential gradient is the motion by which charge transfers through the electrolyte solution. During electrochemical analysis, there is little effect on the mass transport of the electroactive compound as the background solution contains a large quantity of inert electrolyte (typically 0.1 M) which transports most of the charge, meaning there is limited movement of the electroactive compound by migration (Pletcher, 1982).

2.4.3 Convection

Convection is the physical transport of molecules within a solution and can occur naturally due to density gradients, or mechanically by stirring or through forced flow through a channel. If mechanical induced convection, in the form of stirring the solution or using a rotation disc electrode is used, this will be the principal form of mass transport (Pletcher, 1982).

2.5 Voltammetry

Voltammetry is a commonly used electrochemical technique which involves varying the potential (voltage) between the working and reference electrodes, the resulting current flow (amps) is quantified and presented relative to the potential producing a voltammogram. A variety of commonly used voltammetric techniques were used throughout this project and are detailed in the sections below.

2.5.1 Cyclic Voltammetry

One of the most frequently used voltammetric techniques is cyclic voltammetry (CV). Usually, cyclic voltammetry is the technique that is used initially to define and understand the electrochemical processes, this is due to the rate at which scans can be completed and the swift collation and interpretation of data (Pletcher, 2009). A triangular waveform is generated by sweeping the potential of the working electrode linearly as shown in **Figure 2.5.1**. The starting position of the potential applied to the working electrode is E_1, where there is generally no chemical reaction taking place and is swept linearly to E_2. The potential E_2 is generally larger than the potential needed for the oxidation or reduction process of interest thereby allowing the reaction of interest to be recorded. As detailed in **Figure 2.5.1**, it can be identified that the first half of the triangular waveform is alike to that used in Linear Sweep Voltammetry, however, the direction of the sweep is reversed once E_2 is reached, allowing the potential to be scanned back to its primary state (E_1).

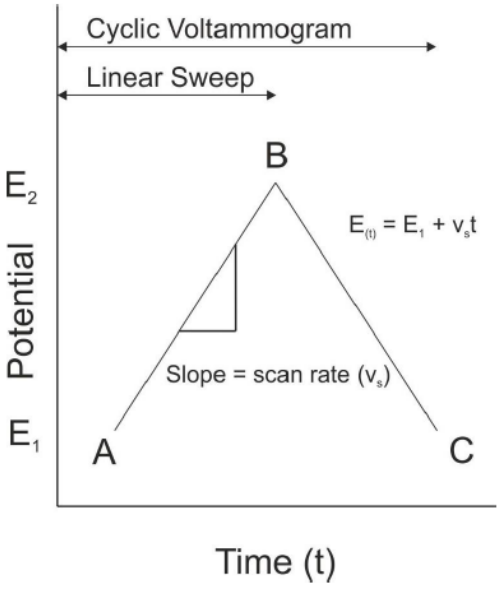

Figure 2.5.1 Triangular waveform used in cyclic voltammetry

After the scan has been completed, with regards to specific scanning parameters, a voltammogram is generated whereby the current is presented against a function of the applied potential. A characteristic cyclic voltammogram presenting the response observed for a reversible reaction in shown in **Figure 2.5.2**.

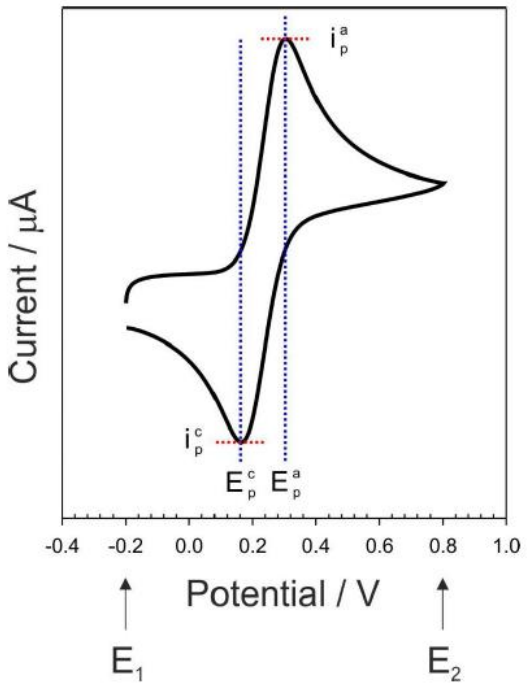

Figure 2.5.2 An example cyclic voltammogram showing reversible redox peaks

The voltammogram presented for a reversible system exhibit some well-defined features:

- The interpeak distance between the oxidation and reduction peak potentials are detailed in **Equation 2.8** and are not aligned with the scan rate.

$$\Delta E = E_p^a - E_p^c = \frac{59}{n}\, mV$$

…Eq.2.8

- The peak ratio of the forward and reverse scans will be equal to one (**Equation 2.9**).

$$\frac{i_p^a}{i_p^c} = 1$$

…Eq.2.9

- Lastly, the peak currents i^a_p / i^c_p are proportional to the square root of the scan rate in a diffusible system.

From **Figure 2.5.3**, we can observe that the current response increases as the scan rate is increased. The change in current can be considered by analysing the size of the diffusion layer along with the length of time taken to complete the scan. Therefore, it can be observed that by increasing the scan rate we will see a quicker rate of scan completion (**Figure 2.5.3 A**). The size of the diffusion layer is then dependant on the scan rate. When the scan rate is increased, the distance the diffusion layer moves away from the electrode will lessen, i.e. a reduced amount of diffusion will happen within the time frame, when compared to a slower scan rate. As a result of increasing the scan rate, there will be a surge in the flux to the surface of the electrode where the current is related to the flux in the direction the electrode. As a result, the size of the current will then be larger at faster scan rates and will be smaller at smaller scan rates (**Figure 2.5.3 B**).

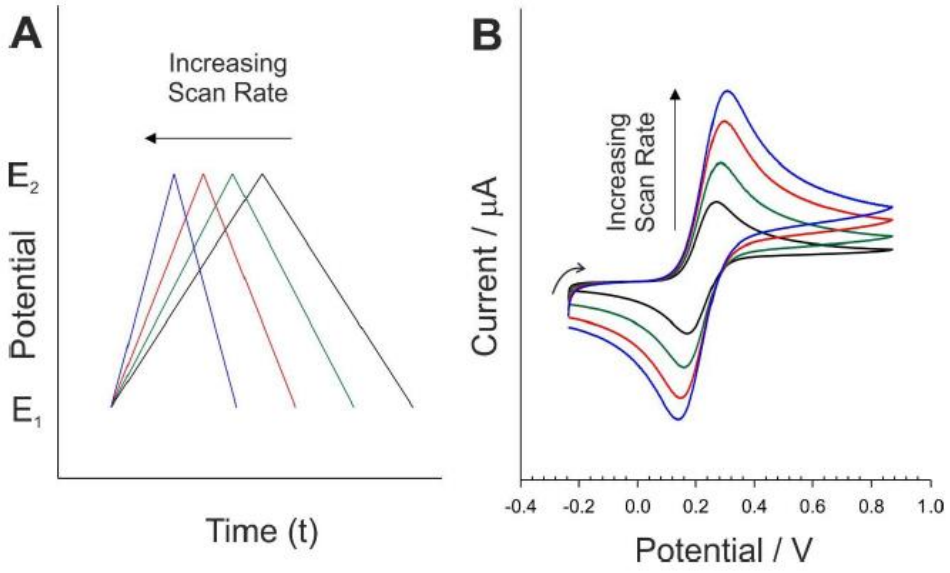

Figure 2.5.3 (A) Triangular waveforms used in cyclic voltammetry displaying different scan rates. (**B)** A series of cyclic voltammograms recorded at increasing scan rates

A graph detailing the peak current against the square root of the scan rate presents a linear relationship and by applying the Randles-Ševčik equation (Equation 2.10) the diffusion coefficient can be calculated.

$$j_p = 2.69\ x\ 10^5\ n^{3/2}\ D^{1/2} c v^{1/2}$$

…Eq.2.10

Where:

j_p = current density (A)

n = number of electrons

D = diffusion coefficient (cm^2/s)

c = concentration (mol/cm^3)

v = scan rate (V/s)

Electrochemical reactions that are reversible tend to demonstrate fast electron kinetics and ensure the equilibrium of concentrations of the oxidised and the reduced species are maintained. This equilibrium can only be maintained if there are sufficient electron kinetics, if the kinetics are not adequate then the reaction is irreversible. The importance of the peak potential of the oxidation and reduction peaks in a standard CV are detailed in **Figure 2.5.4**.

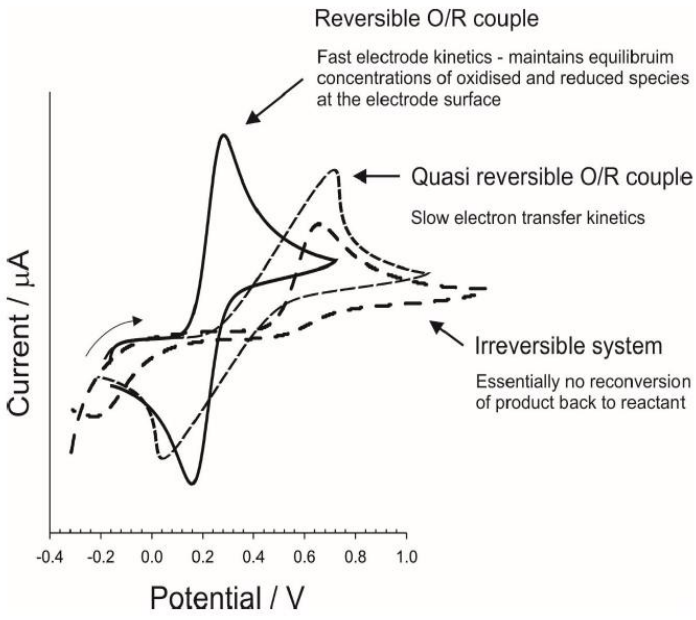

Figure 2.5.4 Cyclic voltammogram detailing the electron kinetics involved in a reversible, quasi reversible and irreversible system

As previously detailed in Equation 2.8, the ideal peak separation for a categorically defined reversible couple would be 59 / n mV, where the rate of transfer of electrons between the working electrode and the redox species is fast and is not affected by a change in scan rate. When the rate of electron transfer kinetics is slower, the oxidation and reduction peaks move away from each other. In this case, the overpotential needed to oxidise the species becomes greater with growing current density, thus resulting in the shift of the oxidation peak to more positive potentials where the peak itself appears broader and elongated in comparison to the sharp peaks of a reversible system. A similar effect is observed in the reduction peak which will appear more drawn out towards more negative potentials. These observations are characteristic of a quasi-reversible couple.

When the rate of transfer of electrons between working electrode and redox species is slow, the oxidation and reduction peaks are much smaller than those observed in a reversible system and are widely separated, this is indicative of an irreversible system. As a result, there is effectively no reconversion of the product back to the reactant. The time it takes for depletion of the surface concentration of the reactant is now much longer, therefore decreasing the flux of the reactant at the peak potential (Pletcher, 2009). An additional observation between reversible and irreversible reactions is that the irreversible couple is reliant on the scan rate.

When the peak current is plotted against the square root of the scan rate a linear relationship is observed when investigating a reversible system, however this is not the case for an irreversible system where the peak current density now must take into account the transfer coefficient (α) and is now defined as:

$$j_p = 3\ x\ 10^5\ n(n\alpha)^{1/2}\ D^{1/2} c v^{1/2}$$

…Eq.2.11

The voltammetric profile and shape of the CV as detailed above is typical of linear diffusion at a macroelectrode. As the dimensions of the electrode with regard to the diffusion layer thickness shrinks, the diffusion layer transforms into a hemispherical shape thus resulting in a noticeable change in the CV profile. The CV shown in **Figure 2.5.5** illustrates near steady-state conditions where the distinctive peak has now disappeared (Compton and Banks, 2011).

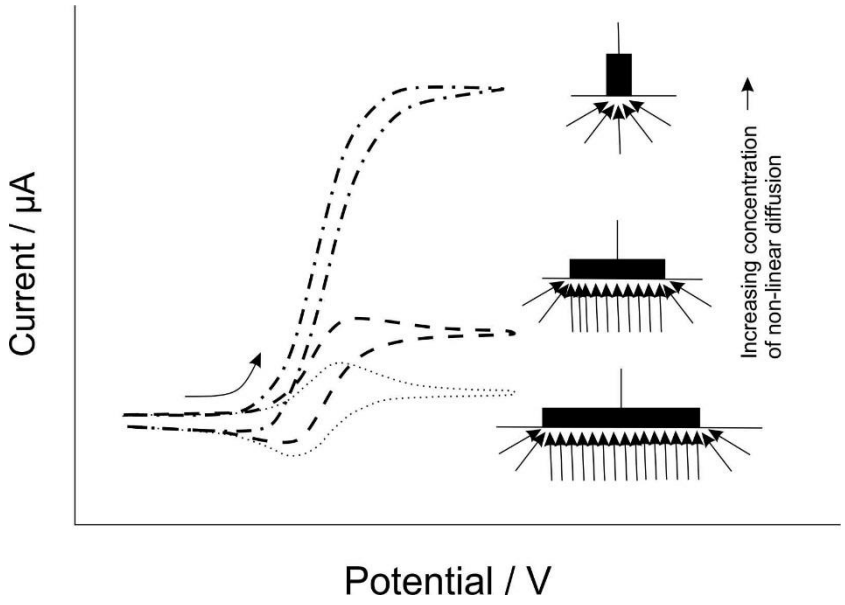

Figure 2.5.5 Relationship observed between the size of the electrode (with respect to the diffusion layer thickness) and the contribution of convergent diffusion and its observed cyclic voltammograms. Adapted from Compton and Banks,2011

Electrodes which dimensions are measured in micrometers are categorised as 'microelectrodes'. When the dimensions of an electrode exceed this size, they are usually termed 'macroelectrodes'. As illustrated in **Figure 2.5.5**, microelectrodes perform in different ways from macroelectodes, especially in terms of non-planar diffusion which gives rise to faster rates of mass transport. Furthermore, microelectrodes possess reduced capacitance in contrast to macroelectrodes as the capacitance is directly proportional to the area of the electrode. Decreasing the dimensions of the electrode immediately reduces the capacitance (Compton and Banks, 2011).

From an analytical perspective, microelectrodes are becoming more popular and are often preferred over macroelectrodes as they offer comparable magnitude voltammetric response with less capacitance background (Davies and Compton, 2005). The production of reproducible microelectrodes can be easily achieved through lithography - typically in cubic or hexagonal arrays or via an easier method implemented by Fletcher and Horne (1999) by facilitating a random distribution (array) of microdisc electrodes into an insulating substrate (RAM^{TM} electrodes) (Stephen Fletcher and Horne, 1999). As mentioned previously, the diffusion profile of microelectrodes differs in comparison to macroelectrodes. Individual diffusion layers will arise in microelectrode arrays, and the subsequent voltammogram is subject to two influences: the dimensions of the diffusion layers in comparison to the area of the individual microelectrode and the dimensions of the diffusion layers against the size of the insulating substrate or the separation between each microelectrode. In accordance with these two influences, Davies and Compton (2005) determined that microelectrode arrays can be allocated to one of four classes which are detailed in **Figure 2.5.6**.

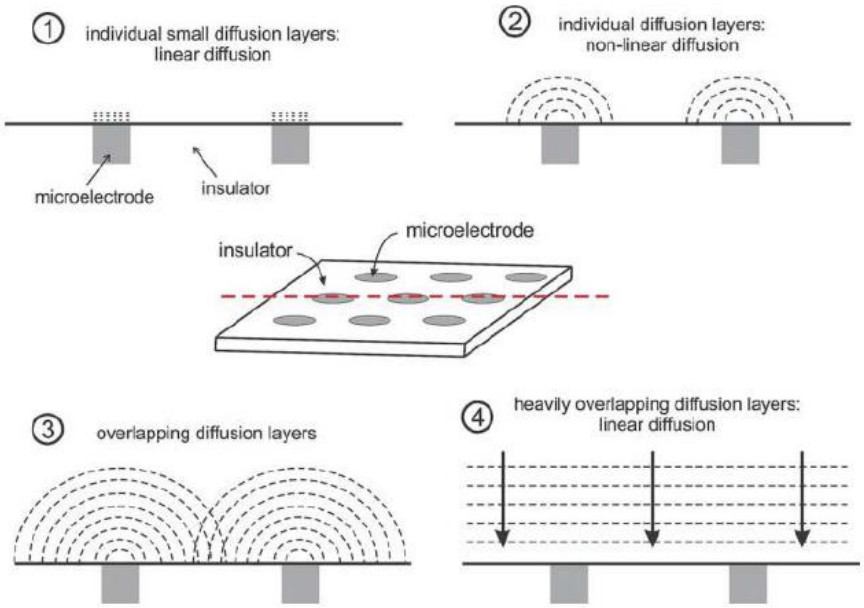

Figure 2.5.6 Schematic diagram of the four categories of diffusion profiles to which a microelectrode array may belong (Davies and Compton, 2005). Reproduced with permission from Elsevier

Traditionally, the majority of microelectrodes that are developed fall into the second category, as this is where the maximum current density is obtained. Steady-state behaviour is achieved within this category where the diffusion layers are greater in size than the microelectrode, but more significantly are smaller than the space between the microelectrodes reinforcing independence. If the distance between the microelectrodes was reduced, as showing in categories 3 and 4, the neighbouring diffusion regions will overlap and therefore give rise to linear diffusion as observed in a microelectrode (Compton and Banks, 2011).

2.5.2 Square Wave Voltammetry

Although cyclic voltammetry can provide qualitative information during electrochemical investigations, square wave voltammetry (SWV) can be used to achieve further quantitative analysis of a sample solution. Unlike CVs - where the potential of the working electrode is swept linearly to form a triangular waveform, with SWV the current is recorded as the potential of the working electrode is swept in a staircase manner and is demonstrated in **Figure 2.5.7**.

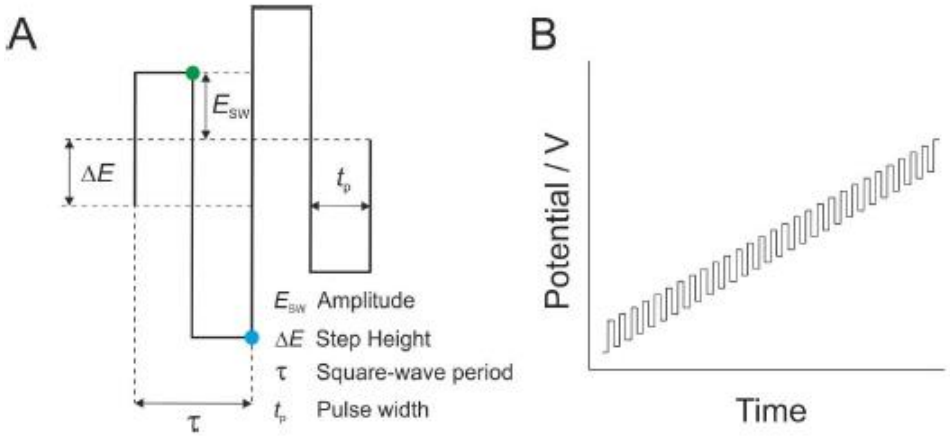

Figure 2.5.7 (A) Detailed waveform and parameters used in square wave voltammetry. (B) Full profile of the staircase waveform used in a square wave scan

The chief principles for SWV are described in **Figure 2.5.7 A**. The duration of one complete square wave cycle or one staircase step is termed the square wave period (τ). The square wave is categorised by two features, the amplitude (E_{sw}) and the pulse width (t_p). The pulse width can also be classified in terms of frequency which is described as $f = 1/\tau$ or $f = 1/2t_p$. The step height ΔE is the step height is applied to determine the scan rate for a square wave voltammetry experiment (Equation 2.12).

$$\text{Scan Rate (mV/sec)} = \frac{\Delta E \text{ (mV)}}{\tau \text{ (sec)}}$$

…Eq.2.12

With the method, during a square-wave period the current is logged twice, this happens as each pulse finishes, which is detailed as the green and blue dots seen in **Figure 2.5.7A**. These are located at the end of the forward current scan - i_f (green dot) and is repeated when the reverse current has been completed - i_r (blue dot). When the forward and reverse currents are recorded, the output is unidirectional sweep as shown in **Figure 2.5.8**. The critical difference between CV and SWV is that the latter is generated from the difference current (Δi) (Bard and Faulkner, 2001).

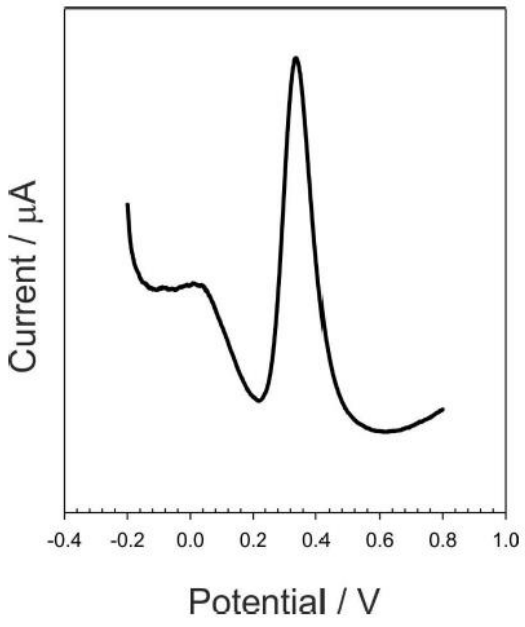

Figure 2.5.8 The difference current displayed in a typical square wave voltammogram

The peak show in **Figure 2.5.8** is positioned at around +0.3 V is representative of redox processes and the size of the peaks in SWV are proportional to the concentration of the analytes present corresponding to **Equation 2.13**.

$$\Delta i_p = \frac{nFAD^{1/2}C}{(\pi t_p)^{1/2}} \Delta\psi_p$$

…Eq.2.13

Where:

Δi_p = differential peak current (A)

n = number of electrons

F = Faraday constant 96485 C mol^{-1}

A = electrode area (cm^2)

D = diffusion coefficient (cm^2/s)

C = concentration (mol/cm^3)

t_p = pulse width in s

$\Delta_{\psi p}$ = dimensionless peak current

Square wave voltammetry is often chosen as a more appropriate method over cyclic voltammetry especially when a high degree of sensitivity is required along with minimal background interface. This is due to the timing of the current measurement. During a CV, current measurement begins directly following the change in potential step, however, during SWV the sensitivity is enhanced as the current is logged twice during each square-wave period at the completion of each pulse, thus resulting in a delay (a few milliseconds) of the recorded current. This delay is significant as upon changing the potential of the electrode surface, there is a reorganisation of ions at the interface which in turn leads to an increase in capacitance current. The current is of greater interest on account of the electron transfer to or from the target biomarker, termed as the Faradaic current. As a consequence of the current measurement delay in square wave voltammetry, the input to the current signal following on from capacitance current is marginal while with cyclic voltammetry, the current measured is the addition of these two current measurements. For this reason, much smaller concentrations can be tested by SWV in contrast to CV since

the small Faradaic current can frequently be masked by the capacitance effects and consequently, by pausing to allow the capacitance dissipate, an improved signal to noise ratio can be achieved and as such greater detection limits can be attained (Bard and Faulkner, 2001).

2.5.3 Amperometry

Amperometric measurements involve stepping the potential of the working electrode, from one potential where there is usually no reaction taking place (E_1) and then stepped to another (E_2) where it is fixed at that potential for a predetermined amount of time as shown in **Figure 2.5.9**. The step in potentials can be used to induce either oxidation or reduction.

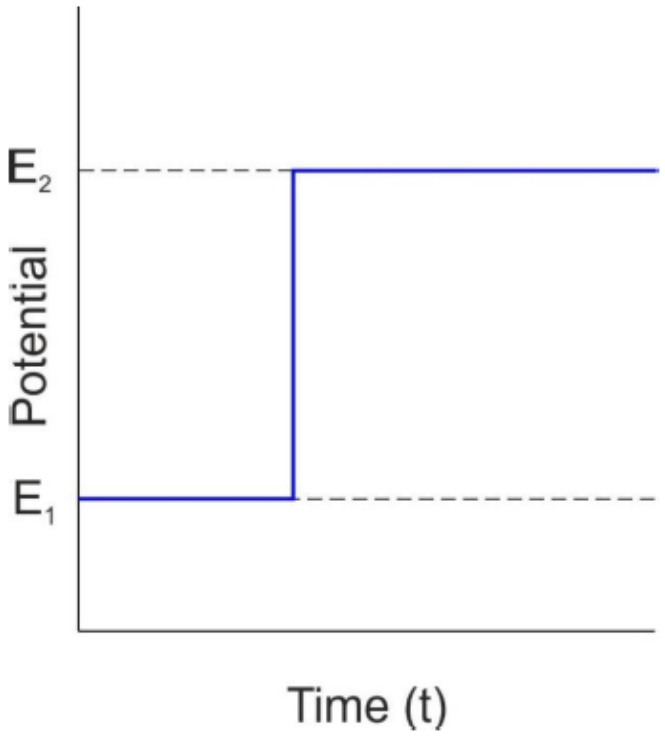

Figure 2.5.9 Potential step procedure used in amperometry

For the duration of this process, the current is measured as a function of time and a typical current response during amperometry is shown in **Figure 2.5.10**. When using a potential step, the performance of the current can be explained by Equation 2.14.

$$i = \frac{E}{R_S} e^{-t/RsCd}$$

…Eq.2.14

Where:

i = current (A)

E = electrode potential (V)

e = electronic charge (C)

t = time (s)

R_s = solution resistance in ohms

C_d = differential capacitance of the double layer in F

`

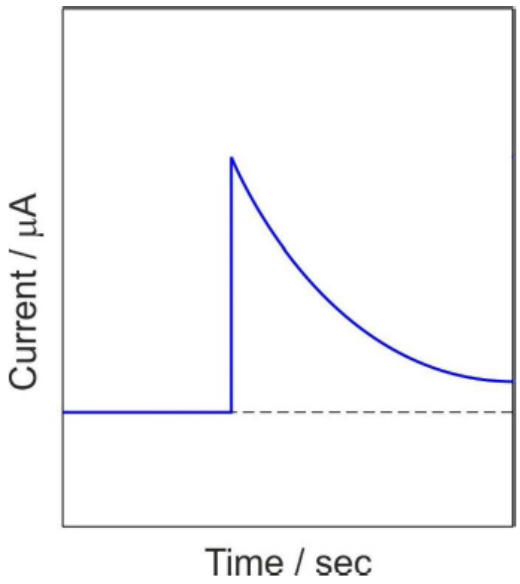

Figure 2.5.10 Example of the current response in amperometry

The current-time response reflects the transformation in the concentration gradient in the electrodes vicinity (**Figure 2.5.11**) as a result it has substantial use in acquiring

physical parameters (electrons transferred, effective electrode areas, diffusion coefficients etc.) of the system under investigation but has limited diagnostic use.

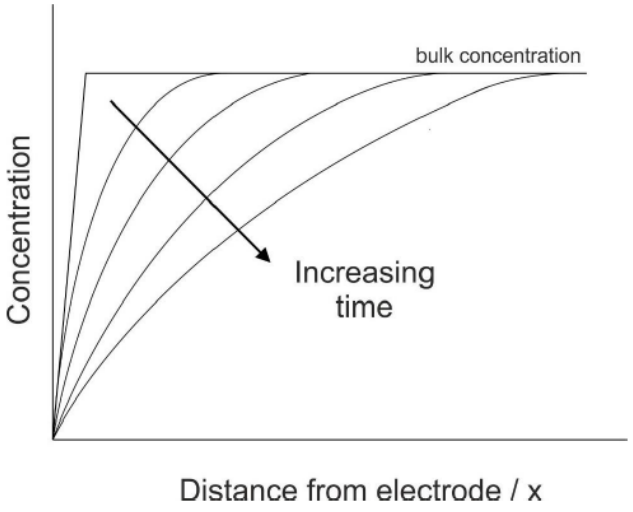

Figure 2.5.11 Concentration profiles for various times into an amperometry experiment

In section 2.4.1, Fick's second law was addressed, which details how diffusion effects the concentration gradient with time. During an amperometric investigation, the potential is stepped from one potential to the next in an effort to stimulate an electrode process; such as oxidation or reduction. The shift in potential will bring about an adjustment in the concentration of the reactant at the electrode surface, causing variation in the reactant concentration close to the electrode surface. This results in the diffusion of the reactant in the direction of the electrode, in doing so it generates concentration differences around the electrode and the extension of the diffusion layer into the bulk solution (Pletcher, 2009). As shown in **Figure 2.5.9** the diffusion layer expands with time along with the concentration gradient and the flux of the reactant towards the electrode surface reduces with time causing a drop in current density versus time (**Figure 2.5.10).**

The falling current density versus time transient will follow the Cottrell equation (Equation 2.15) which is essentially a test for diffusion control and is shown in **Equation 2.15**:

$$j = \frac{nFD^{1/2}c}{\pi^{1/2}t^{1/2}}$$

…Eq.2.15

Where:

j = current density (A)

n = number of electrons

F = Faraday constant 96485 C mol-1

D = diffusion coefficient (cm^2/s)

c = concentration (mol/cm^3)

t = time in (s)

2.5.4 Potentiometry

Unlike all other previously described voltammetric methods, potentiometry measures the potential of the working electrode relative to the reference electrode under zero current and is monitored as a function of time **(Figure 2.5.12).** As zero current is passing through the cell, the configuration of the solution remains unaffected thus allowing quantitative measurements of the solution's composition.

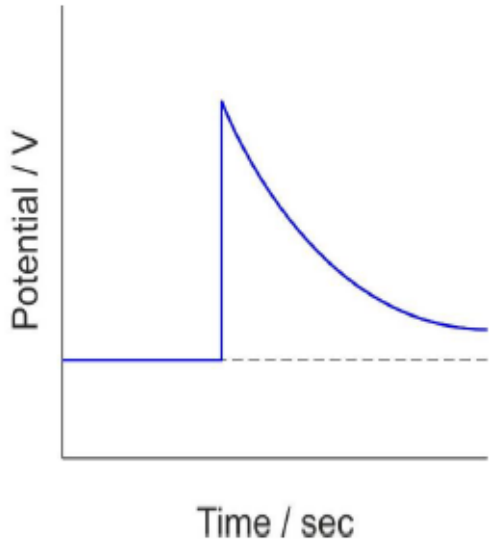

Figure 2.5.12 The potential of the working electrode is measured in relation to the reference electrode and recorded as a function of time

2.6 Surface / Physical Characterisation Methods

The next section will describe a number of surface and physical characterisation techniques that were used throughout the project, these techniques can provide key information regarding physical and chemical composition and surface morphology.

2.6.1 Scanning Electron Microscope

The Scanning Electron Microscope (SEM) is one of the most commonly used surface characterisation techniques. To produce an image, the technique utilises electrons instead of light for imaging. During experimental procedures, materials chosen for electrochemical consideration where first characterised using the SEM to observe surface morphology and structural defects that may be present on the surface of electrode materials. The sample material is scanned using a high energy focused beam of electrons (ranging from 0.5 keV to 40 keV) where the incident beam is scanned in a raster pattern. An electron detector identifies the emitted electrons in each position within the scan area. On the output screen, the brightness of the electronic signal is based on the intensity of the emitted electrons.

An electron gun, equipped with a tungsten source filament, produces a stream of monochromatic electrons. Tungsten can operate with very high voltages and is chosen for this application due to its high melting point and low cost. The filament functions as a cathode, which begins to heat up when a potential is applied, generating an electron beam which travels in the direction of the anode. When the sample is placed onto the sample stage and the entry drawer is sealed, the sample is held under vacuum, where the incident beam moves in a downward motion towards the sample and then towards the detectors. When the focused beam is directed at the sample, backscattered a variety of signals are generated – such as electrons and X-rays. The course taken by the electrons is shown in **Figure 2.6.1**.

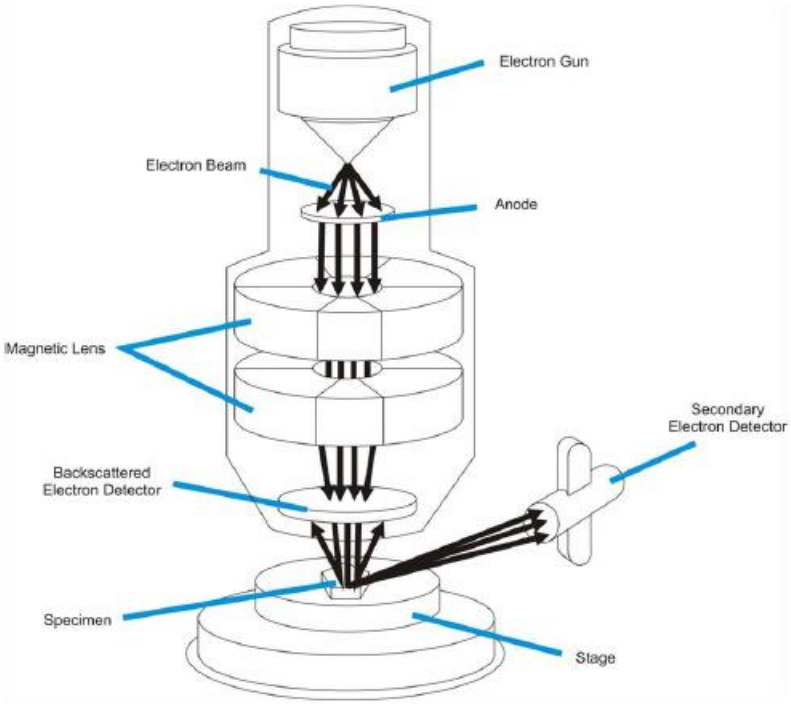

Figure 2.6.1 Diagram of a scanning electron microscope showing the pathway taken by the electrons

When the beam of electrons reaches the sample stage, several signals are generated such as backscattered electrons, secondary electrons, X-rays and auger electrons which are shown in **Figure 2.6.2**. Backscattered electrons originate from the incident beam and are reflected against the sample through elastic scattering. These signals can provide information on the atomic number of the material being examined, where higher atomic number materials absorb more electrons. Secondary electrons arise due to inelastic collisions between primary electrons (the beam) and loosely bound electrons in the outer shells of the sample atoms are ejected due to a transfer of energy from the primary electrons displacing secondary electrons from the sample. Characterisation X-rays are released as the incident beam disconnects an inner shell electron from the sample, triggering a higher energy electron to take its place and emit energy. The released energy is acquired by another electron which is released form the atom. The released electron is known as the Auger electron, together the Auger electron and X-rays provide diagnostic information relating to the surface composition of the sample.

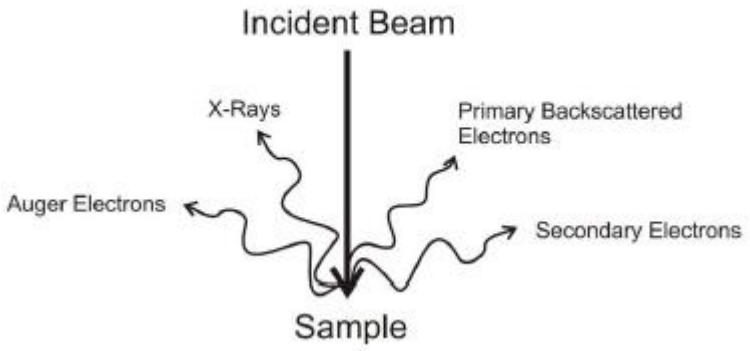

Figure 2.6.2 Several types of signals are produced when an electron beam hits the sample

The SEM has a large depth of field, which allows a large amount of the sample to be in focus at one time, and the technique produces an image which is a reasonable good representation of the 3D topography of the sample. The combination of higher magnification, larger depth of field, greater resolution, compositional and crystallographic information makes the SEM a greater tool for studied surface morphology compared to a traditional light microscope. Samples should be prepared carefully to withstand the vacuum inside the microscope. Because the SEM illuminates the sample with electrons, samples should be made to conduct electricity (insulating samples produce charging). Thin layers of conducting material are sputter coated onto samples where the most commonly used metals are: Au, Au/Pd, Pt, Cr and carbon.

2.6.2 X-Ray Photoelectron Spectroscopy

X-Ray Photoelectron spectroscopy (XPS) is a technique used to characterise the chemical and elemental composition of the uppermost surface regions of a material in the range (30 – 50Å). X-rays from a low energy source (typically Mg Kα (1253.6 eV) or Al Kα (1486.6 eV) X-rays) are directed towards the sample and give rise to the emission of the core and valance electrons from atomic shells of the elements present on the uppermost surface by the photoemission process. The photoelectrons produced possess energies characteristic of the element and the

molecular orbital from which they were emitted. They have measurable kinetic energies.

Valence levels, refer to those electrons that interact with those equivalent valence levels of other atoms to form chemical bonds. Their character and energy will be changed markedly by such interactions. The core levels contain electrons, which are not involved in direct chemical bonding and, so they have energies that are independent of the chemical species in which the atom is bound. Therefore, the identification of the core level binding energy (B.E) is a unique signature for each elemental species.

All elements in the periodic table, except for hydrogen and helium, which do not have core levels, can be identified using this. Quantitative analysis, which yields the atomic concentration of each of the elements detected, requires the measurement of the area under the most intense photoelectron peak for each species, combined with a knowledge of the σ. Typically, the XPS spectrum is plotted as B.E. (x-axis) versus peak intensity in counts/second (y-axis). B.E. is substituted for K.E. to give a direct experimental determination of the electronic energy levels of the different atoms present in the sample.

In **Figure 2.6.3** the electrons emitted from the sample are focused at the entrance of a hemispherical electron energy analyser (HEA) by an electrostatic lens column. A voltage applied across the hemispheres, called the pass energy, allows electrons of specified energy only to travel around the analyser where they are detected by a suitable device such as a channeltron electron multiplier or a channel plate array. Electrons emitted by the sample are slowed to this pass energy by applying a retarding voltage in the region immediately before they enter the electron energy analyser, thus improving the energy resolution. Scanning the voltage across the analyser produces a spectrum of the electron energies detected at each energy value, which corresponds to the elements on the surface of the analysed sample.

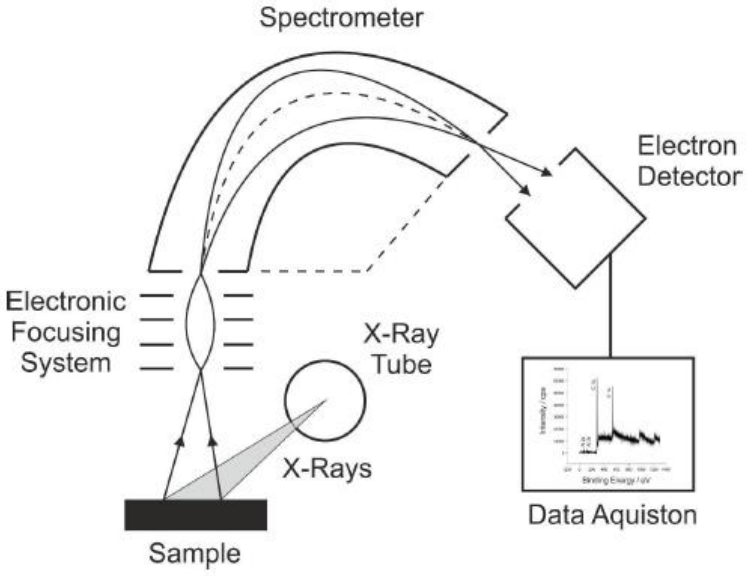

Figure 2.6.3 Diagram of an X-Ray Photoelectron Spectroscopy system

The photoelectrons emitted from the surface region are focussed between inner and outer hemispheres of a Hemispherical Energy Analyser (HEA) via an electrostatic lens assembly. Retarding voltages are used to direct the electrons onto the detector. Peak intensities of the electrons emitted from different orbitals of the same element are not the same because the probability for photoemission, i.e. the photo-ionisation cross-section (σ), from each orbital is different. The probability is also different for a given orbital in a different atom. Thus, the spectral peaks correspond to the number of occupied energy levels in the atoms whose B.E. is lower than the incident X-ray energy ($h\nu$). The position of the peaks then provides a measure of the B.E. of the electrons in the orbitals and identifies the atoms concerned. Correspondingly, the intensities of the peaks depend upon the number of the atoms present and on the value of σ from each orbital concerned. A typical spectrum for carbon is shown in **Figure 2.6.4.**

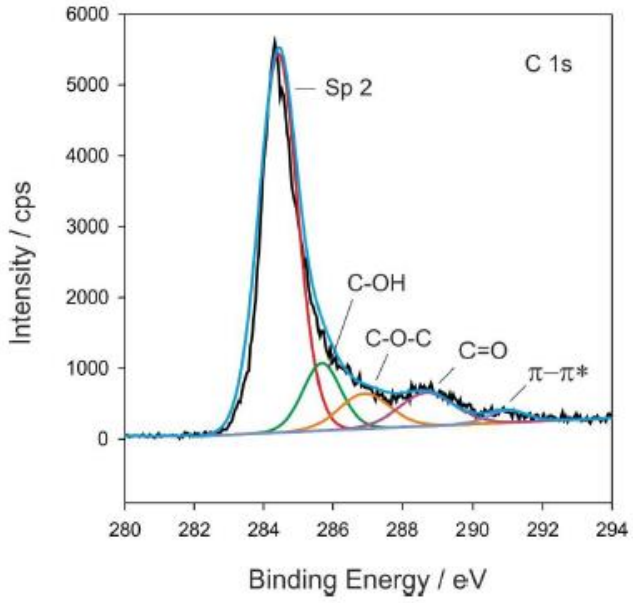

Figure 2.6.4 A typical carbon spectrum obtained from an XPS system showing different binding energies for different chemical states

2.6.3 UV-Vis Spectroscopy

Ultraviolet/visible spectroscopy involves passing electromagnetic radiation through a sample which is placed in a spectrometry cell – typically a quartz cuvette (path length 1cm) held inside the spectrometer. The fundamentals of UV-vis spectroscopy begin when light is passed through the compound, the energy from the light is used to stimulate an electron from a bonding or non-bonding orbital towards one of the vacant anti-bonding orbitals as illustrated in **Figure 2.6.5**.

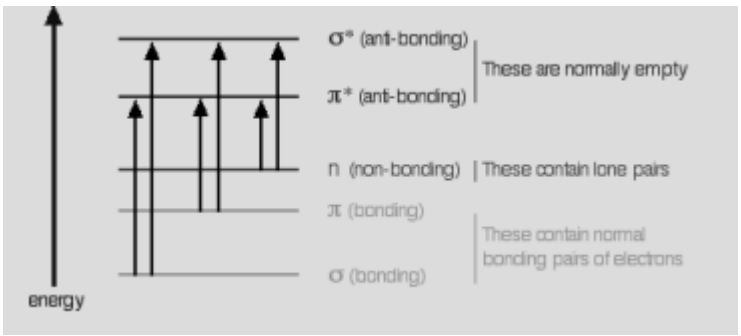

Figure 2.6.5 Electron stimulation from a bonding or non-bonding orbital towards the vacant anti-bonding orbitals

Within each example, an electron is excited from a fully occupied orbital into a vacant antibonding orbital. The energy from each jump is taken from the light, where the larger the jump, the energy required will be bigger. Each specific wavelength of light has a certain energy related to it. If the specific amount of energy is enough to fulfil one of the energy jumps, then the wavelength will be absorbed – as its energy will have been utilised in promoting an electron.

A conventional UV-vis spectrometer functions in a range from around 200 nm (near ultra-violet) to 800 nm (very near infra-red). It is important to note that larger jumps require more energy and therefore absorb light with a shorter wavelength. The most significant jumps are from pi bonding orbitals to pi anti-bonding orbitals, and from non-bonding orbitals to sigma anti-bonding orbitals. Therefore, for light absorption to occur in the area from 200-800 nm, the molecule must possess pi bonds or atoms with nonbonding orbitals. Light absorbing groups that are present in a molecule are known as chromophores.

An example of a typical UV-visible absorbance spectra using Methyl Salicylate is shown in **Figure 2.6.6**. The vertical axis represents absorbance of light, where the larger the value the more of a particular wavelength is being absorbed.

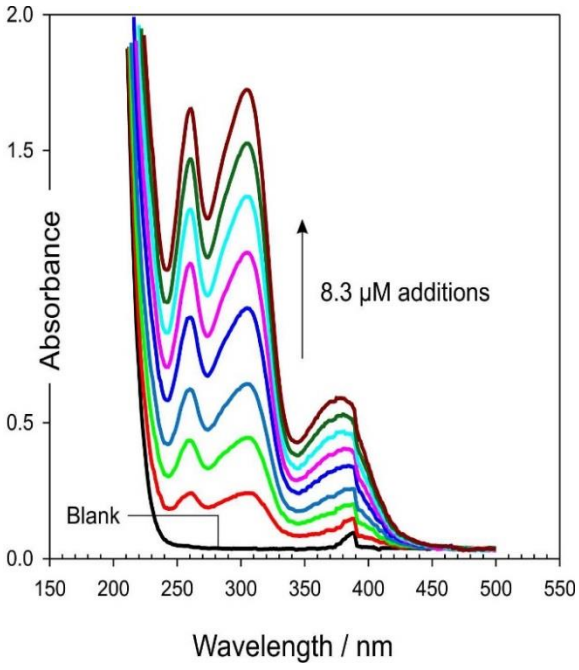

Figure 2.6.6 UV Spectra detailing the additions of methotrexate (2 mM stock, pH 7 buffer)

UV-vis spectroscopy is often used to obtain the absorbance spectra of a particular compound in a solution or solid. The data that is collected spectroscopically is the absorbance of light energy or electromagnetic radiation, which promotes electron excitation from the ground states to the first singlet excited state of the compound of interest. If we consider the electromagnetic spectrum, the area that covers the UV-Visible region spans 1.5 – 6.2 eV which is associated to the wavelength range from 800 -200nm. The theory behind absorption spectroscopy is defined by the Beer-Lambert Law as described in Equation 2.16.

$$A = \varepsilon l c$$

…Eq.2/16

Where:

A = Absorbance

ε = Molar absorptivity of the compound or molecule in solution (mol^{-1} L cm^{-1})

l = Path length of the cuvette or sample holder (usually 1 cm)

c = Concentration of the solution (mol L^{-1}).

There are two types of absorbance spectrometers: single beam and double beam. Each spectrometer has a light source (deuterium or tungsten lamp), a sample container and a detector. A single beam spectrometer contains a monochromator placed between the light source and the sampled to analyse one wavelength. The single beam instrument has a filter or a monochromator between the source and the sample to analyse one wavelength at a time and is demonstrated in **Figure 2.6.7**.

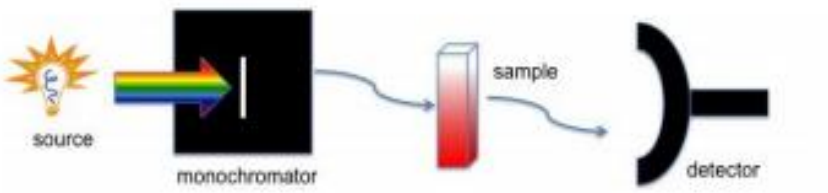

Figure 2.6.7 Schematic of a typical single beam instrument

UV-vis analysis can retrieve both qualitative and quantitative data from the compound sample. In both cases it is necessary to use a reference cell to zero the instrument before the analysis can be undertaken. When quantitative information is required from the sample, calibrating the instrument can be achieved by additions of the compound of interest at known concentrations to the same solvent used in the sample. If confirmation of a compounds presence is only required, it is not necessary to create a calibration graph. Specific scanning parameters for each experiment can be found within the relevant chapter where spectrometry techniques have been used for analysis.

2.7 Surface Modification Techniques

A number of techniques were used throughout the project to improve substrate response or modify the surface of electrode materials. The methods employed are described in detail in the following sections.

2.7.1 Electrochemical Anodisation

Electrochemical anodisation involves the use of the amperometry technique detailed in Section 2.5.3. Within this project, electrochemical anodisation has been employed to alter the electrode surface in order to improve the electrode response towards a number of analytes as previously demonstrated by (Dutt *et al.*, 2005). The electrochemical anodisation and subsequent enhancement of electrode substrates was achieved by amperometric oxidation (+2 V) for various amounts of time (typically 5-300 s) in 0.1M NaOH, where the working electrode acts as the anode (the positive electrode). As a result, hydrogen is released at the cathode (the negative electrode) and oxygen at the surface of the working electrode, which leads to a build-up of hydroxide. This process give rise to the creation of oxygen functionalities (carbonyl, carboxy, hydroxy and quinoid) on the electrode surface, changing the microscopic

texture of the surface as well as the crystal structure of the layers as show in **Figure 2.7.1** (Banks and Compton, 2005a).

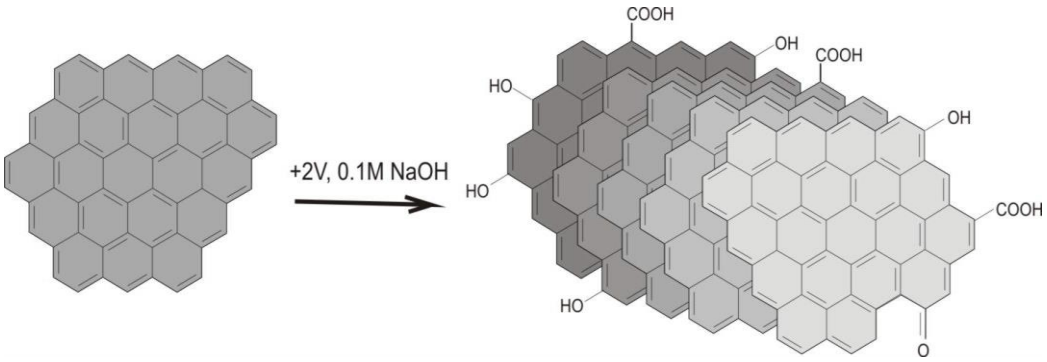

Figure 2.7.1 Effect of electrochemical anodisation on the immediate surface of the graphite particle

By increasing the oxygen functionalities at the electrode surface, fracturing of the carbon is observed leading to the increase in the amount of edge plane sites where faster electron transfer is observed, this gives rise to enhanced electrode performance together with greater voltammetric resolution and sensitivity.

2.7.2 Laser Ablation

Laser ablation of the conductive composite films to create pores was achieved using a 25W CO_2 computer-controlled laser cutter (FB400 series CadCam Technology Ltd, Nottingham, UK). Control over the direction of the laser, speed and output power was controlled via ApS-Ethos software. The laser was typically patterned across the x and y directions of the applicable substrates with a spacing of 2 mm between each pass in order to create a porous network, which will be further detailed in the following chapters. Within this project, controlled laser ablation was used to pattern the surface of the conductive carbon film described in Chapter 1 to create micron sized pores, though which the drug molecules can permeate.

2.8 Film Deposition methods

2.8.1 Solvent Casting

Composite free-standing films were composed of carbon nano powder and cellulous acetate phthalate (CAP) at 1:1 w/w ratio. Cellulose acetate phthalate was first dissolved in acetonitrile and left under continuous stirring until a homogenous, fully dissolved solution was achieved. Following dissolution, the CAP solution was added to the carbon nano powder while mixing with further additions of acetonitrile added until the desired viscosity was achieved. The solution was then free cast onto a flat silicone substrate using a glass pipette and allowed to dry at ambient conditions. Once dry, the film was gently peeled from the silicone substrate and then cut to the required size (typically 0.8 mm x 0.6 mm). The carbon-CAP film sections were thermally sealed within a laminate system to define the electrode area - the full procedure is further detailed in the materials section within the relevant chapters where composite films have been used.

Chapter 3

Electrochemical Manipulation of pH to Aid Controlled Release of Reagents from Barrier Films

Abstract

The development and characterisation of a nanostructured conductive film capable of facilitating the controlled dissolution of enteric coatings is described. Laser treatment of the conductive surface was used to create defined pores. Electrochemical manipulation of the local pH within laser etched pores is shown to initiate the hydrolysis of an attached cellulose acetate phthalate film and facilitate the controlled release of a model drug. Moreover, an innovative approach to the design and operation of microfiber pH probe is critically appraised. X-ray photoelectron spectroscopy of the electrode surface after electrochemical anodization presented an increase in the population of endogenous quinone moieties. The redox profile obtained from the electrochemically anodised microfiber probe was exploited and its application to the prototype drug release system demonstrated.

Part of the research described in this chapter has been published in Anderson, A. & Davis, J., 2015. Next generation transdermal drug delivery – An electrochemical approach to pH manipulation for controlled release within smart patch technologies. *IFMBE Proceedings: World Congress on Medical Physics and Biomedical Engineering*. Volume 51, pp 919-922.

3.1 Introduction

The development and manufacture of conventional controlled release technologies to date have been largely based around encapsulant systems in which a polymeric binder or gel typically responds to changes in the local environment in which the delivery device has been placed. The delivery agents are typically released when the particle, capsule, film or droplet is subjected to the appropriate physio-chemical trigger (typically a change in pH) with the time-release-dose delivery characteristics controlled through manipulation of the encapsulant formulation (Bertz *et al.*, 2013; Hassan, Shakeel Laghari and Rashid, 2016; Kamaly, Yameen, Wu and Omid C. Farokhzad, 2016). Gradual dissolution of the coating leads to the release of the therapeutic agent (Maroni *et al.*, 2016, 2017; Pérez-Ibarbia *et al.*, 2016; Pole *et al.*, 2016). One of the most common formulations is cellulose acetate phthalate (**Figure 3.1.1**), which is stable in acidic environments but dissolves in mild alkaline conditions (Felton and Porter, 2013). The film is designed to protect oral tablet drugs from the acid environment of the stomach and enable safe passage to the colon, where the higher pH induces the dissolution of the film and release of the drug.

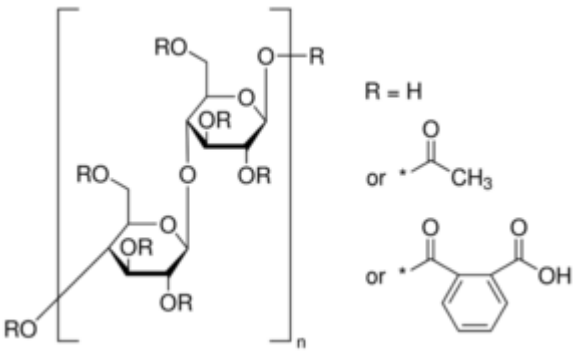

Figure 3.1.1 Chemical structure of cellulose acetate phthalate (CAP)

In this chapter, an adaptation of this core strategy for use in the next generation of transdermal microdevice or smart patch is explored. A key feature of the approach is the ability to electronically trigger the release of the drug on demand.

The strategy within this methodology relies on the electrochemical properties of a carbon-polycarbonate (C-PC) composite film, in which micro-nanoscale pores (typically 0.5 mm diameter) are created through controlled laser ablation. Laser treatment of the film removes small amounts of the encapsulating polymer resulting in greater exposure of conductive carbon around the edges of the pore. In addition, laser ablation causes fracturing of the carbon particles which leads to an increase in the proportion of edge plane sites within the pores, thereby increasing the electron transfer kinetics. This approach has been successfully demonstrated though previous work on carbon fibre electrodes (Ezekiel *et al.*, 2008).

The porous carbon layer was then combined with a conventional pH responsive barrier film (cellulose acetate phthalate) to complete the prototype patch as indicated in **Figure 3.1.2.** Under normal conditions, the enteric coating will remain intact with no diffusion of the drug to the bulk of the solution. Electrolysis of the solution within the latter can be used to raise or lower the pH (Davis and Cooper, 2002; Fomina *et al.*, 2016) and upon imposing a reducing potential to the carbon film top layer, it was anticipated that the local pH within the pores would be dramatically increased, such that hydrolysis of the ester occurs with dissolution of the protective barrier thereby releasing the drug.

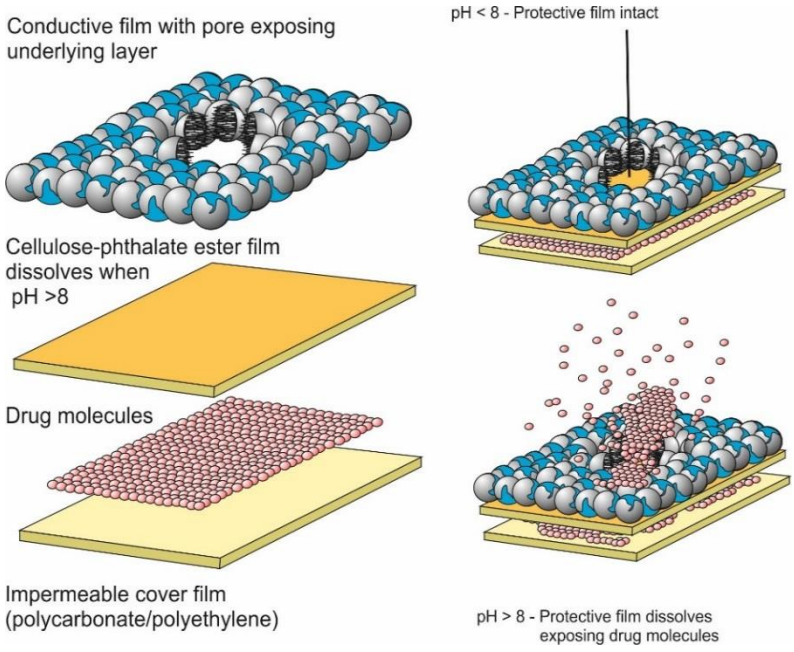

Figure 3.1.2 Proposed configuration of the electrochemical release system

An additional challenge facing this approach was how to determine the pH from within the pore, when the size of the latter is only 0.5 mm in diameter. The problem with using conventional pH measuring systems in this application is not just their incompatible size, they also would have to respond in a rapid manner in determining the pH of the local area and not just the bulk pH. As such, the strategy taken in the present methodology was to use carbon microfiber electrodes (10 µm diameter) encased within thermally sealed laminates, in order to monitor the pH from within the pore. The presence of the pH sensitive quinone functionalities on the surface of the microfiber can be used for the indirect voltammetric sensing of pH in accordance with the Nernst equation (59 mV / pH for a 2 electron-2 proton reaction). Previous methodologies have been able to modify the surface of the electrode via the chemical attachment of quinones (Streeter *et al.*, 2004; Lafitte *et al.*, 2008; Makos *et al.*, 2010; Park and Kim, 2013), however, carbon fibre itself already possess a number of endogenous quinone groups as indicated in **Figure 3.1.3** which could be expected to shift in a similar manner with a change in pH.

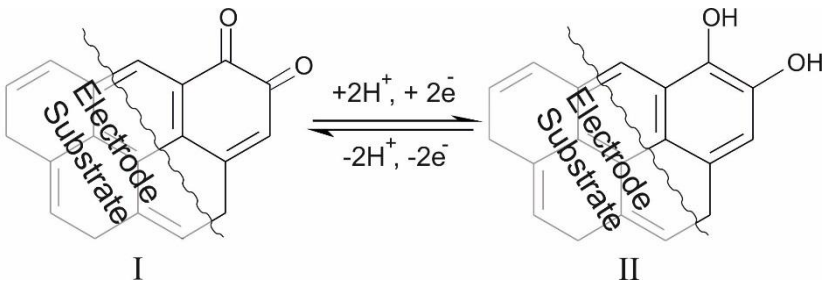

Figure 3.1.3 Possible redox transition of endogenous quinone functionalities

3.2 Experimental Details

3.2.1 Materials

Chemical reagents were of the highest grade available and used without any additional purification. All electrochemical measurements were carried out at 22^{o}C ± 2^{o}C in Britton Robinson (BR) buffer (pH 3-9, adjusted to the appropriate pH value via the addition of sodium hydroxide). The composite carbon-polycarbonate(C-PC)

films, carbon fibre (10 µm diameter filaments) and silver wire (50 µm) reference electrode were supplied by Goodfellow Research Materials. Cellulose acetate phthalate, sodium nitrite and dexamethasone where obtained from Sigma Aldrich.

3.2.2 Electrochemical Setup

Electrochemical analysis and set up was performed using a µAutolab computer controlled potentiostat (Eco-Chemie, Utrecht, The Netherlands). The initial electrochemical arrangement included a three electrode set up comprising of carbon (composite film or microfiber probe, detailed in Section 3.2.3) working electrode, a platinum wire was used as the counter electrode and a standard silver/silver chloride (3 M NaCl) reference electrode. Further measurements used a two electrode configuration comprising a carbon fibre working electrode and a combined counter -reference electrode in the form of a chloridised silver wire. The silver wire (50 µm) was prepared by applying +0.5 V in 1 M KCl for a total of 60 seconds resulting in the deposition of a silver chloride layer. Cyclic voltammetry measurements were conducted at 50 mV/s and square wave voltammograms were scanned from -0.8 V to +0.8 V unless otherwise stated.

3.2.3 Configuration of Release System and Modification

The carbon fibre electrodes were electrochemically anodised by applying a fixed potential of +2 V for varying amounts of time (10-300 seconds) in a solution of 0.1 M NaOH. This process has been shown to increase the presence of carboxyl functionalities on the surface of the carbon (Banks and Compton, 2005b). The carbon microfiber electrode was assembled within a resin backed polyester laminate, modelled to the design shown in **Figure 3.2.1**, which was thermally sealed using a commercial laminator and then cut at the end of the probe to expose a cross section of anodised carbon fibres. A similar approach was utilised for the combined counter silver wire reference, however, a 10 mm length of the chloridised silver wire was exposed.

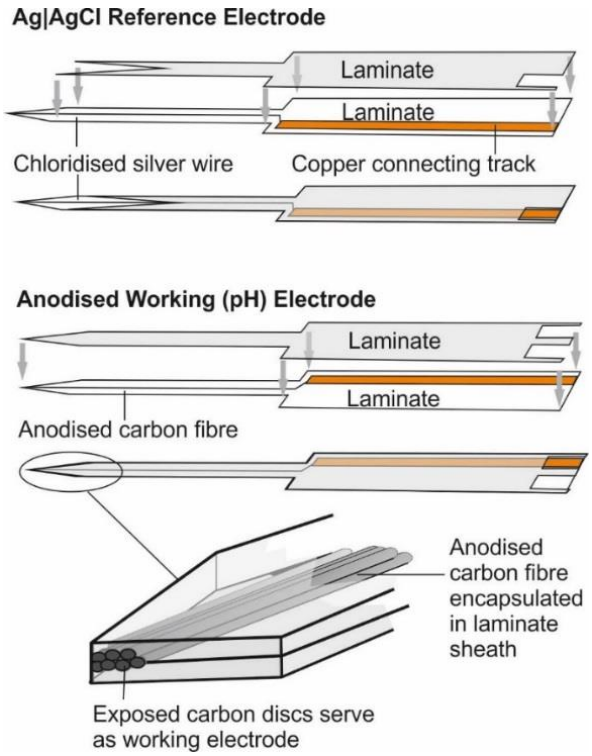

Figure 3.2.1 Schematic of the laminated carbon fibre and reference electrode

Laser enhancement of the conductive C-PC film was achieved using a 25 W CO_2 laser air-cooled computer controlled laser-cutter (FB400 series CadCam Technology Ltd, Nottingham, UK) which created pores on the surface (typically 0.5 mm diameter) and is shown in **Figure 3.2.2**. Controlled laser ablation to pattern the surface also fractures carbon particles increasing the amount of edge plane sites. Before laser enhancement the conductive film is a flat, non-porous structure whereas after laser ablation the surface is modified to create a mesh like interface though which the drug molecules can permeate.

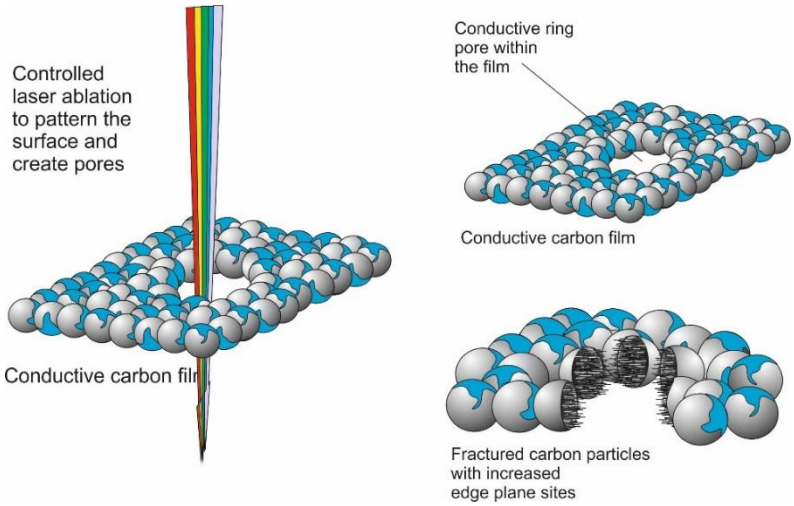

Figure 3.2.2 Fracturing of carbon through laser ablation

It is imperative to note that providing the device is small, the pH will only change at the interface of the pore within the C-PC electrode and will not affect the bulk and hence should not cause any irritation or complication to the patient. Also, crucially as the device is using a negative potential it is unlikely to degrade the drug once released – this may be an issue however if the drug contains nitro functional groups which could, in principle, be converted to the nitroso, hydroxylamine or amine group. The pH sensitive polymer film used in Section 3.3.5 below, was assembled by dissolving cellulose acetate phthalate (CAP) in acetonitrile, which was then cast onto a polyethylene substrate and carefully removed. As part of the overall device schematic, a pH sensitive layer can then be placed below the conductive film along with the drug molecules. The production of the model drug loaded films is described in the following sections.

3.2.4 Film Construction

Sodium Nitrite Loaded Polycarbonate Film

In order to demonstrate model drug release, a polycarbonate film loaded with sodium nitrite (90:10 %w/w) was constructed and placed below the lasered working electrode, where it was possible to monitor the release of a reagent after the

initiation of a negative electrochemical potential. Polycarbonate granules were dissolved in Dichloromethane (DCM) and left to stir for 2 hours. $NaNO_2$ was ground into a fine powder and added to the polycarbonate and left to stir until full integration of the nitrite into the polycarbonate was achieved. A polyethylene sheet was used as a substrate for casting the Polycarbonate/$NaNO_2$ films which were left to dry until the solvent had evaporated.

Dexamethasone Loaded Cellulose Acetate Phthalate Film

A CAP (90%) film loaded dexamethasone (10%) was manufactured in a way similar to the method outlined above. An accurately weighed out amount of dexamethasone was first dissolved in cyclohexane and then added to the CAP and left to stir until the CAP was fully incorporated within the solution. The solution was then cast onto a silicone substrate which, as a consequence of its chemical inertness, was determined to be the most successful route for film removal once the solvent had evaporated.

3.2.5 UV-Visible Spectroscopy

Reagent release from films was monitored using UV-Vis spectroscopy. Spectra were recorded using a Jenway 67 Series spectrometer. Absorbance spectra for the reference and sample solutions were measured in a quartz cuvette (1 cm path length) cell. For each standard solution, a sample was taken and scanned from 200 to 800nm, in order to determine the optimum absorbance.

3.2.6 Model Drug Release

Sodium Nitrite Release

A standard stock solution of 1 mM $NaNO_2$ was prepared in H_2O along with a solution of phloroglucinol (10 mM, pH 3 buffer). A sample of the phloroglucinol solution (3 mLs) was measured into a quartz cuvette and an aliquot of $NaNO_2$ (25 µL) was added to the acidified phloroglucinol. The solution within the quartz cuvette was scanned

from 200 to 500nm were the optimum absorbance selected within an aqueous solution was 319 nm.

Dexamethasone Release

A stock solution of 1 mM Dexamethasone was prepared in methanol and scanned from 200 nm to 500 nm were the ideal absorbance was found to be 243 nm.

3.2.7. XPS Analysis

X-ray photoelectron spectroscopy (XPS) of the carbon fibre probe before and after anodisation was performed using an Axis Ultra DLD spectrometer (Kratos Analytical, Japan) using monochromated Al Ja X-rays (15 kV and 10 mA) with an operating pressure lower than $6x10^{-8}$ Pa. A hybrid lens mode was used throughout examination and charge neutralisation was achieved using an immersion lens with a filament current of between 1.7 and 2.1 mA at a charge balance voltage of between 3.0 and 3.6 V. Three spots were studied for each sample and wide energy survey scans (0–1300 eV binding energy) as well as high resolution spectra for C_{1s} (272.5–297.5 eV) and O_{1s} (519.5–544.5 eV). C-PC films were also analysed, including high resolution spectra for $C_{1s.}$ Pass-energy was 160 eV for the wide energy survey scans and 20 eV for the high-resolution spectra. Quantification of the atomic % oxygen at the surface from the high-resolution spectra was conducted by subtracting a linear background and calculating the area under the peaks on the C_{1s} spectra using Vision 2.2.8 software (Kratos Analytical, Japan).

3.3 Results and Discussion

3.3.1 Microfibre pH Probe Operation and Optimisation

Square wave voltammograms detailing the response of an unmodified carbon fibre electrode under a range of pH conditions are shown in **Figure 3.3.1A**. It can be seen that the voltammetric profile does change with pH, though there are no clearly discernible peaks from which it would be possible to calibrate a range for assessing the pH. The absence of a defined peak for each scan can be attributed to the small number of redox groups present on the surface of the unmodified carbon fibre. In order to improve the electrode response, the carbon fibre electrode was electrochemically anodised with the aim of increasing the population of quinone redox species (**Figure 3.1.3**) and thereby lead to the appearance of a distinct redox peak. The response of the electrode in pH 3 buffer before and after varying the anodisation times are compared in **Figure 3.3.1B**, whereby a noticeable change in the voltammetric profile compared to the unmodified carbon fibre is observed. Significantly, it is now possible to discern a single and unambiguous peak within each of the voltammograms. The magnitude of the peak current is greatly increased and can be associated with a massive increase in quinone population on the carbon surface. The latter is aided by the fact that the anodisation process fractures the carbon – increasing the effective area onto which the quinones can be generated.

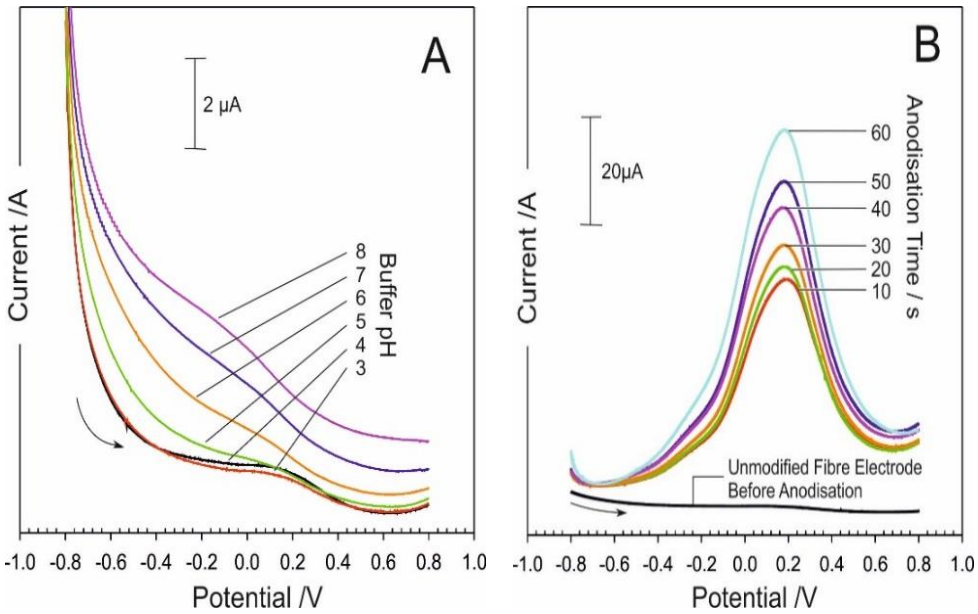

Figure 3.3.1 (A) Response of an unmodified carbon probe to buffers of varying pH. **(B)** Response of the carbon fibre probe to pH 3 buffer solution before and after varying degrees of anodisation

As the square wave scan commences at -0.8 V, the quinone groups present will immediately be reduced to the corresponding hydroquinone (indicated in **Figure 3.1.3**, I→II). As the scan is swept forward to +0.8 V, the hydroquinone moieties are consequently reoxidised (II→I) thus leading to the appearance of a large oxidative peak process as shown in **Figure 3.3.1B**.

The response of the modified carbon fibre probe was tested in buffer solutions across a range of pHs and the scans are detailed in **Figure 3.3.2**. In comparison to the response observed by the unmodified carbon fibre (**Figure3.3.1A**), the electrochemically modified probe presents much more defined (albeit broad) oxidation peaks and, as a result, the peak potential can now be accurately recorded. It can also be observed that as the pH increases, the oxidation peak position moves towards the negative region and is reflective of that observed by previous studies that have used quinones as indicators of pH (Wildgoose, 2003; Lafitte *et al.*, 2008). As the scans progress to more alkaline conditions, the oxidation peak becomes broader and the peak height reduces, this drop in peak height can be due to the deprotonation of the quinones moieties as the background pH solution becomes greater than the pKa which corresponds with earlier work (Abiman *et al.*, 2007). A

calibration graph is showing the peak position against pH is detailed in **Figure 3.3.3.** The peak potentials assigned to each oxidation peak were found to shift with pH (pH 3-9; Epa /V = -0.056 pH + 0.2257; N = 7; R^2 = 0.9916) in manner that is near Nernstian (the ideal being 59 mV / pH) and verifies its suitability for pH measurement.

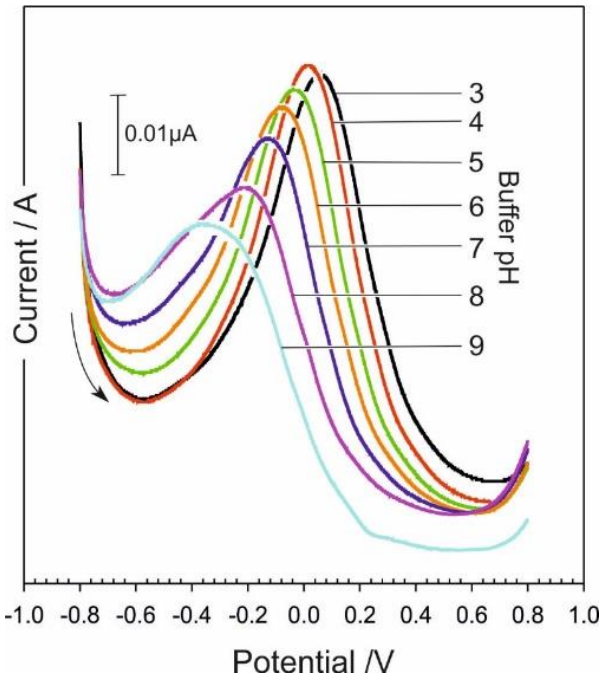

Figure 3.3.2 Square wave voltammograms detailing the response of the anodised carbon fibre probe in buffer solutions of varying pH

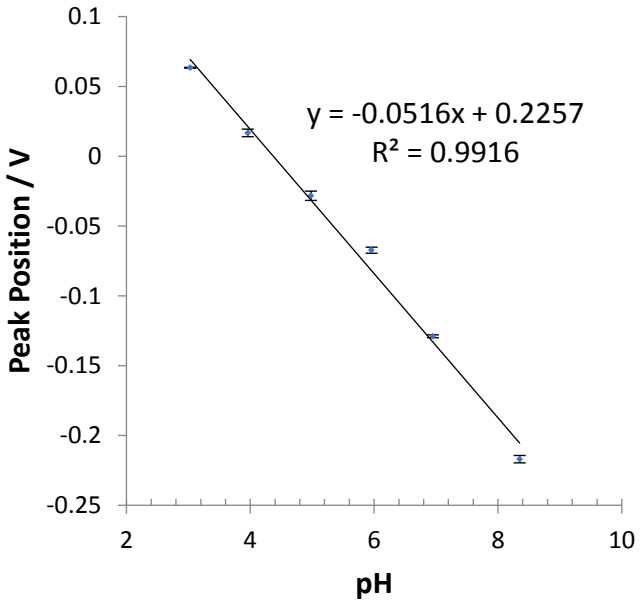

Figure 3.3.3 A plot detailing the linear response found between the peak position and pH

The measurements were recorded three times and the full analysis of the peak position values are recorded in **Table 3.3.1**.

Table 3.3.1 Full analysis of the peak positions obtained during a pH range

	Peak Position / V					
pH	Scan 1	Scan 2	Scan 3	**Mean**	**Standard Deviation**	**Standard Error / mV**
3.03	0.063	0.063	0.064	0.063333	0.0005774	0.0003333
3.96	0.013	0.015	0.022	0.016667	0.0047258	0.0027285
4.98	-0.035	-0.025	-0.025	-0.02833	0.0057735	0.0033333
5.96	-0.069	-0.063	-0.07	-0.06733	0.0037859	0.0021858
6.95	-0.131	-0.128	-0.128	-0.129	0.0017321	0.001
8.35	-0.222	-0.216	-0.213	-0.217	0.0045826	0.0026458

It must be noted that during anodisation, exfoliation of the carbon fibre will produce several structural defects and it has be inferred that this would include a large proportion of oxygen functionalities. The anodisation process is an aggressive, nonspecific weapon and, as a result, it is inevitable that a multitude of quinoid species will occur – each possessing their own unique redox properties. This is displayed in the voltammetric profile detailed in **Figure 3.3.1. B** where it is evident that the broad oxidative peak is liable to comprise of many overlying processes.

3.3.2 XPS Analysis

The influence of the anodisation process on the surface chemistry of the carbon was further investigated using XPS spectroscopy. The spectra obtained for the carbon fibre pre anodisation is comprised of mainly sp^2 carbon as shown in **Figure 3.3.4A**, this can be attributed to the basal nature of the unmodified fibre. Once the carbon fibre has undergone anodisation, there is a marked increase in carbonyl

functionality accounting for 55% of surface carbon moieties. The latter are key elements of the quinone groups (**Figure 3.1.3**) which can be attributed to the observed enhancement in the electrode response highlighted in **Figure 3.3.1B**. There is also an increase in intercalated water which could be expected given the exfoliation of the carbon fibre.

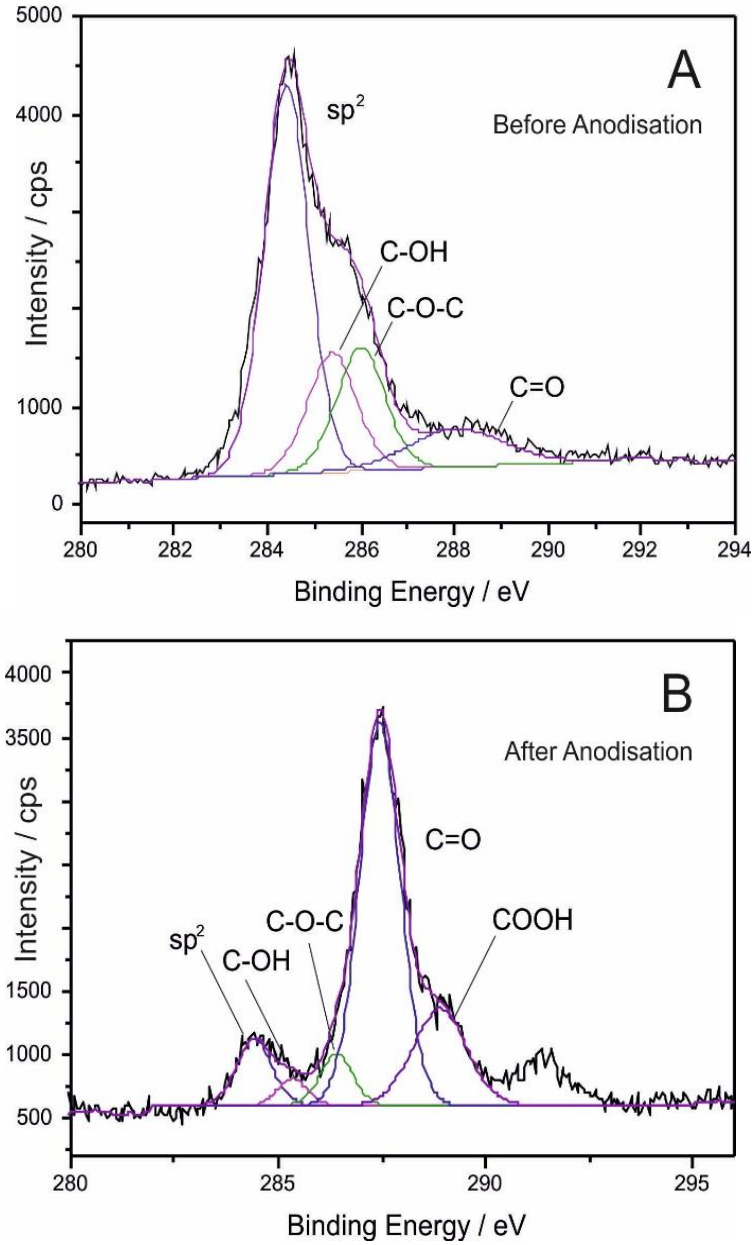

Figure 3.3.4 XPS profiles for the C1s peak obtained from a carbon fibre bundle before (A) and after (B) anodisation

3.3.3 Characterisation of Carbon-Polycarbonate Composite Film

The conductive C-PC film in its unmodified state is a flat, non-porous structure impermeable to the transfer of drug molecules. Laser ablation was therefore used to cut pores within the film as indicated in **Figure 3.3.5**.

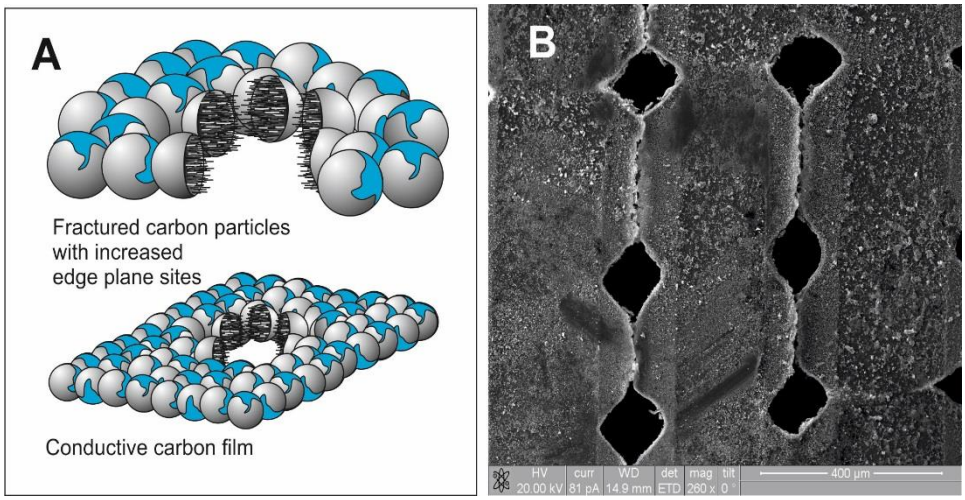

Figure 3.3.5 Pore created on the surface of the conductive film. (A) Result of laser ablation. (B) SEM of pore

The spatial pitch of the pores was 150 µm with an average diameter of 115 µm. It can be seen from the electron micrographs that the pores are not as uniform as anticipated, with a lot of uneven edges. This, however, presents an opportunity for increased surface area of the electrode, from where the pH will be increased. It was also observed that is a small tear in the Y direction, this is attributed to an instrumental artefact and may be due the drag of the laser across the film due to the small distance between each pore. The morphology of the lasered pores should not present any detrimental effects during experimental as the main purpose of the pores are to function as a pathway for drug release.

The electrochemical properties of the C-PC film before and after the various modification steps was assessed through examining the cyclic voltammetric profile of ferrocyanide (2 mM, 0.1 M KCl). Ferrocyanide was selected as a model redox

probe on the basis that it exhibits nearly a reversible electrode reaction without any impediments of proceeding or post chemical reactions. Due to this, ferrocyanide has been chosen as a model redox probe through the years to demonstrate CV.

Cyclic voltammograms detailing the response of an unlasered C-PC electrode to ferrocyanide before and after anodisation are shown in **Figure 3.3.6**. The electrochemical response to C-PC pre anodisation was found to be very poor, where there are no observable oxidation or reduction peaks shown in **Figure 3.3.6A.** The unmodified C-PC contains many basal plane sites where slow electron transfer takes place. In contrast, anodisation (**Figure 3.3.6B**) results in a dramatic change in which the voltammetric profile is characteristic of a microelectrode response.

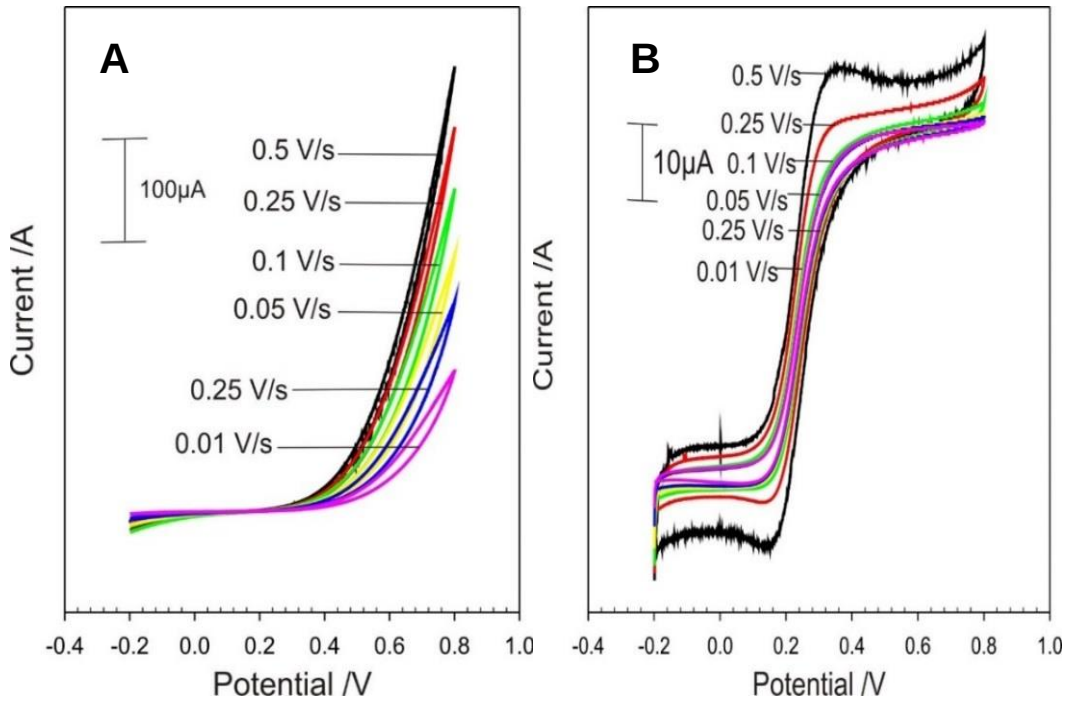

Figure 3.3.6 Cyclic voltammograms presenting the results of the unmodified polycarbonate aluminium electrode towards 2 mM potassium ferrocyanide with variations in scan rate from 10 mV/s to 500 mV/s. Before (A) and after (B) electrochemical anodisation

Similar responses were observed when comparing the lasered C-PC before and after anodisation (**Figure 3.3.7)**. The laser etch does increase the initial (pre anodisation) response to ferrocyanide and this can be attributed to the greater exposures of the encapsulated carbon particles. The response is still far from reversible with a large

overpotential required to elicit any current response. The post anodisation response however is analogous to that recorded with the unlasered C-PC (**Figure 3.3.6B**) where the response is typical of a microelectrode system.

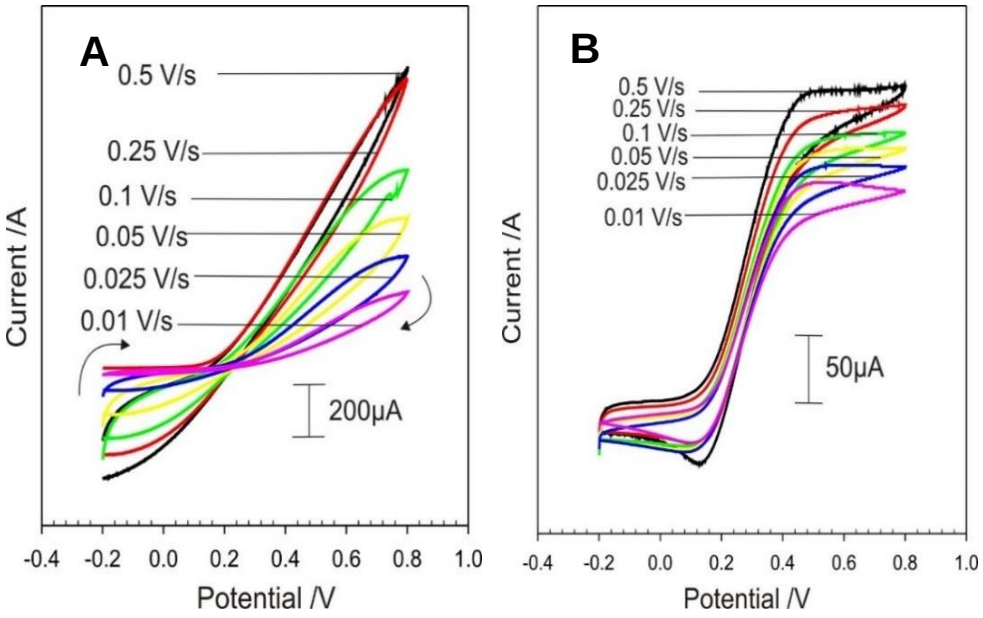

Figure 3.3.7 Cyclic voltammograms presenting the results of the laser modified polycarbonate electrode towards potassium ferrocyanide with variations in scan rate from 10 mV/s to 500 mV/s. Before (A) and after (B) electrochemical anodisation

The anodised electrode responses (irrespective of laser modification) are similar to those expected of a microelectrode system, but as the electrode consists of a 4 x 4 mm square there is clearly a discrepancy. In this case, the electrode consists of particles which are immersed in a sea of polymer, as demonstrated in **Figure 3.3.8**, with only small islands of carbon visible at the surface. Thus, despite a high loading of carbon, the amount of interfacial, and hence electrochemically accessible surface is very limited. This is confirmed when comparing the unanodised responses before and after lasering, where there is a moderate increase in the current as a consequence of more carbon surface being exposed. The microelectrode response can be explained by the occurrence of hemispherical diffusion to the electrode rather than planar diffusion. As the dimensions of the electrode shrink, the diffusion process changes - it becomes much faster and results in a steady state response (sigmoidal shape). Normally, such behaviour is only observed when the electrode dimensions

are at the low micron scale, typically 10 µm in diameter, yet the film substrate being tested is 4mm square. It is also important to note that the current is very large which is to be expected for a large electrode. There is a clear discrepancy in the observed results – the explanation lies in the fact that the film is composed of micron sized particles. Instead of one microelectrode, the film contains a high number of independent micro electrodes, therefore the results present the sigmoidal shape, but also the high current is observed from the cumulative addition of these individual electrodes. The current response is representative of RAM^{TM} electrodes, similar to that observed by Fletcher and Horne (S Fletcher and Horne, 1999). Thus, the interfacial carbon is effectively acting as a random array of microelectrodes (RAM electrode), which were previously introduced in Section 2.5.1.

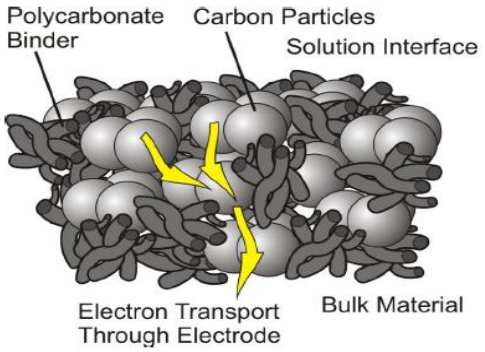

Figure 3.3.8 Schematic of carbon particles within a polycarbonate binder

XPS Analysis of CPC Films

During investigations, the surface composition of the C-PC film was assessed. When we consider the structure of polycarbonate shown in **Figure 3.3.9**, there is very little sp^3, however there are two benzene rings therefore it is expected that there will be a significant sp^2 peak present. It is also important to remember the composition of the film at the interface is largely composed of polycarbonate, with a scattering of carbon (**Figure 3.3.8**). In contrast to the anodisation of the carbon surface, it is unlikely that the electrode process would lead to the destruction of the

polycarbonate backbone and therefore, as polycarbonate is the main component, it is unlikely that there would be much change in the sp^2 peak.

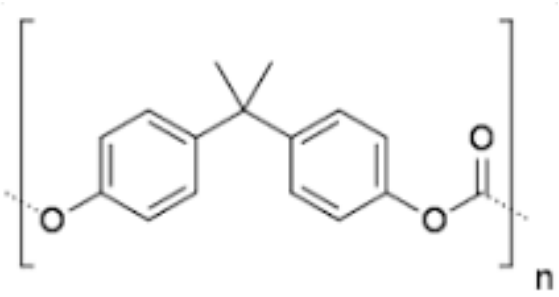

Figure 3.3.9 Structure of polycarbonate

The spectra obtained for the carbon polycarbonate before anodisation (**Figure 3.3.10**) is, as expected comprised of an sp^2 peak attributed to the phenyl ring. Post anodisation, there is an increase in the C=O and COOH groupings – the latter being the more significant as this originates from the exfoliation of the carbon particles.

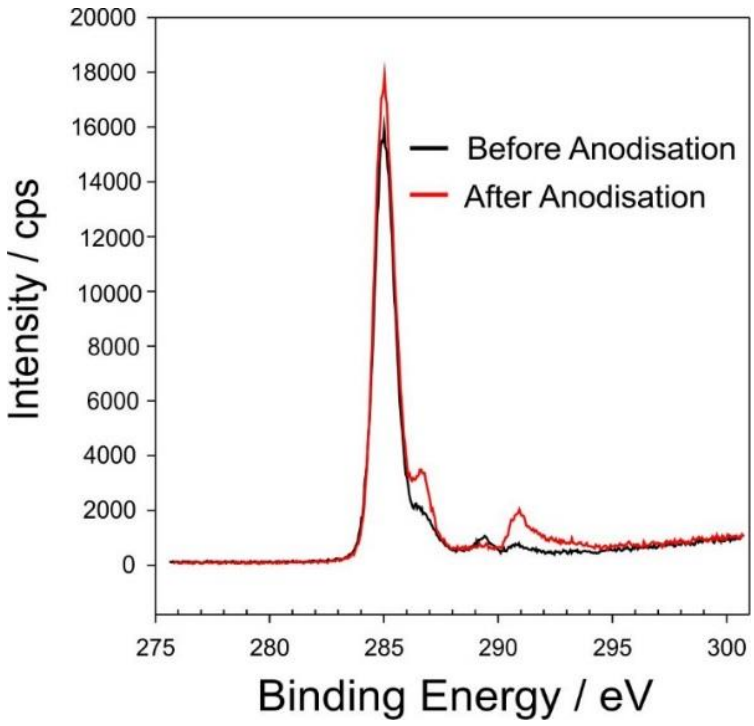

Figure 3.3.10 High resolution spectra for the C1s peak of C-PC

The peak increase at 291 eV is characteristic of carboxylic and carbonate functionality. The formation of these groups is expected after anodisation, with reported literature values of 288.9 eV for carboxylic groups and 290.6 eV to carbonates (Nevskaia and Martin-Aranda, 2003).

3.3.4 Manipulation of Local pH

The next step was to measure the voltammetric behaviour of the carbon fibre probe to assess its suitability for measuring the localised pH. In contrast to earlier investigations employing a single working electrode, this approach required the use of two working electrodes, where the carbon fibre probe was positioned directly above the lasered pores of the carbon-polycarbonate (C-PC) film as demonstrated in **Figure 3.3.11**. A standard Ag|AgCl reference electrode was also used at the same position of the working electrodes. A reservoir was created from the site of the working electrode to a platinum wire, this ensured the level flow of fluid from the working electrode to the counter.

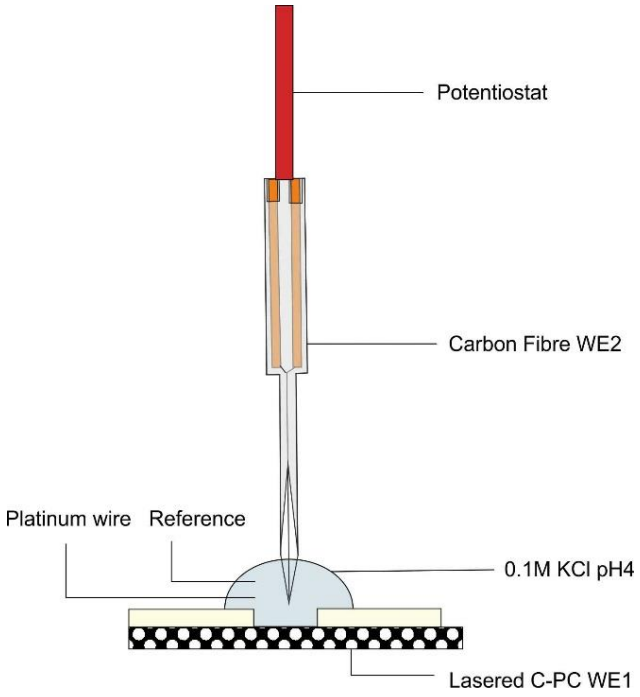

Figure 3.3.11 Microfiber probe arrangement for monitoring changes in pH brought about by electrolysis at the carbon-polycarbonate film

The potential of the C-PC film was held at -2 V for a period of 12 minutes. This had the effect of electrochemically reducing protons within the C-PC pore structures according to Equation 3.1.

$$H^{+}_{(aq)} + e \leftrightarrow \tfrac{1}{2} H_{2\,(g)}$$

…Eq.3.1

The removal of H^{+} from within the pore would have the effect of increasing the pH. The microfibre probe was scanned at 60 s intervals with the resulting scans shown in **Figure 3.3.12**. It can be seen that the oxidation peak associated with the endogenous quinoid moieties is distinct and the peak potential can be assigned without ambiguity.

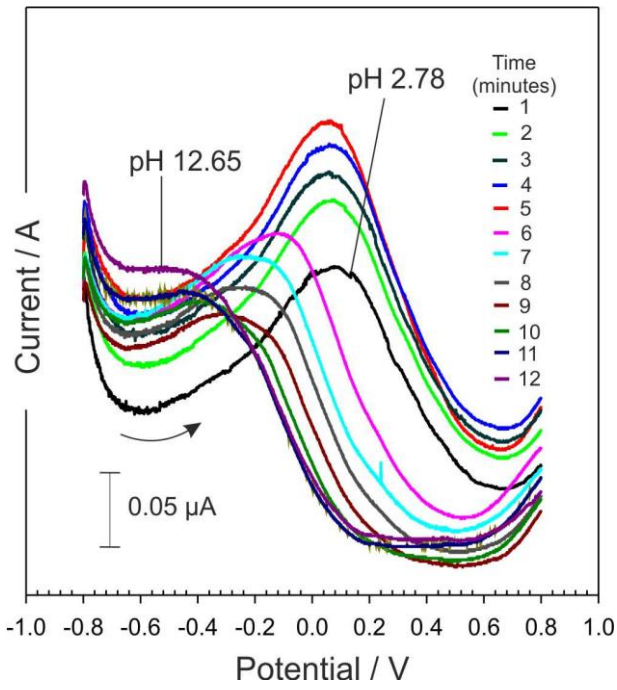

Figure 3.3.12 Voltammograms presenting the response of the probe to change in pH as a result of electrochemically increasing the pH

By recording the position of the quinone oxidation peak, the resulting pH within the micro pore can be determined using the calibration equation (Epa = -0.056 pH + 0.2257) as previously shown in **Figure 3.3.3**. Before the commencement of

electrolysis, the pH within the pore was found to be pH 2.78 and post electrolysis over a conditioning period of 12 minutes the resulting pH was pH 12.65.

The effect of the controlled electrolysis potential applied to the C-PC electrode is shown in **Figure 3.3.13** where by the local pH within the micro pore can be electrochemically controlled over time to produce a steady rise in pH.

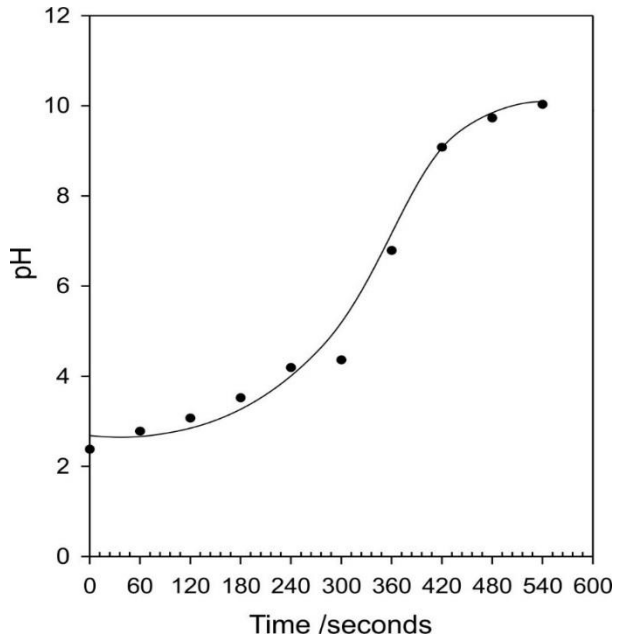

Figure 3.3.13 Influence of film electrolysis time on the local pH recorded by the microfiber probe

3.3.5 Cellulose Acetate Phthalate Dissolution

During the investigations described in the previous section, it was confirmed through voltammetric profiling that it is possible to control and monitor the local pH using the conductive carbon electrode and the carbon fibre micro pH in concert. The next step was to assess the ability of the approach for controlling the dissolution of a cellulose acetate phthalate (CAP) barrier film which protects a model drug film. In this case the CAP film is acting much in the same way as it would be applied to protect oral tablet formulations.

The initial investigations employed sodium nitrite as a model drug and it was selected on the basis of its high solubility in aqueous solution and insolubility in acetonitrile (the solvent used to cast the protective phthalate ester over layer). The preparation and construction of the $NaNO_2$ loaded polycarbonate film is detailed in Section 3.2.4 above. A calibration spectrum for sodium nitrite was generated by analysing a series of 25 µL additions of the $NaNO_2$ stock solution into a 3 mL sample of phloroglucinol and is shown in **Figure 3.3.14**. The resulting absorbance values of each addition where plotted against the concentration of each $NaNO_2$ to produce the calibration graph in **Figure 3.3.15**. The calibration graph was then used to determine the concentration of the $NaNO_2$ released from the loaded polycarbonate film. The determined concentration was then converted to a mass of the $NaNO_2$ released from the film.

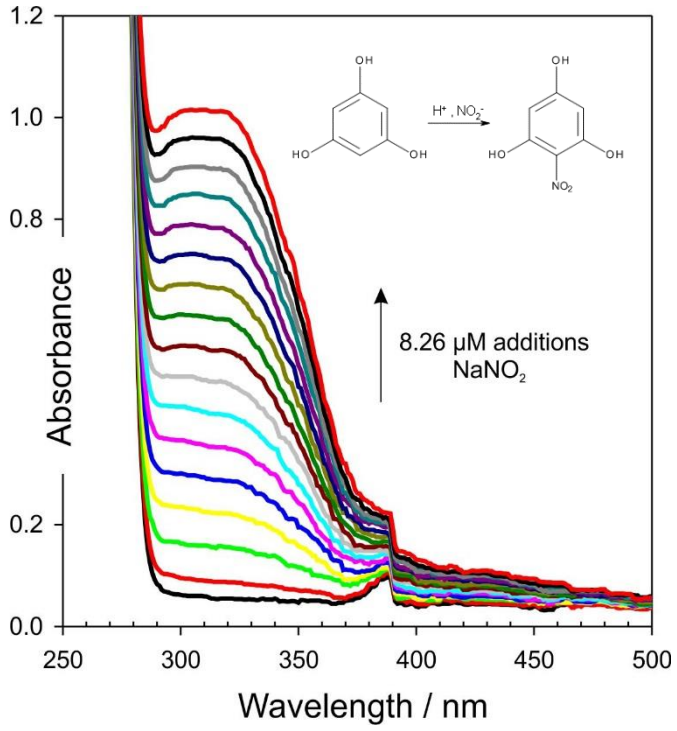

Figure 3.3.14 Spectra of $NaNO_2$ additions to phloroglucinol

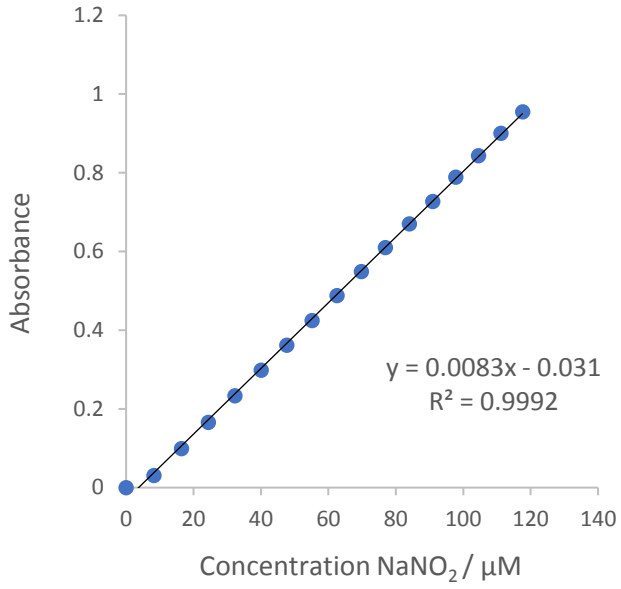

Figure 3.3.15 Calibration graph of $NaNO_2$ additions to phloroglucinol

Before the commencement of electrolysis, the CAP film was tested under the same conditions (-2 V, 20 minutes), as the drug set up to confirm that the hydrolysed CAP itself had no effect on the UV spectrum containing the model drug. The spectra of the reduced CAP results are shown in **Figure 3.3.16**, where there are no ambiguous absorbances associated with CAP in comparison to the pre- electrolysis solution.

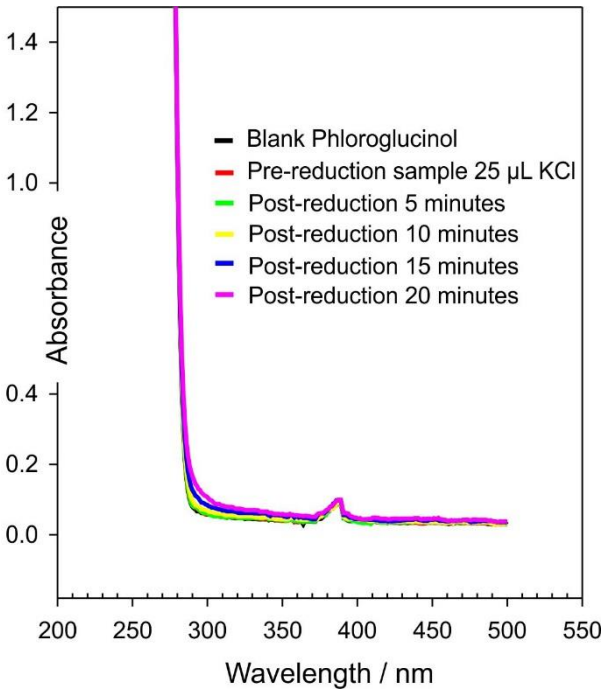

Figure 3.3.16 Reduction of the control CAP film (no $NaNO_2$ present)

Following this, the $NaNO_2$ loaded polycarbonate film acting as the drug reservoir was placed below the protective CAP film and sealed. The lasered carbon-polycarbonate electrode was placed onto the CAP film as shown in **Figure 3.3.17**.

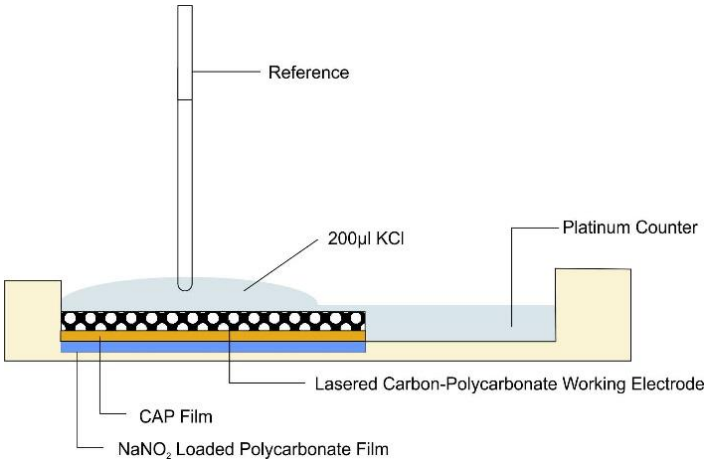

Figure 3.3.17 Electrochemical set up featuring a $NaNO_2$ loaded film below the C-PC working electrode and CAP barrier film

An aliquot of KCl (200 µL, 0.1 M) was deposited onto the conductive polycarbonate electrode, the top layer of the system. A sample of KCl was extracted and placed into the spectrometer in 3 mL of phloroglucinol (10 mM, in pH 3) and a scan was run to confirm that there was no sodium nitrite present at this point. The conductive film was held at -1.5 V, initiating a change in the local pH within the pore. The subsequent dissolution of the CAP film was observed, allowing the surrounding sample of KCl to encounter the $NaNO_2$ loaded film. The solution was then sampled every 5 minutes for nitrite after the commencement of hydrolysis, with the nitrite determined spectroscopically through its reaction with the acidified phloroglucinol. It was found that after commencing electrolysis the nitrite was found to emerge (detected at 319 nm) as indicated in **Figure 3.3.18**.

The inset within **Figure 3.3.18** is the control test where the $NaNO_2$ loaded film was placed in a solution of KCl for two hours and 25 µL additions where sampled from the control solution to demonstrate that the film is stable in aqueous solutions and leeching of the model drug $NaNO_2$ does not occur in solution. A comparison of the

response achieved before and after the commencement of electrolysis is shown in **Figure 3.3.19**.

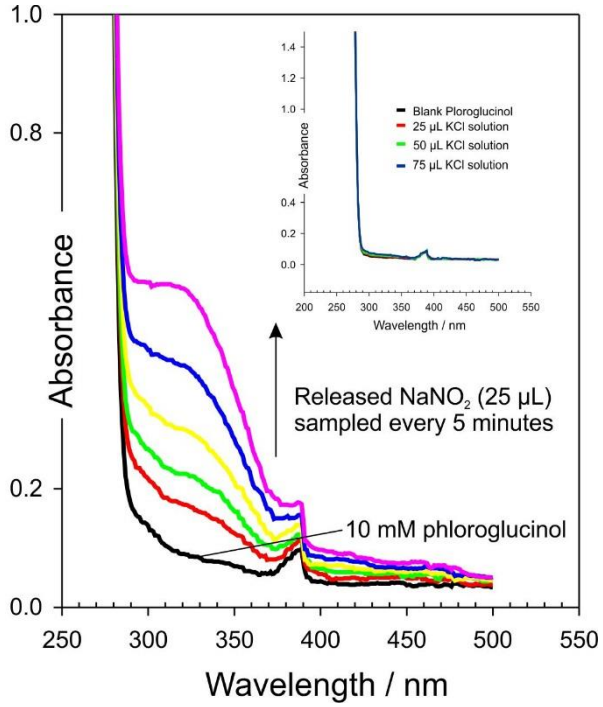

Figure 3.3.18 UV-vis spectra detailing the response of the phloroglucinol towards nitrite – released as a consequence of the electrochemical dissolution of the cellulose phthalate film

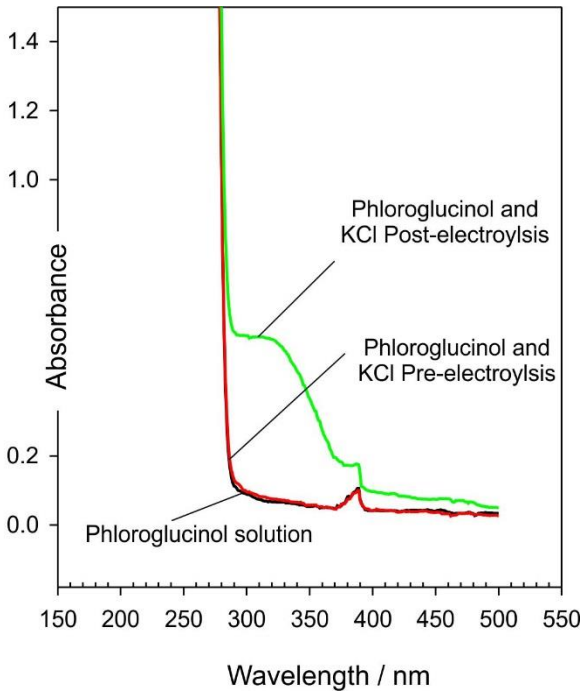

Figure 3.3.19 UV-vis spectra comparing the response before and after the commencement of electrolysis

During electrochemical investigations palladium was also investigated as another ideal candidate for catalysing the reduction of protons and hence electrochemically raising local pH (Zhang *et al.*, 2016a; Cardoso *et al.*, 2017a). Due to this ability, the hydrolysis of the CAP film would be achieved more rapidly owing to the rapid increase in pH leading to the release of more nitrite. This was demonstrated by utilising a similar set up to the C-PC electrode, this time substituting the C-PC for a lasered palladium counterpart and applying a reducing potential. As shown in **Figure 3.3.20**, we can determine that during the same amount of applied electrolysis time, utilising a similar sample removal method as used previously, the reducing potential applied to palladium set up results higher concentrations of release $NaNO_2$.

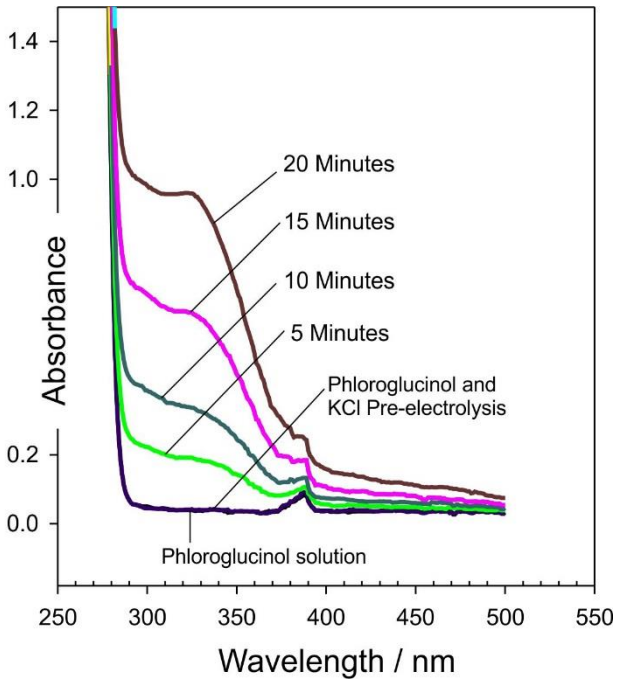

Figure 3.3.20 UV-vis spectra detailing the response of the phloroglucinol towards nitrite – released as a consequence of hydrolysis of the CAP protective film initiated at the palladium working electrode

The merit of using such conductive thin films, lies in the ease from which such thin film can be easily incorporated into systems. The size of the thin films also allows for the facile modification through laser ablation to improve the overall film sensitivity. When used in drug delivery mechanisms as demonstrated above, the pathway to drug release is short and could in principle, be easily incorporated within thin film

transdermal drug delivery systems allowing for the controlled release of therapeutics.

3.3.6 Controlled Release of Dexamethasone From pH Sensitive Film

Dexamethasone, 9α-fluoro-16α-methyl-11β, 17α, 21-trihydroxy-1,4-pregnadiene-3,20-dione, is a synthetic glucocorticoid hydrocortisone which has anti-inflammatory and immunosuppressive properties. The structure of dexamethasone, shown in **Figure 3.3.21**, and has been widely used in clinical applications to treat a variety of conditions such as: rheumatoid arthritis, asthma and ocular diseases (Zilberman, 2005; Saraiya and Goldstein, 2011; Plontke *et al.*, 2014; Kalam, 2016). More notably it is used to suppress an immune response in transplant patients (Wadhwa, Lagenaur and Cui, 2006; Coutinho and Chapman, 2011; Webber *et al.*, 2012). For these reasons, dexamethasone is an ideal candidate for incorporation into transdermal patches as it has the potential to limit skin adverse reactions or irritation that is often associated with puncturing the stratum corneum in order to deliver a drug.

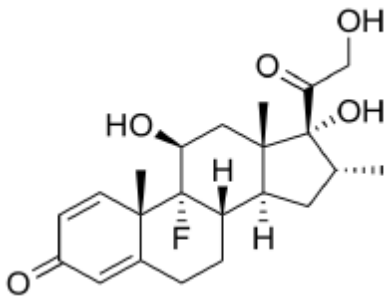

Figure 3.3.21 Structure of dexamethasone

While the approach in Section 3.3.5 utilised a polycarbonate film as an effective drug loaded film, it would be much more effective to control the physical state of the film in a controlled manner to release an entrapped drug, rather than rely on a passive response of releasing the drug from the film as demonstrated by the polycarbonate. Therefore, when hydrolysis is initiated as previously described, the control of the local pH at the site of the drug loaded film could control how much of the drug is released through monitoring the hydrolysis time. Therefore, the next stage was to

transfer the strategy developed with sodium nitrite to the release of dexamethasone. In this scenario, UV-Vis detection was again used to monitor the electrochemically driven release directly from a dexamethasone loaded CAP film, omitting the PC film. A calibration graph was constructed by obtaining the absorbance values from a series of additions of 25-375 µL aliquots from the 1 mM dexamethasone stock solution into a background solution of 0.1M KCl as shown in **Figure 3.3.22**, with accompanying calibration graph **Figure 3.3.23**.

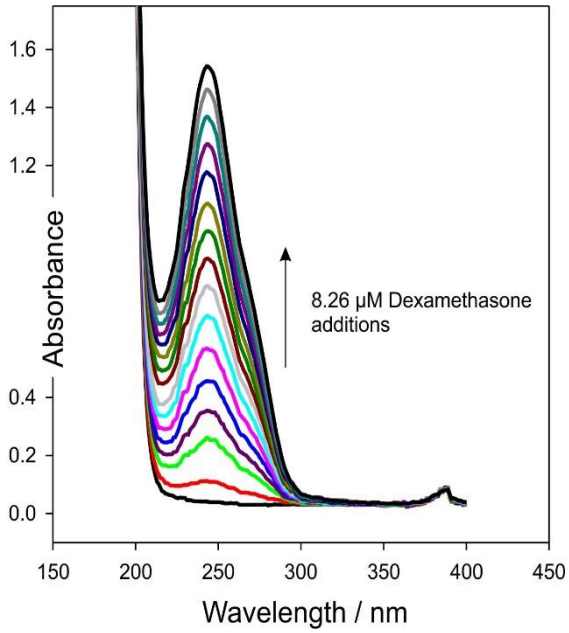

Figure 3.3.22 Calibration spectra of dexamethasone

.

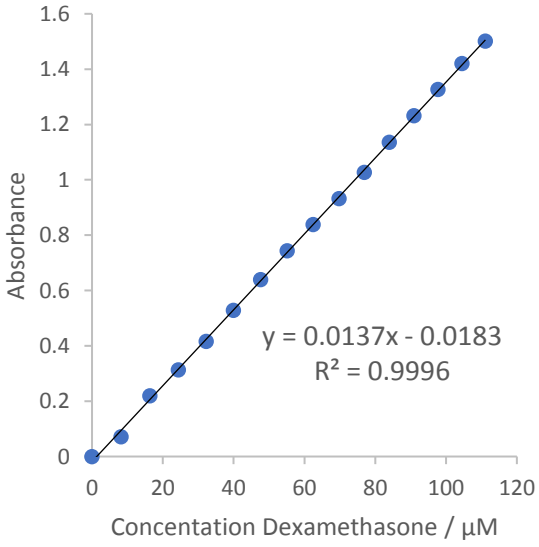

Figure 3.3.23 Calibration graph of stock dexamethasone

The amount of dexamethasone released from the drug loaded CAP film was determined by measuring the absorbance of the dexamethasone into the background solution (0.1 M KCl) and sampling 25 µL of the released solution every 5 minutes into a quartz cell containing a blank solution of 3 mL 0.1 M KCl as shown in **Figure 3.2.24**.

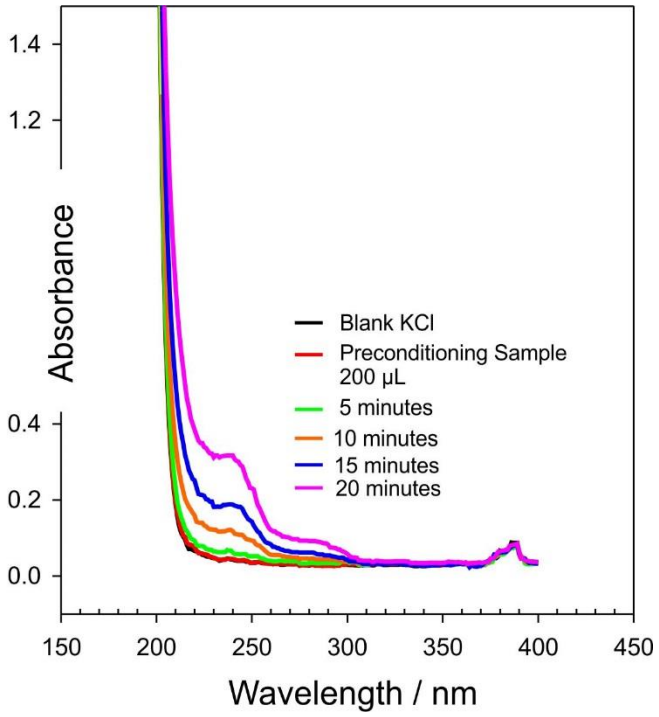

Figure 3.3.24 Release of dexamethasone

3.4 Conclusions

A new approach to pH measurement has been demonstrated and the surface chemistries of several materials characterised. The applicability of the probe was established through measuring variations in the local pH of a novel drug delivery device. The latter permits greater control over the release mechanism and could be used to exploit the more conventional uses of enteric coatings – potentially as transdermal/microneedle patches.

Carbon-polycarbonate films were selected as the base substrate for the electrochemically driven release mechanism. Preliminary investigations sought to control the release of sodium nitrite which had been entrapped within a polycarbonate binder. The use of enteric coatings within conventional drug release is widely established within oral drug formulations and thus the CAP component was chosen to act as a barrier membrane, which served to protect the drug loaded film until the electrochemical trigger was initiated. The application of the electrochemical trigger reduces protons and leads to the removal of H^+ resulting in the increase of local pH. The controlled manipulation of pH within the C-PC pore was shown to lead to the rupture and dissolution of the pH sensitive CAP barrier layer, thereby releasing the sodium nitrite in a controlled but rapid manner, the presence of which was successfully confirmed through spectroscopy.

During electrochemical investigations, palladium was also investigated as another ideal candidate for catalysing the reduction of protons and hence electrochemically raising local pH. From the literature it is known that palladium is commonly used to catalyse hydrogen. This would mean that it would be possible to reach higher pH conditions much quicker. It was postulated that due to this ability, the hydrolysis of the CAP film and subsequent drug release would be achieved much faster than the other conductive component explored. It was determined that conductive polycarbonate film would be used hereon as is proffered a number of advantages over the palladium substrate; including its fairly inexpensive component cost and its ability for successful surface modification (laser ablation and electrochemical anodisation) in order to enhance electrode performance.

The methodology was further developed by encapsulating dexamethasone – a commonly used drug to treat inflammatory diseases, within the CAP layer. This approach was much more effective, as it proffered the opportunity to control the physical state of the film in order to release the entrapped drug. The stability of the film was tested within aqueous solutions and results determined that the CAP binder suitably protected the dexamethasone from leeching into the solution. It was

successfully demonstrated that the application of a suitable reducing potential to the C-PC film, leads to the subsequent swelling and dissolution of the CAP thereby releasing the entrapped dexamethasone.

The main challenges facing drug delivery is device size and response time. Therefore, a device capable of these demands would result in optimal patient outcome. It is imperative to note that providing the device is small the pH will only change at the interface and will not affect the bulk and hence should not cause any irritation or complication to the patient. The response time of the device needs to be improved as part of the development profile, in order to improve response time, the conductive film could be improved by the addition of metals such as platinum or palladium nanoparticles which would catalyse the reduction of protons quicker. The development of the micro pH probe proffers a whole host of advantageous applications, within this project it was used with microtiter plate however it also has the ability to be used *in vivo* in the future.

Chapter 4

Electrochemical Bubble Rip: A New Approach to Controlled Drug Release

Abstract

The controlled dissolution of a cellulose acetate film using electrochemical methods was further investigated. A novel approach employing hydrogen bubble generation has been developed to enable the rapid rupture of barrier film and release of the drug. The ability of the film to be used as a controllable gateway for the release of candidate drugs is critically assessed.

Part of the research described in this chapter has been published in: Anderson, A., McConville, A. & Davis, J., 2015. Electrochemical bubble rip: A new approach to controlled drug release. *Electrochemistry Communications*, 60, pp.88–91.

4.1 Introduction

It was demonstrated in Chapter 3 that the imposition of a negative potential could result in the gradual dissolution of a cellulose acetate phthalate film (CAP) and thereby lead to the release of a therapeutic agent. The rate of dissolution can be relatively slow (depending on applied potential and resulting current) and therefore an alternative strategy was sought to enable rapid release of the drug. Rather than simply relying upon the change of pH at the interface, the next stage was to determine if the hydrogen evolution reaction (HER) could be exploited to yield a mechanical force on the CAP barrier film.

The intention was to fix the film onto a porous carbon fibre (CF) mesh as indicated in **Figure 4.1.1**. The carbon mesh performs a number of functions: it acts as a support for the CAP film, as a gate for a drug reservoir and, as the fibre is conductive, an electrode. The CAP film is impermeable in acidic/neutral pH and thus the drug is effectively entrapped behind the CF mesh. The release methodology was based on employing a suitable reducing potential to the CF electrode, that will initiate the reduction of water, resulting in the production of hydrogen bubbles at the CAP-CF interface.

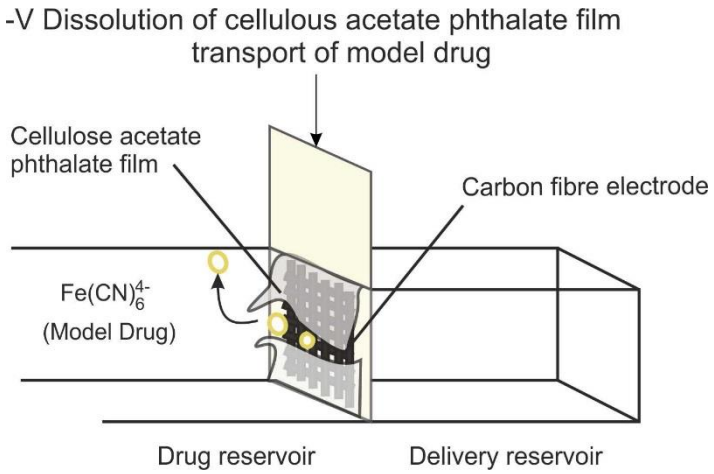

Figure 4.1.1 Schematic of the cell configuration

The reduction of water at electrodes to form hydrogen is well established and the "hydrogen evolution reaction" is a foundation in many electrochemical fuel cells (Lasia, 2010; TONG *et al.*, 2016; Grozovski *et al.*, 2017). In this instance, it was envisaged that the production of gaseous hydrogen and its coalescence into bubbles, would cause sufficient mechanical stress to rupture and dissolve the thin barrier CAP film. Upon fracturing the film, it could be expected that there would diffusion of the drug from the reservoir section of the device through the carbon mesh.

The release strategy is highlighted in the schematic in **Figure 4.1.1** in which ferrocyanide was used as a model drug. The application of the reducing potential will result in an increase in local pH at the working electrode/CAP film interface which will lead to steady dissolution of the film - similar to the solubilisation process that enteric films undergo in their conventional applications. Critically, the solubilisation of the CAP will act in concert with the electrogenerated bubbles, with the dissolution of the film further weakening the mechanical integrity of the film.

The development of electrolytic processes in small scale microdevices has been previously explored and include: dissolution of metallic wrappers (Langer, Santini and Cima, 1999) and the inflation of parylene micro pumps (Gensler, Sheybani, P.-Y. Li, *et al.*, 2012; Uday B. Kompella *et al.*, 2013) but this is the first description of the controlled physical rupture of an impermeable organic seal that could be useful for incorporation within drug delivery devices.

4.2 Experimental Details

4.2.1 Materials

Chemical reagents were of the highest grade available and used without any additional purification. All electrochemical measurements were carried out at 22 ^{o}C ± 2 ^{o}C in Britton Robinson (BR) buffer (pH3-9, adjusted to the appropriate pH value

via the addition of sodium hydroxide). Carbon fibre mat (Toray) was supplied by Goodfellow Research Materials. Methotrexate, (2S)-2-[(4-{[(2,4-Diaminopteridin-6-yl)methyl] (methyl)amino}benzoyl) amino] pentanedioic acid, cellulose acetate phthalate (CAP) and phenolphthalein were obtained from Sigma Aldrich.

4.2.2 Electrochemical Setup

Electrochemical analysis and set up was performed using a μAutolab computer controlled potentiostat (Eco-Chemie, Utrecht, The Netherlands). The initial measurements employed a three electrode configuration comprised of a mat carbon fibre working electrode, a counter electrode in the form of a platinum wire and a standard silver/silver chloride reference electrode. Cyclic voltammetry measurements were recorded at 50 mV/s unless otherwise stated.

4.2.3 Sensor Design and Modification

The carbon fibre mat (Toray) working electrodes (10 μm fibres compressed into a mesh, sheet thickness measured 110 μm and the electrical resistivity through plane is 80 mΩcm^2) were prepared by sandwiching the conductive mesh between polyester laminate sheets that had been pre-patterned to reveal a square window on either side. Circuit connection to the carbon fibre was accomplished though the addition of adhesive copper tape. Cellulose acetate phthalate (Sigma) thin films were prepared by dissolving appropriate number of pellets in acetonitrile solution (10 mg / mL) and solvent cast onto a carbon polyethylene substrate (Goodfellow). These were allowed to dry at ambient conditions until the free-standing CAP film could be carefully removed as shown in **Figure 4.2.1A**.

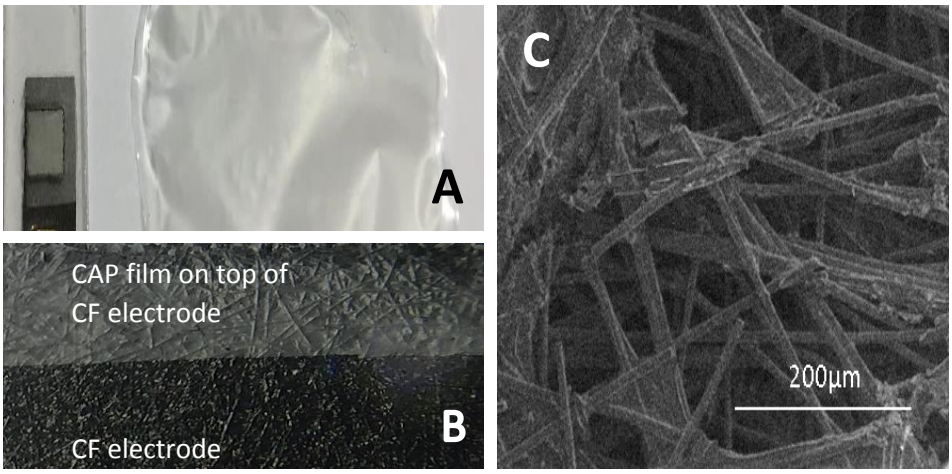

Figure 4.2.1 (A) Mat carbon fibre electrode alongside a free-standing CAP film. (B) Microscope image of CAP after it has been thermally sealed within a CF electrode. (C) Scanning electron micrograph detailing the surface of carbon fibre electrode

The CAP film was carefully removed and placed on top of the unmodified carbon fibre (CF) and both were thermally sealed between polyester laminate sheets. The mat CF/CAP electrode configuration is shown in **Figure 4.2.2**. The basic approach has been described previously (Dutt *et al.*, 2006) but in this instance, rather than have carbon exposed on both sides of the window, the CAP film completely blocks and insulates one side.

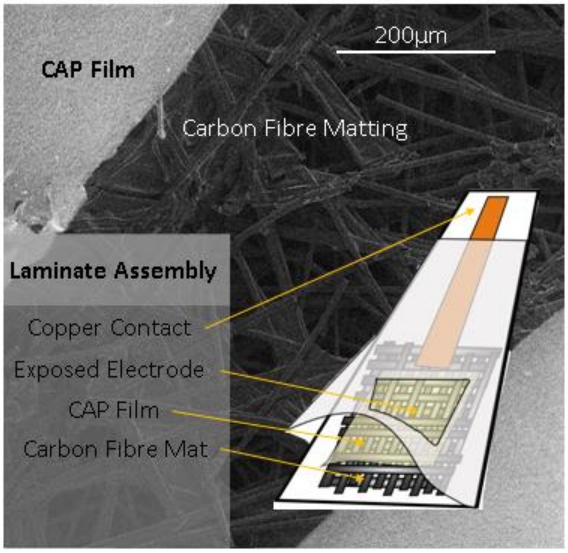

Figure 4.2.2 SEM image and configuration of mat carbon fibre CAP electrode

4.3 Results and Discussion

4.3.1 Characterisation of Carbon Fibre Electrode

In order to evaluate the initial electrochemical performance of the bare carbon fibre, it was necessary to test the CF in the presence of a model redox probe such as ferrocyanide ($Fe(CN)_6^{4-}$), and to benchmark the electrode against a commercial glassy carbon (GC) electrode. A GC electrode is often chosen as a primary substrate in electroanalytical testing, however within this work a GC electrode would be considered too bulky and expensive. Its primary use in this instance is to be employed as a comparison for the evaluation of new electrode materials such as the carbon fibre composite. The response of an unmodified carbon fibre in the presence of 2 mM ferrocyanide is compared against an electrochemically anodised CF electrode and a commercial GC electrode in **Figure 4.3.1**.

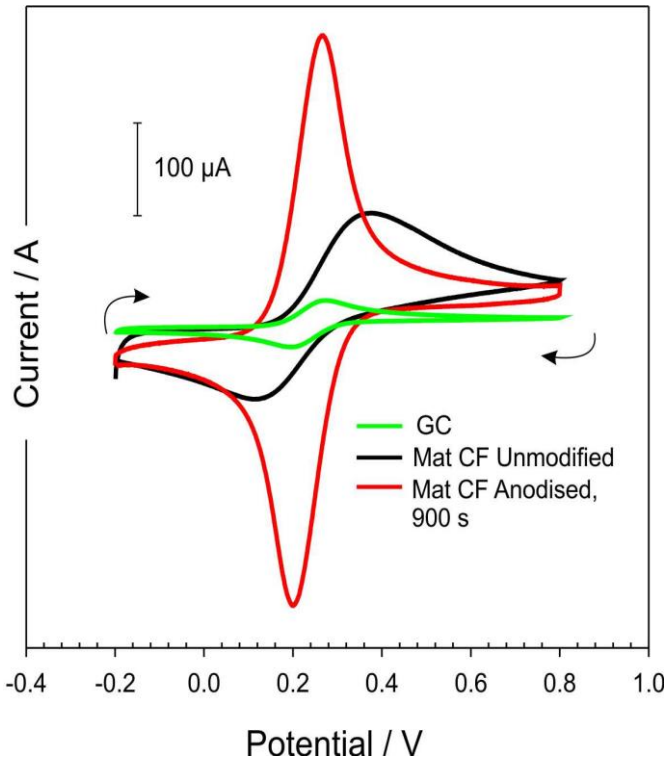

Figure 4.3.1 Cyclic voltammograms comparing the response of a glassy carbon electrode (GC) against carbon fibre electrodes (before and after anodisation) in the presence of ferrocyanide (2 mM, 0.1 M KCl, 50 mV/s)

The response of the GC carbon electrode towards ferrocyanide shows behaviour typical of a reversible system, where there are well defined oxidation and reduction processes with peak separations (ΔEp = 79 mV) close to the 59 mV predicted by Nernst. The peak current ratio is also close to 1 which corroborates the reversibility of the system. In contrast, the unmodified carbon fibre electrode presents broad oxidation (+0.38 V) and reduction (+0.12 V) peaks giving a peak separation of 263 mV and indicating relatively poor electron kinetics. The carbon fibre electrode was electrochemically enhanced by anodising the electrode surface (+2 V, 900 s). Electrochemical modification increases the electrode surface area as it causes exfoliation of the carbon particles and increases the population of edge plane sites, where faster electron transfer can occur (Banks and Compton, 2005). The clarity of the resulting peaks is greatly improved, and the peak current magnitude is greatly increased. The latter can be attributed to the increased surface area arising from the anodisation process. The peak separation is also greatly improved (ΔEp = 65 mV) and is in close agreement with responses from the GC electrode.

4.3.2 Effect of Hydrolysis on CAP Film

The methodology within this chapter relies on the electrochemical initiation of a reducing potential to a CAP modified carbon fibre electrode that has been placed in between two reservoirs, as indicated previously in **Figure 4.1.1**. The CAP side of the electrode acts as an insulating barrier preventing the contact of the detection analyte (2 mM ferrocyanide) with the carbon fibre. The exposed side of the carbon fibre electrode faces to the receiving / delivery reservoir. As the latter contains 0.1 M KCl (adjusted to a lower pH to minimise dissolution of the film) it was anticipated with the CAP barrier in place - there would be effectively no faradaic signal – only the buffer sweep. The application of a reducing potential initiates the production of hydrogen bubbles within the electrode as demonstrated in **Figure 4.3.2.** The consequent removal of protons also causes an increase in local pH within the carbon fibre network. Both events ultimately lead to the disruption of the protective CAP film, allowing the ferrocyanide to travel and then once at the exposed porous CF

electrode, become oxidised to ferrocyanide ($Fe^{(II)}(CN)_6^{4-}$ → $Fe^{(III)}(CN)_6^{3-}$ + e) generating a faradaic signal at the electrode.

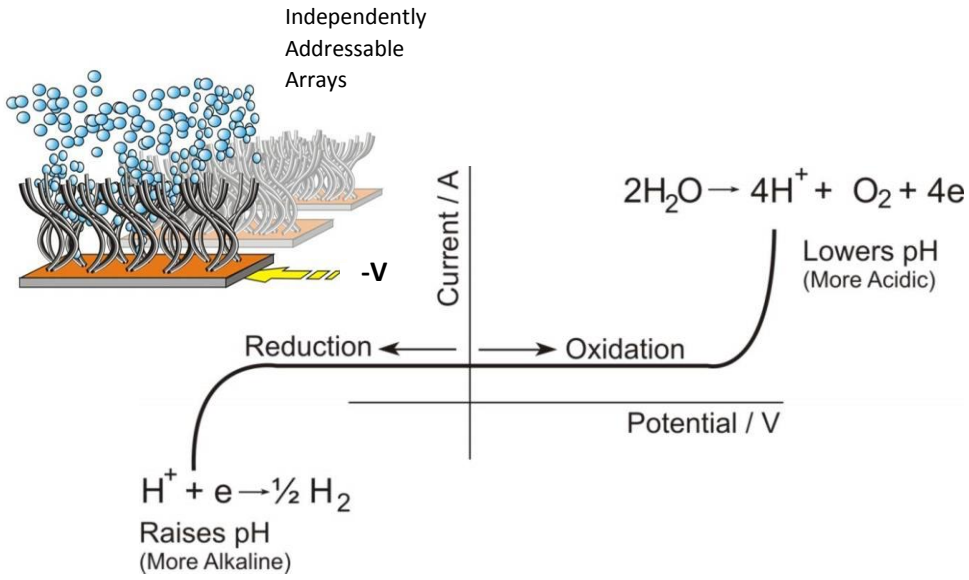

Figure 4.3.2 Mechanism for initiating hydrolysis leading to the evolution of hydrogen bubbles

Both the reference and the counter electrodes were placed in the delivery chamber and completed the electrochemical cell. A cyclic voltammogram was initiated before reduction to confirm that the CAP barrier was intact and there was no leakage of ferrocyanide. This effectively served as the blank response. The carbon fibre electrode was then subjected to a reducing potential -2 V for 30 seconds. As expected, the generation of hydrogen bubbles commenced at the surfaces of the electrode almost immediately. Cyclic voltammograms detailing the response obtained at the carbon fibre electrode after timed intervals - post reduction are shown in **Figure 4.3.3**. The peak responses can be seen to increase with time as, in the absence of the CAP barrier, the ferrocyanide passes through the fibre network and is oxidised to ferrocyanide.

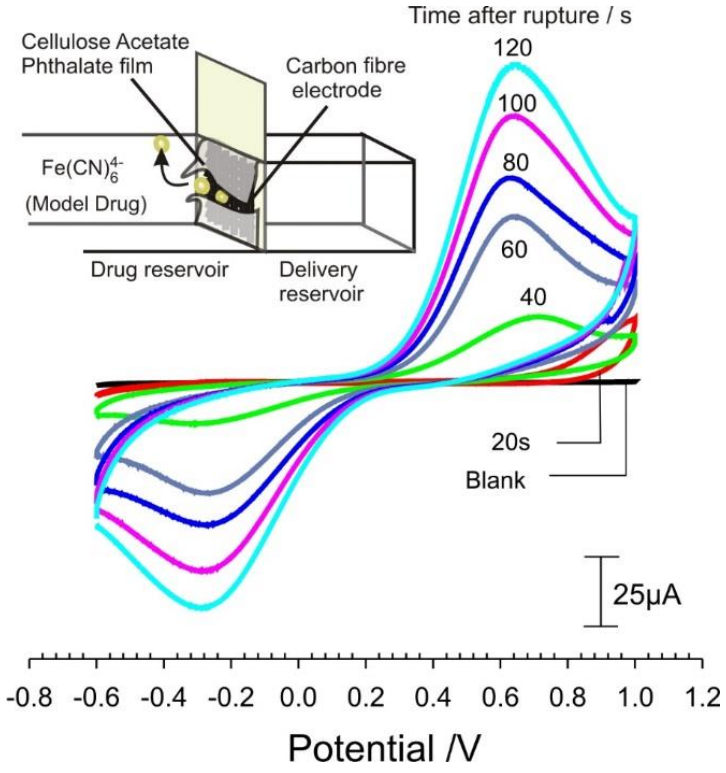

Figure 4.3.3 Cyclic voltammograms detailing the responses recorded at the carbon fibre electrode after electrolysis (−2 V, 30 s) and subsequent rupture of the cellulose acetate phthalate film. Scan rate: 50 mV/s. Inset: schematic of the cell configuration

Confirmation that the film was indeed ruptured by the formation of the bubbles is provided in **Figure 4.3.4**, where video stills capture the effect of electrolysis process pre and post reduction. It can be seen from **Figure 4.3.4B** that a minor tear emerges in the film as the hydrogen bubble emerges from the carbon fibre network.

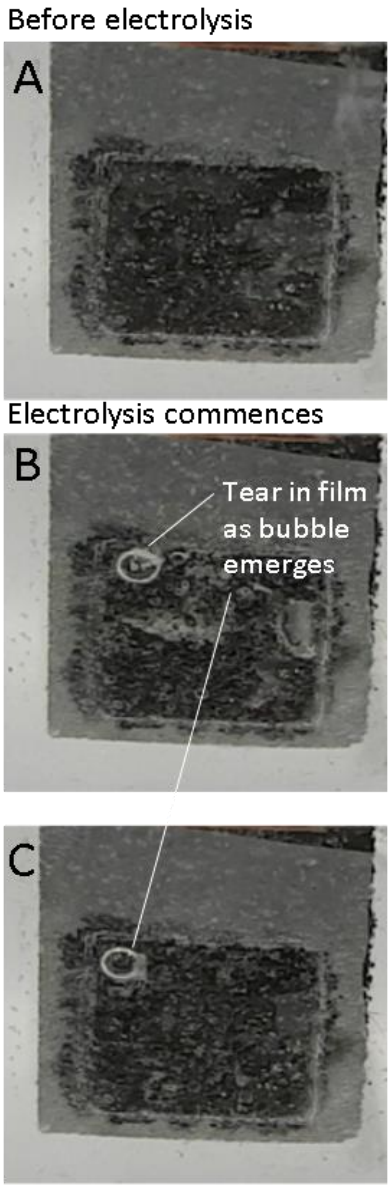

Figure 4.3.4 Pictures of the CAP-CF film before and after commencing the electrolysis

As mentioned previously, the hydrogen evolution reaction will also lead to the increase in the local pH at the carbon fibre interface. The next challenge was to confirm that the latter occurs and to determine the extent to which the pH shifts with the application of a reducing potential.

Assessing Changes in Local pH

The shift in pH at the electrode interface was confirmed through observing the peak position of the quinoid species on the surface of the anodised carbon fibre electrode (Anderson *et al.*, 2014; Lu and Compton, 2014). The carbon surface is populated by a variety of chemical functionality – many of which are electrochemically invisible. Quinoid structures, in contrast, give rise to faradaic processes (**Figure 3.1.3**) which can be observed when conducting voltammetric sweeps. Ordinarily, these species are present at very low concentration, but their population is dramatically increased after anodisation processes and their peak processes can be easily identified (Anderson *et al.*, 2014).

The peak position of these quinone species on the surface of the carbon fibre are pH dependent, this makes them an identifying marker of the local pH. During the present investigation, the carbon fibre was anodised as described previously, and a calibration graph detailing the position of the electrochemically generated quinoid oxidation peak to a range of pH (3-10) is detailed in **Figure 4.3.5.**

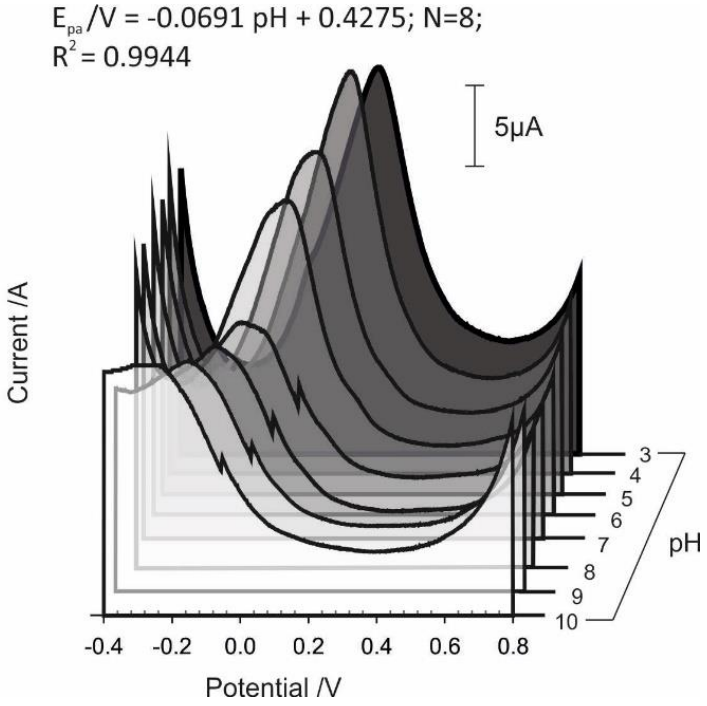

Figure 4.3.5 Square wave voltammograms detailing the response of the anodised carbon fibre probe at various pH regimes

The response was found to be linear (E/V = −0.069 pH + 0.428; N = 8; R^2 = 0.994) although the gradient is larger than Nernstian predictions (Anderson *et al.*, 2014; Lu and Compton, 2014). In order to assess the change in pH within the carbon fibre network during electrolysis, the anodised electrode was scanned in the KCl electrolyte which had been adjusted to pH 3 in accordance with the previous study highlighted in **Figure 4.3.3**. Square wave voltammograms were recorded before and after the imposition of the electrolysis conditioning step (-2 V, 5 s) and are detailed in **Figure 4.3.6.**

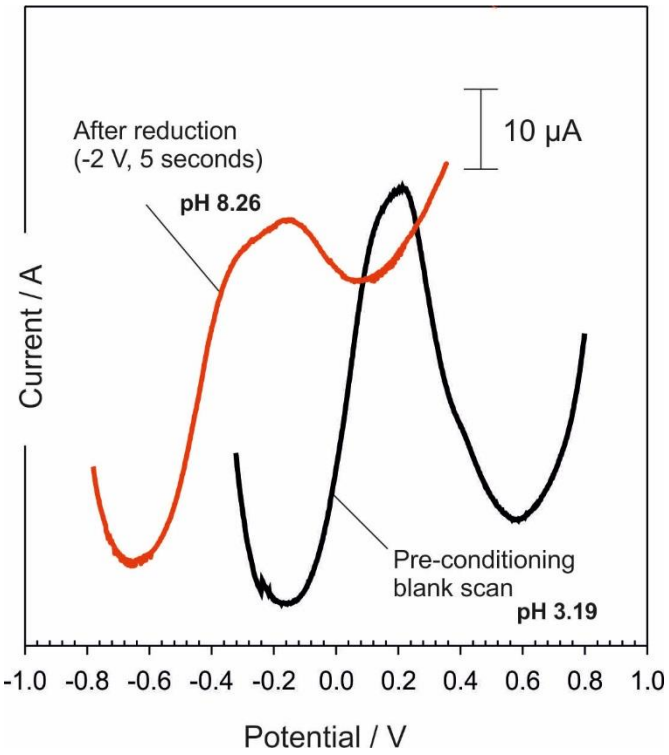

Figure 4.3.6 Square wave voltammograms detailing the influence of local pH on the carbon-quinoid moieties peak position pre and post electrolysis

After the application of the reducing potential (-2 V, 5 s), there is a distinct shift in the peak process towards more negative potentials which, from the results highlighted in **Figure 4.3.5**, are consistent with a change in the local pH to more alkaline conditions. The peak returns to the pre-conditioning position shortly after the electrolysis has finished as the bulk solution dilutes the local concentration of hydroxide and returns the pH to the initial state. From the calibration equation it is possible to determine the pH of the solution directly at the CF interface by using the

calibration equation (**Figure 4.3.5**) and the peak position of the post electrolysis quinone peak (**Figure 4.3.6**). The localised pH was found to have increased from pH 3.19 to pH 8.26 based on holding the electrode at -2 V for 5 s.

The effect of electrolysis was visually investigated through testing the CF electrode in the presence of the pH indicator phenolphthalein. Phenolphthalein is a useful indicator in this study as it remains colourless in acidic conditions, sharply changing colour to pink in alkaline conditions. A reducing potential (-2 V, 60 s) was applied at the CF electrode, where it was envisaged that the onset of a negative potential would increase the local pH environment resulting in a colour change. Although this is not an accurate representation of the true pH change at the electrode, it does however provide a visual indication that the CF electrode does undergoes a change in localised pH. The CF electrode was placed into to a solution of phenolphthalein (1 mM, 0.1 M KCl) along with the reference and counter electrodes. The reducing potential was initiated (-2 V, 60 s) and an image was recorded after every 10 seconds during electrolysis as shown in **Figure 4.3.7**.

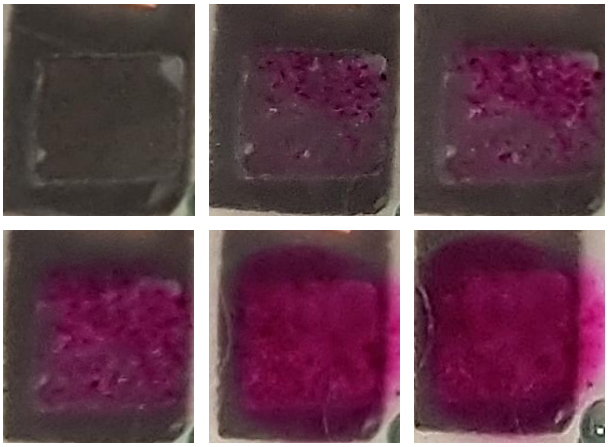

Figure 4.3.7 Mat CF with CAP film under varying times of electrolysis

In addition to this, a screen-printed carbon electrode (SPCE) was used in a similar configuration as described above in order to project a visual change in pH using universal indicator paper. A small section of indicator paper was placed on top of a

SPCE electrode and secured in place. An aliquot of 0.1 M KCl was added, along with the reference electrode and counter wire. A reducing potential (-2 V, 30 s) was initiated at the SPCE, this leads to a colour change within the indicator paper as more basic conditions are achieved - as indicated in **Figure 4.3.8**.

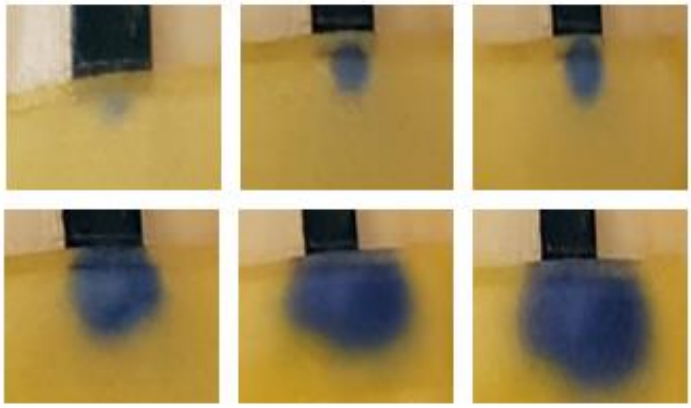

Figure 4.3.8 Application of various electrolysis times to a screen-printed electrode visually monitored with pH indicator paper

It is known that the dissolution of protective CAP films occurs at pH environments of 8 or above and therefore the fact that the pH at the interface of the CF-CAP modified electrode can be manipulated, proffers an alternative approach to controlled release. The electrochemical approach proposed offers two modes of action: rapid release - as a consequence of the mechanical force exerted by the generation of the hydrogen bubbles, and the controlled application of a reducing potential that will lead to more gradual change in local pH and ultimately film dissolution.

4.3.3 Electrochemically Controlled Release of Methotrexate

In order to determine the efficacy of this approach for controlled release systems with an authentic drug, the system utilising ferrocyanide - as described in **Section 4.3.2** , was replaced with methotrexate - a common chemotherapeutic agent (Cipriani *et al.*, 2014; Favalli, Biggioggero and Meroni, 2014). The electrochemical behaviour of the drug is not as distinct as ferrocyanide – it does not exhibit reversible oxidation because of the tertiary amino group. The transport of the drug from

reservoir, through the CF network and into the receiving/delivery reservoir was therefore monitored using UV-Vis spectroscopy. In order to assess the spectral properties of the molecule, a series of additions from a stock solution of methotrexate (1 mM, pH 7 buffer) is shown in **Figure 4.3.9**.

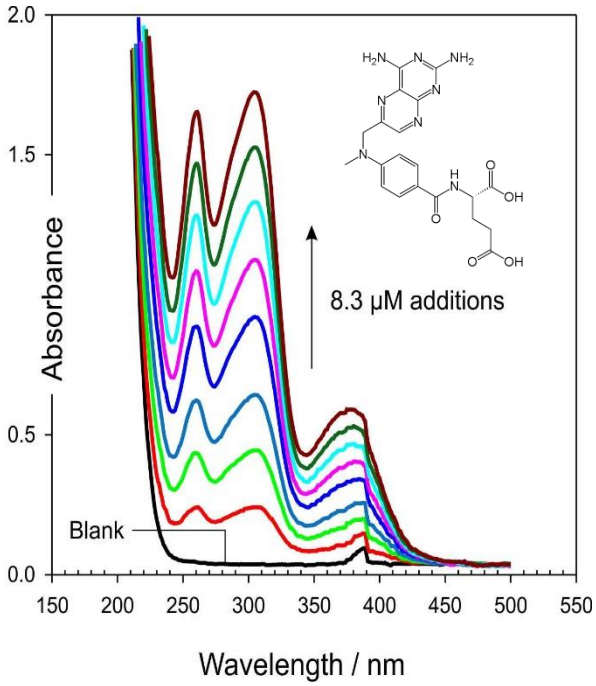

Figure 4.3.9 UV Spectra detailing the additions of methotrexate (2 mM, pH 7 buffer)

A calibration graph detailing influence of concentration on absorbance at 260 nm is shown in **Figure 4.3.10.** The calibration equation was then used to determine the amount of methotrexate that had been displaced from the drug reservoir into the receiving/ delivery reservoir.

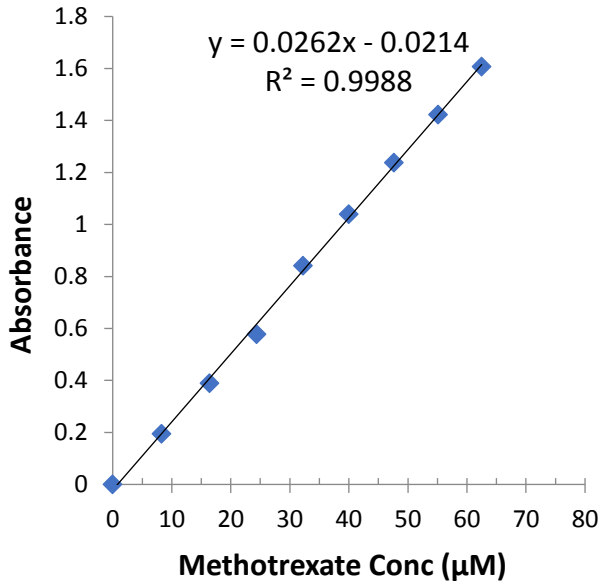

Figure 4.3.10 Relationship observed between peak height and increasing methotrexate concentration (8.3 µM to 62.5 µM, pH 7)

Methotrexate (0.2 mM) was dissolved in pH 7 buffer and placed in the CAP facing drug reservoir) (replacing the ferrocyanide). The delivery reservoir again contained only 0.1 M KCl. Rather than relying on the electrode to detect the transfer of the drug between the reservoirs, samples from the receiving / delivery reservoir were extracted at given time periods. The movement of the methotrexate from the drug reservoir into the delivery reservoir was confirmed by repetitively sampling the delivery reservoir and examining the uv-spectrum. Typical spectra obtained from the investigations are shown in **Figure 4.3.11**. Samples were withdrawn from the delivery reservoir after the initiation of hydrolysis (rupture of the CAP film) every 5 minutes. The spectra show the continued transport of the drug though the carbon fibre gate by diffusion transport.

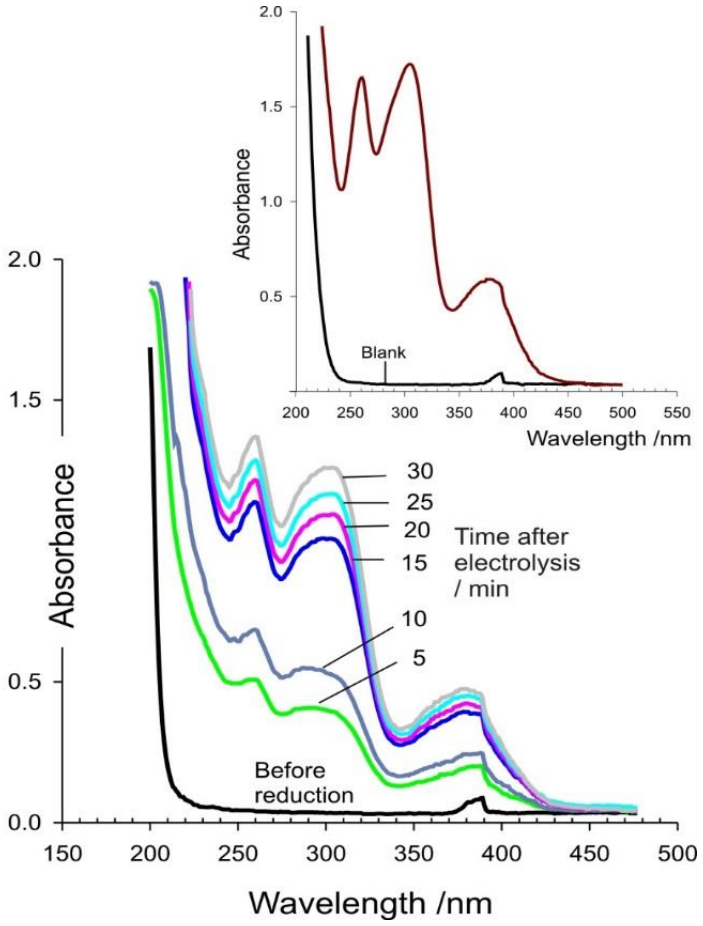

Figure 4.3.11 UV spectra detailing the emergence of methotrexate through the ruptured CAP-CF gate into the delivery chamber. Solution sampled at 5 min intervals following the electrolysis. Inset from calibration additions

The structure of methotrexate is somewhat complex and encompasses several electrochemically active groups and it could be suggested that electrochemical manipulation could lead to the drug being changed and its bioactivity compromised. It must be considered that the electrolysis potential is only applied for a matter of seconds until dissolution or rupture of the film is achieved, therefore, with the exception of the materials directly at the interface, it is unlikely to modify the bulk of the material within the drug reservoir. During hydrolysis, the production and subsequent release of hydrogen - as the bubble rip initiator, must be considered with a small degree of caution, but it must be remembered that the intention is for its application within a microdevice and not at the macro scale. As a result, the amount of hydrogen generated will be very small (assuming 0.18 mm^3 per bubble from visual inspection of the bubble diameter – provides an estimate of some 8 nmol / L) and,

ironically, there have been a number of studies that have demonstrated the beneficial aspects of the gas within physiological systems (Xie *et al.*, 2010; Lekic *et al.*, 2011; Qu *et al.*, 2012) - albeit at low levels. The presence of hydrogen at such levels should not directly impede its consideration.

4.3.4 Modification of Mat CF Electrode Using Iron Oxide Nanoparticles

Nanoparticles designed for biomedical applications have performed favourably in various sensing and diagnostic environments. The use of several metal and metal oxide nanoparticles have been researched, particularly in the fields of regenerative medicine and tissue engineering (Ito and Kamihira, 2011; Khan, Saeed and Khan, 2017; Parveen *et al.*, 2018). The accessibility of magnetic nanoparticles (MNPs) has provided the opportunity to develop conductive composites by utilising much smaller particles than which have been available in the past.

In order to perform favourably within biomedical systems, MNPs should exhibit superparamagnetic properties (SPIONs). SPIONs are small particles containing either a magnetite (Fe_3O_4) or maghemite (γ-Fe_2O_3) core, which have been coated with a biocompatible polymer (Markides, Rotherham and El Haj, 2012). The suitability of iron (Fe) oxide-based MNPs within biological settings is apparent due to their superparamagnetic nature, along with their biocompatibility. The superparamagnetic properties ensure that the nanoparticles will not be attracted to each other and hence the risk of agglomeration in a biological system is reduced. Ferritin is a naturally occurring protein in the human body that stores and release iron in a controlled manner, therefore, nanoparticles containing iron can be considered biocompatible as the body can easily metabolise the particles into its elements, which can be used by the body in subsequent metabolic processes (Markides, Rotherham and El Haj, 2012; Elmas *et al.*, 2018).

The anodised CF electrode was modified through the selective deposition of iron oxide nanoparticles (1 mg/mL, H_2O, Sigma). Iron oxide nanoparticles (0.1 mg) were drop cast onto the surface of an anodised CF electrode and left to dry. The Fe_3O_4 modified electrode was then placed in pH 3 buffer and the resulting square wave voltammogram is compared against an anodised CF electrode in the absence of Fe_3O_4 in **Figure 4.3.12.** The modified electrode contains not only quinoid species native to the carbon fibre but also the addition of the Fe_3O_4 (both Fe^{2+} and Fe^{3+} ions). As the square wave scan commences at the Fe_3O_4 modified electrode, it is possible that as the quinone undergoes oxidation, the iron particles are being reduced leading to a larger and much sharper than the peak recorded for its unmodified counterpart.

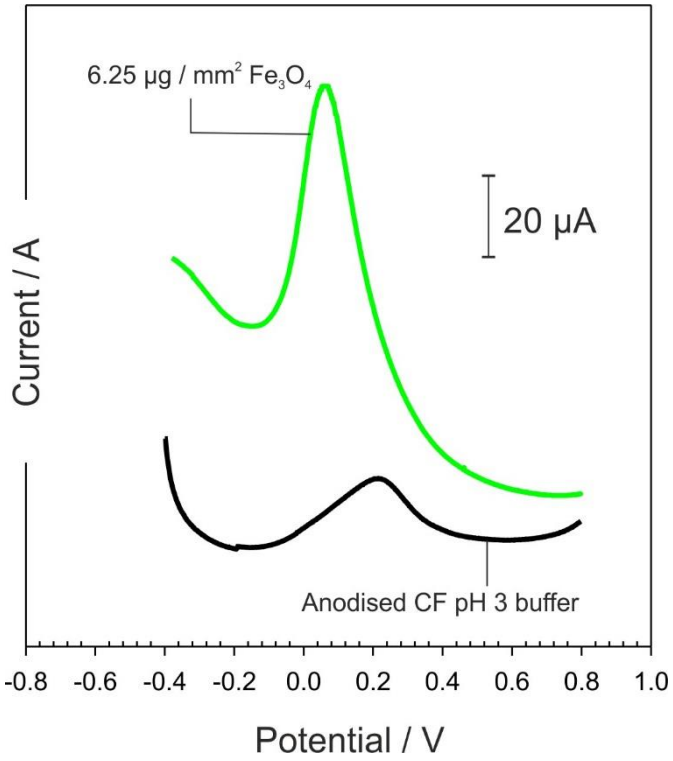

Figure 4.3.12 Anodised CF electrode compared against a Fe_3O_4 modified CF electrode

Incrementing additions (0.02 mg – 0.1 mg) of the Fe_3O_4 were added onto the anodised CF electrode which was investigated in the presence of pH 7 buffer. It was observed in **Figure 4.3.13**, that the peak position in the presence of pH 7 buffer was in the more negative region of the potential window which aligns with previous experimental investigations in **Section 4.3.2.**

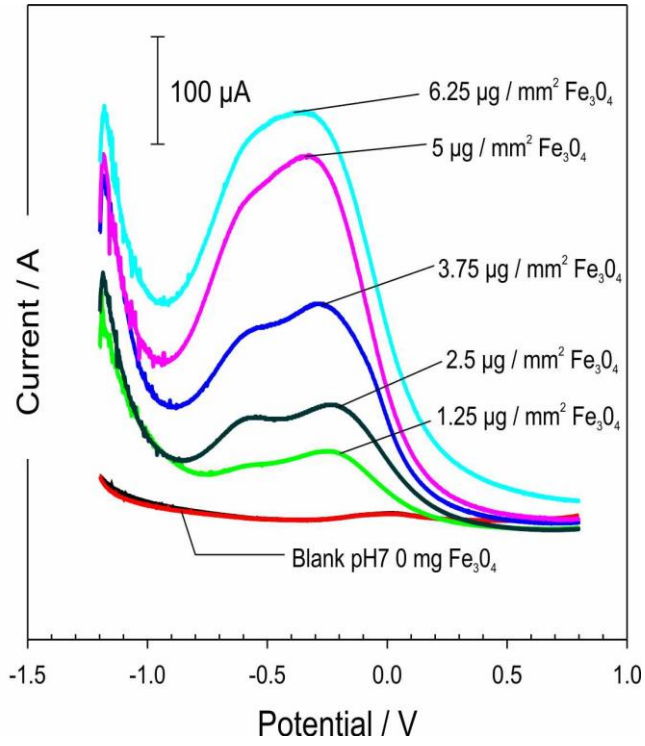

Figure 4.3.13 Square wave voltammograms highlighting the additions of Fe_3O_4 onto modified CF electrode in pH7 buffer

The next step looked at the electrochemical behaviour of the unmodified and Fe_3O_4 modified CF electrodes in the presence of ferrocyanide (2 mM, 0.1 M KCl). The response of the unmodified and Fe_3O_4 modified CF electrodes towards ferrocyanide are shown in **Figure 4.3.14**. Unlike the SWV **(Figure 4.3.12)** which shows a distinct peak, and an increase in electrochemical signal as the additions of Fe_3O_4 are increased, when the Fe_3O_4 modified (0.03 mg) electrodes are tested in ferrocyanide **(Figure 4.3.14)**, the resulting CV is much broader in comparison to the unmodified CF electrode (ΔEp = 220 mV). While the response to ferrocyanide may not be slow, it does not necessarily follow that the response to hydrogen evolution will be likewise.

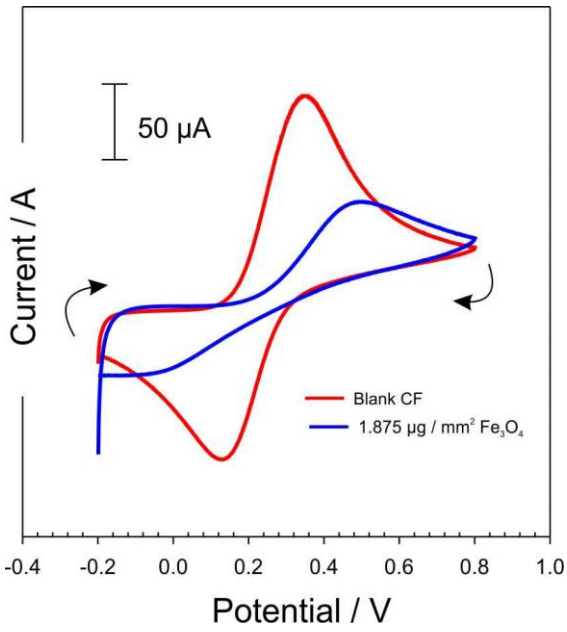

Figure 4.3.14 Cyclic voltammograms comparing the response of the Fe_3O_4 modified electrode to an anodised carbon fibre electrode towards ferrocyanide (2 mM, 0.1 M KCl, 50 mV/s)

Linear sweep voltammograms detailing the response of the modified CF electrodes (anodised CF and IO modified CF (0.1 mg Fe_3O_4)) are shown in **Figure 4.3.15.** The addition of iron oxide nanoparticles onto the CF surface displayed superior HER activity compared to the unmodified CF due to the high dispersity and conductivity of the iron oxide nanoparticles deposited on the surface of the CF.

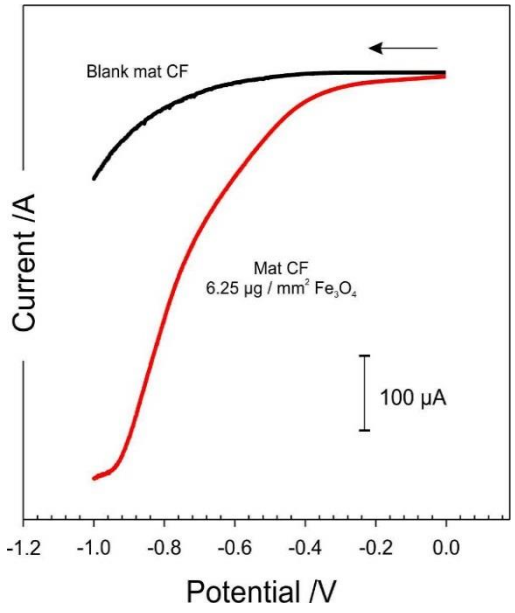

Figure 4.3.15 Linear sweep voltammograms of the unmodified CF and IO modified CF (0.1 M KCl, under nitrogen)

It can be seen that the presence of the Fe_3O_4 particles significantly improves the response to hydrogen reduction and could, in principle, enable the imposition of smaller cathodic potentials to induce more subtler pH changes. The benefit of using the iron oxide is that the system is inherently biocompatible (Markides, Rotherham and El Haj, 2012; Ling and Hyeon, 2013) and could potentially be incorporated into a variety of electrochemically initiated drug release mechanisms.

Graphene Oxide

Graphene research has received a huge amount of attention in the past decade (Nag, Mitra and Mukhopadhyay, 2018). The use of graphene materials - in particular, Graphene Oxide (GO) within electrochemical devices has garnered substantial interest (Ambrosi *et al.*, 2011). Its unique two-dimensional lamellar structure and desirable properties include; high electron conductivity, a fast heterogeneous electron-transfer (HET), a large surface area, and edge reactivity (Zubir *et al.*, 2014; Farooqui, Ahmad and Hamid, 2018). GO is typically formed by the exfoliation of graphite oxide, and possesses a large number of oxygenated functional groups, where, hydroxyl and epoxides reside on the basal plane and carbonyl and carboxyl groups are found at the edges (Zubir *et al.*, 2014).

The addition of GO was employed to assess whether or not its presence would improve the overall performance – both in terms of sensing application but, more importantly, as a means of enhancing the HER process which would be required to initiate an increase in local pH. The optimisation of the unmodified carbon fibre electrodes was further investigated via the deposition of graphene oxide (GO 1 mg / mL H_2O). Additions of the suspended GO solution (0.005 mg – 0.03 mg) were deposited onto the anodised CF and left to dry before their response towards a model redox probe – ferrocyanide, was assessed (**Figure 4.3.16**).

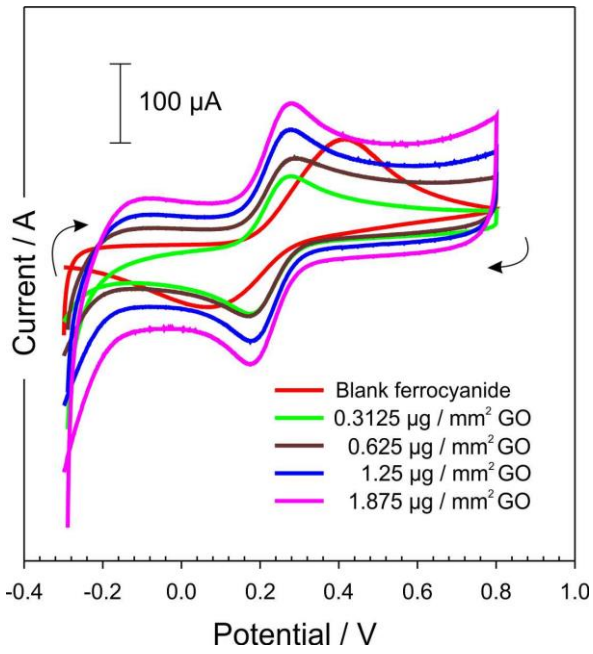

Figure 4.3.16 Cyclic voltammograms detailing the response of the GO modified CF towards ferrocyanide (2 mM, 0.1 M KCl, 50 mV/s)

The additions of GO onto the CF electrode display inherent electrochemistry. By examination of the peak separations in **Table 4.3.1**, it is evident that the electrochemistry of the unmodified CF presents very slow electron transfer of the ferrocyanide couple as shown by the large peak separation values. The values of the GO modified electrodes are much improved with much smaller peak separation values. The better response of the GO modified CF to ferrocyanide can be attributed to the edge plane effects of the GO particles and the structure of GO itself which has quinoid components present (**Figure 4.3.17**)

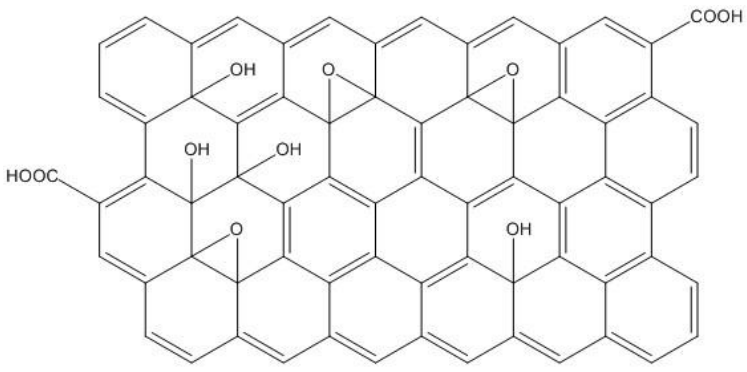

Figure 4.3.17 Structure of graphene oxide

Table 4.3.1 Analysis of peak separation after modification with GO

GO Modifier	Peak Separation
Unmodified CF	353 mV
0.3125 µg /mm^2	101 mV
0.625 µg /mm^2	112 mV
1.25 µg /mm^2	103 mV
1.875 µg /mm^2	105 mV

The influence of the GO on the electrode was found to improve the electrochemical performance as indicated by the improvement in the peak definition and separation. Linear sweep voltammograms detailing the response of the modified CF electrodes (anodised CF, IO modified CF (0.1 mg) and GO modified CF (0.1 mg)) are shown in **Figure 4.3.18**, where it is clear that the addition of both the IO and GO has a dramatic impact on the relative processes.

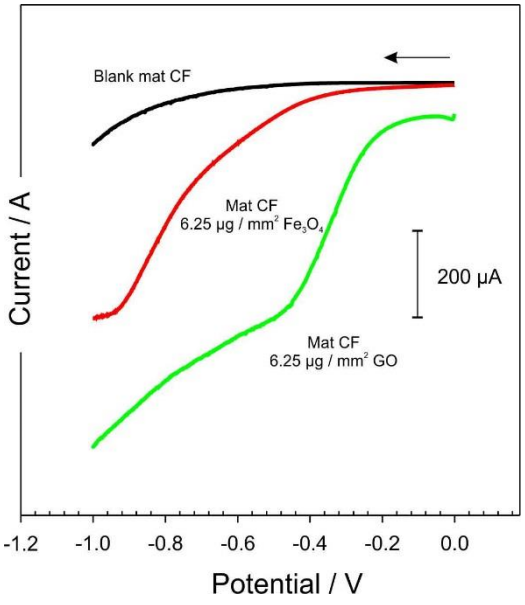

Figure 4.3.18 Linear sweep voltammograms of the unmodified CF and IO and GO modified CF electrodes (0.1 M KCl, under nitrogen)

While the Fe_3O_4 nanoparticles are considered to be the most common and effective biocompatible magnetic nanoparticles for use in biomedical applications – there are still questions over the toxicology of GO. Although the results from the GO modification step demonstrate an improvement in peak separation, there are still questions over the unsatisfactory biocompatibility of GO materials which restricts their use within biological systems (Ambrosi *et al.*, 2011; Guo and Mei, 2014).

4.4 Conclusions

Protective coatings are widely used in conventional drug release systems, but it has been shown in this chapter that electrochemical activation through the imposition of a sufficiently negative potential can induce controlled rupture of a cellulose acetate phthalate film. Electrochemical generation of hydrogen bubbles and the subsequent mechanical strain can enable rapid, on demand, release rather than relying on the gradual solubilisation of the film in solutions of higher pH. It has been demonstrated that potential control of the carbon fibre electrode can not only control the local pH but also enable the dissolution and fracture of protective CAP films. It is possible to exploit this mechanism to selectively control the movement of model drugs from a reservoir to the receiving target. Two approaches have been investigated: electrochemical generation of hydrogen bubbles can enable rapid rupture of the protective film and lower potential dissolution. Proof of concept for the release strategy has been demonstrated using methotrexate as a model drug. Moreover, routes through which the hydrogen evolution reaction could be optimised further were investigated using the immobilisation of iron oxide and graphene oxide nanoparticles. Although preliminary in nature, the results indicate that these systems could be versatile catalysts for further development.

Chapter 5

Controlled Electrochemical Dissolution of pH Sensitive Carbon Composite Electrodes

Abstract

In previous sections, cellulose acetate phthalate (CAP) was employed as a separate film with the electrochemical induced pH dissolution facilitated by electrodes placed near to the film. The methodology proposed herein focuses on integrating the CAP component directly within the electrode substructure – essentially using the former as a pH sensitive binder. The design and fabrication of a novel nanostructured conductive film, based on a composite of carbon nanoparticles and cellulose acetate phthalate (CAP) is presented and its ability to serve as drug releasing actuator is explored.

5.1 Introduction

The work described within the previous chapter exploited a conductive carbon fibre electrode combined with a pH sensitive barrier film applied as a separate layer. The assembly can be complicated due to the need for precise alignment between the carbon fibre, cellulose acetate phthalate (CAP) film and the encapsulating laminate. The next stage was to simplify the process and determine if the CAP component could be directly incorporated within the conductive element. Rather than using carbon fibre filaments - the central design rationale here revolved around using the CAP polymer to bind together nanoparticulate carbon particles to form a conductive sheet. In contrast to conventional carbon films, a novel element was to be introduced whereby the CAP component could be eroded under the imposition of a reducing potential. In this respect it shared similar principles to the approach investigated in Chapter 4. The core methodology relating the film to controlled drug release is highlighted in **Figure 5.1.1**. It was envisaged that the carbon-CAP composite film would retain conductivity and thus the imposition of a suitable cathodic potential would begin to generate hydrogen. The pH would be expected to increase at the film interface and induce the solubilisation of the CAP film. The end result would be the removal of the CAP binder allowing the passage of the drug through the pores left behind.

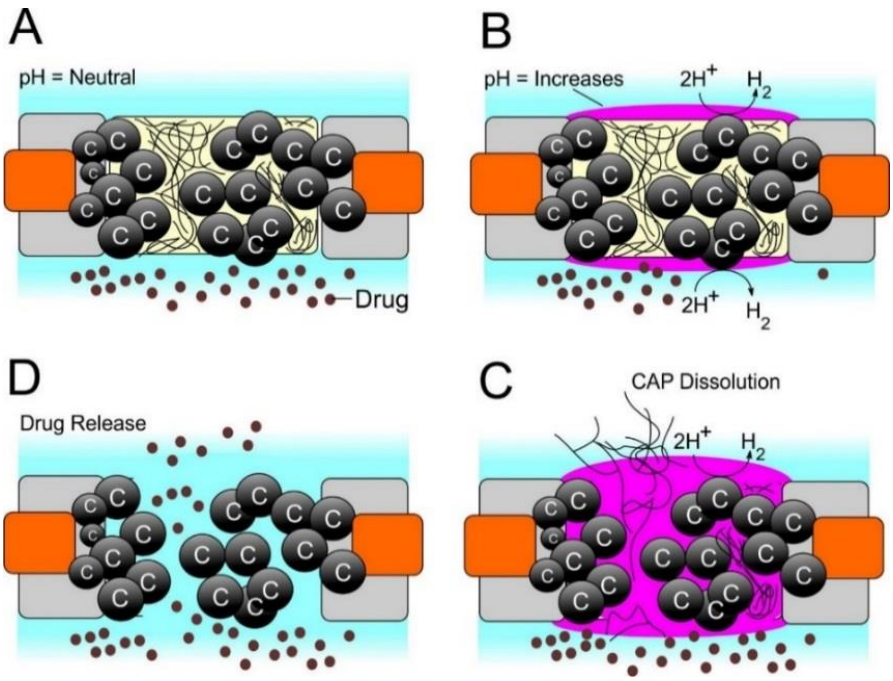

Figure 5.1.1. (A) Stable carbon-CAP film before the commencement of reduction (B) Application of reducing potential leads to hydrogen generation (C) The pH at the interface of the film increases, leading to gradual film solubilisation (D) The removal of the CAP binder results in the transportation of the drug through the film pores

The application of a reducing potential was once again used as the rational towards the development of an electrochemically controllable gate and, in this instance, the system could be considered to be more readily capable of being integrated into micro drug delivery reservoirs.

5.2 Experimental Details

5.2.1 Materials

Chemical reagents were of the highest grade available and used without any additional purification. All electrochemical measurements were carried out at 22 ^{o}C ± 2^{o}C in Britton Robinson (BR) buffer (pH 3-9, adjusted to the appropriate pH value via the addition of sodium hydroxide). Nano carbon powder with a mean particle size of 100 nm and cellulose acetate phthalate (CAP) were obtained from Sigma Aldrich.

5.2.2 Electrochemical Setup

Electrochemical analysis and set up was performed using a µAutolab computer controlled potentiostat (Eco-Chemie, Utrecht, The Netherlands). The initial measurements involved a three electrode configuration comprising of CAP-C composite working electrode, a counter electrode in the form of a platinum wire and a standard silver/silver chloride (3 M NaCl, BAS Technicol UK) reference electrode. Cyclic voltammetry measurements were conducted at 50 mV/s unless otherwise stated.

5.2.3 Sensor Design and Modification

The construction of the carbon loaded films was generally achieved through the simple mixing and dispersion of the carbon nano powder within the CAP (50 / 50 wt %) that had previously been dissolved in a suitable solvent, such as acetonitrile. The composite solution was then cast onto a silicone substrate and allowed to dry. After drying, the films were carefully removed from the substrate and assembled into the electrode configuration. Electrical connections to the carbon composite films were made via the addition of strips of adhesive backed copper shielding tape (100 µm thick) available from RS Electronics, UK. Small sections of the CAP-C film were assembled between sleeves of a resin polyester lamination pouch with a film thickness of 75 µm (Rexel, UK). The laminate sleeves were pre-patterned to reveal a square window on either side and were sealed using a standard office laminator. The final electrode configuration is shown in **Figure 5.2.1**. To improve the conductivity of the composite films for electron microscopy, the CAP-C electrodes were sputtered with a thin layer of Palladium using an 80:20 Pd/Au target at 30 mA for 3 minutes (Emitech K500X Sputter Coater, Quorum Technologies Ltd, England). Iron (II, III) oxide (Fe_3O_4) - which contains a mixture of $Iron^{2+}$ and $Iron^{3+}$ ions and graphene oxide (GO) were employed as chemical modifiers during experiments.

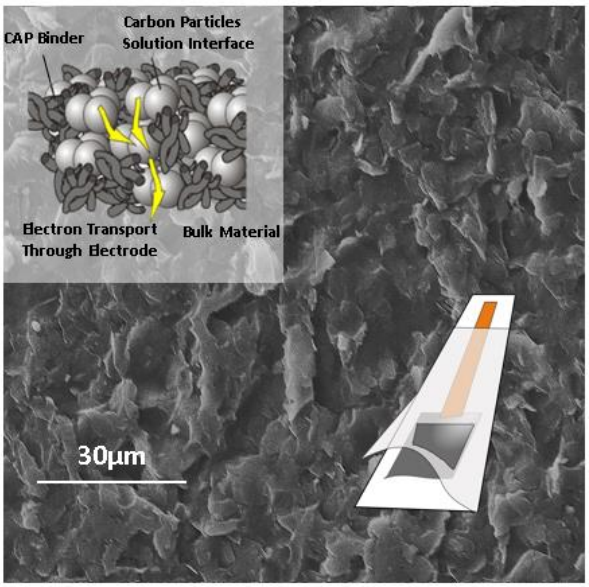

Figure 5.2.1 Schematic of the CAP-C electrode configuration along with electron micrographs of the cellulose acetate phthalate-nano carbon composite microstructure

5.2.4 Biocompatibility Studies

The biocompatibility of the nano carbon-cellulose acetate composite was assessed in relation to skin irritation (DIN EN ISO 10993-10:2014) and cytotoxicity (DIN EN ISO 10993-5:2009) and were conducted by Bioserv Analytik Un Medizinprodukte GMBH (Rostock Germany) under GLP conditions. A summary of the procedure undertaken is described:

Skin irritation assessments were conducted using healthy young female albino rabbits with a weight not less than 2 kg (as per ISO recommendations). The rabbits were kept caged for at least 5 days prior to the test to enable acclimatisation and were immunised against myxomatosis and RHD. The fur on the back of the rabbits was closely clipped on both sides of the spinal column (10 x 15 cm) 4 hours before the test procedure was initiated. The test material (CAP-C) was applied directly to the clipped skin along with gauze patches that served as a control (25 x 25 mm). The sites were then covered with a non-occlusive gauze patch and then wrapped with an occlusive bandage for a period of 4 hours. At the end of the test, the dressings were removed, and any residual substances were washed with warm water and the skin blown dry. The application sites were typically monitored at 1, 24, 48 and 72 hours

after removal of the material and scored in terms of extent of erythema, eschar and edema formation. The results indicated that there was no skin irritation at any point in the course of the 72 hour observation.

Cytotoxicity studies were conducted using 6 cm^2 samples of the CAP-C material. Polypropylene and DMSO were used as the negative and positive control samples respectively. Extracts were prepared in accordance with ISO 10993-12:2012 using Dulbecco's Modification of Eagle Medium with 10% fetal calf serum (DMEM-FCS). The extraction processes were run with gentle shaking for 24 hours at 37^oC. Cell cultures were prepared using L 929 cells (ATCC CCL 1, NCTC clone 929, connective tissue mouse) as per recommendations in 10993-5:2009. Cells were grown in DMEM-FCS at 37^oC and 5% CO_2 in a humidified incubator. Cells were harvested 24 hours before determination of cytotoxicity using a trypsin / EDTA solution and re-suspended in fresh DMEM-FCS. The cell density was adjusted to $1.75x10^5$/ mL. The wells of a tissue culture plate were then inoculated with 1 mL of the cell suspension and incubated for 24 hours - during which the cells formed a subconfluent monolayer. Serial dilutions of the CAP-C extract were prepared to give a concentration range of 100, 66, 44, 30 and 20% using DMEM-FCS as diluent. Each dilution extract was then tested through triplicate pipetting of 1mL aliquots into the respective cell culture wells (after removal of the culture medium). The well plate was then incubated for 24 hours prior to assessment. The cell culture plates were examined microscopically and graded according to their reactivity (0: no growth inhibition/no cell lysis through to 4: almost complete destruction of the cell layers). The cell layers were also quantitatively assessed through staining with 0.25% crystal violet, washed, dried and the cell bound stain extracted with 33% glacial acetic acid. The dissolved stain samples were read by microplate reader at 550 nm. The absorbance for each sample was determined in triplate with the mean value of the negative polypropylene estimated at 100% cell growth. The relative inhibition of cell growth (ICG) was calculated as %ICG= 100-(100 x A_{550} test / A_{550} negative control) whereby, in accordance with ISO 10993-5, an ICG of more than 30% is regarded as a cytotoxic effect. The extract solutions all fell below this threshold and along with the overall assessment indicated that the material did not cause any relevant

toxicological or biological damage to the subconfluent monolayer of L929 cells under the test conditions of DIN EN ISO 10993-5:2009.

5.3 Results and Discussion

5.3.1 Preliminary Characterisation of CAP-C Films

The primary batch of composite electrodes were comprised solely of CAP and carbon nanopowder (CAP-C). The electrochemical performance of the CAP-C electrodes in the presences of ferrocyanide (2 mM, 0.1 M KCl) – a model redox probe, is shown in **Figure 5.3.1 A**. The CAP-C electrode displays very poor electrode kinetics with a poorly defined oxidation peak. No reduction peak was observed on the reverse scan. This is in contrast to the responses observed with a Glassy Carbon electrode and the carbon fibre systems detailed previously in **Figure 4.3.1**. The response of the CAP-C film was then tested in Ruthenium hexamine ($Ru(NH_3)_6^{2+/3+}$ (2 mM, 0.1 M KCl) under nitrogen (**Figure 5.3.1 B**). There is a marked improvement in electrochemical response towards the ruthenium hexamine in comparison to the ferrocyanide. The disparity can be attributed to the difference in the nature of the compounds and their interaction with the carbon surface. The ferrocyanide probe is a classic negatively charged inner sphere complex whereas the ruthenium hails from a positive charged outer sphere system (Brownson *et al.*, 2011) and it could be that electron transfer is preferentially faster at the latter.

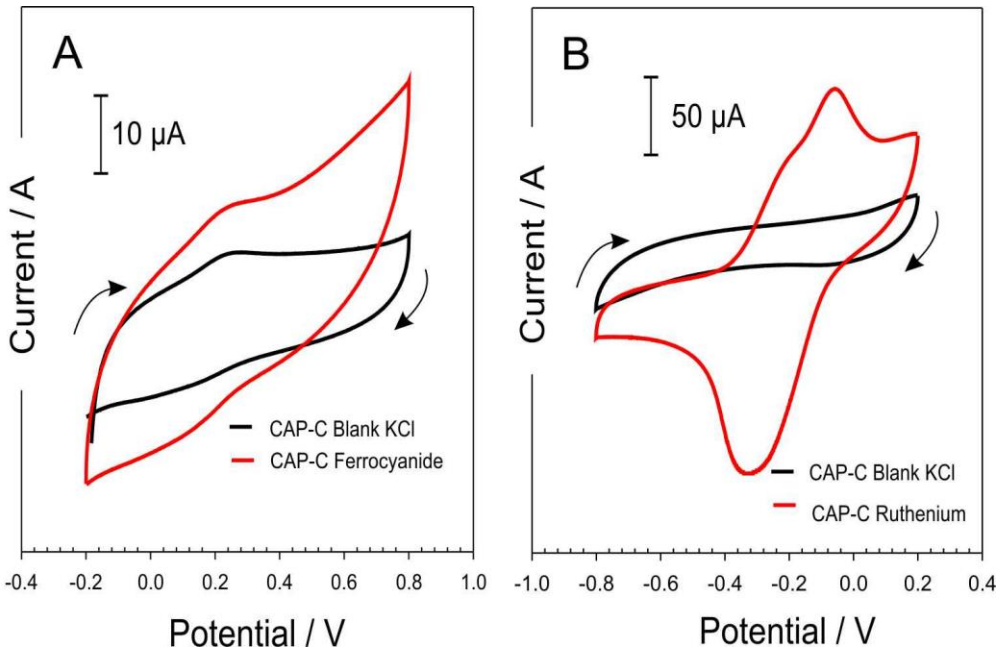

Figure 5.3.1 Cyclic voltammograms detailing the response of the cellulose acetate phthalate-nano carbon films towards ferrocyanide (A) and ruthenium hexamine (B). Each redox probe present at 2 mM in 0.1 M KCl. Scan rate: 50 mV/s

It is clear from the voltammograms highlighted in **Figure 5.3.1** that the background current is very large and can, at least in part, be attributed to uncompensated resistance within the film and the capacitive background associated with the surface area arising from the nanoparticle interface. The is due to the composite nature of the film, in which the carbon content has to be reduced in order to have sufficient polymeric binder that the film integrity is not compromised. Going beyond the 50:50 ratio of carbon : CAP has the effect of either increasing resistance (too much binder) or the film becomes too powdery (too much carbon).

While in previous chapters it was possible to improve the electroanalytical response to ferrocyanide through anodisation of the carbon surface and thereby increasing the edge plane/quinoid functional group population, the same option is not possible in this case. Electrochemical anodisation is not appropriate as due to the pH sensitive nature of the CAP binder. The highly alkaline anodisation solution (0.1 M NaOH) would immediately compromise the structure of the CAP-C films resulting in immediate dissolution and destruction of the film.

5.3.2 Controlled Electrochemical Dissolution of CAP-C Electrodes

Exploitation of the pH sensitivity of the polymer for use in electrochemically controlled drug release has been described previously in Chapter 4, but in the context of its use as a film encapsulating a drug loaded reservoir with a distinct/separate conductive element. The stability of the CAP-C composite film was first assessed in the presence of ruthenium hexamine (2 mM, 0.1 M KCl) and is shown in **Figure 5.3.2**. The addition of 150 µL of 0.1 M NaOH to the ruthenium hexamine solution yield a pH of 11.55 and it was envisaged that as the bulk pH was dramatically increased, dissolution of the CAP-C electrode begins. This would ultimately decrease the electrochemical signal of the ruthenium hexamine.

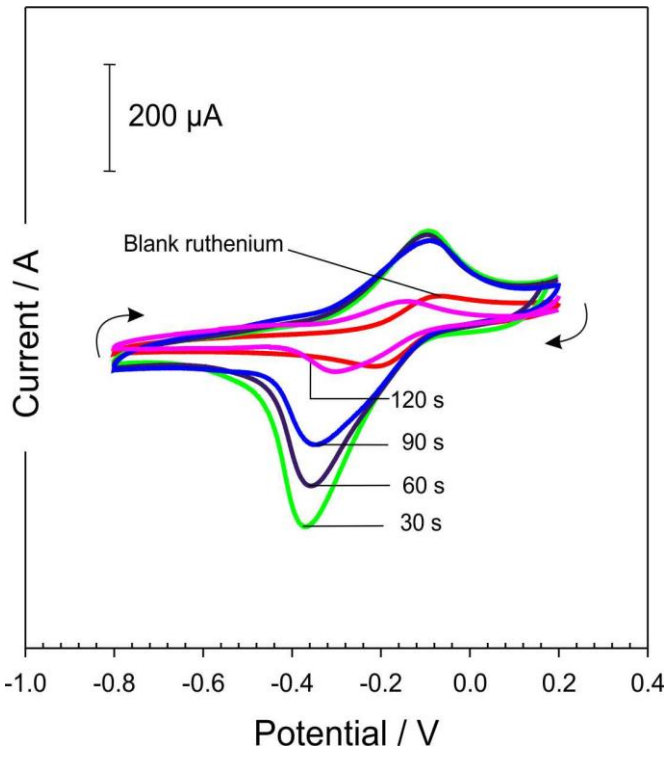

Figure 5.3.2 Response of the CAP-C electrode towards 2 mM ruthenium before and after pH adjustment using NaOH. Scan rate: 50 mV/s

It was observed that soon after change the pH of the bulk ruthenium (30 s) that the signal becomes much more amplified (green scan) compared to the scan that was initiated before the addition of NaOH. An explanation for the increase in electrochemical signal can be that when the NaOH is initially added to the solution,

it leads to the dissolution of the surface CAP thereby exposing more of the carbon resulting in a greater signal. After the time intervals, it was observed that this initial spike in signal then begins to decrease as more and more of the CAP is dissolved and the carbon is also lost when the electrode begins to disintegrate. To prove that this result was indeed a result of the dissolution of the CAP-C and not a consequence of the pH changes to the ruthenium, a commercial glassy carbon electrode was exposed to the same conditions as shown in **Figure 5.3.3**.

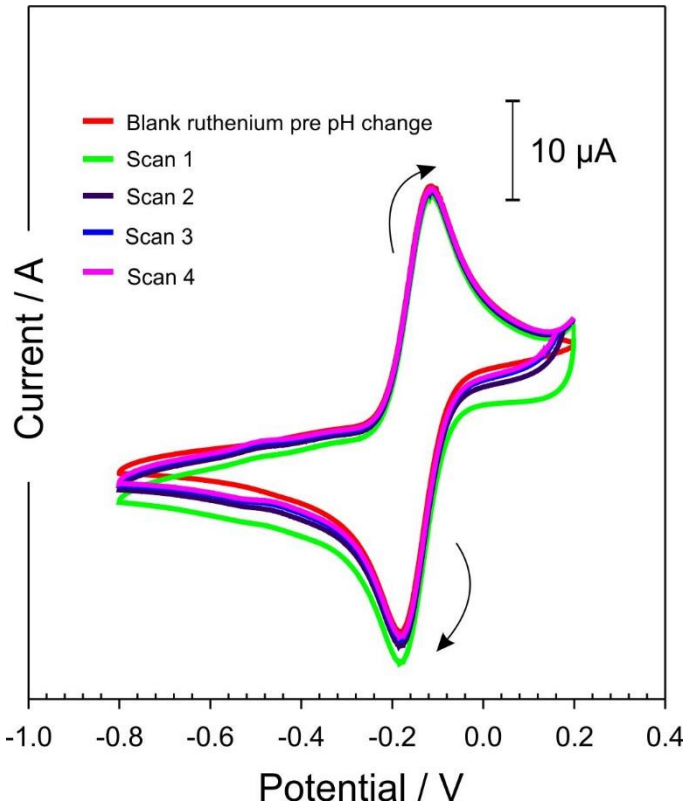

Figure 5.3.3 Response of the GC electrode towards 2 mM ruthenium before and after pH adjustment to pH 11.55 using NaOH. Scan rate: 50 mV/s

The glassy carbon response remains constant; therefore, it was concluded that the response of the CAP-C was not just simply a case of a pH effect of the solution on the ruthenium hexamine, rather a response to the presence of lots of hydroxyl ions dissolving the CAP binder – and therein compromising the structural integrity of the film as indicated in **Figure 5.1.1**. Visual confirmation that electrochemical control of the potential (-2 V, 30 s) and hence the local pH can induce the dissolution and

subsequent failure of the film is highlighted in **Figure 5.3.4)**. It could be anticipated that were drugs to be entrapped within the network at the time of formulation, then the electrochemically induced swelling could allow control over their release.

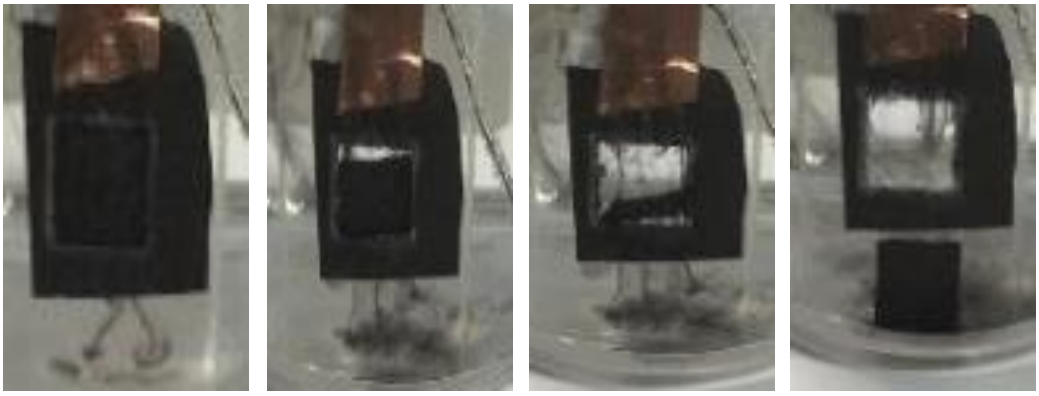

Figure 5.3.4 Dissolution of the CAP-C film before and after the initiation of electrolysis

The next step was to assess the ability to control the swelling or dissolution of the CAP-C film in the presence of ruthenium hexamine. The CAP-C electrodes where assembled into the laminate assembly, where a filter paper sleeve was placed on either side of the CAP-C film and thermally sealed within the electrode. The incorporation of the filter paper into the system was used to ensure that residual particles of carbon and CAP were entrapped after the application of the reducing potential yet allowing redox transitions of the ruthenium hexamine to be detected through the porous membrane. Voltammograms were recorded before the application of a cathodic potential to serve as a control. Again, it was envisaged that the imposition of a cathodic potential would increase the pH and lead to the swelling or dissolution of the CAP binder within the core of the film, as such, the surface area of the electrode would change. The latter could therefore be assessed through changes in the peak magnitude of the ruthenium hexamine. Thus, the ruthenium hexamine voltammograms were recorded before and after each cathodic step. Cyclic voltammograms detailing the response of the CAP-C filter paper electrodes to ruthenium hexamine (2 mM, 0.1 M KCl) before and after the imposition of a potential of -2 V are detailed in **Figure 5.3.5**. Before the cathodic potential is applied, the

voltammetric response of the CAP-C film to ferrocyanide is consistent with that observed in **Figure 5.3.1B**.

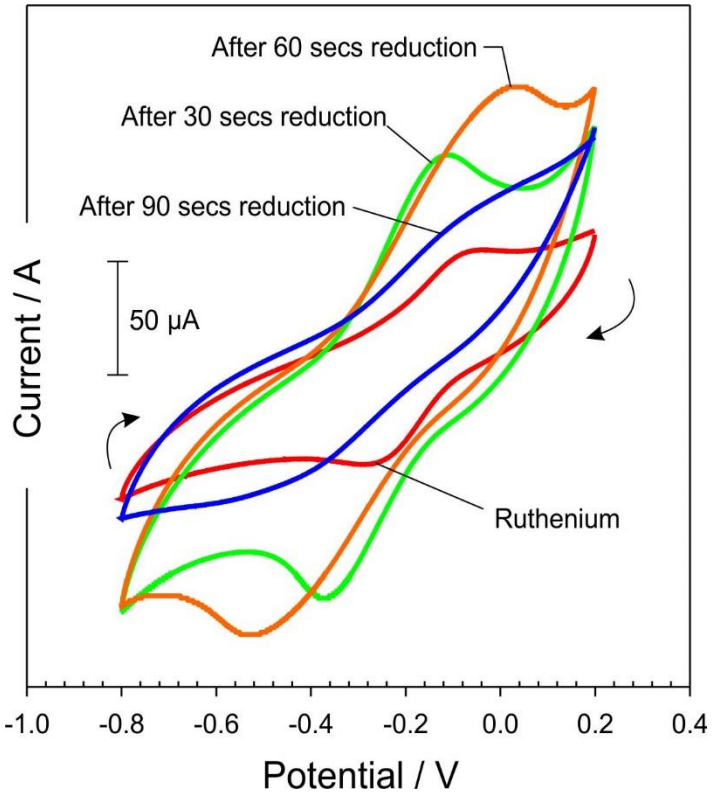

Figure 5.3.5 Cyclic voltammograms detailing the response of the CAP-C filter paper electrode to 2 mM Ruthenium before and after holding the electrode at -2 V for given time periods. Scan rate: 50 mV/s

Upon the initiation of hydrogen evolution, the profile changes dramatically, where the scan recorded after 30 s of reduction at -2 V appears much larger with a more defined peak. This aligns with the previous result shown in **Figure 5.3.2**, where after the first period of reduction the resulting scan presents a much larger signal – again this can be related back to the fact that as the local pH is increasing, the surface CAP is being removed therefore exposing more carbon particles resulting in a greater signal. This trend continues 60 s post reduction; however, the peak begins to lose definition, becoming much broader. After 90 s of an applied reducing potential the electrode losses much of its response as full dissolution of the electrode has been achieved and the conduction between the carbon particles is significantly reduced. The results from above (**Figure 5.3.5**) were repeated without the filter paper within

the electrode configuration in order to draw a comparison. It was predicted that the local pH within the filter paper configuration would give rise to greater changes in pH as the local sensing area had been confined within the filter paper, therefore leading to more rapid dissolution. Cyclic voltammograms detailing the response of the CAP-C electrode without filter paper before and after the imposition of a potential of -1.5 V are shown in **Figure 5.3.6**. The voltammetric response of the CAP-C electrode to ruthenium hexamine is consistent with that observed in **Figure 5.3.2**.

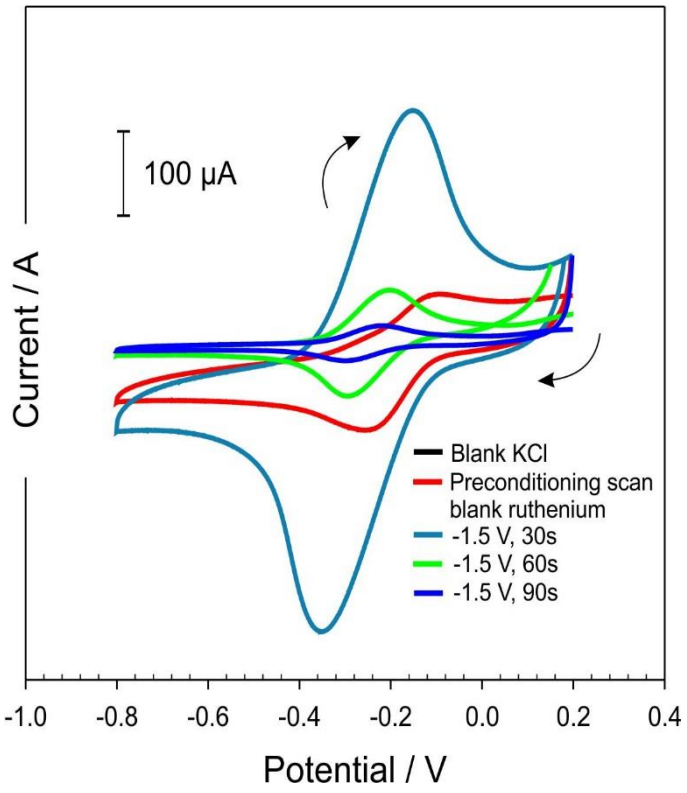

Figure 5.3.6 Cyclic voltammograms detailing the response of the CAP-C electrode (without filter paper) to 2 mM Ruthenium before and after holding the electrode at -1.5 V for given time periods Scan rate: 50 mV/s

After imposing the reducing potential for 30 s, a large well-defined peak is observed which is much larger in comparison to the electrode with filter paper. This can be attributed to the fact that the diffusion of the ruthenium hexamine to the electrode surface is faster in the absence of the filter paper. The latter also means that diffusion of the CAP away from the electrodes is also more rapid and hence the drop in the signal is much more pronounced.

To demonstrate that the signal drop is, in fact, due to the dissolution of the CAP-C electrode as a result of hydrolysis, a mat CF electrode was exposed to the same conditioning potential as the CAP C. Cyclic voltammograms detailing the response of a carbon fibre towards ruthenium hexamine before and after the commencement of hydrolysis are shown in **Figure 5.3.7**. It was observed that the carbon fibre electrode remains stable after the onset of a reducing potential, confirming that it is the deterioration of the CAP-C electrode – due to the change in local pH, that ultimately leads to a decrease in electrode sensitivity.

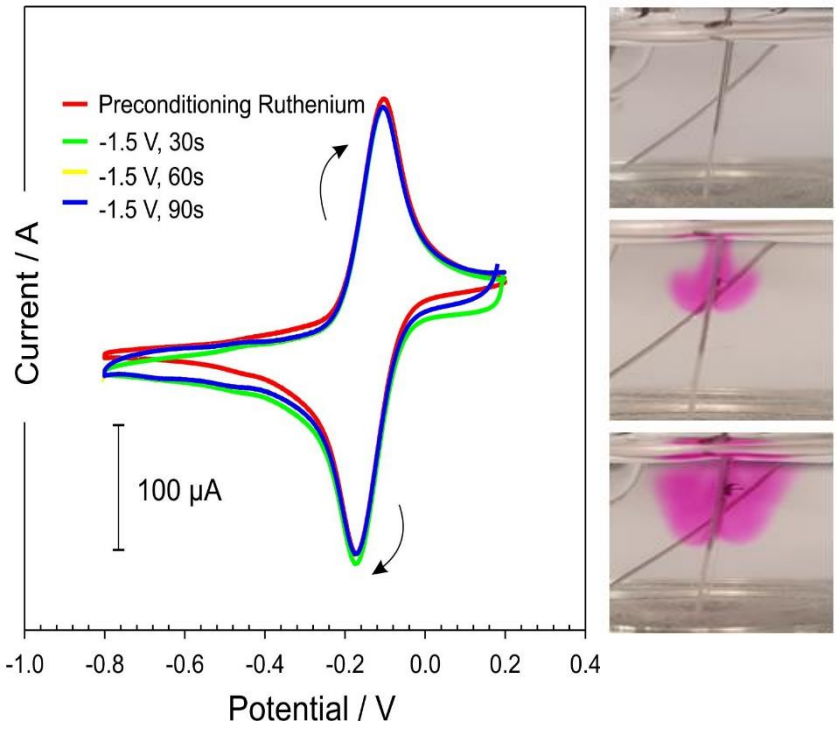

Figure 5.3.7 Cyclic voltammograms detailing the response of a carbon fibre electrode towards 2 mM ruthenium before and after holding the electrode at -1.5 V for given time periods. Scan rate: 50 mV/s Inset: Carbon fiber electrode in the presence of phenolphthalein (1 mM, 0.1 M KCl) during electrolysis

During electrolysis, the carbon fibre was also assessed in the presence of phenolphthalein (1 mM, 0.1 M KCl). As the reducing potential was initiated at the carbon fibre electrode, images were captured during electrolysis at specific time periods to confirm the increase in local pH (**Figure 5.3.7** Inset).

5.3.3 Alizarin Modified Electrode for Voltammetric pH Sensing

In the following section, square wave voltammetry was used as the electrochemical probe of the system. It was envisaged that monitoring the peak position of alizarin (1 mM in ethanol) would provide the diagnostic data for measuring the extent to which local pH changed as a consequence of electrolysis. In previous investigations it was possible to utilise the position of quinone peaks endogenous to the carbon surface as an indicator of pH. This requires a large population of the quinone which was generally created through the process of anodisation. The latter is clearly inappropriate for the CAP-C system and therefore a quinone indicator system had to be directly added to the film using conventional casting methods. Square wave voltammetry was used to probe the impact of pH on the position of the solution based alizarin. The redox reaction of alizarin is shown in **Figure 5.3.8** below, where the peak potential should theoretically vary by 59.2 mV per pH unit according to the Nernst Equation (Bard and Faulkner, 2001).

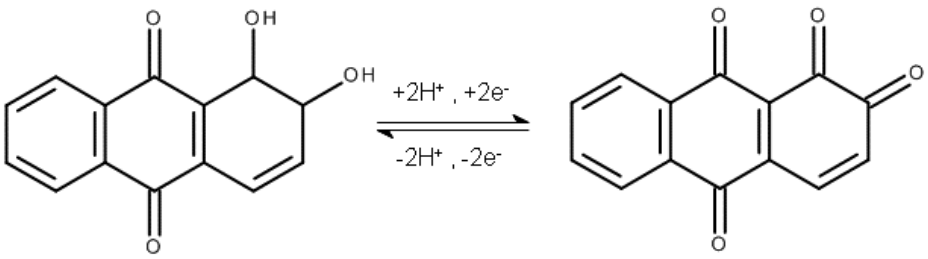

Figure 5.3.8 The electrochemical redox reaction of the alizarin

The CAP binder could not be used in acquisition of the calibration data in this instance due to its pH sensitivity. To overcome this issue, the CAP was substituted for polycarbonate (pH insensitive binder) and the composite film assembled as described in Section 5.2.3 and electrochemically anodised (+2 V, 300 s). The carbon-polycarbonate film's response towards alizarin (1 mM, ethanol, 25 µL deposited each side) under a range of different pH regimes are shown in **Figure 5.3.9**.

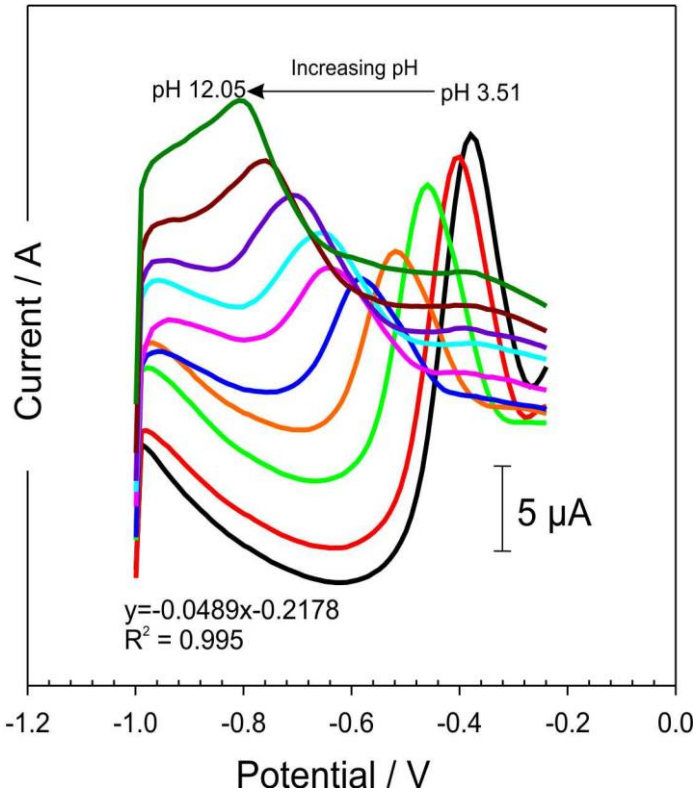

Figure 5.3.9 Square wave voltammograms of the alizarin modified carbon-polycarbonate electrode towards a series of pH buffers

The peak of the alizarin shifted to the more negative region as the pH of the solution increases to a more alkaline environment as expected, and the plot of peak potential against pH shows a good linear relationship with a shift of 48.9 mV per pH unit. A calibration graph detailing peak position against pH (3-12) is detailed in **Figure 5.3.10**. The equation of the line was E_{pAliz} / V = -0.0489 [pH] + 0.2178; R^2 = 0.995; *N* = 10).

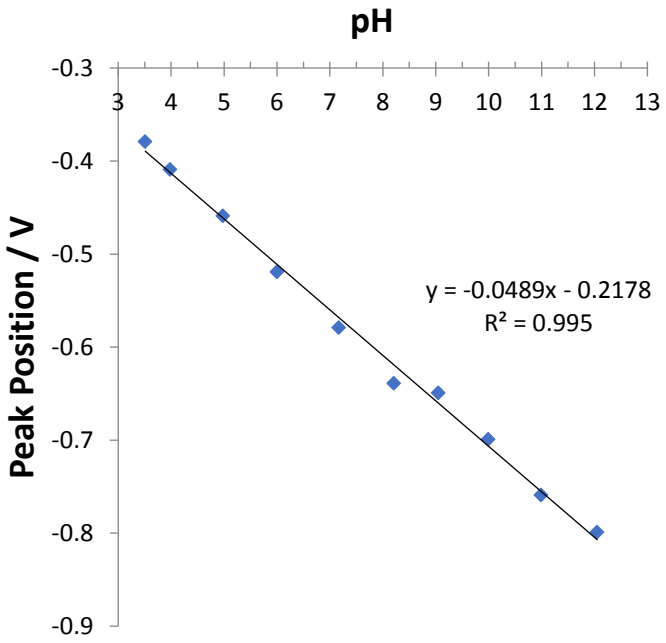

Figure 5.3.10 Relationship between the oxidation peak position of alizarin and solution pH

One of the next objectives within this work was to modify the CAP-C electrode through the addition of alizarin for pH sensing within an unbuffered solution (0.1 M KCl). A CAP-C electrode was modified through the drop casting of an aliquot of alizarin as described above with the carbon-polycarbonate. The stability of the CAP-C film was tested in the presence of 0.1 M KCl that had been adjusted to pH 3.51 through the addition of 0.1 M HNO_3. The CAP-C-Alizarin film was then assessed after the imposition of a moderate reducing potential (-1 V, increments of 30 s) as shown in **Figure 5.3.11**. After the application of the reducing potential the peak magnitude begins to decrease (detailed in **Table 5.3.1**). There is no significant shift in the potential of the oxidation peak – this can be attributed to the fact the reducing potential (-1 V) is not sufficiently negative to induce a marked increase in proton reduction and hence pH such the local pH re-establishes to the bulk pH (pH 3.51) almost immediately. Thus, when the actual scan is initiated after the reducing potential – the solution pH has returned and thus no peak shift.

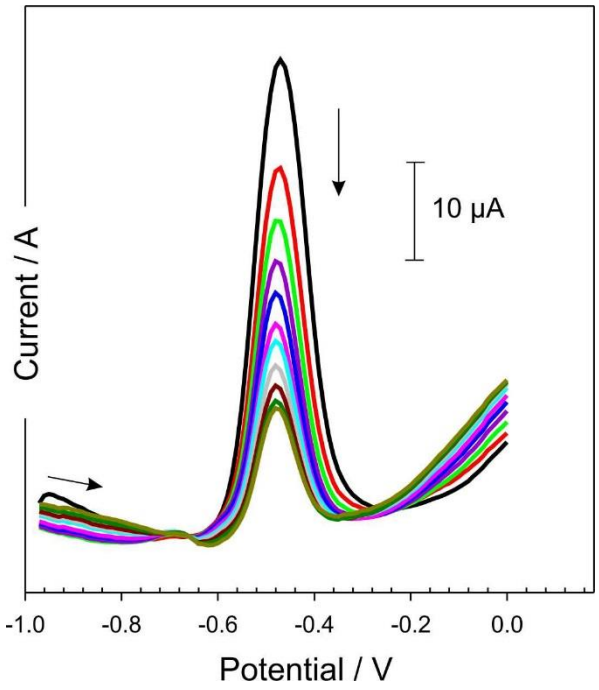

Figure 5.3.11 Square wave voltammograms detailing the influence of the reducing potential (-1 V, 30 s) on the alizarin modified CAP C films

Table 5.3.1 Peak height measurement of the alizarin before and after various reduction times

	Peak Position / V	Peak Height / µA
Preconditioning	-0.47	47.39
-1 V, 30 s	-0.47	36.42
-1 V, 60 s	-0.48	31.31
-1 V, 90 s	-0.48	27.27
-1 V, 120 s	-0.48	23.4
-1 V, 150 s	-0.48	20.14
-1 V, 180 s	-0.48	18.49
-1 V, 210 s	-0.48	16.24
-1 V, 240 s	-0.48	14.57
-1 V, 270 s	-0.48	12.81
-1 V, 300 s	-0.48	12.19

Since the CAP-C-alizarin modified electrode showed a reasonable Nernst response under various pH regimes, it was necessary to test the performance of this electrode for the voltammetric sensing of local pH, before and after the commencement of hydrolysis. The performance of the alizarin modified electrode was assessed by measuring the pH at the interface of the electrode in 0.1 M KCl. The determined pH by the electrode before the commencement of the reducing potential is equal to 4.74

and is shown in **Figure 5.3.12**. A further measurement of the pH was conducted after the reducing potential (-2 V, 30 s) and is equal to 9.86. Additional scans were continued after the reducing step and show that after repetition the peak begins to disappear as the electrode is begins to disintegrate where the results are shown in **Table 5.3.2**.

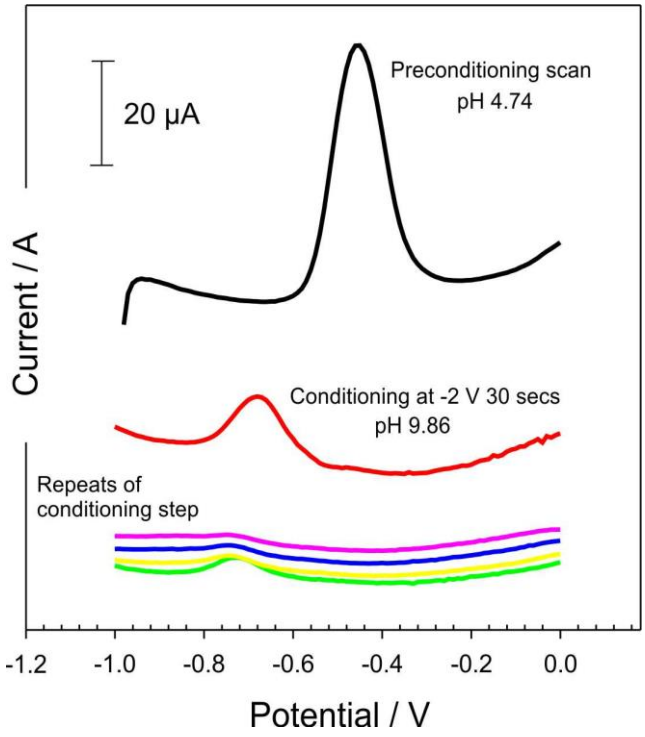

Figure 5.3.12 Square wave voltammograms detailing the influence of local pH on the alizarin peak position pre and post electrolysis

Table 5.3.2 The measurement of pH in 0.1 M KCl by the CAP-C alizarin modified electrode

	Peak Position / V	**Peak Height / µA**
Preconditioning	-0.45	44.76
-2 V, 30 s	-0.7	11.15
-2 V, 60 s	-0.75	3.49
-2 V, 90 s	-0.76	2.19
-2 V, 120 s	-0.76	1.83
-2 V, 150 s	-0.76	1.37

The peak position of the alizarin for both conditioning potentials (-1 V and -2 V) with increasing scan number is compared in **Figure 5.3.13**. The relationship between the peak position of the alizarin and scan number for the lower conditioning potential (-

1 V) is a relatively stable process with little shift in peak position, in contrast to the larger conditioning potential (-2 V) which shows a large shift towards the negative region as the local pH is increased at the surface of the CAP-C alizarin electrode.

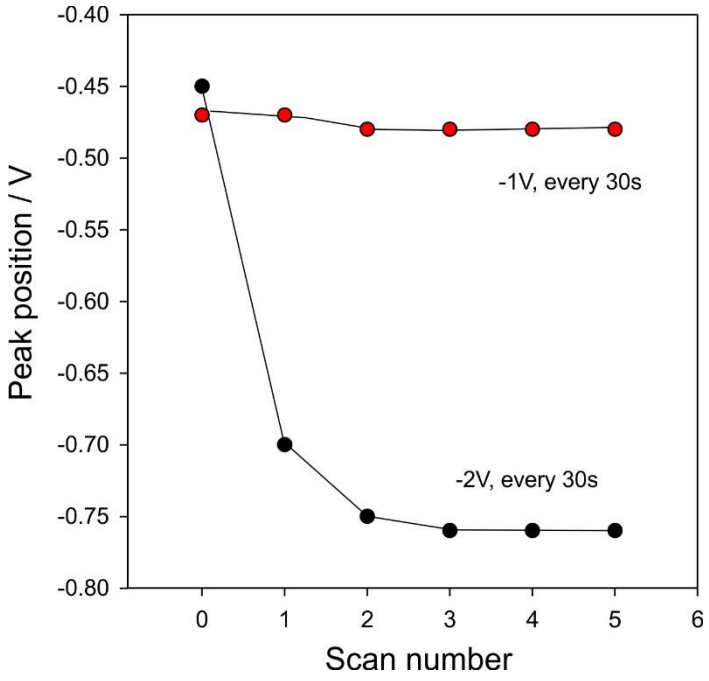

Figure 5.3.13 Plot of alizarin peak position against the scan number during electrolysis

The next stage was to assess the impact of electrolysis on the electrode current at the different electrodes. The electrodes assessed where; the carbon-polycarbonate electrode, the CAP-C-Alizarin electrode and the CAP-C-Alizarin electrode after dissolution, resulting in the loss of the sensing area. All three electrodes were reduced at -2 V, and the effect on the current was measured using chronoamperometry (**Figure 5.3.14**). After the imposition of the reducing potential the carbon-polycarbonate alizarin electrode remains stable and is unaffected by the electrolysis. This is in contrast to the CAP-C-alizarin electrode were the current drops very fast after the onset of reduction, after which the sensing window falls from the electrode as the CAP becomes unstable. This electrode was then rinsed and placed in a fresh solution of 0.1 M KCl and the process repeated. The electrode is without a sensing window at this point- represented by the red line, where there is a very small amount of current, but not zero current, this is due to the remaining carbon that is

still exposed at the edge of the window where the working area of the electrode has fallen out.

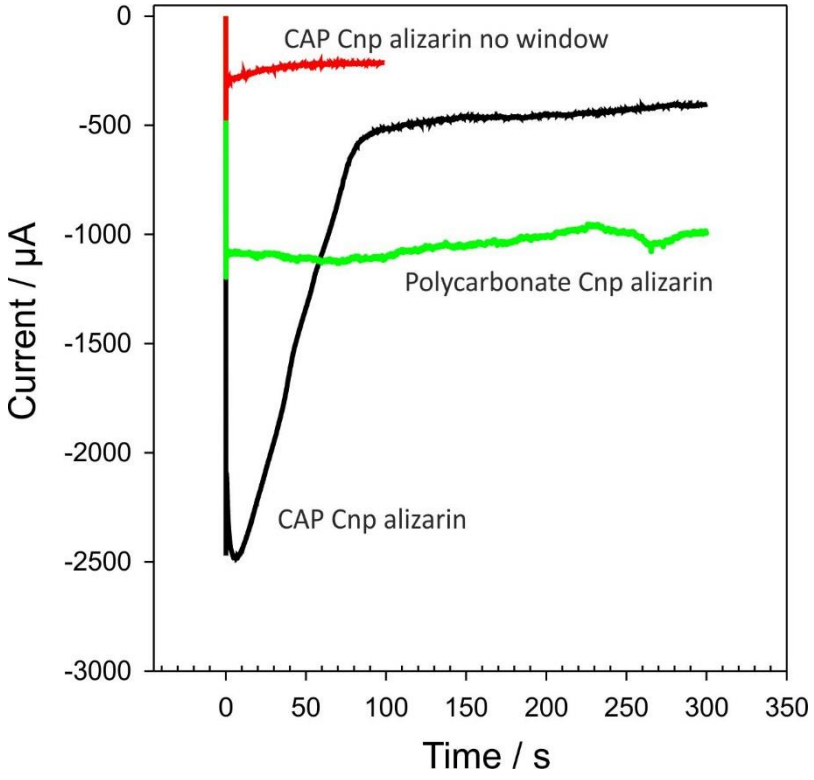

Figure 5.3.14 Effect of electrolysis on the measured current of each electrode tested; CAP-C-alizarin (blank line), CAP-C-alizarin no window (red line) and polycarbonate-C-alizarin (green line)

5.3.4 Ion-Exchange Properties of the CAP-C film

It was anticipated that the CAP-C film, upon electrochemical reduction could exhibit ion exchange activities with cations. The CAP polymer has, by nature of its composition, the capability of being transformed into an anionic film. There is an abundance of carboxylic acid groups on the structure (as per the phthalate residues) and thus while these would be expected to be protonated at low pH, the imposition of the reducing potential increases the pH and will simultaneously deprotonate the acid groups leading to a net negative charge. The latter can then pick up cationic species from the bulk solution. This is highlighted in **Figure 5.3.15**. The effect is relatively short lived unless a stable complex is formed and thus the cation will drift back into solution as the local pH is returned to the low pH of the bulk.

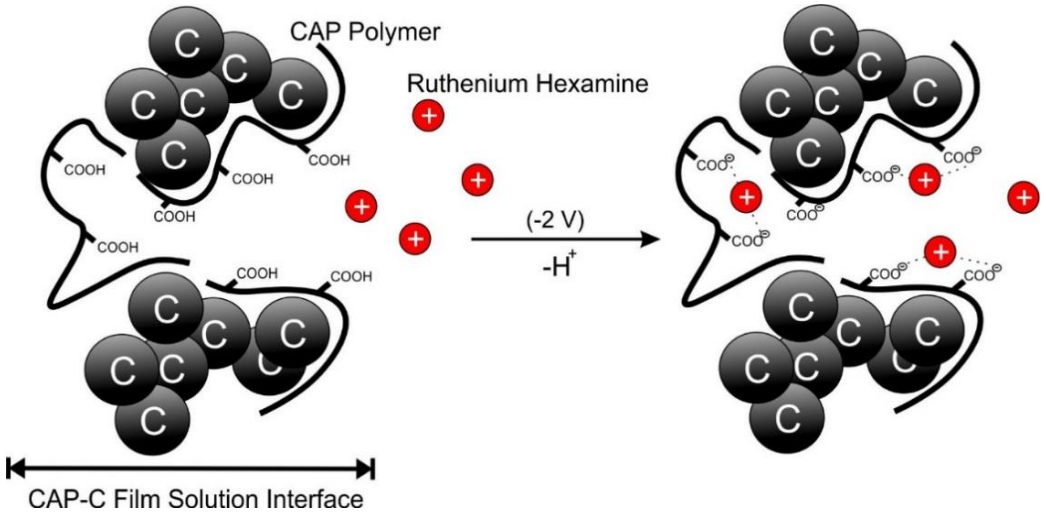

Figure 5.3.15 Ion exchange mechanism

The CAP-C electrode was immersed in a solution of ruthenium hexamine (2 mM, 0.1 M KCl) and held at -2 V for 1 second as shown in **Figure 5.3.16** (green line). The electrochemical signal becomes larger than the scan before reduction (black line) as expected. As the conditioning potential continues for 10 seconds more (green line) the CAP binder begins to deteriorate exposing more of the carbon, however after 30 seconds (purple line) much of the CAP-C has been lost as the electrode structure diminishes resulting in a loss in signal.

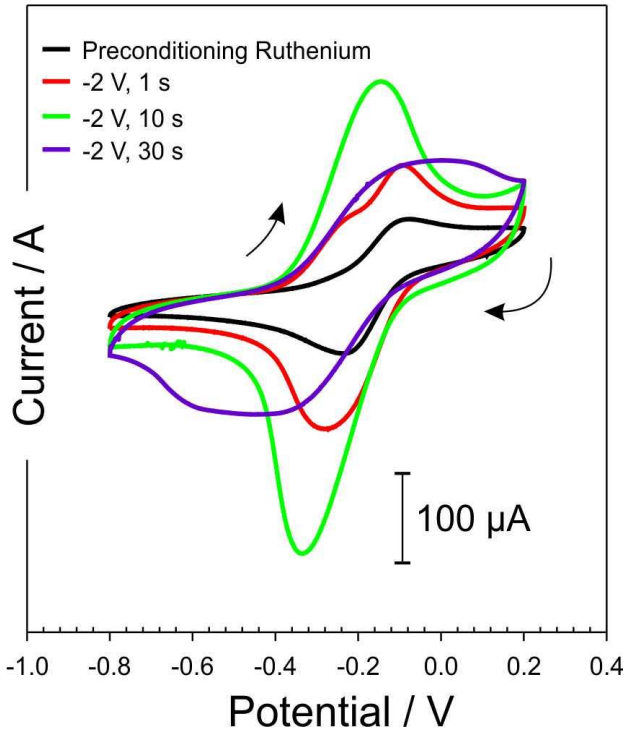

Figure 5.3.16 Cyclic voltammograms detailing the response of the CAP-C electrode to 2 mM Ruthenium before and after holding the electrode at -2 V for given time periods. Scan rate: 50 mV/s

The still intact CAP-C film was then removed from the ruthenium solution, rinsed and placed in a fresh solution of 0.1 M KCl with no ruthenium hexamine present. A series of cyclic voltammograms were initiated and are shown in **Figure 5.3.17.** Ruthenium hexamine peaks are still visible during the scan confirming that ion exchange into the polymer has occurred. As there is no additional reducing potential to maintain a high local pH, the internal voids with residual CAP-COO^- $Ru(NH_3)_6^{3+}$ return to the bulk pH and the ruthenium hexamine slowly diffuses out into the solution – as evidenced by the successive reduction in the peak height.

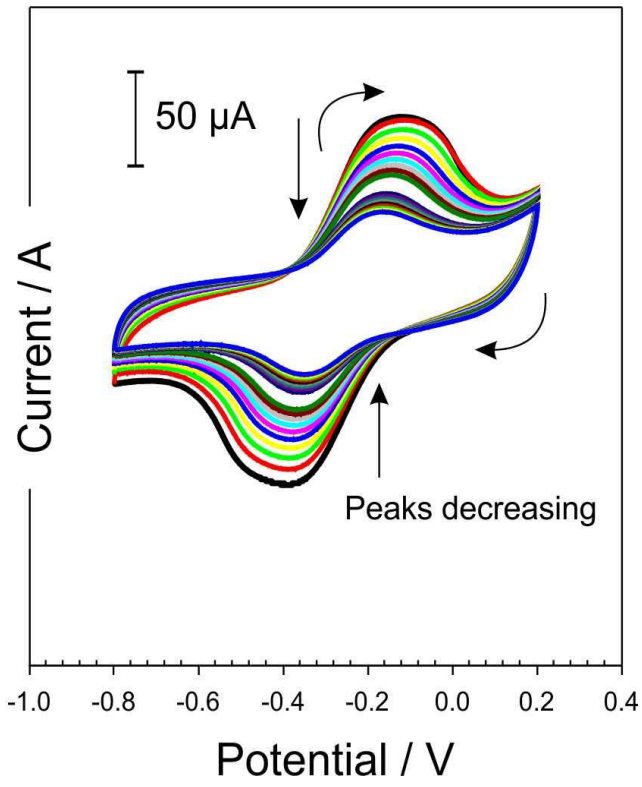

Figure 5.3.17 Cyclic voltammograms detailing the response of the CAP-C films (post reduction in 2 mM Ruthenium Hexamine) in fresh 0.1 M KCl. Scan rate:50 mV/s

This observation is interesting, as it was initially believed that when the conditioning potential was applied that the increase in signal was simply due to the increase the surface wettability and hence more active area and therefore a larger current. However, when the reducing potential (-2 V) is initiated, there is an immediate pH change at the interface and considering the CAP is full of acid groups, it effectively deprotonates the remainder - meaning the interface is now net negative. The ruthenium complex is 2^+ / 3^+ and results in ion exchange into the film - hence the preconcentration effect and larger signal. In principle, this could serve as another means of drug delivery and in some respects, mirrors the early work with drug ion exchanged into polypyrrole films and delivered via cochlear implants (discussed previously in **Section 1.4.2)** (Richardson *et al.*, 2009; Kaur *et al.*, 2015). It must be recognised that the delivery load will be much more limited than using the reservoir configuration previously described.

In order to confirm the potential for delivery of an actual drug – dopamine (10m M, pH7) was selected as a model. The CAP-C film's direct voltammetric response towards increasing concentrations of dopamine (0-196 µM, 0.1 M KCl) are shown in **Figure 5.3.18**.

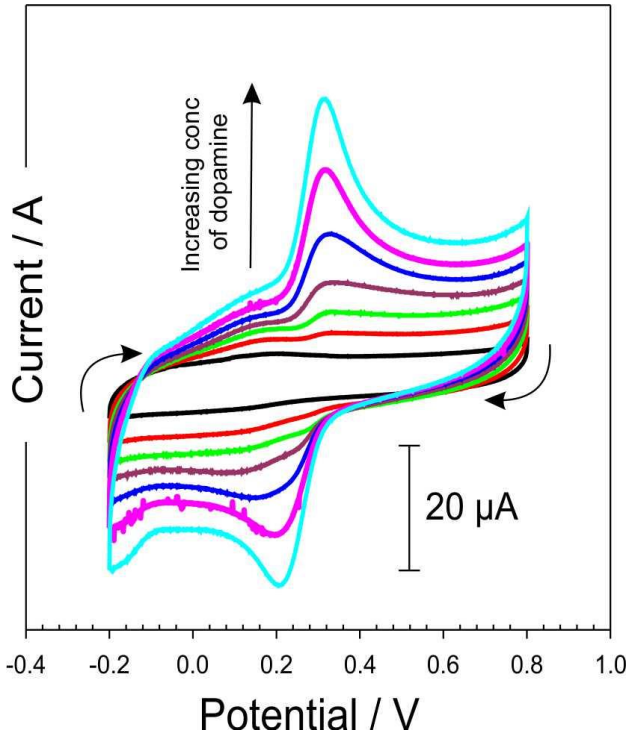

Figure 5.3.18 Cyclic voltammetric response of the CAP-C towards increasing additions of dopamine (0-196 µM, 0.1 M KCl). Scan rate:50 mV/s

Dopamine will have a net positive charge as a consequence of the protonation of primary amino group (pKa ~11) and therefore should have the potential to ion exchange into the film after imposing the reduction potential (**Figure 5.3.19 A**) in much the same way as the ruthenium hexamine (**Figure 5.3.16**). A similar decrease in dopamine peak magnitude was observed when the reduced electrode was removed, rinsed and tested in fresh 0.1 M KCl as shown in **Figure 5.3.19 B**.

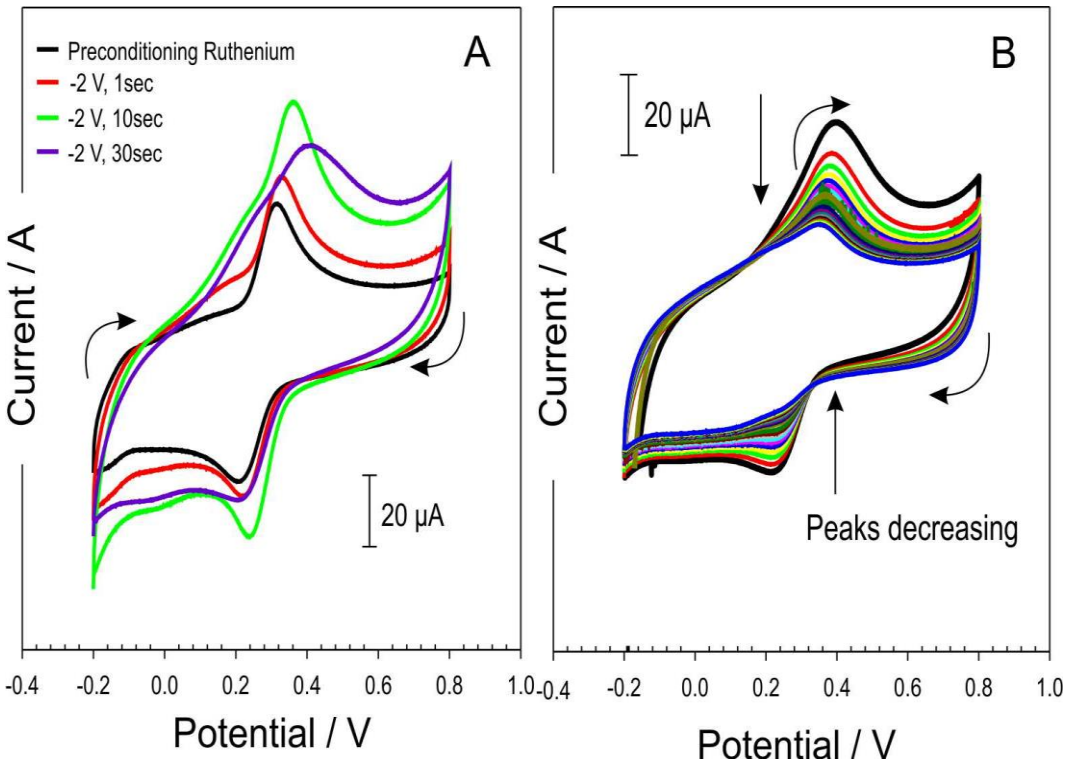

Figure 5.3.19 (A) Cyclic voltammograms detailing the response of the CAP-C electrode towards dopamine (196 µM, pH 7) before and after holding the electrode at -2 V for given time periods. **(B)** Cyclic voltammograms detailing the response of the CAP-C films (post reduction) in 0.1 M KCl. Scan rate: 50 mV/s

5.3.5 Enhancement of Electrode Response

Surface modification of an electrode substrate is often employed to improve the electron transfer kinetics, various surface interactions and overall sensing performance. In this this case, the use of Graphene Oxide (GO) is electrochemically characterised using model redox probes, specifically potassium ferrocyanide and ruthenium hexamine to evaluate the ability of GO modifiers to enhance the HER process.

The CAP-C film's response towards ferrocyanide before and after the deposition of Graphene Oxide (GO) was investigated in a similar manner to the work previously reported in Chapter 4. Modification of the CAP-C film was achieved through the selective deposition of GO which had been previously sonicated in deionized water (1 mg / mL). An aliquot of GO suspended in solution (0.005 mg) was accurately drop cast onto the electrode surface (2.5 µL each side) and allowed to dry under ambient

conditions. Cyclic voltammograms detailing the response to ferrocyanide are shown in **Figure 5.3.20.** The improvement in the CAP-C-GO electrode response resulting from the GO modification can be attributed to the increase in the availability of carboxylic acid groups and edge plane sites that present themselves with the addition of GO (*cf.* **Section 4.3.4**). It is important to acknowledge that the GO in this instance is serving much the same purpose as electrochemical anodisation but without the need to strong alkaline solutions and thus preserving the integrity of the CAP-C film.

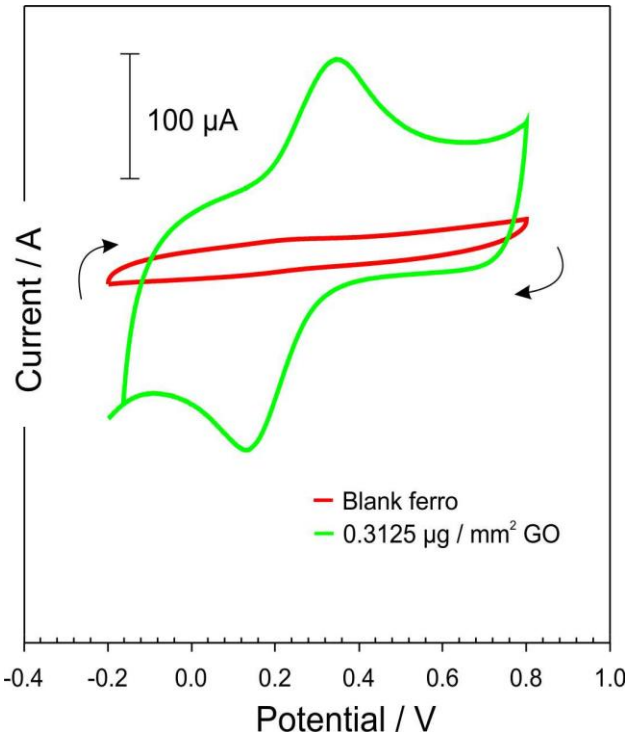

Figure 5.3.20 Cyclic voltammograms detailing the response of the CAP-C towards ferrocyanide (2 mM, 0.1 M KCl), before (red line) and after (green line) the addition of graphene oxide (0.3125 µg / mm^2 GO)

A similar response was observed after the CAP-C film was modified via the addition of Iron (II,II) oxide nano powder. The unmodified film displays a poor response towards ferrocyanide, after which a solution of Fe_3O_4 was prepared in deionised water as described above (1 mg/ mL). A small amount of the Fe_3O_4 solution (0.03 mg) was dropped onto the electrode (15 µL each side) and left to dry. The CAP-C film responses towards ferrocyanide before and after Fe_3O_4 modification are shown in **Figure 5.3.21**.

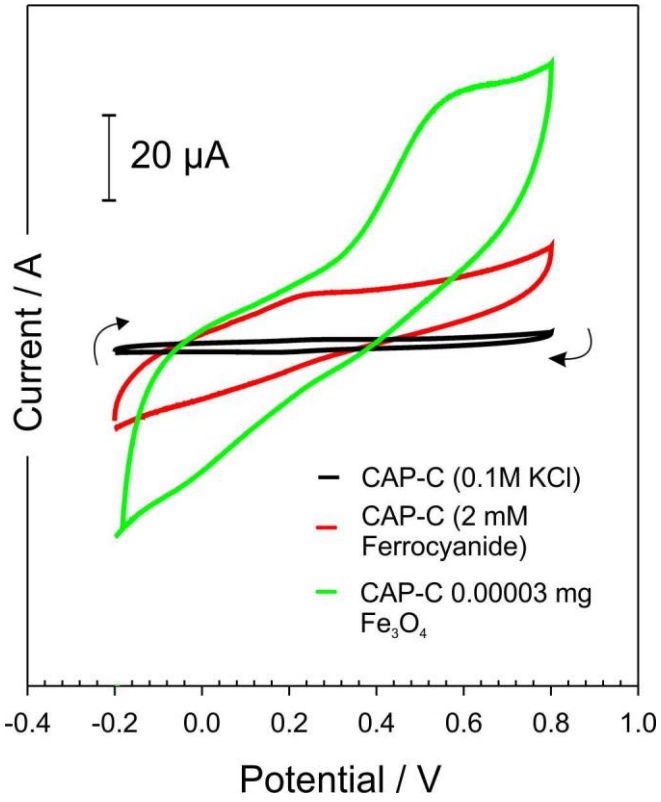

Figure 5.3.21. Cyclic voltammograms detailing the response of the CAP-C towards ferrocyanide (2 mM, 0.1 M KCl), before (red line) and after (green line) the addition of Iron (II, II) oxide nano powder (1.875 µg / mm^2 Fe_3O_4)

Modification of the CAP-C film through the addition of Fe_3O_4 nano particles displays very poor electrode kinetics towards ferrocyanide with a broad oxidation peak and no observable reduction peak. This can be explained by the structure of the CAP-C film, where the carbon nanoparticles are effectively trapped within the polymer binder and therefore only small areas of the surface of the carbon particles are exposed as a sensing area. The CAP-C film's response towards increasing additions of Fe_3O_4 (0.005 mg to 0.03 mg) was then assessed in the presence of ruthenium hexamine (2 mM, 0.1 M KCl) and is recorded in **Figure 5.3.22**.

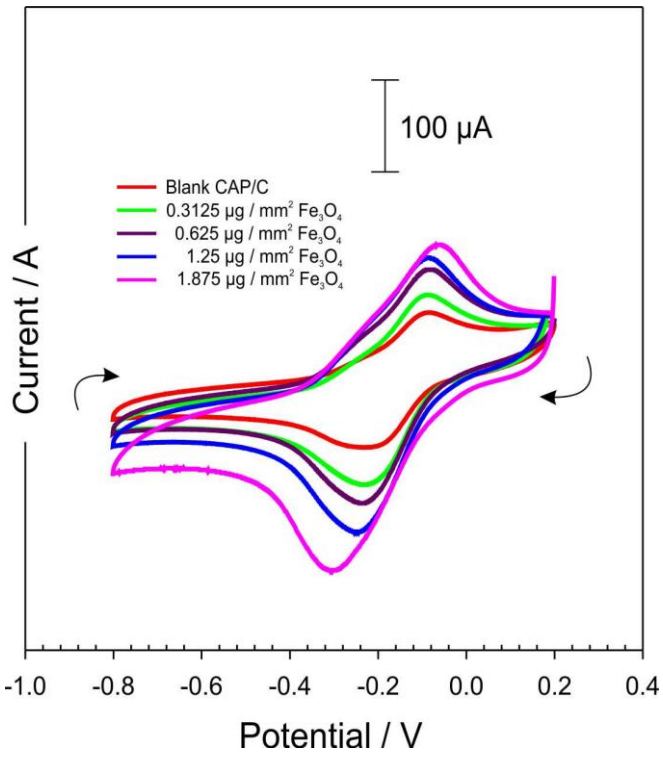

Figure 5.3.22 Cyclic voltammograms detailing the CAP-C film's response towards ruthenium hexamine (2 mM, 0.1 M KCl) with increasing additions of Fe_3O_4

Each subsequent addition of Fe_3O_4 was found to increase the electrode sensitivity towards ruthenium hexamine and can be attributed to the increased presence of metal oxide particle facilitating electron transfer. The central interest however lies in the ability of the modified electrode to improve the dynamics of the hydrogen evolution reaction.

Linear sweep voltammograms of the unmodified CAP-C against the CAP-C-GO and CAP-C-Fe_3O_4 are detailed in **Figure 5.3.23**. The responses to proton reduction show that the GO and Fe_3O_4 modifiers perform more favourably than the CAP-C alone. For the modified electrodes, the potential at which reduction occurs is less negative as supported by the linear sweep voltammograms. Although the modification of GO and Fe_3O_4 present an interesting approach for successful electrode modification and these preliminary findings are positive, the fabrication aspects, reproducibility and stability were poor and thus they were not used.

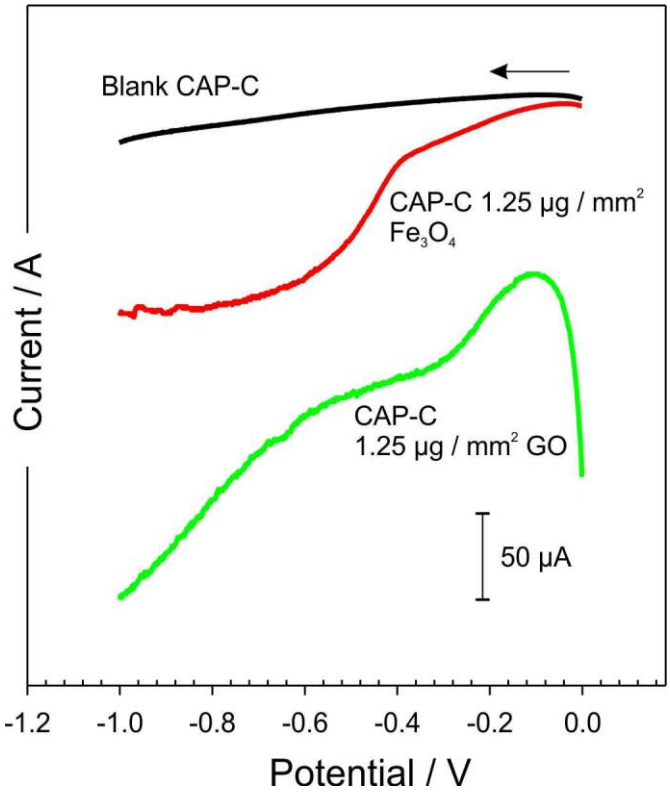

Figure 5.3.23 Linear sweep voltammograms of the unmodified, Fe_3O_4 modified and GO modified CAP-C films in 0.1 M KCl. Scan rate: 50 mV/s.

The GO modified electrode (green line) is offset from the other two electrodes during the linear sweep, due to the capacitance background of the GO on the electrode. However, it should be noted that during reduction (-0.3 V, green line), is not H^+ reduction – it is quinone reduction. The reduction of H^+ at GO occurs at -0.6 V, which is a much more improved response that the CAP-C electrode alone.

5.4 Conclusions

The dissolution of a conductive composite film through the application of a specified potential trigger is described. Nano carbon loaded polymer films were chosen such that they would retain conductivity and thus the imposition of a suitable cathodic potential would begin to generate hydrogen. It has been demonstrated that a change in local pH, brought about by the application of a reducing potential was able to induce the solubilisation of the CAP-C film. In application, the

electrochemically controllable film could be incorporated within existing drug delivery technology where the removal of the binder would allow the passage of the drug through the pores left behind.

Results from biocompatibility testing in accordance with of DIN EN ISO 10993-5:2009 indicated that the CAP-C film did not cause any relevant toxicological or biological damage to the subconfluent monolayer of L929 cells under the test conditions. These results show promise for the further development of the conductive film to be investigated within drug delivery applications which interact with biological systems. The simplification of the CAP-C film in comparison to previous designs outlined in Chapter 4, show that the conductive film serves as a function to both control the local pH and initiate dissolution concurrently. Although the CAP-C film was constructed as a film, the production of the film could also be modified to function as a conductive ink which offers desirable conductivity for a wide range of applications.

During electrochemical characterisation, there was a marked improvement in electrochemical response towards the ruthenium hexamine in comparison to the ferrocyanide. The disparity can be attributed to the difference in the nature of the compounds and their interaction with the carbon surface. The ferrocyanide probe is a classic negatively charged inner sphere complex, whereas the ruthenium hails from a positive charged outer sphere system and it could be that electron transfer is preferentially faster at the latter.

The modification of the CAP-C electrode through the addition of alizarin for pH sensing within an unbuffered solution was also assessed. The deposition of alizarin resulted in an unambiguous peak which enhanced the diagnostic capability of the quinone voltammetric signal allowing for the measurement of the local pH. The determined pH by the electrode before the commencement of the reducing potential was equal to 4.74 and after the reducing potential (-2 V, 30 s) the pH increased to 9.86.

The film was modified through the addition of Iron (II,III) oxide nano powder and graphene oxide in order to increase the electrode response towards the chosen redox probes – ferrocyanide and ruthenium. The responses to proton reduction show that the GO and Fe_3O_4 modifiers perform more favourably then the CAP-C alone. For the modified electrodes, the potential at which reduction occurs is less negative as supported by the linear sweep voltammograms. While this method of modification initially presented promising potential towards the sensing application, it was found that fabrication aspects – reproducibility and stability of the deposited nano particles where poor, thus the modification step was omitted.

Chapter 6

Controlled Electrochemical Dissolution of pH Sensitive Carbon Composite Microneedle Arrays

Abstract

A new approach to the production of conductive microneedles is presented. The methodology proposed herein focuses on the formulation of nano particulate carbon along with pH sensitive cellulose acetate phthalate as a polymeric binder for the production of microneedle patches. Under normal conditions (open circuit), the conductive coating remains intact but, through exploiting hydrogen evolution at the microneedle array, changes in local pH is shown to induce swelling within the needle structure. The design and characterisation of the carbon composite microneedles, the ability to electrochemically manipulate the structural integrity of the needles and the surface modification of the carbon needles with palladium and cysteine is critically assessed from sensing and drug delivery perspectives.

Part of the research described in this chapter has been published in Martin, A., McConville, A., Anderson, A., McLister, A., and Davis, J. Microneedle Manufacture: Assessing Hazards and Control Measures. *Safety* 2017, *3*, 25.

6.1 Introduction

Microneedle systems are increasingly being proclaimed as a technological advancement in drug delivery applications and can proffer a wealth of advantages over traditional needle based approaches (Prausnitz, 2004; Cheung and Das, 2014; Larrañeta *et al.*, 2016). These microneedle (MN) systems characteristically consist of an array of sub millimetre sized needles (50-900 μm) and, counter to traditional hypodermic inoculations, are suitably minute that the shallow puncture depth usually does not illicit a response from the dermal nerve network (Prausnitz, 2004; Birchall *et al.*, 2011). The virtually painless perforation of the skin barrier can facilitate the delivery of a substantial range of drug therapies and vaccines to the microcirculation below the stratum corneum and the generic nature of the approach has resulted in an exponential increase in publications (Cheung and Das, 2014).

Naturally formed microneedle structures can be found in a range of species – plant, insect and animal and are used as defence mechanism to protect the host system from various predation threats. A common example is the stinging hairs that are found on the stem and the underside of the leaves of a stinging nettle – a common weed found in almost all parts of the UK. The stinging hair of *Urtica dioica*, is shown in the micrograph in **Figure 6.1.1**. The stinging hair consists of one tapered, elongated stinging cell with a bulbous base, which is surrounded with sheathing pedestal cells at the stem (Fu *et al.*, 2007; Cummings and Olsen, 2011). Upon contact with an external trigger, the ball tip breaks off and transforms the stinging hair into a micron sized hypodermic needle capable of penetrating the skin and releasing its constituents resulting in the typical rash.

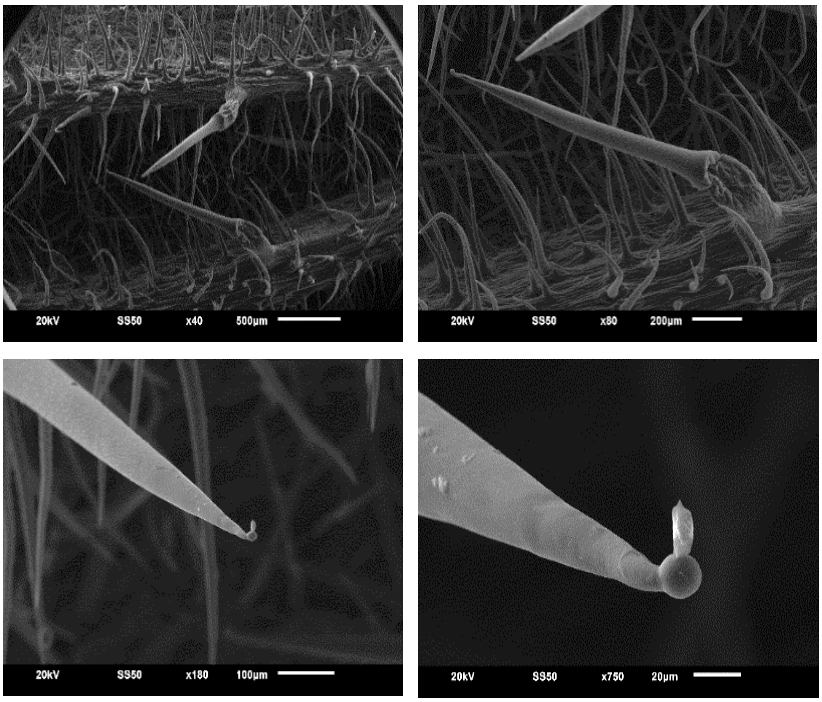

Figure 6.1.1 SEM micrograph detailing the morphology of stinging nettle hairs

Many of the primary models of microneedle systems have been fostered by designs taken from nature, which provides a very effective method of puncturing the skin. While nature has had many millennia to perfect her designs, laboratory based MN manufacture is rather more basic. In general, there are five categories of MN system: solid, coated, hollow, dissolvable and swellable. Each individual types has its own advantageous qualities and limitations which have been comprehensively reviewed (Cheung and Das, 2014; Larrañeta *et al.*, 2016). As MN technologies have progressed, there has been a gradual accessibility of the technologies necessary to manufacture them. The availability of silicone moulds enables rapid, low cost, soft lithographic construction of MNs within the standard laboratory setting (Prausnitz, 2004; Birchall *et al.*, 2011; Cheung and Das, 2014; Larrañeta *et al.*, 2016; McConville and Davis, 2016). The procedures can be modified for formulating all forms of MNs - with the exception of hollow systems. An example of a commercial silicon microneedle mould and the resulting microneedle array are shown in **Figure 6.1.2 A**. A comparison between traditional hypodermic needle, suture needle and microneedle tips are highlighted in **Figure 6.1.2 B**.

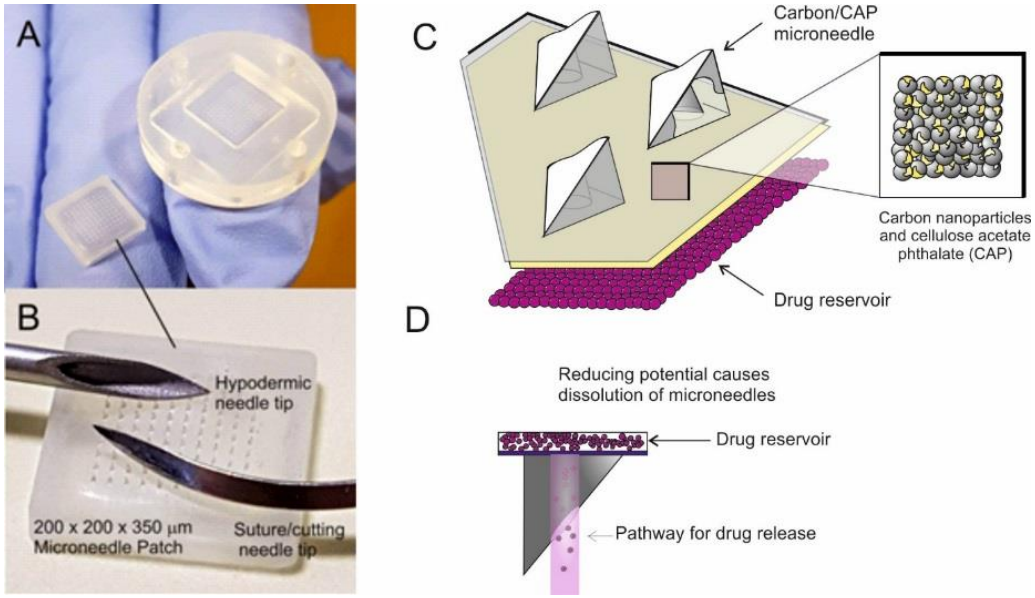

Figure 6.1.2 (A) Micropoint™ 200x200x350 micron needle mould template and an example of the resulting polymer cast microneedle patch. (B) Comparison of conventional sharps alongside a 350 micron microneedle patch. (C) Configuration of CAP-C microneedle patch above a drug containing reservoir. (D) Schematic of drug release mechanism after the initiation of a suitable reducing potential

The aim of the methodology within this chapter has been to investigate the development of solid microneedles based on nano carbon that has been encapsulated within a polymer network (CAP) as shown in **Figure 6.1.2 C**. This research follows on from the previous chapter, where the development of a conductive film of the same components was exploited as a pH sensitive and electrochemically controllable film. The intention in this chapter is to further investigate the conductive polymer blend and, therefore, to construct electrochemically controllable microneedle arrays. The MN arrays could, in principle, offer the capability for electrochemical procedures to be applied such that the microneedle patches could acquire sensing capabilities but, more significantly, could also be used to control drug release as shown in **Figure 6.1.2 D**. The latter is situated at the core of the approach as the electrochemical manipulation of the release mechanism could offer a novel approach in MN design.

The rationale implemented here is subject to the use of cellulose acetate phthalate (CAP) as the binding polymer used to preserve the structural integrity of the needle assembly. Contrary to more benign polymer systems used in MN production (i.e. polycarbonate or polystyrene (McConville and Davis, 2016)), CAP is soluble in higher pH environments and has previously been extensively used in a large variety of oral drug formulations (Kelley *et al.*, 2012; Bertz *et al.*, 2013; Hanafi, Nograles, Abdullah, Shamsudin and Rosli, 2013; Larrañeta *et al.*, 2016; Wong *et al.*, 2017a). Manipulation of the pH responsiveness of the polymer for use in electrochemically controlled drug release has been discussed in Chapters 3 and 4. In the latter, it was used as a thin film encapsulating a drug payload (Ashleigh Anderson, McConville and Davis, 2015). The core objective within this work was to use the CAP matrix as the binding agent in which nano carbon particles would be interspersed to produce a pH sensitive composite microneedle. The application of an appropriate reducing potential to the MN array would lead to the swelling or dissolution of the MNs due to changes in the local pH as a result of electrolysis. The latter is linked to the hydrogen evolution reaction (HER) by which an increase in local pH at the electrode occurs as an after effect of the reduction process (Ashleigh Anderson, McConville and Davis, 2015). Therefore, it could be foreseen that, were the HER reaction to be applied direct to the MN array, the increase in local pH would occur, leading to the swelling (and subsequent dissolution) of the CAP polymer that composes the needle structure. Hence, were drugs to be encapsulated within the polymer composite complex at the time of construction, then the electrochemically initiated swelling could permit control over their release.

The final incorporation of the proposed electrochemically driven approach is shown within a MN system and is highlighted in **Figure 6.1.3.** There is rapidly growing interest in the use of dissolvable and swellable MN systems for drug release (Lahiji, Dangol and Jung, 2015; Thakur *et al.*, 2016; Ita, 2017b) and though the construction method is comparable to that investigated in this work, the release is markedly different as the release process for those systems is inherently passive. Within this work it the objective was to investigate whether the addition of nano carbon particles

could expedite the development of a controlled release mechanism and to critically assess the merits and restrictions that these systems would present for transdermal drug delivery.

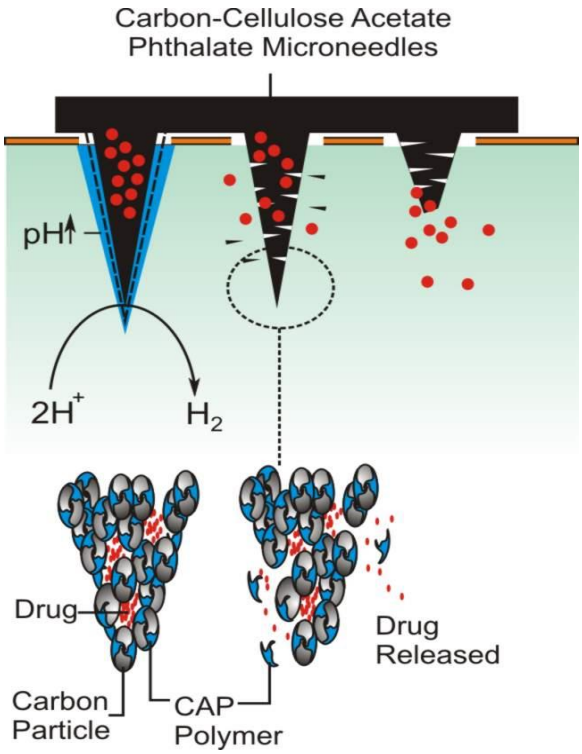

Figure 6.1.3. Overview of the proposed electrochemically initiated release mechanism

6.2 Experimental Details

6.2.1 Materials

Chemical reagents were of the highest grade available and used without any additional purification. All electrochemical measurements were carried out at 22 ^{o}C ± 2^{o}C in Britton Robinson (BR) buffer (pH 3-9, adjusted to the appropriate pH value via the addition of sodium hydroxide). Nano carbon powder was supplied by Sigma Aldrich with a mean particle size of 100 nm. Silicone MPatch™ microneedle templates were purchased from Micropoint Technologies Pte Ltd. (CleanTech Loop, Singapore).

6.2.2 Electrochemical Setup

Electrochemical analysis and set up was performed using a μAutolab computer controlled potentiostat (Eco-Chemie, Utrecht, The Netherlands). The initial measurements involved a three electrode configuration comprising of carbon-polymer composite MN working electrode, a counter electrode in the form of a platinum wire and a standard silver/silver chloride (3 M NaCl, BAS Technicol UK) reference electrode.

6.2.3 Sensor Design and Modification

CAP/Carbon Microneedle Fabrication: Production of the MNs was generally achieved through the simple mixing and dispersion of the nano carbon (Sigma-Aldrich) within the polymer (50/50 wt%) that had previously been dissolved in a suitable solvent such as cyclohexanone. The silicone moulds were obtained from Micropoint Technologies Pte Ltd. (CleanTech Loop, Singapore) and typically comprised of a 10 x 10 MN array. The needle dimensions used in the studies were either 200 x 200 x 350 micron or 200 x 200 x 700 micron. During investigations, silicon moulds were also produced inhouse using a SLYGARD 184 Silcone Eleastomer Kit. The elastomer and curing agent were mixed at a ratio of 10 parts to 1 and gently stirred until a viscous mixture was achieved. The mixture was left to settle until all bubbles had disappeared from the solution. The PDMS solution was then applied to a polycarbonate microneedle array with dimensions 200 x 200 x 400 micron and inspected to ensure full coverage of the needles. The PDMS mould was baked in the oven under vacuum for two hours at 80 ^{o}C and then left to set for 48 hours at room temperature. When the PDMS was fully cured, the microneedle substrate was then carefully removed, and the finished mould is shown in **Figure 6.2.1** below. The moulds were cleaned by sonication in methanol and the polymer-carbon mixture added and the solvent allowed to evaporate. The use of a vacuum oven (under ambient temperature) was found to greatly improve the speed of the production process and needle quality through accelerating the removal of trapped solvent.

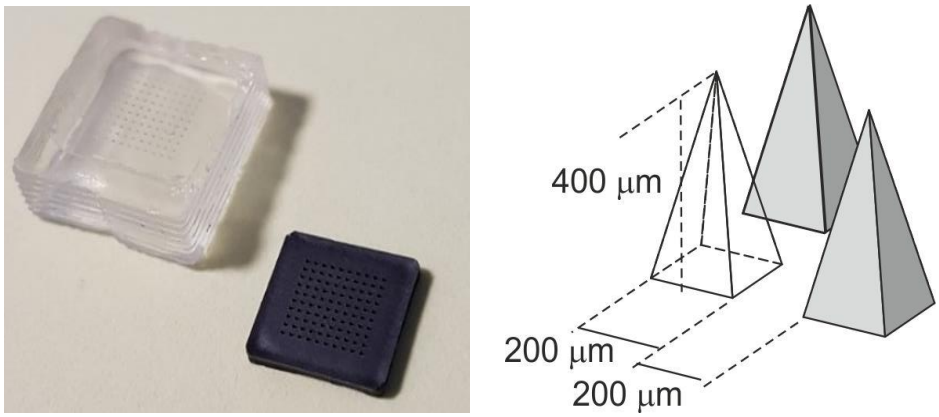

Figure 6.2.1 In-house manufactured PDMS 200 x 200 x 400 μm microneedle mould and the resulting CAP-C microneedle array

Toluidine Blue O /CAP/Carbon Microneedle Fabrication: Production of the Toluidine Blue O (TBO) loaded composite MNs was achieved by first dissolving TBO (5 wt%) in a solution of cyclohexanone. CAP was then added to the TBO solution and left to stir until full dissolution was achieved, at this point the nano carbon (Sigma Aldrich) was added to the TBO/polymer solution (50/50 wt%). The TBO/CAP/C solution was then cast onto the microneedle moulds with dimensions of 200 x 200 x 700 micron. The moulds were then held under vacuum (at ambient temperature) as described in the methodology above, then removed and allowed to dry at room temperature for 48 hours. The microneedles were then carefully removed from the moulds and rinsed thoroughly to remove interfacial TBO.

Microneedle Modification. The nano CAP-carbon microneedles were sputtered with a thin layer of Palladium using an 80:20 Pd/Au target at 30 mA for 3 minutes (Emitech K500X Sputter Coater, Quorum Technologies Ltd, England). X-ray photoelectron spectroscopy (XPS) of the Palladium samples before and after modification with cysteine was performed using an Axis Ultra DLD spectrometer (Kratos Analytical, Japan) using monochromated Al Ja X-rays (15 kV and 10 mA) with an operating pressure lower than $6x10^{-8}$ Pa. A hybrid lens mode was used during analysis and charge neutralisation was achieved using an immersion lens with a filament current

of between 1.7 and 2.1 mA at a charge balance voltage of between 3.0 and 3.6 V. Three spots were analysed per sample and wide energy survey scans (0–1300 eV binding energy) as well as high resolution spectra for Pd3d, C1s, N1s and O1s and S2p. Pass-energy was 160 eV for the wide energy survey scans and 20 eV for the high-resolution spectra.

Alginate Gel Preparation: Alginic acid sodium salt was added to a solution of ferrocyanide (2 mM, 0.1 M KCl) to produce a 1.5% w/v viscous solution. The solution (typically 10 mL) was left to stir for 4 hours at 45 °C, after which a solution of 0.2 M calcium chloride (5 mL, deionised water) was added drop wise to the alginate/ferro solution and left overnight to ensure cross-linking was complete.

Gelatin Preparation: Gelatin (2 g) was added to 0.1M KCl (typically 18 mL) and was stirred for 2 h at 40 °C until the solution was full dissolved. The pH of the gel was measured to ensure that release was not initiated from the pH environment of the gel. The gelatin solution was then transferred into a petri dish and left to set.

6.3 Results and Discussion

6.3.1 Characterisation of CAP Microneedle Array

CAP is an ideal candidate for enteric coatings as it contains many carboxylic acid groups and has a pKa of around 5.28 (Rando *et al.*, 2006). Thus, when it is exposed to the lower pH conditions of the stomach, the carboxylic acid groups will not be fully dissociated and therefore the CAP will be resistant to dissolution. As the pH is increased to that of the intestine (pH 7-8), deprotonation is near complete resulting in the polymer chains having greater hydrophilicity and hence solubility. Scanning electron micrographs detailing the structure of a MN array (700 μm) cast from a solution of CAP alone are highlighted in **Figure 6.3.1**.

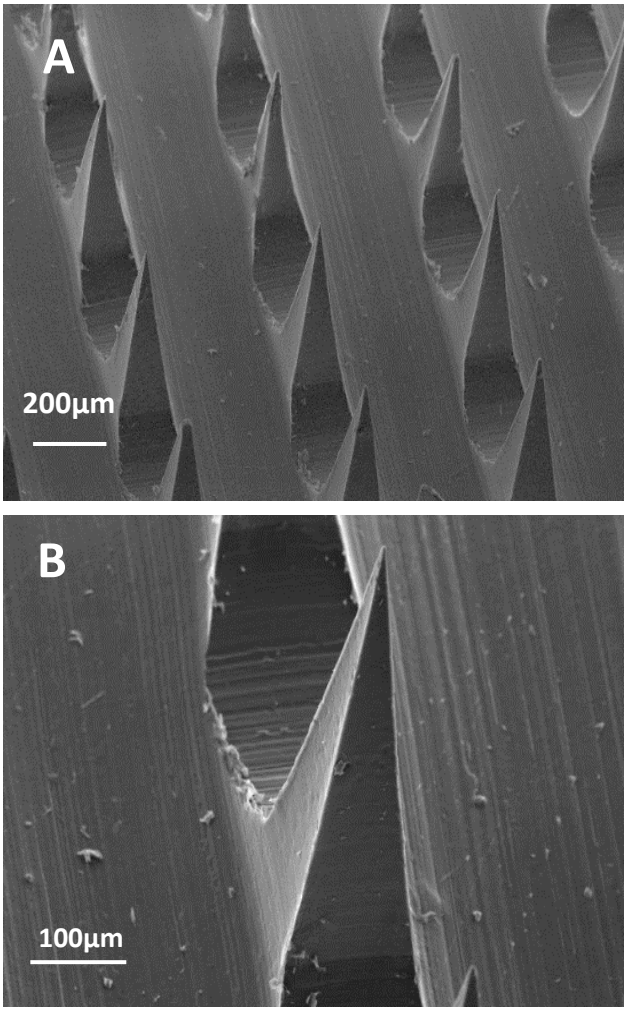

Figure 6.3.1 (A) Electron micrograph of a 10 x 10 microneedle array formed from the solution casting of CAP. (B) Individual morphology of a 400 x 400 x 700 micron CAP microneedle

Scanning electron micrographs detailing the structure of a MN array (height: 350 µm) cast from a solution of CAP without any additional components are highlighted in **Figure 6.3.2**. Well defined tips were attained which were found to be stable in solutions where the pH is acid/neutral. The microneedle array was then exposed to pH 8 buffer and the successive images recorded after 1, 3 and 5-minute intervals. The MN structure gradually dissolves and confirms the pH sensitivity of the system as indicated in the electron micrographs (B-D).

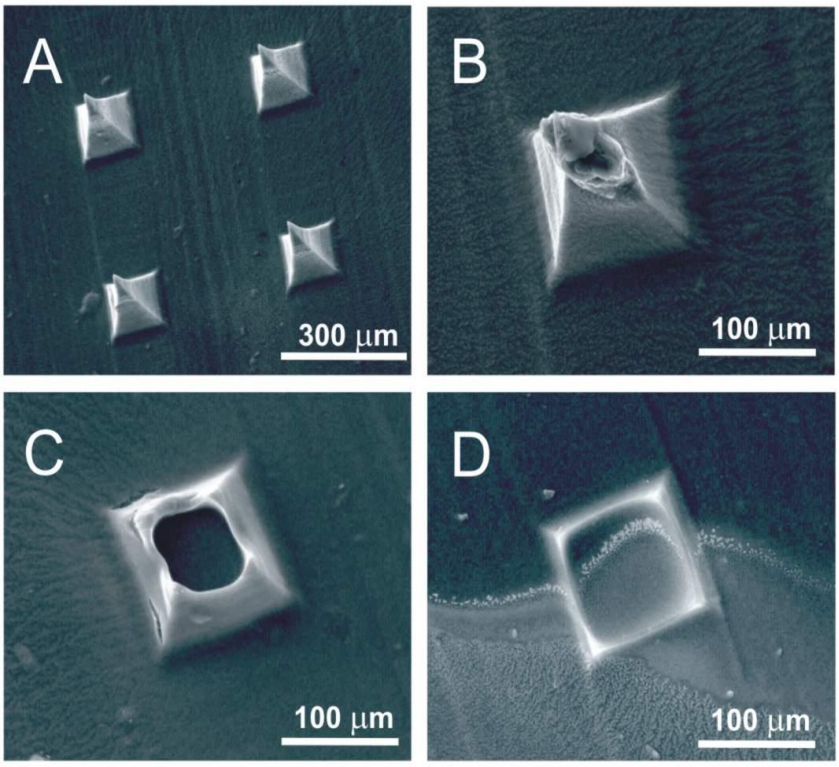

Figure 6.3.2 Scanning electron micrographs of the cellulose acetate phthalate microneedles upon exposure to pH 8 Britton Robinson buffer. Recorded at (A) 0 minutes (B) 1minute (C) 3 minutes and (D) 5 minutes. Microneedles: 200 x 200 x 350 μm

6.3.2 Characterisation of Carbon Nano Powder-CAP Microneedle Array

The process was repeated but using the nano carbon CAP (CAP-C) formulation. The electron micrographs detailed in **Figure 6.3.3** highlight a markedly increased surface roughness which can be attributed to the particulate nature of the nano carbon particles (mean diameter 100 nm).

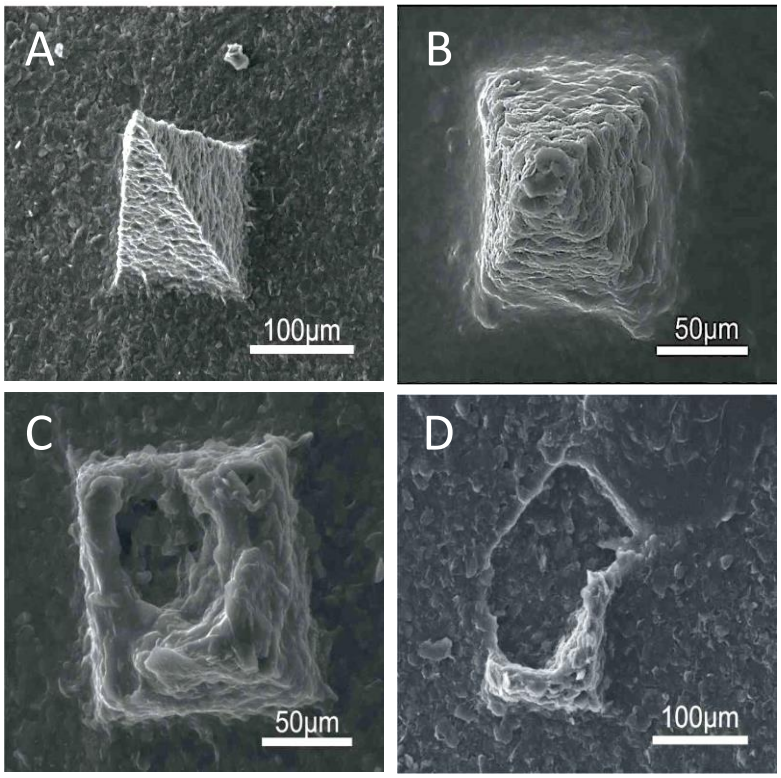

Figure 6.3.3 Scanning electron micrographs of the cellulose acetate phthalate-nano carbon microneedles upon exposure to pH 8 britton robinson buffer. Recorded at (A) 0 minutes (B) 1 minute (C) 3 minutes and (D) 5 minutes. Microneedle: 200 x 200 x 350 µm.

The microstructure of the carbon nano particles are shown in **Figure 6.3.4 A** and the aggregation of the nano carbon particles with the CAP binder is highlighted in **Figure 6.3.4 B,** where a platelet type structure predominates. The MNs are however distinct and behave in a similar fashion to those composed purely of CAP.

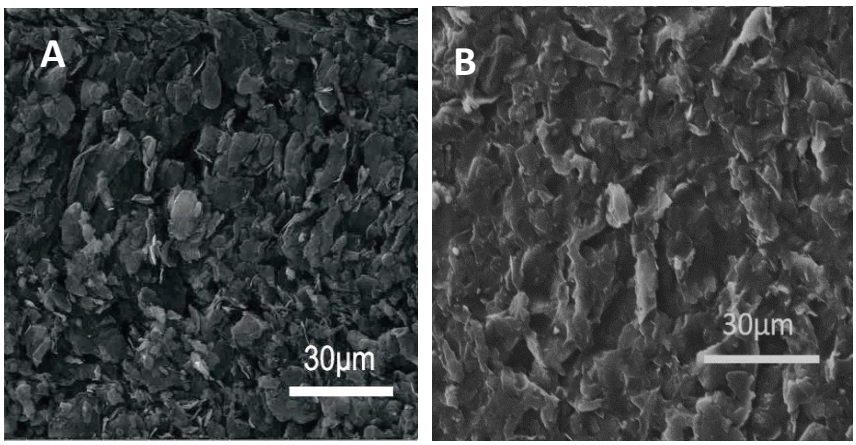

Figure 6.3.4 Electron micrographs of the (A) Carbon nanoparticles and (B) Cellulose acetate phthalate-nano carbon microstructure

Electrochemical Characterisation

Cyclic voltammograms detailing the response of the CAP-C MN array (200 x 200 x 350 µm) towards ferrocyanide and ruthenium hexamine (each solution containing 2 mM redox probe, 0.1 M KCl, 50 mV/s) are highlighted in **Figures 6.3.5 A** and **B** respectively. In both cases, well defined peaks are attained, however, there is noticeable nonconformity from the ideal peak separations of 59 mV. This can be accredited to the composite characteristics of the MN array and a similar performance has been observed with composite Pd-polystyrene microneedle (McConville and Davis, 2016). Nevertheless, the capability of the needles to perform as functional electrochemical sensors is evident.

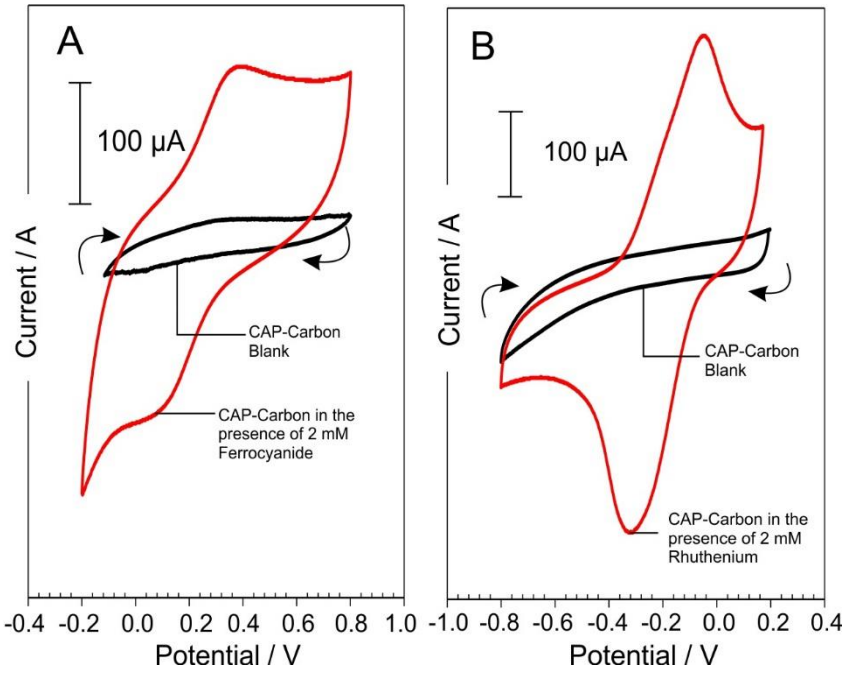

Figures 6.3.5 Cyclic voltammograms detailing the response of the cellulose acetate phthalate-nano carbon microneedles to ferrocyanide (A) and ruthenium hexamine (B). Each redox probe present at 2 mM in 0.1 M KCl. Scan rate: 50 mV/s

6.3.3 Optimisation of Microneedle Response

Palladium is commonly employed to improve the HER process (Zhang *et al.*, 2016b; Lin and Lasia, 2017) and has been applied in the manner of clusters and coatings with graphite (Bhowmik, Kundu and Barman, 2016), carbon nanotubes

(Ramakrishna *et al.*, 2016), graphene (Ghasemi *et al.*, 2015; Cardoso *et al.*, 2017b) and numerous metal alloy systems (Zhuang *et al.*, 2015; Jović *et al.*, 2017) for use in fuel cell applications. The principal methodology here is not to exploit the hydrogen being generated but rather to utilize the change in local pH that occurs as a result of the electrolysis. Given that carbon is a quite poor substrate for the HER process, it was believed that the deposition of the Pd on the MN array would allow a much more effective response.

The CAP-C microneedles were then sputtered with a thin layer of Palladium using an 80:20 Pd/Au target at 30 mA for 3 minutes (Emitech K500X Sputter Coater, Quorum Technologies Ltd, England). This was done to further improve the electrochemical behavior in relation to enhancing the hydrogen evolution reaction, which would be necessary to promote swelling of the needles. The Pd sputtered microneedle array's response towards ferrocyanide (2 mM, 0.1 M KCl) at varying scan rates is detailed in **Figure 6.3.6**.

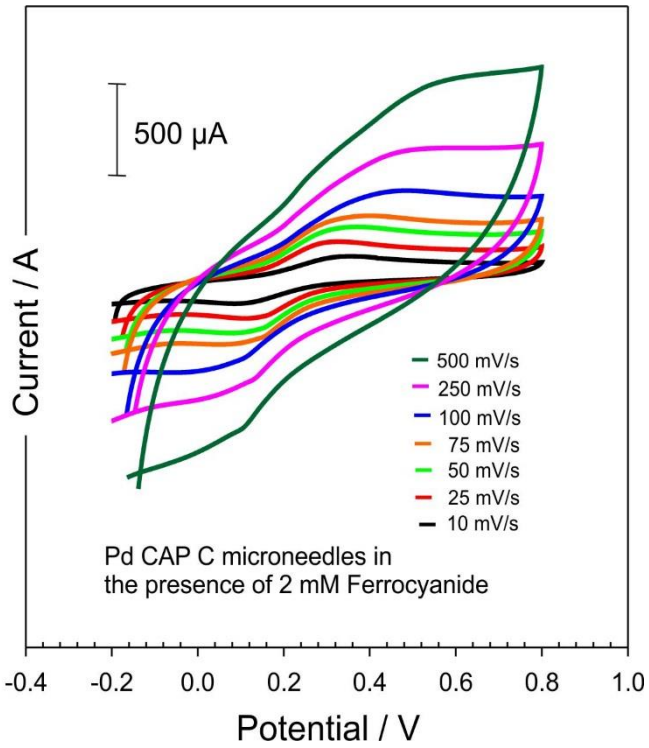

Figure 6.3.6. Cyclic voltammograms detailing the response of the CAP-C-Pd modified microneedles to 2 mM Ferrocyanide at various scan rates

It was observed that the Pd layer enhanced the electrochemical performance as shown by the improvement in the peak definition and separation. Further optimization was carried through the adsorption of a cysteine layer onto the Pd surface as per the work by Macfie (2012) and Feliciano-Ramos (2010) and colleagues (Feliciano-Ramos *et al.*, 2010; Macfie *et al.*, 2012). Cyclic voltammograms detailing the response of the cysteine modified Pd-CAP-C microneedles towards ferrocyanide are compared with the simple CAP-C and Pd-CAP-C needles in **Figure 6.3.7 A**. The peak definition of the former is much improved after the cysteine modification step. The addition of the cysteine onto Pd layers was verified through XPS analysis and comparison of the S_{2p} peak before and after modification as indicated in **Figure 6.3.7 B**.

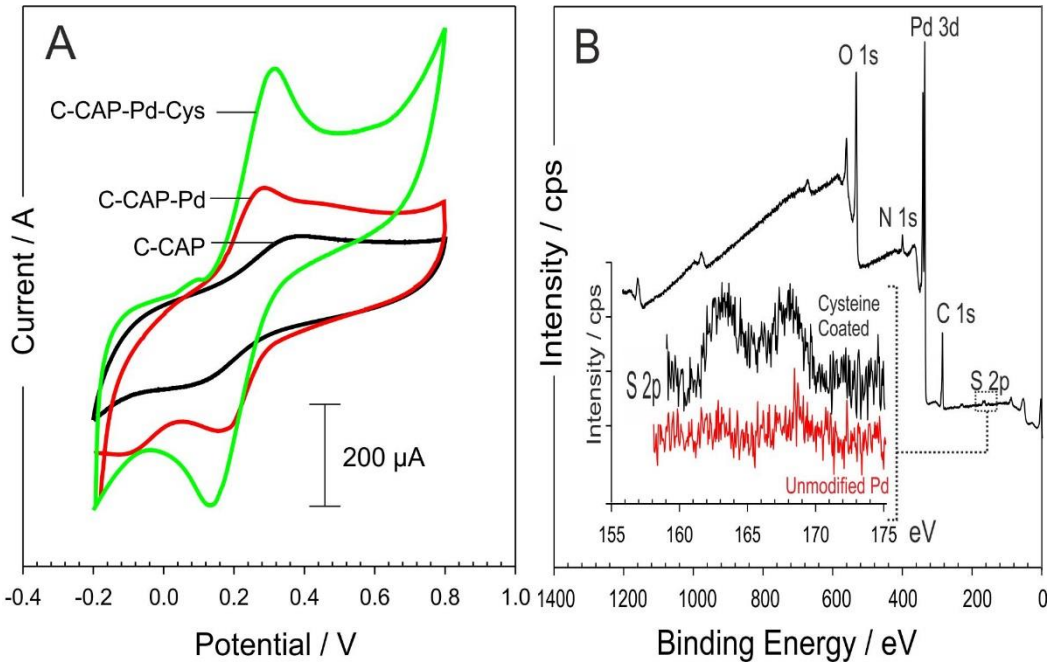

Figure 6.3.7 (A) Cyclic voltammograms comparing the response of the cellulose acetate phthalate-nano carbon microneedles to 2 mM Ferrocyanide before and after modification with palladium and cysteine. Scan rate: 50 mV/s. (B) XPS spectra highlighting the modification of palladium with cysteine

It was predicted that the application of the large reducing potential required to commence HER would also have reduced the Pd-thiol bond, which has been previously demonstrated with gold electrodes (Salvarezza and Carro, 2017), and thus the cysteine modification step was excluded. The advantage of employing the Pd layer can be seen in the linear sweep voltammograms shown in **Figure 6.3.8** where

two difference sets of MN arrays (CAP-C and CAP-C-Pd) where compared under two distinct pH environments. It is evident that the Pd coating provides a significant catalytic effect on the hydrogen evolution reaction.

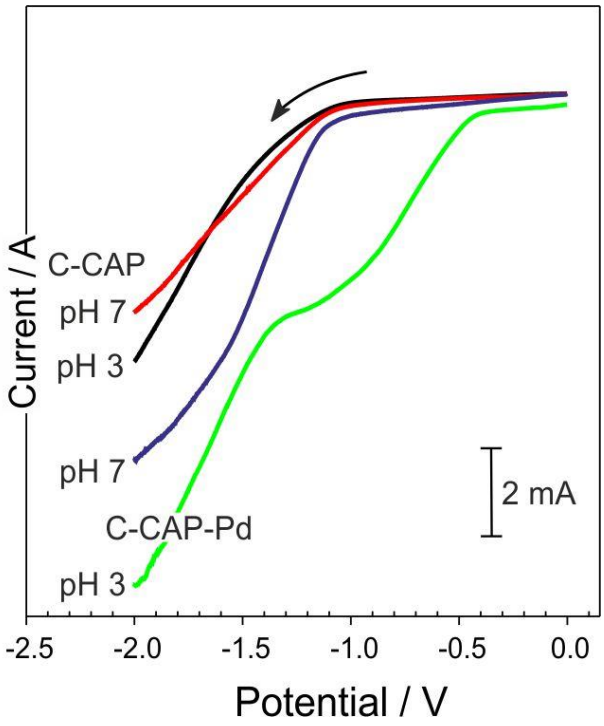

Figure 6.3.8 Linear sweep voltammograms of the unmodified and Pd coated microneedles in pH 3 and pH 7 Britton Robinson buffer. Scan rate: 50 mV/s

6.3.4 Microneedle Response Pre and Post Electrolysis

In order to evaluate the effect of a reducing potential directly at the MN substrate, the Pd sputtered MNs were assessed before the commencement of electrolysis, where distinct oxidation and reduction peaks are observed in **Figure 6.3.9**. A reducing potential of -2 V was then applied in 10 second increments following which a CV was recorded. Post reduction, the peaks become gradually broader and it is difficult to define specific peak potentials. This can be attributed to the fact that as the reducing potential is applied, the binding CAP polymer slowly begins to dissolve thereby exposing more carbon particles resulting in a larger signal. This effect continues until full dissolution of the sensing area of the MN array occurs

thus resulting the signal deteriorating. As dissolution of the CAP binder progresses, connection the structural integrity of the system is compromised as the carbon particles become isolated leading to a reduction in the overall signal.

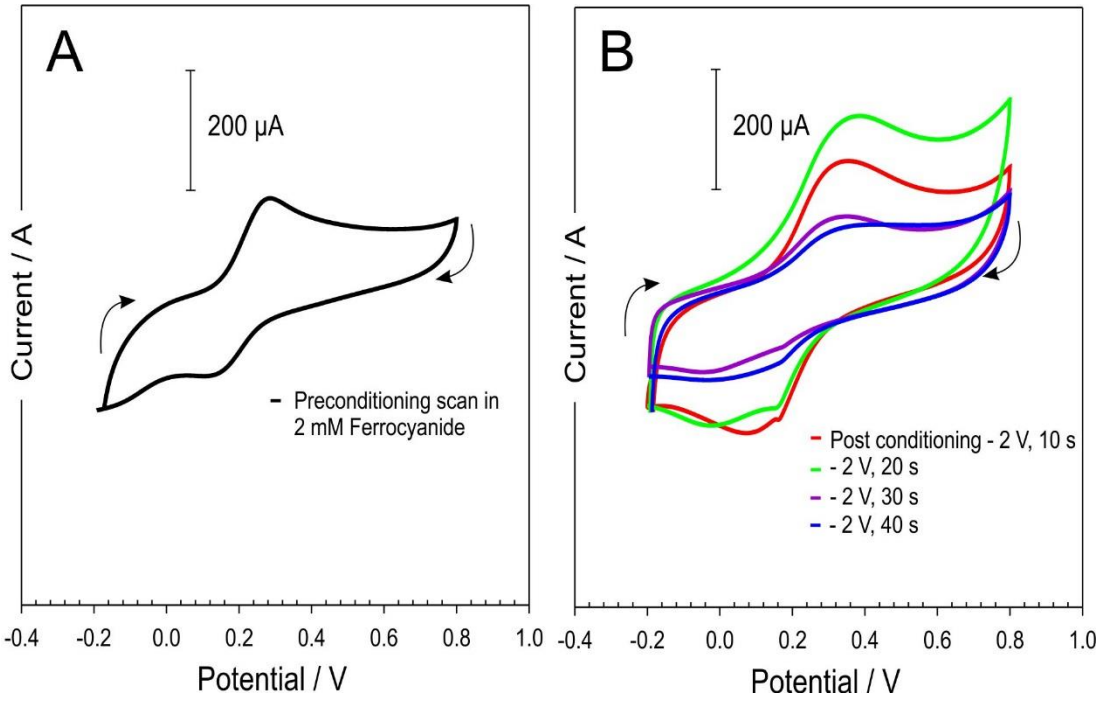

Figure 6.3.9 Cyclic voltammograms detailing the response of the cellulose acetate phthalate-nano carbon-palladium microneedles to 2 mM ferrocyanide (A) before and (B) after holding the electrode at -2 V for given time periods. Scan rate: 50 mV/s

Transdermal Mimics – Simulated Drug Delivery

The next step was to evaluate the ability to control the swelling or dissolution of the MN arrays. A skin mimic system based on calcium crosslinked alginate gel was formulated which contained 2 mM Ferrocyanide, the set-up is detailed in **Figure 6.3.10** and follows the basic procedure developed by McConville and Davis, 2016. The pH of the redox loaded gel was adjusted prior to the addition of the calcium crosslinker to ensure that the gel matrix itself did not lead to the dissolution of the microneedles. A methodology was proposed to mimic the skin's stratum corneum, and was adapted from previous work demonstrated by the Donnelly Group, where a thin layer of parafilm was stretched over the gel in order to closely mimic MN insertion into the skin (Larrañeta *et al.*, 2014). The Pd sputtered microneedles were

then pressed onto the parafilm layer (100 µm) through the application of thumb pressure, with the needle tips penetrating through the polymer film into the gel beneath. A reference electrode (3 M NaCl Ag | AgCl) and Pt counter were then incorporated through the parafilm to complete the cell. Ferrocyanide was incorporated within the gel to act as an *in situ* redox probe that could be utilized to evaluate the structural integrity of the microneedle.

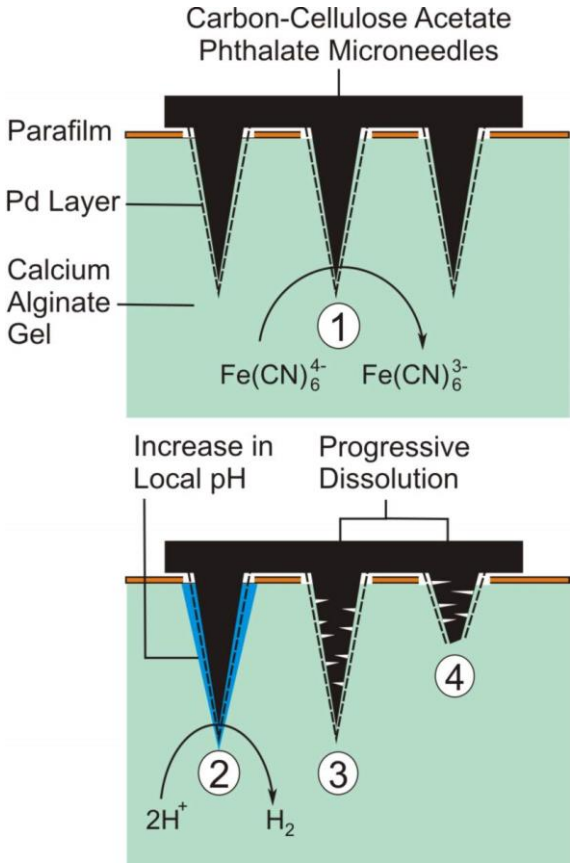

Figure 6.3.10 Representation of the skin mimic assembly highlighting the use of ferrocyanide as a probe to determine in situ the integrity of the needles and the subsequent effects of imposing a cathodic potential

Pd sputtered MNs where compared against cysteine sputtered MNs in the ferrocyanide loaded gel to determine the optimum mode of modification as shown in **Figure 6.3.11.** In this case the Pd sputtered MNs were chosen for further investigation. Due to the implications of the reducing potential that could potentially result in the reduction the Pd-thiol bond, the cysteine modification step was omitted.

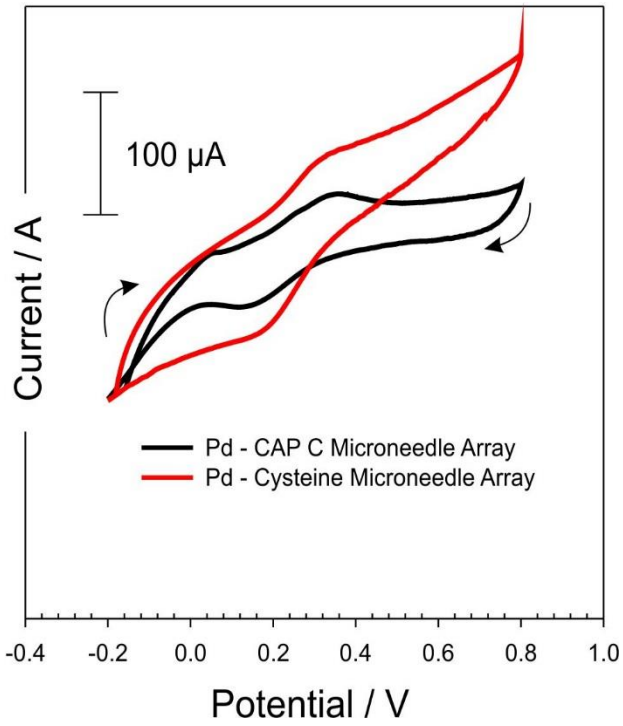

Figure 6.3.11 Cyclic voltammograms comparing the response of the CAP-C microneedles to 2 mM ferrocyanide (within the gel) before and after modification with palladium and cysteine. Scan rate: 50 mV/s

It was envisaged that the application of a cathodic potential would lead to an increase in pH and result in the swelling or dissolution of the CAP binder. As the latter makes up the core structure of the needle array, the surface area of the needles would be transformed. The latter could consequently be measured through variations in the peak magnitude of the ferrocyanide within the gel. Cyclic voltammograms were recorded prior to the commencement of the cathodic potential as a control measure. The ferrocyanide voltammograms were recorded before and after each cathodic step. Cyclic voltammograms presenting the performance of the MN array within the ferrocyanide loaded alginate layer before and after the application of a potential of -2 V are shown **Figure 6.3.12.** Prior to the application of the negative potential, the voltammetric response of the MN array to ferrocyanide is consistent with that observed in **Figure 6.3.11**.

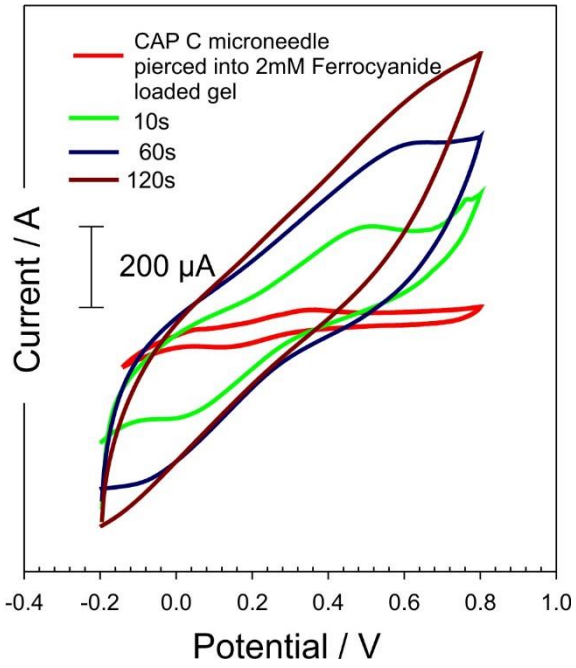

Figure 6.3.12 Cyclic voltammograms detailing the response of the cellulose acetate phthalate-nano carbon-palladium microneedles to 2 mM Ferrocyanide before and after holding the electrode at -2 V for given time periods. Scan rate: 50 mV/s

The voltammetric profile however transforms markedly upon initiating hydrogen evolution with a loss of peak definition. The absence of peak definition be accredited to amplified resistance within the bulk of the needle assembly because of the CAP swelling and expanding the three-dimensional separation among the carbon particles. The swelling and dissolution of the MN was corroborated through surveying the needle morphology following the application of the cathodic potential at various time intervals. Electron micrographs detailing the influence of holding the electrode at negative potentials (-1 V, -1.5 V and -2 V) on the dissolution of the microneedle assembly are shown in **Figure 6.3.13.** In each case - the electrode was held for a period of 30 s. The dissolution of the assembly is perceptible at -1.5 V and is complete after holding at -2 V for 30 s. It is evident, from examining the cyclic voltammograms, that the resistance enlarges considerably upon the application of the cathodic potential for very brief cycles demonstrating that swelling occurs relatively promptly, but dissolution necessitates much more vigorous conditions. The continual response detailed in **Figure 6.3.12** after the perceptible dissolution of the

needle (indicated in **Figure 6.3.13 D**) is accredited to the remaining electroactivity of the base plate.

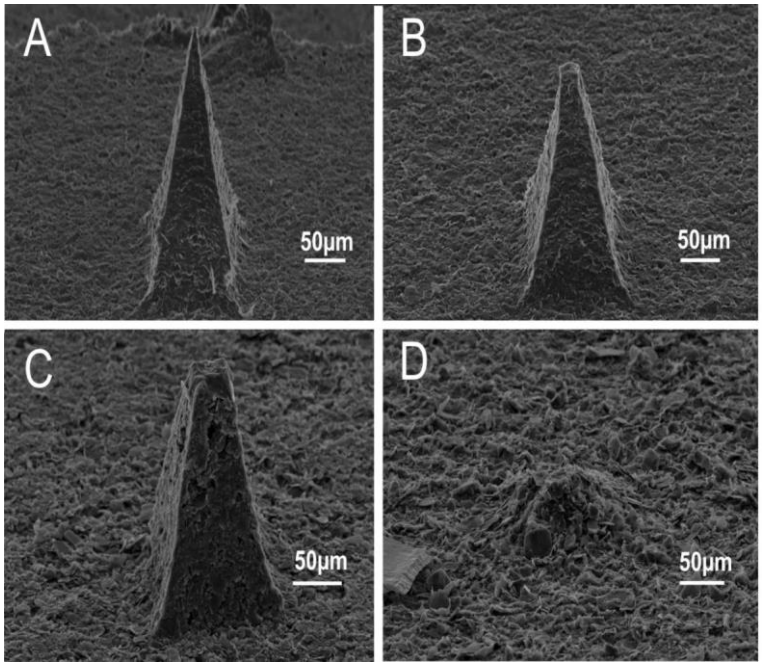

Figure 6.3.13 Scanning electron micrographs of the cellulose acetate phthalate-nano carbon microneedles after imposing the reducing potential. (A) Open circuit (B) -1 V for 30 s (C) -1.5 V for 30 s (D) -2 V for 30 s. Microneedle: 200 x 200 x 700 µm

It must be taken into account however that, provided that the needles are suitably shallow, residual needle fragments are likely to be removed from the skin through normal skin shedding in the external layers which would typically happen over a period of weeks (Baran and Maibach, 2010). The biocompatibility studies of the CAP-C material - detailed in Chapter 5, deliver some encouraging insights into the possible use of the material with no evident skin irritation nor cytotoxicity nevertheless these need to be regarded with some caution – especially where the devices may be used for long term purposes where sensitisation may transpire.

6.3.5 Model Drug Release

Prior to the commencement of the controlled electrochemical release studies, the modified CAP-C MNs were inserted into a gelatin matrix preloaded with phenolphthalein (1 mM, 0.1 M KCl). The latter remains colourless in acidic conditions and turns pink when exposed to pH environments greater than pH 7. A sample of the gel was tested as a control, an aliquot of 0.1 M NaOH was added to the gel to confirm that the phenolphthalein had been adequately dispersed within the gel. The MNs were then pressed into the gelatin. Visual inspection of the gel interface (**Figure 6.3.14)** confirmed that the needles penetrate the gel and are intact. The MNs were then removed from the gel and the site of insertion remained colourless.

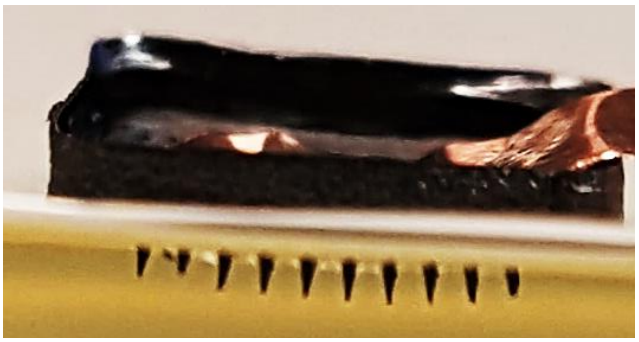

Figure 6.3.14 Cross-section of MN array piercing through gelatin

A reducing potential of -2 V was applied to the CAP-C MNs for increments of 10 s, after which the MN arrays were removed, and the puncture site inspected. After the initiation of the cathodic potential to the MNs, there will be an increase in pH directly at the needle site thus changing to colour of the phenolphthalein loaded gel from colourless to pink. After each reducing increment, the microneedles where removed and inspected as shown in **Figure 6.3.15**.

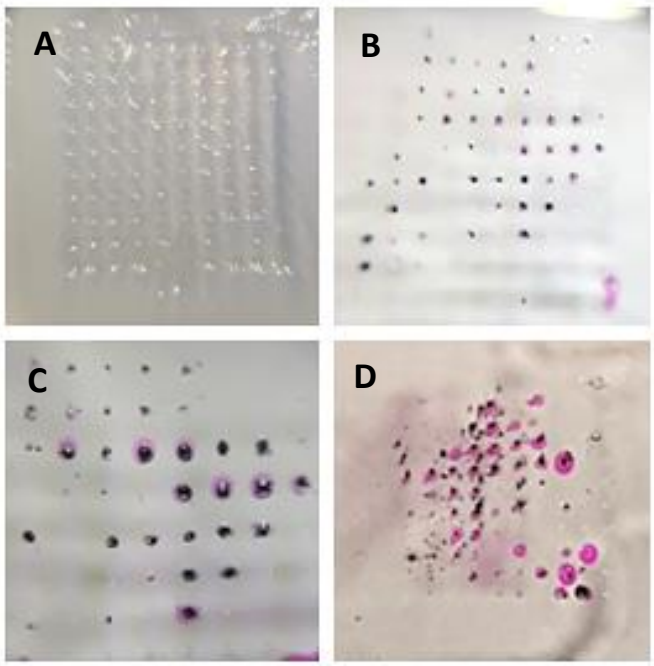

Figure 6.3.15 Images captured of the phenolphthalein loaded gel (A) Before reduction (B) -2 V, 20 s (C) -2 V, 40 s (D) -2 V, 60 s

The next step was to assess the efficacy of the release method with a model drug – Toluidine Blue O (TBO). The CAP-C was added to a solution of TBO in cyclohexanone and stirred until a viscous solution was achieved. TBO was chosen as the release agent as it could be easily monitored through visual inspection. Thus, the initiation of the reducing potential would release the entrapped TBO and it was expected that it would slowly permeate through the gelatin matrix. Prior to the commencement of electrolysis, the MNs were pierced into pH adjusted gelatin (pH 4.02) and removed to ensure there were no observable traces of released TBO. Electrochemical release was induced through holding the potential at −2 V, at 10 s increments (up to 50 s) and then visually inspected after the application of each cathodic cycle (**Figure 6.3.16)**. Although a strong blue colour was observed upon changing the pH, there is a possibility that there is release of TBO from the baseplate which is in contact with the gelatin. To ensure the TBO was released exclusively from the needles, the MN array was first pierced through a layer of parafilm, which acted as a skin mimic, before being placed in the gel in order to separate the baseplate from the gelatin. Therefore, after the application of the reducing potential to the microneedle array

as shown in **Figure 6.3.16**, any blue colour observed in the gel can be attributed to the release from the microneedles exclusively.

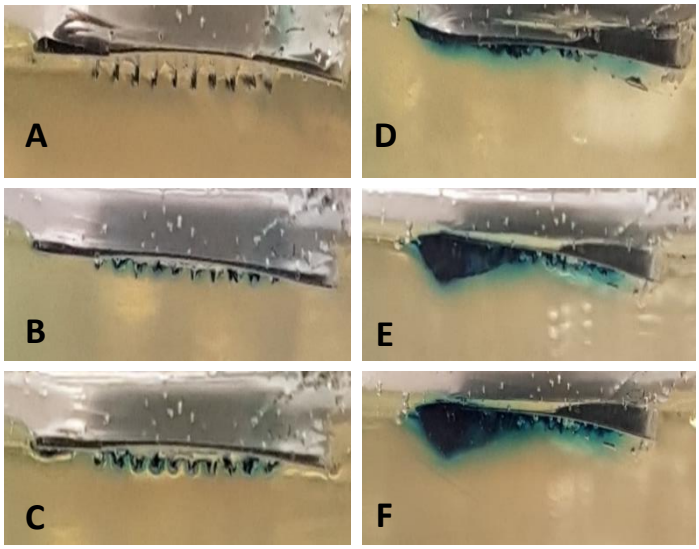

Figure 6.3.16 CAP-C MNs loaded with TBO before and after the commencement of electrolysis for varying times. (A) Before electrolysis (B) – 2 V, 20 s (C) – 2 V, 40 s (D) – 2 V, 60 s (E) – 2 V, 80 s (F) – 2 V, 100 s

Drug Delivery Candidates

In recent years, the development of microneedles for drug and vaccine delivery has been extensively studied. In vivo studies using MN arrays have demonstrated the successful delivery of several drug candidates, including; insulin delivery (Cegla, 2015; Xie, Li and Yu, 2015), low molecular weight heparin (Gomaa *et al.*, 2012) and human growth hormone delivery (Lee *et al.*, 2011). Each category of microneedles has been comprehensively studied for a number of different applications, examples of which are detailed in **Table 6.3.1**.

At the present time, there are a number of companies that are currently developing MN-based products which include : 3M (USA), Becton - Dickinson (BD) Technologies (USA), Nanopass Technologies (Israel), Valeritas (USA) and Lohmann Therapie – Systeme AG (Germany / USA) the largest manufacturer of transdermal patches. Currently, there are no MN array-based drug delivery products on the market. Nanopass technologies have developed a combination microneedle system equipped with four hallow silicon microneedles which can be attached to a syringe driver. This

MN-based medical system is not a true MN array for drug delivery, rather it is a delivery system combined with microneedles (no release from microneedles) which aids the delivery of a drug from a syringe driver through the stratum corneum.

Table 6.3.1 Drug delivery from MN systems and their applications

MN Type	MN Material	Drug Loaded	Drug Content Delivered	Application	Reference
Dissolving polymeric MN array	Poly (methyl vinyl ether / maleic Acid) (PMVE / MA)	Ibuprofen sodium	33 mg over 24 hr.	Non-steroidal anti-inflammatory drugs (NSAIDs)	(McCrudden *et al.*, 2014)
Dissolving polymeric MN array	Poly (vinylpyrrolidone) (PVP) and Poly(methyl vinyl ether/ maleic acid) (PMVE /MA)	Aspirin Lisinopril dihydrate Atorvastatin calcium trihydrate	3924 ± 1011 µg 687.9 ± 101.3 µg 126.3 ± 18.1 µg	NSAID Angiotensin-converting-enzyme inhibitor (ACE inhibitor) Statin	(Quinn *et al.*, 2015)
Dissolving MN patch	Sodium carboxymethyl cellulose (SCMC)	Anti - calcitonin gene – related peptide (CGRP8-37)	1.42 $\pm$ 0.65 µg	Analgesic effects for localized neuropathic pain	(Xie *et al.*, 2017)
Dissolving MN patch	Hydroxypropyl cellulose (HPC)	Cyclosporin A (CyA)	34 $\pm$ 6.5 µg after 60 min.	Treatment of psoriasis	(Jeong *et al.*, 2018)
Tip-loaded dissolving microneedles	MN Tips - hydroxy-propyl-methyl-cellulose (HPMC) Baseplate – carboxy-methyl cellulose (CMC)	Donepezil hydrochloride (DPH)	179.9 µg	Alzheimer's disease	(Kim *et al.*, 2016)
Tip-dissolving microneedles	Polyvinylpyrrolidone (PVP)	Meloxicam (MX)	272.96 µg	NSAIDs	(Chen et al., 2017)
Hydrogel-forming microneedles with integrated drug film	15% w/w Gantrez S-97, 7.5% w/w PEG, 10,000 and 3% w/w Na_2CO_3	Donepezil hydrochloride (DPH)	854.71 ± 122.71 µg	Alzheimer's disease	(Kearney *et al.*, 2016)

It is envisaged that the MN array patch system within this work could be utilised to deliver high potency and low yield drug candidates, such as buprenorphine and fentanyl. Transdermal fentanyl patches have long been established for the effective treatment of chronic pain associated with cancer (Cachia and Ahmedzai, 2011; Othman, Mohamad and Sayed, 2016). This novel approach to delivery using drug loaded MN arrays may potentially lead to a reduction in opioid abuse as previously discussed in Section 1.1. There is also potential for the MN needle arrays to combat some of the issues surrounding patient compliance. Cognitive impairment is a significant issue in geriatric patients who have been diagnosed with Alzheimer's disease (AD) (Lima *et al.*, 2016). The transdermal route for delivery is particularly useful in this case as it does not require the patient to remember to take their medication and provides stable dosage over an extended period of time.

It is also important to highlight the factors which can limit the delivery of drug within this methodology. For example, an issue would be the delivery of pH sensitive compounds such as proteins which, due to the exposure of the high pH environment during electrolysis could lead to denaturation. Also, crucially as the device is using a negative potential, issues may arise if the drug loaded within the MN array contains nitro functional groups which could, in principle, be converted to the nitroso, hydroxylamine or amine group.

Due to the lack of commercially available microneedle products, and their relative infancy of development, there are currently no regulatory requirements documented for MN array systems. No doubt this concern will be addressed in the forthcoming years when companies who intend to commercialise MN technologies proceed with commercialisation procedures, after issues with scale up production methods have been successfully addressed.

6.4 Conclusions

The applied potentials used in this work are significantly negative and have been selected on the basis of allowing gross characteristics to be observed with relative ease for the intention of confirming proof of concept. The use of more moderate potentials would certainly reduce the degree of pH modification and thus, rather than initiating a rapid release, could permit a much more controlled rate of dosage devoid of the rapid deterioration of the microneedle structure. The result of using less negative potentials also lessens the potential migration of nano carbon/Pd particles into the skin. The approach reported underlines a new route through which microneedle structures could be controlled in situ and thereby offer alternative means of controlling dosage.

The micro moulding method undoubtedly offers a facile means of constructing high quality microneedles which, through astute selection of the casting constituents, could possibly be translated to numerous of sensing and drug delivery applications. The nano-carbon assemblies are conductive and present effective electrochemical properties which could be employed in analytical situations. The modification with Pd is simply accomplished through using standard sputtering techniques employed for coating SEM samples, however the Pd sputtering treatment can deliver substantial improvement to the voltammetric performance. The core impact of the work illustrated however is centred on the ability to electrochemically control the integral structure of the microneedle through regulating the cathodic potential directed to the needles themselves. It is easy to envision the integration of an appropriate drug candidate within the carbon-CAP solution at the time of casting. Drug yield will however be a matter of concern given the restrictions in the dimensions of the microneedle structure. This is a common issue encountered during the development of most microneedle systems and it is expected that the MN assembly developed in this work would only intended for low yield - high potency agents. The application of the cathodic potential, while essential to initiate the polymer swelling, may, in principle, result in the reduction of functional groups within

the drug – for example nitro groups – thereby excluding such reagents from use in the MN system. The likelihood of disintegration and the loss of carbon/Pd particulates should also be considered.

Chapter 7

Smart Sutures – A Novel Approach to Electrochemical Drug Release from Micro-Wires

Abstract

The work described within this chapter assesses the use of a gold microwire loaded with cellulose acetate phthalate encapsulated drug droplets as a novel approach for the electrochemically driven drug release from a suture. The imposition of hydrogen evolution reaction at the wire leads to an increase in the local pH and the subsequent dissolution of the pH sensitive cellulose acetate phthalate polymer binder and release of the drug. Precise control over the electrochemically induced dissolution-release mechanism has the potential to give rise to the further development of smart suture design where more responsive and accurate dosing could be achieved.

Part of the research described in this chapter has been published in Morelli, F., Anderson, A., McLister, A., Fearon, J. J., & Davis, J. (2017). Electrochemically driven reagent release from an electronic suture. *Electrochemistry Communications*, 81(May), 70–73.

7.1 Introduction

Sutures are an instrumental tool in the mending and physical restoration of major wounds, injuries or lacerations where they present a facile means of joining apposing tissues and, in effect, can assist in wound healing (Seitz *et al.*, 2015; Dennis, Sethu, Nayak, Mohan, Y. Y. Morsi, *et al.*, 2016a; Alshomer *et al.*, 2017; Wu *et al.*, 2017). While the general technique of wound closure has altered little over the years, the materials selected in the manufacture of sutures have advanced significantly. Biodegradability, physical structure and chemical composition are the main features subject to modification or adaption and there is an abundance of commercially available forms (Alshomer *et al.*, 2017; Wu *et al.*, 2017). Sutures which possess antimicrobial properties are now commonplace and have been employed as a consequence of the enduring issues surrounding surgical site infection (SSI) (Wu *et al.*, 2017). The latter are commonly recognised as being the most regularly encountered postoperative complication and correspond to 15–20% of all nosocomial infections that develop after surgery (Owens and Stoessel, 2008; De Angelis *et al.*, 2010). It has been established that sutures loaded with antimicrobial agents (such as triclosan or silver nanoparticles) decrease recurrence of infection and aid wound healing (Catanzano *et al.*, 2014; Zhang *et al.*, 2014; Gallo *et al.*, 2016; Yamashita *et al.*, 2016; Alshomer *et al.*, 2017; Wu *et al.*, 2017). The mechanical properties of sutures can be tailored to meet the functional requirements of the wound site and can be achieved by braiding or coating the surface of the suture material. A commercially available braided black silk suture is shown in **Figure 7.1.1**. Regardless of design, conventional sutures are characteristically based on a thread-like arrangement to supply the mechanical strength necessary to bind the wound edges together and, subsequently, the antimicrobial attributes are consistently supplied through passive contact with the adjacent tissue (Alshomer *et al.*, 2017).

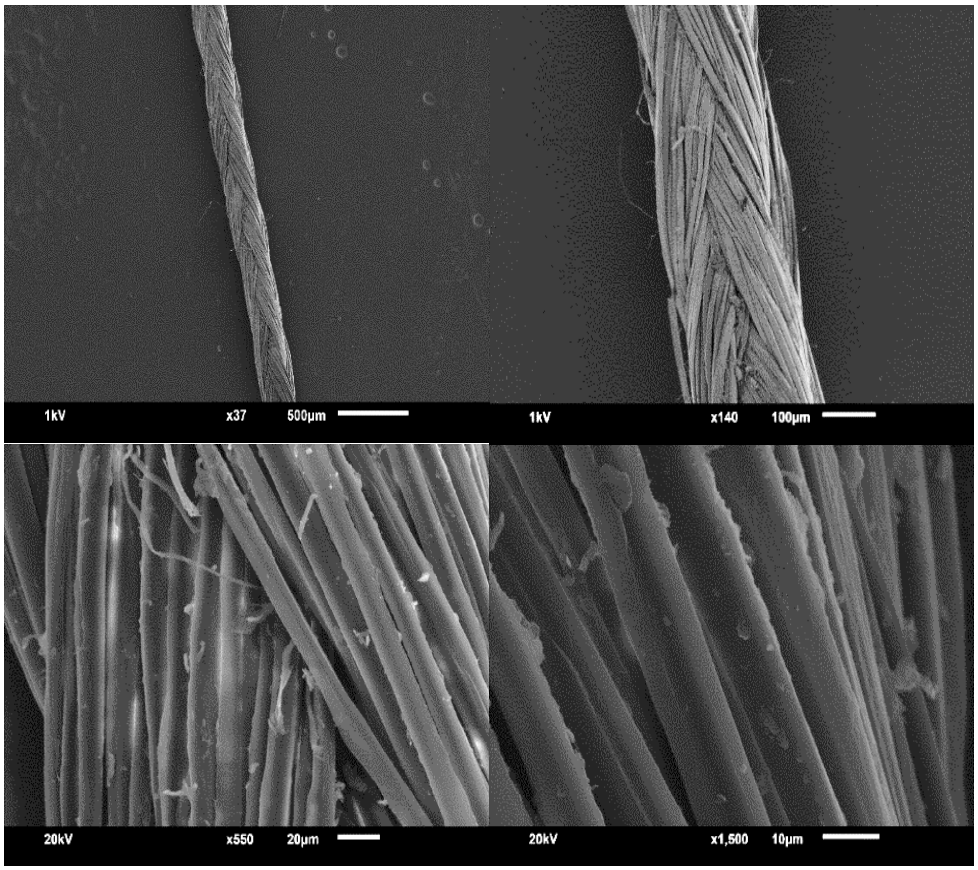

Figure 7.1.1 Electron micrograph of braided black silk suture

Taking into the account the growing concerns over antimicrobial resistance, there is a necessity for additional advances in suture design where the latter can provide a more functional role – either through imparting diagnostic telemetry of the wound healing rate or allowing the direct delivery of drugs to the infection location. The aim of this chapter is to assess the use of a gold–silver composite thread as a structure through which the electronically controlled release of a chemical agent from a suture could be achieved. Previous work by Kim and colleagues (2012) investigated the development of a microfabricated strip sensor equipped with sensory feedback modules and actuation capabilities which has given way to a step change in suture design (Kim *et al.*, 2012b). The current investigation has likewise sought to advance the controlled actuation mechanism through a potentially straight forward, though more adaptable and easily employed electrochemical route. The under lying principle involves the loading of the model drug (Toluidine Blue O, TBO) within cellulose acetate phthalate (CAP) binder droplets which have spread and distributed along the length of a gold microwire (25-100 µm diameter) as illustrated in **Figure 7.1.2**. The

CAP polymer binder is pH responsive as noted in previous chapters (Kelley *et al.*, 2011; Dasan and Rekha, 2012; Bertz *et al.*, 2013; Hanafi, Nograles, Abdullah, Shamsudin, Rosli, *et al.*, 2013; Ashayer-Soltani, Hunt and Thomas, 2016; Wong *et al.*, 2017b). Similarly, it was envisaged that the application of a reducing potential (-1 V to -2 V) at the gold electrode microwire would lead to an increase in the local pH and the CAP binder should dissolve and in doing so release the entrapped drug (A. Anderson, McConville and Davis, 2015). The gold wire itself does not possess the required tensile strength to draw the wound edges together but it can be reinforced by braiding the wire within a conventional suture thread. During investigations, a commercial silver thread was employed to improve mechanical suture strength and served as a second electrode in the electrochemical set up. This work assesses the electrochemical response of several mechanisms and examines the capability of the proposed release mechanism.

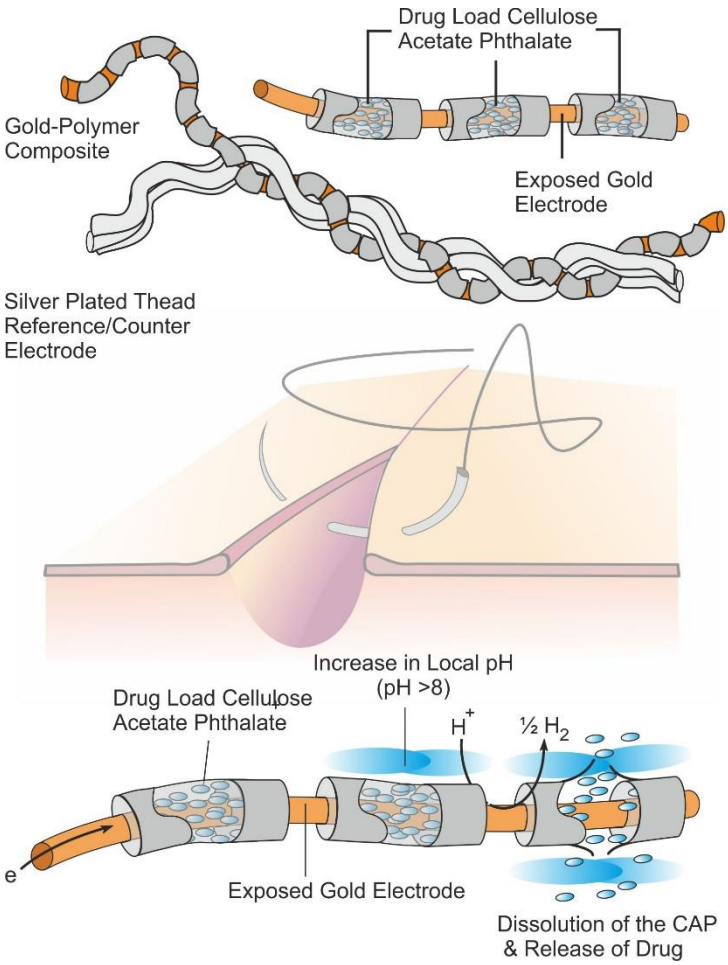

Figure 7.1.2 Proposed controlled release methodology

7.2 Experimental Details

7.2.1 Materials

Chemical reagents were of the highest grade available and used without any additional purification. All electrochemical measurements were carried out at 22^{o}C ± 2^{o}C in Britton Robinson (BR) buffer (pH 3-9, adjusted to the appropriate pH value via the addition of sodium hydroxide). Cellulose acetate phthalate and Toluidine Blue O were supplied by Sigma Aldrich. Gold and silver wires were supplied by Goodfellow Ltd (Huntingdon, UK). Conductive silver thread (0.4 Ω/cm) was supplied by Kitronik Ltd (Nottingham, UK).

7.2.2 Electrochemical Setup

Electrochemical analysis and set up was performed using a μAutolab computer controlled potentiostat (Eco-Chemie, Utrecht, The Netherlands). The initial electrochemical measurements involved a three electrode configuration, comprised of a conductive wire working electrode, a platinum wire counter electrode and a standard silver/silver chloride (3 M NaCl, BAS Technicol UK) reference electrode. A two electrode set-up was used in further experiments which employed a conductive silver thread, utilised as a combined counter-reference electrode. The conductive silver thread (0.4 Ω/cm) is comprised of 96 singular filaments, each coated with a micron-thick layer of silver. The production procedure involves a primary twist comprising 16 filaments of cotton. Two primary twists are then wound together to form the secondary twist and finally three of the latter are combined to yield the final thread consisting of 96 filaments and is approximately 18 denier.

7.2.3 Sensor Design and Modification

The Toluidine Blue O (TBO) (5 wt%) was first dissolved in a solution of acetonitrile and the CAP was added to this mixture and left to stir until the CAP was fully dissolved and incorporated within the solution. The TBO/CAP mixture was then dropped and spread along the length of the gold wire. Although it was originally anticipated that addition of the TBO/CAP mixture to the gold would have led to an evenly coated film, the polymer spontaneously merged into isolated droplets along the length of the wire as an effect of surface poor wetting as indicated in **Figure 7.2.1**.

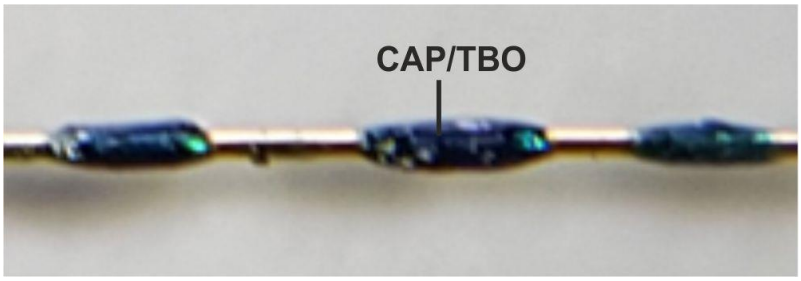

Figure 7.2.1 Image of the CAP-TBO modified gold wire

This coating procedure was repeated up to 4 times to enhance the yield of TBO. The modification steps and the configuration of the gold – polymer composite electrode with the combined counter-reference electrode are detailed in **Figure 7.2.2**. Electrochemical release was initiated through holding the potential of the coated wire at potentials ranging from -1 V to -2 V for a given period (typically 10 s) in line with the previous methodology followed within Chapter 6, to induce polymer swelling and dissolution of the protective CAP binder. The released TBO was then sampled by recording the absorbance spectrum (200-800 nm) in a 1 cm^3 volume cuvette.

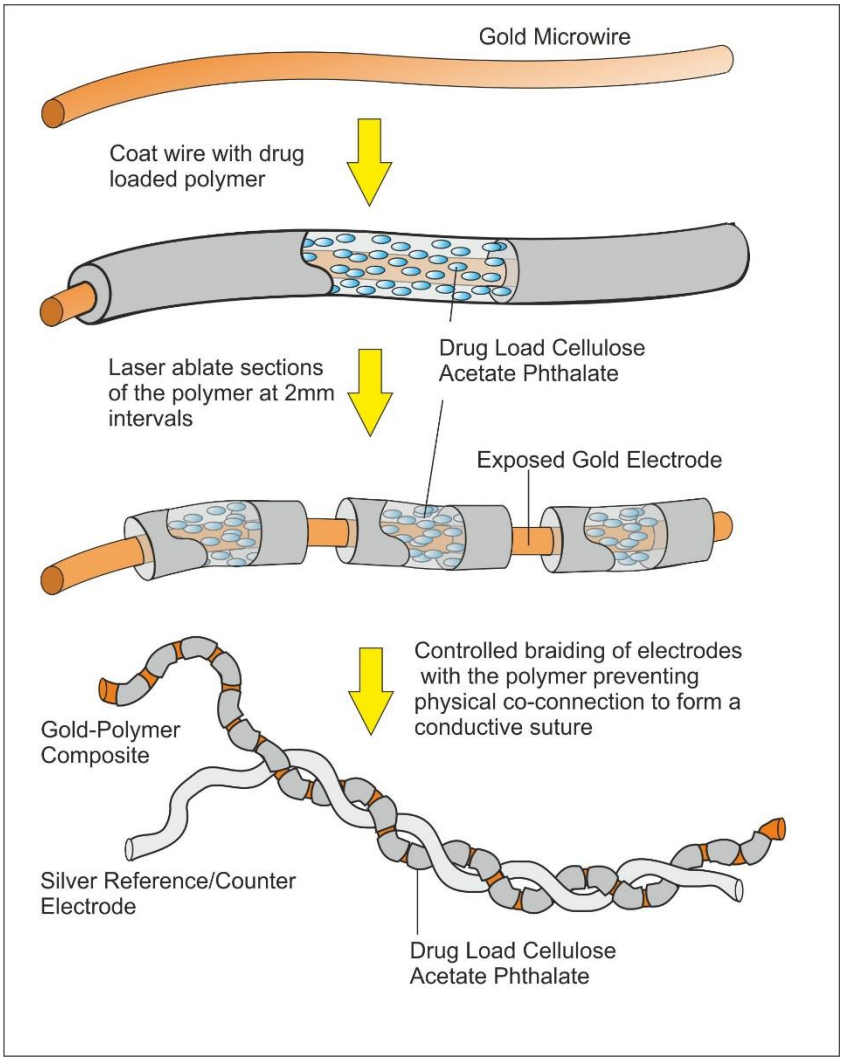

Figure 7.2.2 Modification steps of gold wire

7.3 Results and Discussion

Characterisation of the Thread Reference Electrode

The potentiometric response of the silver thread to a range of chloride concentrations was tested in a range of chloride solutions (1 mM to 1 M). A plot of average potential against the Log of the chloride concentration was found to be linear and exhibited Nernstian behaviour ($E/V = -0.060 \log[Cl^-] + 0.0103$; $N = 4$; $R^2 = 0.999$) with a 60 mV shift with each decade shift in chloride concentration as shown in **Figure 7.3.1.**

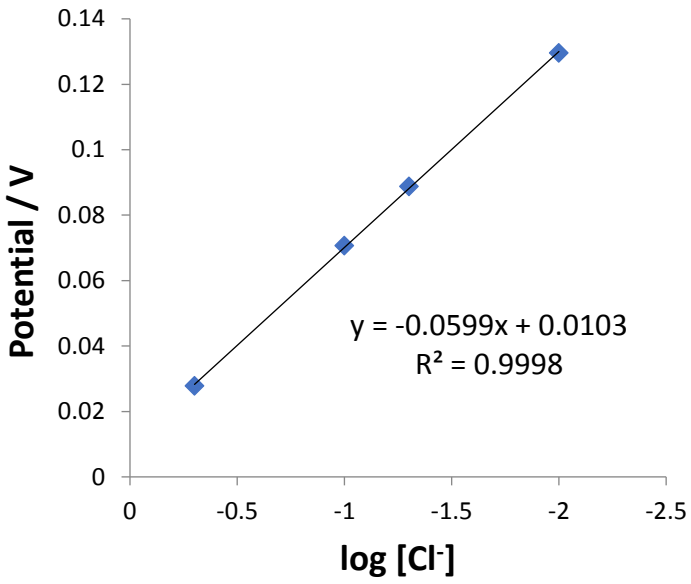

Figure 7.3.1 Silver thread reference potentiometric response to chloride concentration

7.3.1 Characterisation of Gold Wire and Toluidine Blue O Coating

The practicality of employing cellulose acetate phthalate as the controlled release polymer was briefly evaluated using gelatin as the simulated tissue matrix. Toluidine Blue O was utilised as a model drug as its release could be readily observed through visual examination or, as reported later, through UV–vis spectroscopy (λmax = 591 nm, ε = 2.98 × 103 L^{-1} mol cm^{-1}). The first step was to thoroughly rinse the coated wire to remove any interfacial TBO, to ensure that the only dye present was trapped within the polymer matrix. The thread was then submersed in specific pH adjusted gelatin and left in the sample for 48 h. The results from the pH - time study are shown in **Figure 7.3.2 A-F**, where it is evident that the TBO layer remains intact at pH 6 and where the blue coloration only appears when the TBO coating is exposed to alkaline conditions.

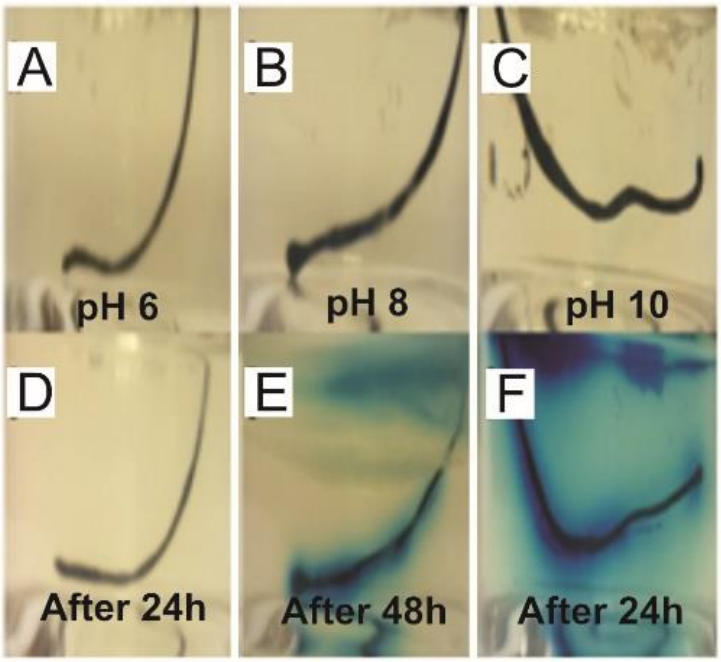

Figure 7.3.2 A-F Release of Toluidine Blue O from cellulose acetate polymer coating on thread immersed in gelatin of varying pH (A–F)

During the time study, it was observed that the dissolution of the CAP occurred very slowly from neutral or mildly alkaline (pH 8) where the outwards diffusion of the TBO into the gelatin matrix was observed after 48 hours. The CAP/TBO droplets arranged on the gold wire (100 µm) are presented in **Figure 7.3.3 A**, although their visible arrangement is overstated for clarity. The construction of the conductive thread is shown in **Figure 7.3.3 B** and it can be observed that while each individual fibre has been silver coated, however upon closer inspection, it can be seen that there are some areas where the underlying cotton is exposed.

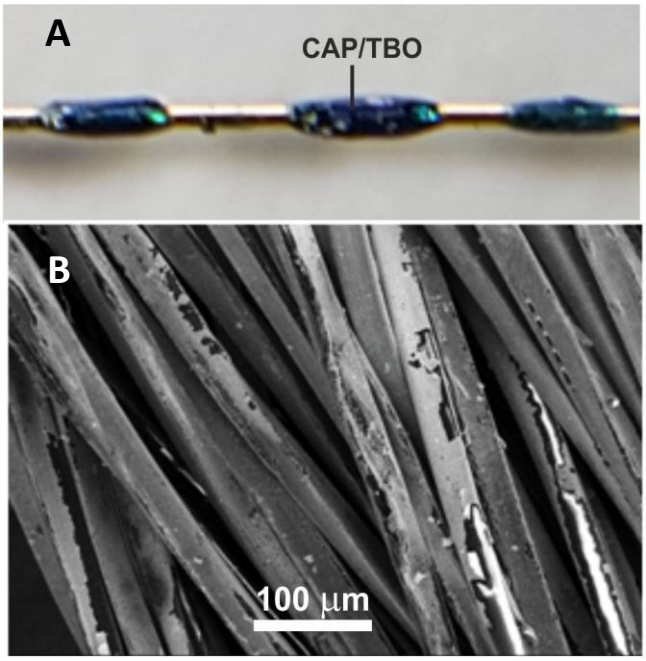

Figure 7.3.3 (A) Gold microwire (100 μm) modified with CAP/TBO droplets. (B) Electron micrograph of the silver suture thread

This aligns with earlier reports of electroless deposition of silver on fabrics and can be anticipated where the plating suspension has not been successful with nucleation on specific areas or perhaps where the thread braiding has inhibited adequate penetration (Ashayer-Soltani, Hunt and Thomas, 2016; Liu, Hu and Yang, 2016; Lui *et al.*, 2017). Nonetheless, the silver deposition undoubtedly spreads along the length of the thread and is suitably consistent to maintain conductivity when twisted or sewn, which is ideal for the intended application. It should be noted that the core rationale for the commercialisation of the thread was directed at developing 'e-fabrics' and wearable electronics and was constructed exclusively for sewn and woven purposes. The capability of the thread to function as a feasible reference/counter electrode was evaluated through comparing the potentiometric response to chloride ion whereby a Nernstian response (−59 mV) was obtained.

7.3.2 Toluidine Blue O Release in pH Buffer

Quantitative assessments of TBO release from the microwire were conducted using UV-Vis spectroscopy. A section of wire, previously coated in the CAP/TBO solution, was thoroughly rinsed to remove any residual TBO and placed in pH 4.75 buffer and left for 1 hour. A blank scan was initiated and revealed that no TBO was released into the background solution as shown in **Figure 7.3.4** (green line). The process was repeated with a new section of wire and placed in a buffer solution at pH 9.75 and was subjected to the same conditions. Upon completion of the scan, it was evident that the higher pH environment had indeed initiated successful release of the TBO into the solution (blue line).

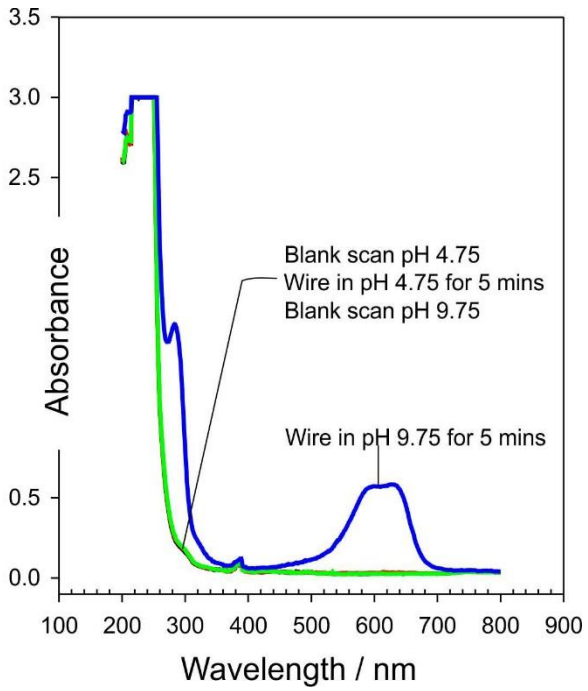

Figure 7.3.4 Spectra detailing the absence of TBO in pH 4.75 buffer (green line) and the emergence of TBO in pH 9.75 buffer (blue line)

Tensile Strength Testing

The tensile strength of the conductive silver thread was tested and was found to be 1.6 N/Tex (% RSD = 9.1; N = 6) which behaved favourable when measured against a conventional Vicryl® braided suture (0.57 N/Tex) (Kelley *et al.*, 2011). It could then be envisaged that the electronic thread structural support to bring together the apposing wound edges together and facilitate closure. The electrochemical response of a gold microwire (50 µm diameter) in the presence of ferrocyanide (2 mM, 0.1 M KCl) is detailed in **Figure 7.3.5** utilising a conventional three-electrode set up with a 3 M NaCl half cell reference and a platinum wire served as a counter electrode.

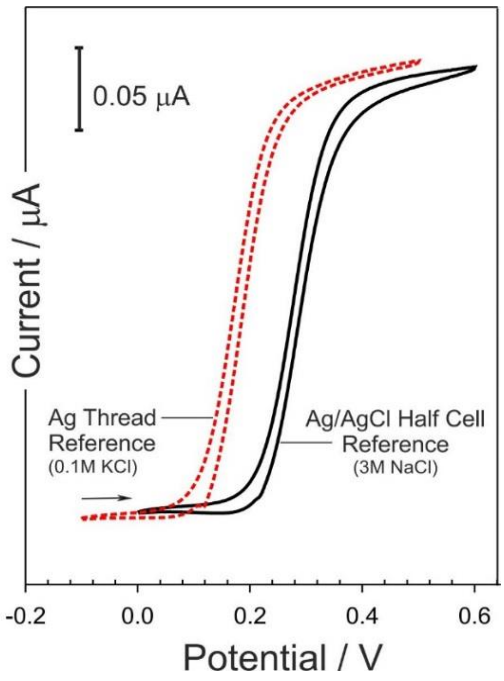

Figure 7.3.5 Cyclic voltammograms detailing the response of a gold wire (50 µm) towards ferrocyanide (2 mM, 0.1 M KCl, 5 mV/s) using three-electrode (solid line) and two-electrode (dashed line) configurations. Silver thread was used as the combined reference counter in the two electrode (prototype suture) investigation

The voltammetric profile generates a sigmoidal cyclic voltammogram distinctive of microelectrode performance (Stephen Fletcher and Horne, 1999), as expected due to the small dimensions of the gold microwire. It was observed that after altering the cell configuration to a two-electrode set up where the silver thread was used as a combined counter-reference electrode – as would be the situation in the final

electronic suture design, the voltammetric profile maintained the sigmoidal profile but has shifted to the lower end of the potential window. The potential shift can be accredited to the fact that the thread is in the presence of bulk chloride concentration (0.1 M KCl) instead of the local concentration characteristic to the 3 M internal solution within the half cell. It is evident that the silver thread could be employed as a functional reference-counter electrode with the deposited silver offering a larger surface area in contrast to the gold wire working electrode. The reliance on the chloride concentration within the solution may be problematic when investigating the exploitation of the thread within sensing applications where disparities in the chloride concentration could result in uncertainty in assigning peak positions. Nevertheless, it is probable that the homeostatic regulation of chloride ion within the tissues (usually 0.1 M) would decrease the extent of any peak shift. It must be stated however that the release mechanism proposed here applies large reducing potentials that are not likely to be influenced by negligible shifts in the reference potential.

7.3.3 Electrochemical Release

Prior to the release studies, a calibration graph was constructed from a stock solution of TBO (1 mM, pH 7 buffer) to assess the spectral properties of the molecule and is shown in **Figure 7.3.6**. The calibration equation was then used to determine the amount of entrapped TBO that had been electrochemically released from CAP coated suture.

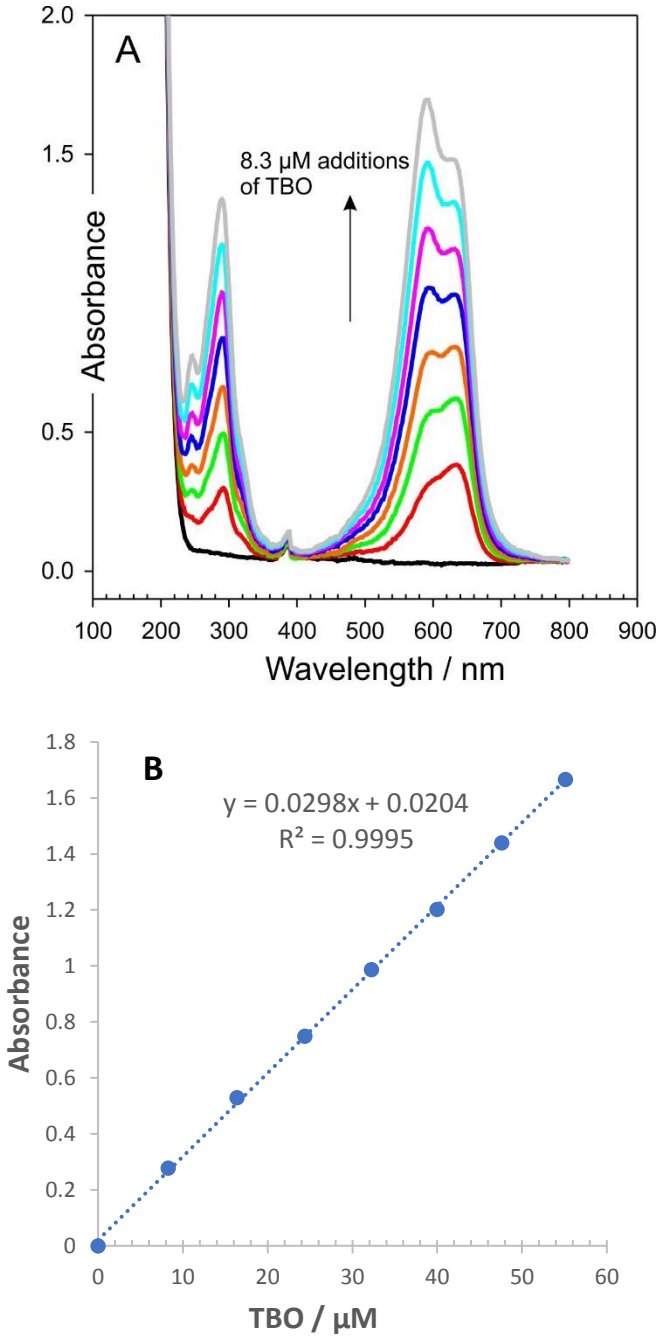

Figure 7.3.6 (A) UV Spectra detailing the additions of TBO (1 mM, pH 7 buffer). (B) Relationship observed between peak height and increasing TBO concentration (8.3 µM to 55.1 µM, pH 7)

The TBO/CAP modified suture was assembled along with the reference and counter electrodes and placed in a small quartz cuvette and held at varying reducing potentials and the subsequent release of the TBO into the solution of 0.1 M KCl was observed through UV spectroscopic analysis. As per the proposed methodology

outlined in Chapter 4, the application of a sufficient reducing potential at the working electrode, it is possible to increase the local pH thereby initiating the dissolution of the CAP binder and releasing the entrapped TBO.

Larger negative potentials were applied as it was found that a reducing potential of -1 V was found to be too slow to initiate any dissolution of the CAP binder. As illustrated in **Figure 7.3.7** there is no evidence of TBO emergence after 5 minutes reduction at -1 V.

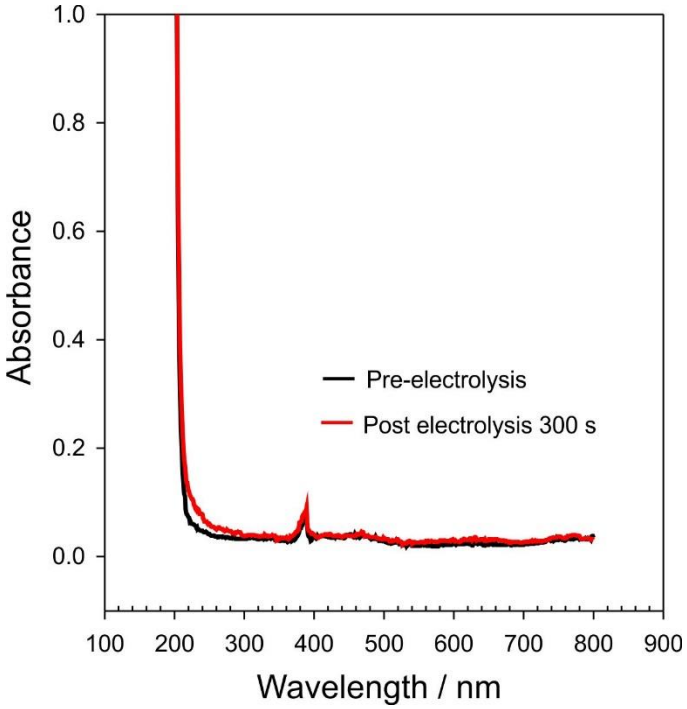

Figure 7.3.7 Spectra detailing the absence of TBO before and after the commencement of hydrolysis, -1 V for 300 s

After applying a reducing potential of -1.75 V, it is possible to observe the released TBO as shown in **Figure 7.3.8 A,** along with a quantitative examination of the drug yield per 10 s cycle shown in **Figure 7.3.8B.** The absorbance peak of TBO at 591 nm intensifies after each reducing cycle, which presents a linear response during the preliminary reducing phase with each 10 s increment releasing around 2 µg of the TBO. The concentration of TBO released will evidently depend on the manufacturing of the suture coating (**Figure 7.389B** inset) and the quantity of drug loading and, as

anticipated, there are some mild inconsistencies between each reducing potential due to the initial characterisation of manufacture presented here.

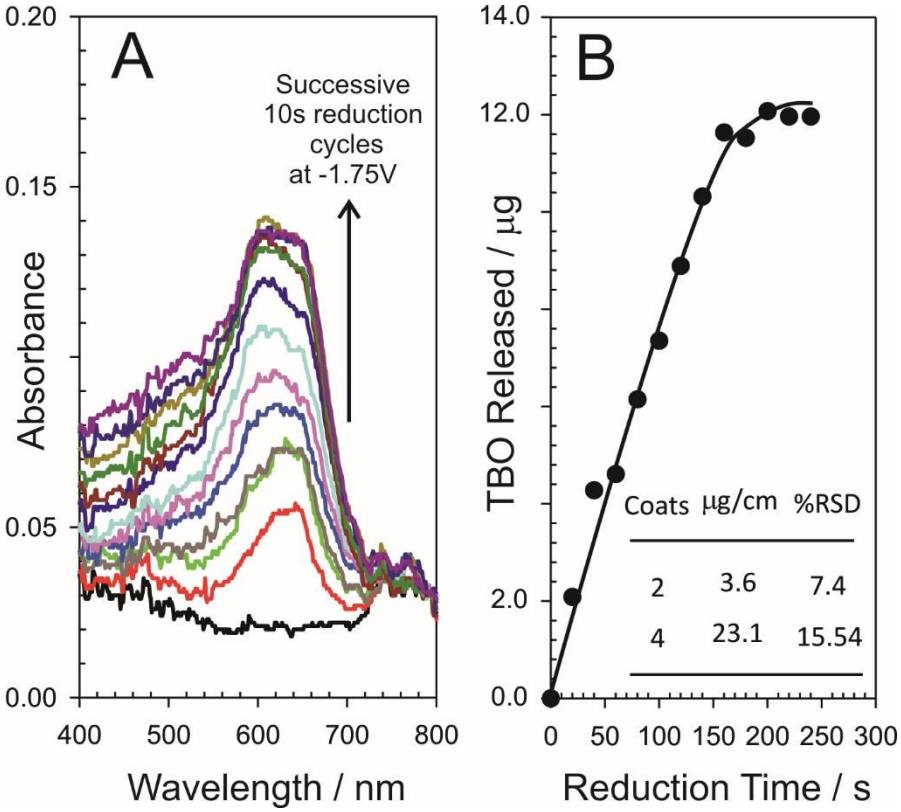

Figure 7.3.8 A) Spectra detailing the release of TBO after successive applications of a reducing potential (−1.75 V for 10 s increments) from a 5 cm length of 100 µm CAP coated gold wire. B) Yield of drug (µg) per 10 s reduction cycle. Inset: Typical yield per length of suture depending on coating

7.4 Conclusions

It is evident that the release of TBO can be electrochemically initiated through the application of an appropriate potential to the suture. The size of the reducing potential must be necessarily large to induce rapid disruption of the pH sensitive binder (CAP), although it can be anticipated that this could be lessened through using less harsh negative potentials. The crucial principle is that the potential is adequate to induce the hydrogen evolution. Regulating the time through which the potential is applied is another option.

The principal benefit of the system described here lies in the ability to meter the dosing of the model drug through generating a change in the local pH. It must also be noted that the change in local pH only continues while the electrode potential is maintained at large negative potentials and the natural buffer elements within the matrix will swiftly proceed to re-establish the pH to that of the bulk solution. The release mechanism can be manipulated to be relatively brief and will cease when the reducing potential is removed. One limiting issue with the technique is that it should be noted that the drug itself should not contain any reducible functionality (i.e. nitro groups) which may be unintentionally altered during the application of the reducing potential. Even though more rigorous methods of manufacture would enhance the reproducibility of delivery, it is clear that the current approach offers a versatile mechanism through which exploitation of the applied potential or the duration over which it is applied can easily control the release process.

Chapter 8

Conclusions and Scope for Future Work

8.1 Conclusions

While many of the materials and mechanisms for controlled release are promising contenders for effective drug delivery, only a few have been used in combination with micro – nanofabrication technologies. By linking the novel research from these 'smart' materials into appropriate micro devices, it may be possible to tune the specificity of drug loading and control over release during the delivery phase. It is clear that patients suffering from chronic illnesses would be among the key recipients for the use controllable release systems, by delivering medication through a more discrete and more accessible route. Currently, there is a pressing need to further develop current transdermal patch technologies and explore the potential for the addition of feedback systems, initiating the development of smart patch drug delivery systems. The convenience of an electrochemically controlled smart device that could be worn by an outpatient could address many of the issues associated with delays in drug delivery and treatment regime adherence. These can offer much better outcomes especially when it comes to patient compliance where all too often, human error can lead to the treatment regime becoming ineffective and can compromise the overall condition of the patient.

Innovations in the fabrication of electronic devices for drug delivery have now reached a size which can be similar to those present within the physiological environment of the body. This outlook creates exciting prospects for combining microelectronics and biosensor technology to develop novel mechanisms with unparalleled ability and potential. The miniaturization of device size and design of these drug delivery systems means they have the ability to release a multifaceted

drug therapy profile in a controlled manner in order to optimize the therapeutic outcome of the drug treatments. These would have the capability to deliver a more efficient method to drug release by taking into account the quantity of drug to be delivered and at the correct time in response to an appropriate electrochemical trigger. It could also be invaluable in weaning patients off opioid medications in a much more controlled manner. The outcome would be to develop a platform technology that is at the forefront of electronic delivery.

Chapter 3 detailed the development and characterisation of a nanostructured conductive carbon-polycarbonate (C-PC) film capable of facilitating the controlled dissolution of enteric coatings. Modification of the conductive film was achieved using laser treatment to create pores. Electrochemical manipulation of the local pH within laser etched pores was shown to initiate the hydrolysis of the cellulous acetate phthalate film and facilitate the controlled release of a model drug. Dexamethasone was chosen as an ideal model drug candidate for incorporation into enteric film. Dexamethasone has been widely used in clinical applications to treat a variety of conditions and its suitability to be used in transdermal form was confirmed. The methodology presented proffers the opportunity to achieve local transdermal delivery of dexamethasone for the treatment of rheumatoid arthritis in a controlled manner. Furthermore, an innovate approach to the design and operation of microfiber pH probe based on electrochemically generated quinoid moieties on the surface of the carbon fibre probe was critically appraised.

Carbon fibre was selected as the base substrate onto which a CAP film was fixed onto within Chapter 4. The carbon fibre mesh acted as a support for the CAP film, as well as a gate for a drug reservoir and, as the fibre is conductive, an electrode. A novel approach employing controlled electrolysis was developed as a means through which the electrochemically initiated rupture and subsequent dissolution of a pH sensitive barrier film could be used as a controllable gateway for the release of candidate drugs. The application of a reducing potential to the conductive carbon fibre substrate initiated the generation of hydrogen bubbles, along with a change in local

pH, and the former was shown to enable rapid removal of the cellulose acetate phthalate (CAP) film thereby inducing reagent release.

The shift in pH at the electrode interface was confirmed through observing the peak position of the quinoid species on the surface of the anodised carbon fibre electrode. The peak position of these quinone species on the surface of the carbon fibre are pH dependent, this makes them an identifying marker of the local pH. After the application of the reducing potential (-2 V, 5 s), there was a distinct shift in the peak process towards more negative potentials which are consistent with a change in the local pH to more alkaline conditions. The localised pH was found to have increased from pH 3.19 to pH 8.26 based on holding the electrode at -2 V for 5 s.

A reservoir approach was developed to determine the efficacy of the approach for the delivery of a model drug (methotrexate) to be transported to the delivery chamber via the application of the electrochemical trigger. After the commencement of electrolysis, the successful detection of the model drug within the delivery reservoir, thus confirming the suitability of the methodology for controlled release applications.

Modification of the carbon fibre electrode through the selective deposition of conductive nanoparticles was investigated. The addition of iron oxide and graphene oxide nanoparticles displayed superior HER activity compared to the unmodified CF due to the high dispersity and conductivity on the surface of the carbon fibre. The addition of the nanoparticles, in principle, could enable the imposition of smaller cathodic potentials to induce more subtler pH changes. The benefit of using the iron oxide is that the system is inherently biocompatible and could potentially be incorporated into a variety of electrochemically initiated drug release mechanisms, while further study is required to determine the full toxicological effects of graphene oxide.

Chapter 5 investigated a new approach to simplify the electrode construction process and served to determine if the CAP component could be directly incorporated with the conductive element. In this methodology the carbon fibre filaments were substituted with nanoparticulate carbon particles which were bound together using the CAP polymer to form a conductive sheet. In contrast to conventional carbon films, a novel element was introduced whereby the CAP component could be eroded under the imposition of a reducing potential. Under normal conditions, the conductive coating remained intact but, upon imposing a reducing potential on the carbon composite layer, the pH at the interface was increased, which resulted in the solubilisation of the pH sensitive CAP binder components.

Modification of the film using iron oxide and graphene oxide nanoparticles was undertaken and, in this respect, it shared similar principles to the approach investigated in Chapter 4. It was important to acknowledge that the GO in this instance served the same purpose as electrochemical anodisation but without the need to expose the film to strong alkaline solutions and thus preserving the integrity of the CAP-C film. The central interest however was the ability of the modified electrode to improve the dynamics of the hydrogen evolution reaction. The responses to proton reduction showed that the GO and Fe_3O_4 modifiers performed more favourably than the CAP-C alone. For the modified electrodes, the potential at which reduction occurs was less negative. Although these preliminary findings were positive, the fabrication aspects, reproducibility and stability were poor and thus they were not used.

The biocompatibility of the nano carbon-cellulose acetate composite was assessed in relation to skin irritation and cytotoxicity conducted by Bioserv Analytik Un Medizinprodukte GMBH (Rostock Germany). The overall assessment indicated that the material did not cause any relevant toxicological or biological damage and possessed good overall biocompatibility. The proposed mechanism has potential to work as an effective drug delivery method were, if a drug component were loaded into the film, controlled release of the therapeutic could be achieved, thus serving as an ideal candidate for incorporation into drug delivery and electrochemical microsystems.

Chapter 6 focused on the further investigation of the conductive polymer blend detailed in Chapter 5, which was employed to construct electrochemically controllable microneedle arrays. Manipulation of the pH responsiveness of the polymer for use in electrochemically controlled drug release has been discussed in Chapters 3 and 4. In the latter, it was used as a thin film encapsulating a drug payload. Under normal conditions (open circuit), the conductive microneedle array remained intact but, through exploiting hydrogen evolution at the microneedle array, changes in local pH were shown to induce swelling within the needle structure.

A skin mimic system based on crosslinked alginate gel, was formulated. Ferrocyanide was incorporated within the gel to act as an in situ redox probe that could be utilized to evaluate the structural integrity of the microneedle. A cathodic potential was applied directly to the microneedle array which lead to an increase in pH and swelling of the CAP binder. Upon initiating hydrogen evolution, the microneedles were periodically scanned, and it was observed that the voltammetric profile of the ferrocyanide began to deteriorate. The efficacy of the release method was also tested with a model drug – Toluidine Blue O (TBO). The TBO loaded MNs were placed in a gelatin matrix and visually inspected after the application of each cathodic conditioning step. A strong blue colour was observed upon removing the MNs after changing the pH, thus confirming the ability to release an entrapped agent on demand.

Hence, were drugs to be encapsulated within the polymer composite complex at the time of construction, then the electrochemically initiated swelling could permit control over their release. The latter is situated at the core of the approach as the electrochemical manipulation of the release mechanism could offer a novel approach in MN design. Biocompatibility studies of the CAP-C material - detailed in Chapter 5, delivered some encouraging insights into the possible use of the material with no evident skin irritation nor cytotoxicity nevertheless these need to be regarded with some caution – especially where the devices may be used for long term purposes where sensitisation may transpire.

The release mechanism detailed in Chapter 7 followed on from previous chapters which have employed the application of a negative potential, where in this case the potential was applied to a gold microwire. The gold microwire was loaded with cellulose acetate phthalate encapsulated drug droplets (TBO) as a novel approach for the electrochemically driven drug release from a suture.

A conductive silver thread was utilised as a combined counter-reference electrode. The capability of the thread to function as a feasible reference/counter electrode was evaluated through comparing the potentiometric response to chloride ion whereby a Nernstian response (−59 mV) was obtained. Electrochemical release was initiated through holding the potential of the coated wire at potentials ranging from -1 V to -2 V for a given period (typically 10 s) in line with the previous methodology followed within Chapter 6, to induce polymer swelling and dissolution of the protective CAP binder. After each reducing cycle it was determined that around 2 μg of the TBO was released from the gold wire. It is clear that the current approach offers a versatile mechanism through which exploitation of the applied potential or the duration over which it is applied can easily control the release process, thus proffering a novel approach to electrochemically controlled drug release from micro wires.

8.2 Scope for Future Work

The focus of the present thesis is directed towards electrochemical approaches to drug delivery given the compatibility with modern electronics which should, in principle, provide opportunities for the delivery devices to become much smaller and less obtrusive with greater dose control and much more rapid response times. Through the development of functional materials whose properties can be controlled, it is possible, to create advanced systems that could deliver a drug, antidote or treatment upon activation by an electrochemical trigger. These “smart” materials could ultimately be incorporated into a micro device or smart patch that would be capable of acting autonomously to deliver a drug therapy.

The further development of transdermal systems will also see the addition of complex electronic systems into the device itself, where considerations surrounding power requirements and the finished product size will have to be considered for future ‘smart’ delivery systems to achieve their full potential.

References

Abiman, P., Crossley, A., Gregory G. Wildgoose, Jones, J. H. and Richard, G. C. (2007) 'Investigating the Thermodynamic Causes Behind the Anomalously Large Shifts in pKa Values of Benzoic Acid-Modified Graphite and Glassy Carbon Surfaces', *Langmuir*. American Chemical Society, 23(14), pp. 7847–52.

Adler, G., Mueller, B. and Articus, K. (2014) 'The transdermal formulation of rivastigmine improves caregiver burden and treatment adherence of patients with Alzheimer's disease under daily practice conditions', *International Journal of Clinical Practice*, 68(4), pp. 465–470.

Agboola, S. O., Ball, M., Kvedar, J. C. and Jethwani, K. (2013) 'The future of Connected Health in preventive medicine', *QJM*, 106(9), pp. 791–794.

Agnello, S., Gasperini, L., Reis, R. L., Mano, J. F., Pitarresi, G., Palumbo, F. S. and Giammona, G. (2016) 'Micro fl uidic production of hyaluronic acid derivative micro fi bers to control drug release', 182, pp. 309–313.

Ai, Y., Yalcin, S. E., Gu, D., Baysal, O., Baumgart, H., Qian, S. and Beskok, A. (2010) 'A low-voltage nano-porous electroosmotic pump', *Journal of Colloid and Interface Science*, 350(2), pp. 465–470.

Akagi, T., Kaneko, T., Kida, T. and Akashi, M. (2005) 'Preparation and characterization of biodegradable nanoparticles based on poly (g -glutamic acid) with l -phenylalanine as a protein carrier', 108, pp. 226–236.

Albertsson, A.-C., Carlfors, J. and Sturesson, C. (1996) 'Preparation and characterisation of poly(adipic anhydride) microspheres for ocular drug delivery', *Journal of Applied Polymer Science*. Wiley Subscription Services, Inc., A Wiley Company, 62(4), pp. 695–705.

Alizadeh, N. and Shamaeli, E. (2014) 'Electrochemically controlled release of anticancer drug methotrexate using nanostructured polypyrrole modified with cetylpyridinium: Release kinetics investigation', *Electrochimica Acta*, 130, pp. 488–496.

Almeida, P. F. and Almeida, A. J. (2004) 'Crosslinked alginate gelatine beads a new matrix for controlled release of pindolol', *Journal of Controlled Release*, 97, pp. 431–439.

Alshomer, F., Madhavan, A., Pathan, O. and Song, W. (2017) 'Bioactive Sutures: A Review of Advances in Surgical Suture Functionalisation', *Current Medicinal Chemistry*, 24(2), pp. 215–223.

Alzheimer's Society (2010) 'Drug treatments for Alzheimer's disease', *Society*, pp. 1–7.

Ambrosi, A., Bonanni, A., Sofer, Z., Cross, J. S. and Pumera, M. (2011) 'Electrochemistry at chemically modified graphenes', *Chemistry - A European Journal*, 17(38), pp. 10763–10770.

Amidon, S., Brown, J. E. and Dave, V. S. (2015) 'Colon-targeted oral drug delivery systems: design trends and approaches.', *AAPS PharmSciTech*. Springer, 16(4), pp. 731–41.

Anandhakumar, S., Krishnamoorthy, G., Ramkumar, K. M. and Raichur, A. M. (2017) 'Preparation of collagen peptide functionalized chitosan nanoparticles by ionic gelation method : An effective carrier system for encapsulation and release of doxorubicin for cancer drug delivery', *Materials Science & Engineering C*. Elsevier B.V., 70, pp. 378–385.

Anderson, A. and Davis, J. (2015) 'Next generation transdermal drug delivery – An electrochemical approach to pH manipulationfor controlled release within smart patch technologies', *IFMBE Proceedings : World Congress on Medical Physics and Biomedical Engineering*. Springer International Publishing.

Anderson, A., McConville, A. and Davis, J. (2015) 'Electrochemical bubble rip: A new approach to controlled drug release', *Electrochemistry Communications*, 60, pp. 88–91.

Anderson, A., McConville, A. and Davis, J. (2015) 'Electrochemical bubble rip: A new approach to controlled drug release', *Electrochemistry Communications*, 60.

Anderson, A., Phair, J., Benson, J., Meenan, B. and Davis, J. (2014) 'Investigating the use of endogenous quinoid moieties on carbon fibre as means of developing micro pH sensors', *Materials Science and Engineering: C*. Elsevier, 43, pp. 533–537.

De Angelis, G., Murthy, A., Beyersmann, J. and Harbarth, S. (2010) 'Estimating the impact of healthcare-associated infections on length of stay and costs', *Clinical Microbiology and Infection*, 16(12), pp. 1729–1735.

Ashayer-Soltani, R., Hunt, C. and Thomas, O. (2016) 'Fabrication of highly conductive stretchable textile with silver nanoparticles', *Textile Research Journal*. SAGE PublicationsSage UK: London, England, 86(10), pp. 1041–1049.

Askarian, S., Abnous, K., Darroudi, M., Kazemi, R. and Ramezani, M. (2016) 'Biologicals Gene delivery to neuroblastoma cells by poly (L -lysine) -grafted low molecular weight polyethylenimine copolymers', *Biologicals*. Elsevier Ltd, 44(4), pp. 212–218.

Badran, M. M., Kuntsche, J. and Fahr, A. (2009) 'Skin penetration enhancement by a microneedle device (Dermaroller®) in vitro: Dependency on needle size and applied formulation', *European Journal of Pharmaceutical Sciences*. Elsevier, 36(4–5), pp. 511–523.

Bagherifam, S., Griffiths, G. W., Mælandsmo, G. M., Hasirci, V., Hasirci, N., Bagherifam, S., Griffiths, G. W. and Mælandsmo, G. M. (2015) 'Poly (sebacic anhydride) nanocapsules as carriers : effects of preparation parameters on properties and release of doxorubicin parameters on properties and release of doxorubicin', *Journal of Microencapsulation*, 32(2), pp. 166–174.

Banks, C. E. and Compton, R. G. (2005a) 'Exploring the electrocatalytic sites of carbon nanotubes for NADH detection: an edge plane pyrolytic graphite electrode study', *The Analyst*, 130(9), p. 1232.

Banks, C. E. and Compton, R. G. (2005b) 'Exploring the electrocatalytic sites of carbon nanotubes for NADH detection: an edge plane pyrolytic graphite electrode study', *The Analyst*, 130(9), p. 1232.

Baran, R. (Robert) and Maibach, H. I. (2010) *Textbook of cosmetic dermatology*.

Informa Healthcare.

Bard, A. J. and Faulkner, L. R. (2001) *Electrochemical methods : fundamentals and applications*. Wiley.

Benicewicz, B. C. and Hopper, P. K. (1991) 'Polymers for Absorbable Surgical Sutures - Part II', *Journal of Bioactive and Composite Polymers*, 6(1), pp. 64–94.

Bertz, A., Wöhl-Bruhn, S., Miethe, S., Tiersch, B., Koetz, J., Hust, M., Bunjes, H. and Menzel, H. (2013) 'Encapsulation of proteins in hydrogel carrier systems for controlled drug delivery: Influence of network structure and drug size on release rate', *Journal of Biotechnology*, 163(2), pp. 243–249.

Bhowmik, T., Kundu, M. K. and Barman, S. (2016) 'Palladium Nanoparticle–Graphitic Carbon Nitride Porous Synergistic Catalyst for Hydrogen Evolution/Oxidation Reactions over a Broad Range of pH and Correlation of Its Catalytic Activity with Measured Hydrogen Binding Energy', *ACS Catalysis*. American Chemical Society, 6(3), pp. 1929–1941.

Bhutani, U., Laha, A., Mitra, K. and Majumdar, S. (2016) 'Sodium alginate and gelatin hydrogels : Viscosity effect on hydrophobic drug release', *Materials Letters*. Elsevier, 164, pp. 76–79.

Birchall, J. C., Clemo, R., Anstey, A. and John, D. N. (2011) 'Microneedles in Clinical Practice–An Exploratory Study Into the Opinions of Healthcare Professionals and the Public', *Pharmaceutical Research*, 28(1), pp. 95–106.

Bloom Cerkoney, K. A. and Hart, L. K. (1980) 'The Relationship Between the Health Belief Model and Compliance of Persons with Diabetes Mellitus', *Diabetes Care*, 3(5), pp. 594–598.

Bohl, A., Rohm, H. W., Ceschi, P., Paasche, G., Hahn, A., Barcikowski, S., Lenarz, T., Stöver, T., Pau, H.-W., Schmitz, K.-P. and Sternberg, K. (2012) 'Development of a specially tailored local drug delivery system for the prevention of fibrosis after insertion of cochlear implants into the inner ear.', *Journal of materials science. Materials in medicine*, 23(9), pp. 2151–62.

Bollella, P., Fusco, G., Tortolini, C., Sanzò, G., Favero, G., Gorton, L. and Antiochia, R. (2017) 'Beyond graphene: Electrochemical sensors and biosensors for biomarkers detection', *Biosensors and Bioelectronics*. Elsevier, 89, pp. 152–166.

Bourouina, T., Bossebuf, A. and Grandchamp, J.-P. (1997) 'Design and simulation of an electrostatic micropump for drug-delivery applications', *Journal of Micromechanics and Microengineering*. IOP Publishing, 7(3), pp. 186–188.

Braunecker, J., Baba, M., Milroy, G. E. and Cameron, R. E. (2004) 'The effects of molecular weight and porosity on the degradation and drug release from polyglycolide', 282, pp. 19–34.

Brownson, D. A. C., Munro, L. J., Kampouris, D. K. and Banks, C. E. (2011) 'Electrochemistry of graphene: not such a beneficial electrode material?', *RSC Advances*, 1(6), p. 978.

Cachia, E. and Ahmedzai, S. H. (2011) 'Transdermal opioids for cancer pain', *Current Opinion in Supportive and Palliative Care*, 5(1), pp. 15–19.

Cai, B., Engqvist, H. and Bredenberg, S. (2015) 'Development and evaluation of a tampering resistant transdermal fentanyl patch.', *International journal of pharmaceutics*, 488(1–2), pp. 102–107.

Cardoso, J. A. S. B., Amaral, L., Metin, Ö., Cardoso, D. S. P., Sevim, M., Sener, T., Sequeira, C. A. C. and Santos, D. M. F. (2017a) 'Reduced graphene oxide assembled Pd-based nanoalloys for hydrogen evolution reaction', *International Journal of Hydrogen Energy*. Pergamon, 42(7), pp. 3916–3925.

Cardoso, J. A. S. B., Amaral, L., Metin, Ö., Cardoso, D. S. P., Sevim, M., Sener, T., Sequeira, C. A. C. and Santos, D. M. F. (2017b) 'Reduced graphene oxide assembled Pd-based nanoalloys for hydrogen evolution reaction', *International Journal of Hydrogen Energy*, 42(7), pp. 3916–3925.

Casettari, L. and Illum, L. (2014) 'Chitosan in nasal delivery systems for therapeutic drugs.', *Journal of controlled release : official journal of the Controlled Release Society*, 190, pp. 189–200.

Catanzano, O., Acierno, S., Russo, P., Cervasio, M., Del Basso De Caro, M., Bolognese, A., Sammartino, G., Califano, L., Marenzi, G., Calignano, A., Acierno, D. and Quaglia, F. (2014) 'Melt-spun bioactive sutures containing nanohybrids for local delivery of anti-inflammatory drugs', *Materials Science and Engineering: C*, 43, pp. 300–309.

Cegla, J. (2015) 'Microneedle-array patches loaded with hypoxia-sensitive vesicles provide fast glucose-responsive insulin delivery', *Annals of Clinical Biochemistry*, 52(6), p. 720.

Chaloupka, K., Malam, Y. and Seifalian, A. M. (2010) 'Nanosilver as a new generation of nanoproduct in biomedical applications.', *Trends in biotechnology*. Elsevier, 28(11), pp. 580–8.

Chan, M., Estève, D., Fourniols, J.-Y., Escriba, C. and Campo, E. (2012) 'Smart wearable systems: Current status and future challenges', *Artificial Intelligence in Medicine*, 56(3), pp. 137–156.

Chen, D. W., Hsu, Y.-H., Liao, J.-Y., Liu, S.-J., Chen, J.-K. and Ueng, S. W.-N. (2012) 'Sustainable release of vancomycin, gentamicin and lidocaine from novel electrospun sandwich-structured PLGA/collagen nanofibrous membranes', *International Journal of Pharmaceutics*, 430(1–2), pp. 335–341.

Chen, J., Huang, W., Huang, Z., Liu, S., Ye, Y., Li, Q. and Huang, M. (2017) 'Fabrication of Tip-Dissolving Microneedles for Transdermal Drug Delivery of Meloxicam', *AAPS PharmSciTech*. AAPS PharmSciTech, (25).

Chen, Y.-F., Hu, Y.-H., Chou, Y.-I., Lai, S.-M. and Wang, C.-C. (2010) 'Surface modification of nano-porous anodic alumina membranes and its use in electroosmotic flow', *Sensors and Actuators B: Chemical*, 145(1), pp. 575–582.

Cheng, L.-J. and Chang, H.-C. (2011) 'Microscale pH regulation by splitting water', *Biomicrofluidics*, 5(4), p. 46502.

Cheung, K. and Das, D. B. (2014) 'Microneedles for drug delivery: trends and progress', *Drug Delivery*, 23(7), pp. 1–17.

Choonara, B. F., Choonara, Y. E., Kumar, P., Bijukumar, D., du Toit, L. C. and Pillay, V.

(2014) ‘A review of advanced oral drug delivery technologies facilitating the protection and absorption of protein and peptide molecules.’, *Biotechnology advances*, 32(7), pp. 1269–82.

Cima, M. J., Lee, H., Daniel, K., Tanenbaum, L. M., Mantzavinou, A., Spencer, K. C., Ong, Q., Sy, J. C., Santini, J., Schoellhammer, C. M., Blankschtein, D. and Langer, R. S. (2014) ‘Single compartment drug delivery.’, *Journal of controlled release : official journal of the Controlled Release Society*, 190, pp. 157–71.

Cipriani, P., Ruscitti, P., Carubbi, F., Liakouli, V. and Giacomelli, R. (2014) ‘Methotrexate: an old new drug in autoimmune disease’, *Expert Review of Clinical Immunology*, 10(11), pp. 1519–1530.

Compton, R. G. and Banks, C. E. (2011) *Understanding voltammetry*. Imperial College Press.

Constantin, M., Bucatariu, S., Doroftei, F. and Fundueanu, G. (2017) ‘Smart composite materials based on chitosan microspheres embedded in thermosensitive hydrogel for controlled delivery of drugs’, *Carbohydrate Polymers*. Elsevier Ltd., 157, pp. 493–502.

Costache, M. C., Qu, H., Ducheyne, P. and Devore, D. I. (2010) ‘Polymer–xerogel composites for controlled release wound dressings’, *Biomaterials*, 31(24), pp. 6336–6343.

Coutinho, A. E. and Chapman, K. E. (2011) ‘The anti-inflammatory and immunosuppressive effects of glucocorticoids, recent developments and mechanistic insights.’, *Molecular and cellular endocrinology*. Elsevier, 335(1), pp. 2–13.

Cummings, A. J. and Olsen, M. (2011) ‘Mechanism of action of stinging nettles’, *Wilderness and Environmental Medicine*. Elsevier Inc., 22(2), pp. 136–139.

Dailey, G., Kim, M. S. and Lian, J. F. (2001) ‘Patient compliance and persistence with antihyperglycemic drug regimens: evaluation of a medicaid patient population with type 2 diabetes mellitus’, *Clinical Therapeutics*, 23(8), pp. 1311–1320.

Dasan, K. P. and Rekha, C. (2012) ‘Polymer blend microspheres for controlled drug

release: the techniques for preparation and characterization: a review article.', *Current drug delivery*, 9(6), pp. 588–95.

Davies, T. J. and Compton, R. G. (2005) 'The cyclic and linear sweep voltammetry of regular and random arrays of microdisc electrodes: Theory', *Journal of Electroanalytical Chemistry*. Elsevier, 585(1), pp. 63–82.

Davis, J. and Cooper, J. M. (2002) 'Electrochemical manipulation of localised pH: application to electroanalysis', *Journal of Electroanalytical Chemistry*, 520(1–2), pp. 13–17.

Dennis, C., Sethu, S., Nayak, S., Mohan, L., Morsi, Y. and Manivasagam, G. (2016) 'Suture materials - Current and emerging trends', *Journal of Biomedical Materials Research - Part A*, 104(6), pp. 1544–1559.

Dennis, C., Sethu, S., Nayak, S., Mohan, L., Morsi, Y. Y. and Manivasagam, G. (2016a) 'Suture materials - Current and emerging trends', *Journal of Biomedical Materials Research Part A*, 104(6), pp. 1544–1559.

Dennis, C., Sethu, S., Nayak, S., Mohan, L., Morsi, Y. Y. and Manivasagam, G. (2016b) 'Suture materials - Current and emerging trends', *Journal of Biomedical Materials Research Part A*, 104(6), pp. 1544–1559.

Dong, Z., Wang, Q. and Du, Y. (2006) 'Alginate/gelatin blend films and their properties for drug controlled release', *Journal of Membrane Science*, 280(1–2), pp. 37–44.

Donnelly, R. F., Garland, M. J., Morrow, D. I. J., Migalska, K., Singh, T. R. R., Majithiya, R. and Woolfson, A. D. (2010) 'Optical coherence tomography is a valuable tool in the study of the effects of microneedle geometry on skin penetration characteristics and in-skin dissolution', *Journal of Controlled Release*. Elsevier, 147(3), pp. 333–341.

Donnelly, R. F., McCrudden, M. T. C., Zaid Alkilani, A., Larrañeta, E., McAlister, E., Courtenay, A. J., Kearney, M.-C., Singh, T. R. R., McCarthy, H. O., Kett, V. L., Caffarel-Salvador, E., Al-Zahrani, S. and Woolfson, A. D. (2014) 'Hydrogel-Forming Microneedles Prepared from "Super Swelling" Polymers Combined with Lyophilised Wafers for Transdermal Drug Delivery', *PLoS ONE*, 9(10), p. e111547.

Donnelly, R. F., Singh, T. R. R., Alkilani, A. Z., McCrudden, M. T. C., O'Neill, S., O'Mahony, C., Armstrong, K., McLoone, N., Kole, P. and Woolfson, A. D. (2013) 'Hydrogel-forming microneedle arrays exhibit antimicrobial properties: Potential for enhanced patient safety', *International Journal of Pharmaceutics*. Elsevier, 451(1–2), pp. 76–91.

Donnelly, R. F., Singh, T. R. R., Garland, M. J., Migalska, K., Majithiya, R., McCrudden, C. M., Kole, P. L., Mahmood, T. M. T., McCarthy, H. O. and Woolfson, A. D. (2012) 'Hydrogel-Forming Microneedle Arrays for Enhanced Transdermal Drug Delivery', *Advanced Functional Materials*. WILEY-VCH Verlag, 22(23), pp. 4879–4890.

Dosio, F., Arpicco, S., Stella, B. and Fattal, E. (2016) 'Hyaluronic acid for anticancer drug and nucleic acid delivery ☆', *Advanced Drug Delivery Reviews*. Elsevier B.V., 97, pp. 204–236.

Dul, M., Stefanidou, M., Porta, P., Serve, J., O'Mahony, C., Malissen, B., Henri, S., Levin, Y., Kochba, E., Wong, F., Dayan, C., Coulman, S. and Birchall, J. (2017) 'Hydrodynamic gene delivery in human skin using a hollow microneedle device', *Journal of Controlled Release*. Elsevier, 265, pp. 120–131.

Dutt, J. S. N., Cardosi, M. F., Livingstone, C. and Davis, J. (2005) 'Diagnostic implications of uric acid in electroanalytical measurements', *Electroanalysis*, 17(14), pp. 1233–1243.

Dutt, J. S. N., Cardosi, M. F., Wilkins, S. J., Livingstone, C. and Davis, J. (2006) 'Characterisation of carbon fibre composites for decentralised biomedical testing', *Materials Chemistry and Physics*. Elsevier, 97(2–3), pp. 267–272.

Einmahl, S., Cohen, F. B., Hermies, D., Rudaz, S., Tabatabay, C., Renard, G. and Gurny, R. (2016) 'A New Poly (Ortho Ester) -Based Drug Delivery System as an Adjunct Treatment in Filtering Surgery', 42(3), pp. 1–6.

Elliott Donaghue, I. and Shoichet, M. S. (2015) 'Controlled release of bioactive PDGF-AA from a hydrogel/nanoparticle composite', *Acta Biomaterialia*, 25, pp. 35–42.

Elmas, Ş. N. K., Güzel, R., Say, M. G., Ersoz, A. and Say, R. (2018) 'Ferritin based bionanocages as novel biomemory device concept', *Biosensors and Bioelectronics*.

Elsevier, 103, pp. 19–25.

Escobar-Chávez, J. J., Bonilla-Martínez, D., Villegas-González, M. A., Molina-Trinidad, E., Casas-Alancaster, N. and Revilla-Vázquez, A. L. (2011) 'Microneedles: a valuable physical enhancer to increase transdermal drug delivery.', *Journal of clinical pharmacology*, 51(7), pp. 964–77.

Evans, D. F., Pye, G., Bramley, R., Clark, A. G., Dyson, T. J. and Hardcastle, J. D. (1988) 'Measurement of gastrointestinal pH profiles in normal ambulant human subjects.', *Gut*, 29(8), pp. 1035–41.

Ezekiel, H. B., Sharp, D., Villalba, M. M. and Davis, J. (2008) 'Laser-anodised carbon fibre: Coupled activation and patterning of sensor substrates', *Journal of Physics and Chemistry of Solids*, 69(11), pp. 2932–2935.

Fan, C. and Wang, D. (2016) 'Journal of Materials Science & Technology Novel Gelatin-based Nano-gels with Coordination-induced Drug Loading for Intracellular Delivery', *Journal of Materials Science & Technology*. Elsevier Ltd, 32(9), pp. 840–844.

Fan, L., Ge, H., Zou, S., Xiao, Y., Wen, H., Li, Y., Feng, H. and Nie, M. (2016) 'International Journal of Biological Macromolecules Sodium alginate conjugated graphene oxide as a new carrier for drug delivery system', 93, pp. 582–590.

Farooqui, U. R., Ahmad, A. L. and Hamid, N. A. (2018) 'Graphene oxide: A promising membrane material for fuel cells', *Renewable and Sustainable Energy Reviews*. Elsevier Ltd, 82(August 2016), pp. 714–733.

Favalli, E. G., Biggioggero, M. and Meroni, P. L. (2014) 'Methotrexate for the treatment of rheumatoid arthritis in the biologic era: Still an "anchor" drug?', *Autoimmunity Reviews*. Elsevier, 13(11), pp. 1102–1108.

Feliciano-Ramos, I., Caban-Acevedo, M., Aulice Scibioh, M. and Cabrera, C. R. (2010) 'Self-assembled monolayers of l-cysteine on palladium electrodes', *Journal of Electroanalytical Chemistry*, 650(1), pp. 98–104.

Felton, L. A. and Porter, S. C. (2013) 'An update on pharmaceutical film coating for drug delivery', *Expert Opinion on Drug Delivery*, 10(4), pp. 421–435.

Fletcher, S. and Horne, M. . (1999) 'Random assemblies of microelectrodes (RAM™ electrodes) for electrochemical studies', *Electrochemistry Communications*, 1(10), pp. 502–512.

Fletcher, S. and Horne, M. D. (1999) 'Random assemblies of microelectrodes (RAM™ electrodes) for electrochemical studies', *Electrochemistry Communications*. Elsevier, 1(10), pp. 502–512.

Fomina, N., Johnson, C. A., Maruniak, A., Bahrampour, S., Lang, C., Davis, R. W., Kavusi, S., Ahmad, H., Duchen, M. R., Forman, H. J., Fricker, M. D., Gems, D., Halestrap, A. P., Halliwell, B., Jakob, U., Johnston, I. G., Jones, N. S., Logan, D. C., Morgan, B., Müller, F. L., Nicholls, D. G., Remington, S. J., Schumacker, P. T., Winterbourn, C. C., Sweetlove, L. J., Meyer, A. J., Dick, T. P. and Murphy, M. P. (2016) 'An electrochemical platform for localized pH control on demand', *Lab Chip*. The Royal Society of Chemistry, 16(12), pp. 2236–2244.

Fu, H.-Y., Chen, S.-J., Chen, R.-F., Kuo-Huang, L.-L. and Huang, R.-N. (2007) 'Why do Nettles Sting? About Stinging Hairs Looking Simple but Acting Complex', *Functional Plant Science and Biotecnology*, 1(1), pp. 46–55.

Fu, Y. and Kao, W. J. (2010) 'Drug release kinetics and transport mechanisms of non-degradable and degradable polymeric delivery systems.', *Expert opinion on drug delivery*. NIH Public Access, 7(4), pp. 429–44.

Gallo, A. L., Paladini, F., Romano, A., Verri, T., Quattrini, A., Sannino, A. and Pollini, M. (2016) 'Efficacy of silver coated surgical sutures on bacterial contamination, cellular response and wound healing', *Materials Science and Engineering: C*, 69, pp. 884–893.

Gasmi, H., Siepmann, F., Hamoudi, M. C., Danede, F., Verin, J., Willart, J. and Siepmann, J. (2016) 'Towards a better understanding of the different release phases from PLGA microparticles : Dexamethasone-loaded systems', *International Journal of Pharmaceutics*. Elsevier B.V., 514(1), pp. 189–199.

Genina, N., Jukarainen, H., Khajeheian, M., Holl, J., Sandler, N., Rosling, A. and Ermei, M. (2016) 'Three-Dimensional Printed PCL-Based Implantable Prototypes of Medical Devices for Controlled Drug Delivery', 105.

Gensler, H., Sheybani, R., Li, P.-Y., Mann, R. Lo and Meng, E. (2012) 'An implantable MEMS micropump system for drug delivery in small animals', *Biomedical Microdevices*, 14(3), pp. 483–496.

Gensler, H., Sheybani, R., Li, P. Y., Mann, R. Lo and Meng, E. (2012) 'An implantable MEMS micropump system for drug delivery in small animals', *Biomedical Microdevices*, 14(3), pp. 483–496.

George, P. M., Lavan, D. a., Burdick, J. a., Chen, C. Y., Liang, E. and Langer, R. (2006) 'Electrically controlled drug delivery from biotin-doped conductive polypyrrole', *Advanced Materials*, 18(5), pp. 577–581.

George, P. M., Lyckman, A. W., LaVan, D. A., Hegde, A., Leung, Y., Avasare, R., Testa, C., Alexander, P. M., Langer, R. and Sur, M. (2005) 'Fabrication and biocompatibility of polypyrrole implants suitable for neural prosthetics', *Biomaterials*. Elsevier, 26(17), pp. 3511–3519.

Ghasemi, S., Hosseini, S. R., Nabipour, S. and Asen, P. (2015) 'Palladium nanoparticles supported on graphene as an efficient electrocatalyst for hydrogen evolution reaction', *International Journal of Hydrogen Energy*, 40(46), pp. 16184–16191.

Gokhale, A. (2014) 'Achieving Zero-Order Release Kinetics Using Multi-Step Diffusion-Based Drug Delivery', *Pharmaceutical Technology*, 38(5), p. 46.

Gomaa, Y. A., Garland, M. J., McInnes, F., El-Khordagui, L. K., Wilson, C. and Donnelly, R. F. (2012) 'Laser-engineered dissolving microneedles for active transdermal delivery of nadroparin calcium', *European Journal of Pharmaceutics and Biopharmaceutics*, 82(2), pp. 299–307.

Grozovski, V., Vesztergom, S., Láng, G. G. and Broekmann, P. (2017) 'Electrochemical Hydrogen Evolution: H + or H 2 O Reduction? A Rotating Disk Electrode Study', *Journal of The Electrochemical Society*, 164(11), pp. E3171–E3178.

Guo, X. and Mei, N. (2014) 'Assessment of the toxic potential of graphene family nanomaterials', *Journal of Food and Drug Analysis*. Elsevier, 22(1), pp. 105–115.

Gupta, B., Jain, R. and Singh, H. (2008) 'Preparation of antimicrobial sutures by

preirradiation grafting onto polypropylene monofilament', *Polymers for Advanced Technologies*. John Wiley & Sons, Ltd., 19(12), pp. 1698–1703.

Gupta, J., Gill, H. S., Andrews, S. N. and Prausnitz, M. R. (2011) 'Kinetics of skin resealing after insertion of microneedles in human subjects.', *Journal of controlled release : official journal of the Controlled Release Society*. NIH Public Access, 154(2), pp. 148–55.

Hanafi, A., Nograles, N., Abdullah, S., Shamsudin, M. N. and Rosli, R. (2013) 'Cellulose Acetate Phthalate Microencapsulation and Delivery of Plasmid DNA to the Intestines', *Journal of Pharmaceutical Sciences*, 102(2), pp. 617–626.

Hanafi, A., Nograles, N., Abdullah, S., Shamsudin, M. N., Rosli, R., Sahul, H. A., Wang, Y. F. and Tong, G. Z. (2013) 'Cellulose acetate phthalate microencapsulation and delivery of plasmid DNA to the intestines.', *Journal of pharmaceutical sciences*. Elsevier, 102(2), pp. 617–26.

Hassan, A., Shakeel Laghari, M. and Rashid, Y. (2016) 'Micro-Encapsulated Phase Change Materials: A Review of Encapsulation, Safety and Thermal Characteristics', *Sustainability*, 8(10), p. 1046.

Huang, H. and Dasgupta, P. K. (1997) 'Renewable liquid film-based electrochemical sensor for gaseous hydroperoxides', *Talanta*, 44(4), pp. 605–615.

Hurrell, S. and Cameron, R. E. (2002) 'The effect of initial polymer morphology on the degradation and drug release from polyglycolide', 23, pp. 2401–2409.

Hyun, D. C. (2015) 'Magnetically-controlled , pulsatile drug release from poly (ε - caprolactone) (PCL) particles with hollow interiors', *Polymer*. Elsevier Ltd, 74, pp. 159–165.

Illum, L. (2012) 'Nasal drug delivery - recent developments and future prospects.', *Journal of controlled release : official journal of the Controlled Release Society*, 161(2), pp. 254–63.

Indermun, S., Luttge, R., Choonara, Y. E., Kumar, P., Du Toit, L. C., Modi, G. and Pillay, V. (2014) 'Current advances in the fabrication of microneedles for transdermal

delivery', *Journal of Controlled Release*. Elsevier B.V., 185(1), pp. 130–138.

Isaac, M. and Holvey, C. (2012) 'Transdermal patches: the emerging mode of drug delivery system in psychiatry.', *Therapeutic advances in psychopharmacology*, 2(6), pp. 255–63.

Ita, K. (2017a) 'Dissolving microneedles for transdermal drug delivery: Advances and challenges', *Biomedicine & Pharmacotherapy*. Elsevier Masson, 93, pp. 1116–1127.

Ita, K. (2017b) 'Dissolving microneedles for transdermal drug delivery: Advances and challenges', *Biomedicine & Pharmacotherapy*, 93, pp. 1116–1127.

Ito, A. and Kamihira, M. (2011) 'Tissue Engineering Using Magnetite Nanoparticles', in *Progress in molecular biology and translational science*, pp. 355–395.

Jämstorp, E., Forsgren, J., Bredenberg, S., Engqvist, H. and Strømme, M. (2010) 'Mechanically strong geopolymers offer new possibilities in treatment of chronic pain', *Journal of Controlled Release*, 146(3), pp. 370–377.

Jeong, H.-R., Kim, J.-Y., Kim, S.-N. and Park, J.-H. (2018) 'Local dermal delivery of Cyclosporin A, a hydrophobic and high molecular weight drug, using dissolving microneedles', *European Journal of Pharmaceutics and Biopharmaceutics*.

Ji, J., Tay, F. E., Miao, J. and Iliescu, C. (2006) 'Microfabricated Silicon Microneedle Array for Transdermal Drug Delivery', *Journal of Physics: Conference Series*. IOP Publishing, 34(1), pp. 1127–1131.

Jin, J., Sklar, G. E., Min Sen Oh, V. and Chuen Li, S. (2008) 'Factors affecting therapeutic compliance: A review from the patient's perspective.', *Therapeutics and clinical risk management*, 4(1), pp. 269–86.

Jin, Z., Güven, G., Bocharova, V., Halámek, J., Tokarev, I., Minko, S., Melman, A., Mandler, D. and Katz, E. (2012) 'Electrochemically controlled drug-mimicking protein release from iron-alginate thin-films associated with an electrode', *ACS Applied Materials and Interfaces*, 4(1), pp. 466–475.

Joseph, B., George, A., Gopi, S., Kalarikkal, N. and Thomas, S. (2017) 'Polymer sutures for simultaneous wound healing and drug delivery – A review', *International Journal*

of Pharmaceutics. Elsevier B.V., 524(1–2), pp. 454–466.

Jović, B. M., Jović, V. D., Branković, G., Radović, M. and Krstajić, N. V. (2017) 'Hydrogen evolution in acid solution at Pd electrodeposited onto Ti2AlC', *Electrochimica Acta*, 224, pp. 571–584.

Jung, W., Han, J., Choi, J.-W. and Ahn, C. H. (2015) 'Point-of-care testing (POCT) diagnostic systems using microfluidic lab-on-a-chip technologies', *Microelectronic Engineering*, 132, pp. 46–57.

Kalam, M. A. (2016) 'Development of chitosan nanoparticles coated with hyaluronic acid for topical ocular delivery of dexamethasone', *International Journal of Biological Macromolecules*. Elsevier, 89, pp. 127–136.

Kamaly, N., Yameen, B., Wu, J. and Farokhzad, O. C. (2016) 'Degradable Controlled-Release Polymers and Polymeric Nanoparticles : Mechanisms of Controlling Drug Release'.

Kamaly, N., Yameen, B., Wu, J. and Farokhzad, O. C. (2016) 'Degradable Controlled-Release Polymers and Polymeric Nanoparticles: Mechanisms of Controlling Drug Release', *Chemical Reviews*. American Chemical Society, 116(4), pp. 2602–2663.

Karrout, Y., Neut, C., Wils, D., Siepmann, F., Deremaux, L., Flament, M.-P., Dubreuil, L., Desreumaux, P. and Siepmann, J. (2009) 'Novel polymeric film coatings for colon targeting: Drug release from coated pellets', *European Journal of Pharmaceutical Sciences*. Elsevier, 37(3–4), pp. 427–433.

Kaur, G., Adhikari, R., Cass, P., Bown, M. and Gunatillake, P. (2015) 'Electrically conductive polymers and composites for biomedical applications', *RSC Advances*. Royal Society of Chemistry, 5(47), pp. 37553–37567.

Kearney, M. C., Caffarel-Salvador, E., Fallows, S. J., McCarthy, H. O. and Donnelly, R. F. (2016) 'Microneedle-mediated delivery of donepezil: Potential for improved treatment options in Alzheimer's disease', *European Journal of Pharmaceutics and Biopharmaceutics*. Elsevier B.V., 103, pp. 43–50.

Kelley, K. E., Hernández-Díaz, S., Chaplin, E. L., Hauser, R. and Mitchell, A. A. (2011)

'Identification of Phthalates in Medications and Dietary Supplement Formulations in the United States and Canada', *Environmental Health Perspectives*, 120(3), pp. 379–384.

Kelley, K. E., Hernández-Díaz, S., Chaplin, E. L., Hauser, R. and Mitchell, A. A. (2012) 'Identification of phthalates in medications and dietary supplement formulations in the United States and Canada.', *Environmental health perspectives*. National Institute of Environmental Health Science, 120(3), pp. 379–84.

Khan, I., Saeed, K. and Khan, I. (2017) 'Nanoparticles: Properties, applications and toxicities', *Arabian Journal of Chemistry*. Elsevier.

Kim, D.-H., Wang, S., Keum, H., Ghaffari, R., Kim, Y.-S., Tao, H., Panilaitis, B., Li, M., Kang, Z., Omenetto, F., Huang, Y. and Rogers, J. A. (2012a) 'Thin, Flexible Sensors and Actuators as "Instrumented" Surgical Sutures for Targeted Wound Monitoring and Therapy', *Small*. Wiley-Blackwell, 8(21), pp. 3263–3268.

Kim, D.-H., Wang, S., Keum, H., Ghaffari, R., Kim, Y.-S., Tao, H., Panilaitis, B., Li, M., Kang, Z., Omenetto, F., Huang, Y. and Rogers, J. A. (2012b) 'Thin, Flexible Sensors and Actuators as "Instrumented" Surgical Sutures for Targeted Wound Monitoring and Therapy', *Small*. WILEY-VCH Verlag, 8(21), pp. 3263–3268.

Kim, J. H., Shin, J. U., Kim, S. H., Noh, J. Y., Kim, H. R., Lee, J., Chu, H., Jeong, K. Y., Park, K. H., Kim, J. D., Kim, H. K., Jeong, D. H., Yong, T.-S., Park, J.-W. and Lee, K. H. (2018) 'Successful transdermal allergen delivery and allergen-specific immunotherapy using biodegradable microneedle patches', *Biomaterials*. Elsevier, 150, pp. 38–48.

Kim, J. Y., Han, M. R., Kim, Y. H., Shin, S. W., Nam, S. Y. and Park, J. H. (2016) 'Tip-loaded dissolving microneedles for transdermal delivery of donepezil hydrochloride for treatment of Alzheimer's disease', *European Journal of Pharmaceutics and Biopharmaceutics*. Elsevier B.V., 105, pp. 148–155.

Kim, K. and Lee, J.-B. (2006) 'High aspect ratio tapered hollow metallic microneedle arrays with microfluidic interconnector', *Microsystem Technologies*. Springer-Verlag, 13(3–4), pp. 231–235.

Kleiner, L. W., Wright, J. C. and Wang, Y. (2014) 'Evolution of implantable and

insertable drug delivery systems', *Journal of Controlled Release*. Elsevier B.V., 181(1), pp. 1–10.

Kompella, U. B., Amrite, A. C., Pacha Ravi, R. and Durazo, S. A. (2013) 'Nanomedicines for back of the eye drug delivery, gene delivery, and imaging', *Progress in Retinal and Eye Research*, 36, pp. 172–198.

Kompella, U. B., Amrite, A. C., Pacha Ravi, R. and Durazo, S. A. (2013) 'Nanomedicines for back of the eye drug delivery, gene delivery, and imaging.', *Progress in retinal and eye research*, 36, pp. 172–98.

Kumar, S., Kumar, S., Pandey, C. M. and Malhotra, B. D. (2016) 'Conducting paper based sensor for cancer biomarker detection', *Journal of Physics: Conference Series*. IOP Publishing, 704(1), p. 12010.

Lafitte, V. G. H., Wang, W., Yashina, A. S. and Lawrence, N. S. (2008) 'Anthraquinone–ferrocene film electrodes: Utility in pH and oxygen sensing', *Electrochemistry Communications*, 10(12), pp. 1831–1834.

Lahiji, S. F., Dangol, M. and Jung, H. (2015) 'A patchless dissolving microneedle delivery system enabling rapid and efficient transdermal drug delivery.', *Scientific reports*. Nature Publishing Group, 5, p. 7914.

Lane, M. E. (2013) 'The transdermal delivery of fentanyl.', *European journal of pharmaceutics and biopharmaceutics : official journal of Arbeitsgemeinschaft für Pharmazeutische Verfahrenstechnik e.V*, 84(3), pp. 449–55.

Langer, R., Santini, J. T. and Cima, M. J. (1999) 'A controlled-release microchip.', *Nature*, 397(6717), pp. 335–338.

Larrañeta, E., Lutton, R. E. M., Woolfson, A. D. and Donnelly, R. F. (2016) 'Microneedle arrays as transdermal and intradermal drug delivery systems: Materials science, manufacture and commercial development', *Materials Science and Engineering: R: Reports*, 104, pp. 1–32.

Larrañeta, E., Moore, J., Vicente-Pérez, E. M., González-Vázquez, P., Lutton, R., Woolfson, A. D. and Donnelly, R. F. (2014) 'A proposed model membrane and test

method for microneedle insertion studies', *International Journal of Pharmaceutics*, 472(1–2), pp. 65–73.

Lasia, A. (2010) 'Hydrogen evolution reaction', in *Handbook of Fuel Cells*. Chichester, UK: John Wiley & Sons, Ltd.

Lee, D.-S., Li, C. G., Ihm, C. and Jung, H. (2018) 'A three-dimensional and bevel-angled ultrahigh aspect ratio microneedle for minimally invasive and painless blood sampling', *Sensors and Actuators B: Chemical*. Elsevier, 255, pp. 384–390.

Lee, H. S., Park, S. H., Lee, J. H., Jeong, B. Y., Ahn, S. K., Choi, Y. M., Choi, D. J. and Chang, J. H. (2013) 'Antimicrobial and biodegradable PLGA medical sutures with natural grapefruit seed extracts', *Materials Letters*, 95, pp. 40–43.

Lee, J. W., Choi, S.-O., Felner, E. I. and Prausnitz, M. R. (2011) 'Dissolving Microneedle Patch for Transdermal Delivery of Human Growth Hormone', *Small*. WILEY-VCH Verlag, 7(4), pp. 531–539.

Lee, J. W., Han, M.-R. and Park, J.-H. (2013) 'Polymer microneedles for transdermal drug delivery', *Journal of Drug Targeting*, 21(3), pp. 211–223.

Lehmann, K. (1994) 'Coating of Multiparticulates Using Polymeric Solutions', in, pp. 51–78.

Lekic, T., Manaenko, A., Rolland, W., Fathali, N., Peterson, M., Tang, J. and Zhang, J. H. (2011) 'Protective Effect of Hydrogen Gas Therapy After Germinal Matrix Hemorrhage in Neonatal Rats', in *Acta neurochirurgica. Supplement*, pp. 237–241.

Leprince, L., Dogimont, A., Magnin, D. and Demoustier-Champagne, S. (2010) 'Dexamethasone electrically controlled release from polypyrrole-coated nanostructured electrodes.', *Journal of materials science. Materials in medicine*, 21(3), pp. 925–30.

Lhernould, M. S. (2013) 'Optimizing hollow microneedles arrays aimed at transdermal drug delivery', *Microsystem Technologies*. Springer-Verlag, 19(1), pp. 1–8.

Li, P.-Y., Shih, J., Lo, R., Saati, S., Agrawal, R., Humayun, M. S., Tai, Y.-C. and Meng, E.

(2008) ‘An electrochemical intraocular drug delivery device’, *Sensors and Actuators A: Physical*, 143(1), pp. 41–48.

Li, P. Y., Sheybani, R., Gutierrez, C. a., Kuo, J. T. W. and Meng, E. (2010) ‘A parylene bellows electrochemical actuator’, *Journal of Microelectromechanical Systems*, 19(1), pp. 215–228.

Liakos, I., Rizzello, L., Bayer, I. S., Pompa, P. P., Cingolani, R. and Athanassiou, A. (2013) ‘Controlled antiseptic release by alginate polymer films and beads.’, *Carbohydrate polymers*, 92(1), pp. 176–83.

Liakos, I., Rizzello, L., Scurr, D. J., Pompa, P. P., Bayer, I. S. and Athanassiou, A. (2014) ‘All-natural composite wound dressing films of essential oils encapsulated in sodium alginate with antimicrobial properties.’, *International journal of pharmaceutics*, 463(2), pp. 137–45.

Lima, S., Gago, M., Garrett, C. and Pereira, M. G. (2016) ‘Medication adherence in Alzheimer’s disease: The mediator role of mindfulness’, *Archives of Gerontology and Geriatrics*. Elsevier, 67, pp. 92–97.

Lin, C.-H., Chen, C.-H., Lin, Z.-C. and Fang, J.-Y. (2017) ‘Recent advances in oral delivery of drugs and bioactive natural products using solid lipid nanoparticles as the carriers’, *Journal of Food and Drug Analysis*. Elsevier, 25(2), pp. 219–234.

Lin, D. and Lasia, A. (2017) ‘Electrochemical impedance study of the kinetics of hydrogen evolution at a rough palladium electrode in acidic solution’, *Journal of Electroanalytical Chemistry*, 785, pp. 190–195.

Ling, D. and Hyeon, T. (2013) ‘Chemical design of biocompatible iron oxide nanoparticles for medical applications’, *Small*, 9(9–10), pp. 1450–1466.

Litster, S., Ha, B., Kim, D. and Santiago, J. G. (2007) ‘A Two-Liquid Electroosmotic Pump for Portable Drug Delivery Systems’, in *Volume 11: Micro and Nano Systems, Parts A and B*. ASME, pp. 963–964.

Liu, B., Wang, Y., Yang, F., Wang, X., Shen, H., Cui, H. and Wu, D. (2016) ‘Colloids and Surfaces B : Biointerfaces Construction of a controlled-release delivery system for

pesticides using biodegradable PLA-based microcapsules', *Colloids and Surfaces B: Biointerfaces*. Elsevier B.V., 144, pp. 38–45.

Liu, L., Gao, Q., Lu, X. and Zhou, H. (2016) 'In situ forming hydrogels based on chitosan for', *Asian Journal of Pharmaceutical Sciences*. Elsevier B.V., 11(6), pp. 673–683.

Liu, S., Hu, M. and Yang, J. (2016) 'A facile way of fabricating a flexible and conductive cotton fabric', *J. Mater. Chem. C*. The Royal Society of Chemistry, 4(6), pp. 1320–1325.

Liu, Y., Nguyen, A., Allen, A., Zoldan, J., Huang, Y. and Chen, J. Y. (2016) 'Regenerated cellulose micro-nano fi ber matrices for transdermal drug release', *Materials Science & Engineering C*. Elsevier B.V.

Loizidou, E. Z., Williams, N. A., Barrow, D. A., Eaton, M. J., McCrory, J., Evans, S. L. and Allender, C. J. (2015) 'Structural characterisation and transdermal delivery studies on sugar microneedles: Experimental and finite element modelling analyses', *European Journal of Pharmaceutics and Biopharmaceutics*. Elsevier, 89, pp. 224–231.

Low, L.-M., Seetharaman, S., He, K.-Q. and Madou, M. J. (2000) 'Microactuators toward microvalves for responsive controlled drug delivery', *Sensors and Actuators B: Chemical*, 67(1–2), pp. 149–160.

Lu, M. and Compton, R. G. (2014) 'Voltammetric pH sensing using carbon electrodes: glassy carbon behaves similarly to EPPG', *The Analyst*. The Royal Society of Chemistry, 139(18), pp. 4599–4605.

Luft, G., Kuehl, D. and Richter, G. J. (1978) 'Electro-osmotic valve for the controlled administration of drugs', *Medical & Biological Engineering & Computing*, 16(1), pp. 45–50.

Lui, H., Zhu, L. L., He, Y. and Cheng, B. W. (2017) 'A novel method for fabricating elastic conductive polyurethane filaments by in-situ reduction of polydopamine and electroless silver plating', *Materials & Design*. Elsevier, 113, pp. 254–263.

Luo, X., Matranga, C., Tan, S., Alba, N. and Cui, X. T. (2011) 'Carbon nanotube nanoreservior for controlled release of anti-inflammatory dexamethasone',

Biomaterials, 32(26), pp. 6316–6323.

Luo, X., Matranga, C., Tan, S., Alba, N. and Cui, X. T. (2011) 'Carbon nanotube nanoreservior for controlled release of anti-inflammatory dexamethasone.', *Biomaterials*, 32(26), pp. 6316–23.

Luo, Y., Pan, K. and Zhong, Q. (2015) 'Casein / pectin nanocomplexes as potential oral delivery vehicles', *International Journal of Pharmaceutics*. Elsevier B.V., 486(1–2), pp. 59–68.

Macfie, G., Simpson, L. V., McColl, D. and Cardosi, M. F. (2012) 'Mechanism of 2-Mercaptoethanesulphonate Adsorption onto Sputtered Palladium Films: Influence of Surface Oxide Species', *The Journal of Physical Chemistry C*. American Chemical Society, 116(18), pp. 9930–9941.

Mahor, A., Kumar, S., Verma, A. and Gupta, R. (2016) 'Journal of Drug Delivery Science and Technology Development , in-vitro and in-vivo characterization of gelatin nanoparticles for delivery of an anti-in fl ammatory drug', *Journal of Drug Delivery Science and Technology*. Elsevier Ltd, 36, pp. 55–61.

Majumdar, A., Sahoo, J., Roy, G. and Kamalanathan, S. (2015) 'Improper sharp disposal practices among diabetes patients in home care settings: Need for concern?', *Indian journal of endocrinology and metabolism*. Wolters Kluwer -- Medknow Publications, 19(3), pp. 420–5.

Makos, M. A., Omiatek, D. M., Ewing, A. G. and Heien, M. L. (2010) 'Development and Characterization of a Voltammetric Carbon-Fiber Microelectrode pH Sensor', *Langmuir*. American Chemical Society, 26(12), pp. 10386–10391.

Mansoor, I., Liu, Y., Häfeli, U. O. and Stoeber, B. (2013) 'Arrays of hollow out-of-plane microneedles made by metal electrodeposition onto solvent cast conductive polymer structures', *Journal of Micromechanics and Microengineering*. IOP Publishing, 23(8), p. 85011.

Margetts, L. and Sawyer, R. (2007a) 'Transdermal drug delivery: principles and opioid therapy', *Continuing Education in Anaesthesia, Critical Care & Pain*, 7(5), pp. 171–176.

Margetts, L. and Sawyer, R. (2007b) 'Transdermal drug delivery: principles and opioid therapy', *Continuing Education in Anaesthesia, Critical Care & Pain*, 7(5), pp. 171–176.

Markides, H., Rotherham, M. and El Haj, A. J. (2012) 'Biocompatibility and toxicity of magnetic nanoparticles in regenerative medicine', *Journal of Nanomaterials*, 2012, pp. 13–15.

Maroni, A., Del Curto, M. D., Zema, L., Foppoli, A. and Gazzaniga, A. (2013) 'Film coatings for oral colon delivery.', *International journal of pharmaceutics*, 457(2), pp. 372–94.

Maroni, A., Moutaharrik, S., Zema, L. and Gazzaniga, A. (2017) 'Enteric coatings for colonic drug delivery: state of the art', *Expert Opinion on Drug Delivery*. Taylor & Francis, 14(9), pp. 1027–1029.

Maroni, A., Zema, L., Cerea, M., Foppoli, A., Palugan, L. and Gazzaniga, A. (2016) 'Erodible drug delivery systems for time-controlled release into the gastrointestinal tract', *Journal of Drug Delivery Science and Technology*, 32, pp. 229–235.

Maroni, A., Zema, L., Loreti, G., Palugan, L. and Gazzaniga, A. (2013) 'Film coatings for oral pulsatile release.', *International journal of pharmaceutics*, 457(2), pp. 362–71.

Martanto, W., Moore, J. S., Couse, T. and Prausnitz, M. R. (2006) 'Mechanism of fluid infusion during microneedle insertion and retraction', *Journal of Controlled Release*. Elsevier, 112(3), pp. 357–361.

Martanto, W., Moore, J. S., Kashlan, O., Kamath, R., Wang, P. M., O'Neal, J. M. and Prausnitz, M. R. (2006) 'Microinfusion Using Hollow Microneedles', *Pharmaceutical Research*. Springer-Verlag, 23(1), pp. 104–113.

Martin, C. J., Allender, C. J., Brain, K. R., Morrissey, A. and Birchall, J. C. (2012) 'Low temperature fabrication of biodegradable sugar glass microneedles for transdermal drug delivery applications', *Journal of Controlled Release*. Elsevier, 158(1), pp. 93–101.

Maurya, A., Repka, M. A., Cegu, P. and Murthy, S. N. (2014) 'Pre-treatment with

chemical penetration enhancers in dermal/transdermal drug delivery', *Journal of Drug Delivery Science and Technology*, 24(3), pp. 251–254.

McAllister, D. V., Wang, P. M., Davis, S. P., Park, J.-H., Canatella, P. J., Allen, M. G. and Prausnitz, M. R. (2003) 'Microfabricated needles for transdermal delivery of macromolecules and nanoparticles: Fabrication methods and transport studies', *Proceedings of the National Academy of Sciences*, 100(24), pp. 13755–13760.

McConville, A. and Davis, J. (2016) 'Transdermal microneedle sensor arrays based on palladium: Polymer composites', *Electrochemistry Communications*, 72, pp. 162–165.

McCrudden, M. T. C., Alkilani, A. Z., McCrudden, C. M., McAlister, E., McCarthy, H. O., Woolfson, A. D. and Donnelly, R. F. (2014) 'Design and physicochemical characterisation of novel dissolving polymeric microneedle arrays for transdermal delivery of high dose, low molecular weight drugs', *Journal of Controlled Release*. Elsevier B.V., 180(1), pp. 71–80.

Meng, E. and Hoang, T. (2012) 'MEMS-enabled implantable drug infusion pumps for laboratory animal research, preclinical, and clinical applications.', *Advanced drug delivery reviews*. NIH Public Access, 64(14), pp. 1628–38.

Moon, J. M. and Chun, B. J. (2011) 'Fentanyl Intoxication Caused by Abuse of Transdermal Fentanyl', *The Journal of Emergency Medicine*, 40(1), pp. 37–40.

Van den Mooter, G. and Kinget, R. (1995) 'Oral colon-specific drug delivery: a review', *Drug Delivery*. Informa UK Ltd UK, 2(2), pp. 81–93.

Mounteney, J., Giraudon, I., Denissov, G. and Griffiths, P. (2015) 'Fentanyls: Are we missing the signs? Highly potent and on the rise in Europe.', *The International journal on drug policy*, 26(7), pp. 626–31.

Muheem, A., Shakeel, F., Jahangir, M. A., Anwar, M., Mallick, N., Jain, G. K., Warsi, M. H. and Ahmad, F. J. (2016) 'A review on the strategies for oral delivery of proteins and peptides and their clinical perspectives.', *Saudi pharmaceutical journal : SPJ : the official publication of the Saudi Pharmaceutical Society*. Elsevier, 24(4), pp. 413–28.

Nag, A., Mitra, A. and Mukhopadhyay, S. C. (2018) 'Graphene and its sensor-based

applications: A review', *Sensors and Actuators, A: Physical*. Elsevier B.V., 270, pp. 177–194.

Narayanan, R. P., Melman, G., Letourneau, N. J., Mendelson, N. L. and Melman, A. (2012) 'Photodegradable iron(III) cross-linked alginate gels', *Biomacromolecules*, 13(8), pp. 2465–2471.

Nevskaia, D. M. and Martin-Aranda, R. M. (2003) 'Nitric acid-oxidized carbon for the preparation of esters under ultrasonic activation', *Catalysis Letters*, 87(3–4), pp. 143–147.

Nguyen, D. N., Raghavan, S. S., Tashima, L. M., Lin, E. C., Fredette, S. J., Langer, R. S. and Wang, C. (2008) 'Biomaterials Enhancement of poly (orthoester) microspheres for DNA vaccine delivery by blending with poly (ethylenimine)', 29, pp. 2783–2793.

NICE (2007) *Costing statement : Medicines adherence : involving patients in decisions about prescribed medicines and supporting adherence*, *Excellence, National Institue for Health and Clinical*.

Othman, A. H., Mohamad, M. F. and Sayed, H. A.-R. (2016) 'Transdermal Fentanyl for Cancer Pain Management in Opioid-Naive Pediatric Cancer Patients', *Pain Medicine*. Oxford University Press, 17(7), pp. 1329–1336.

Owens, C. D. and Stoessel, K. (2008) 'Surgical site infections: epidemiology, microbiology and prevention', *Journal of Hospital Infection*, 70, pp. 3–10.

Paik, S.-J., Byun, S., Lim, J.-M., Park, Y., Lee, A., Chung, S., Chang, J., Chun, K. and Cho, D. 'Dan' (2004) 'In-plane single-crystal-silicon microneedles for minimally invasive microfluid systems', *Sensors and Actuators A: Physical*. Elsevier, 114(2–3), pp. 276–284.

Park, J.-H., Allen, M. G. and Prausnitz, M. R. (2005) 'Biodegradable polymer microneedles: Fabrication, mechanics and transdermal drug delivery', *Journal of Controlled Release*. Elsevier, 104(1), pp. 51–66.

Park, W. and Kim, S. (2013) 'Triggerable single-component two-electrode voltammetric pH sensors using dyad molecules', *Electrochemistry Communications*,

26, pp. 109–112.

Parveen, S., Wani, A. H., Shah, M. A., Devi, H. S., Bhat, M. Y. and Koka, J. A. (2018) 'Preparation, characterization and antifungal activity of iron oxide nanoparticles', *Microbial Pathogenesis*. Academic Press, 115, pp. 287–292.

Penalva, R., Esparza, I., Agüeros, M., Gonzalez-navarro, C. J., Gonzalez-ferrero, C. and Irache, J. M. (2015) 'Food Hydrocolloids Casein nanoparticles as carriers for the oral delivery of folic acid', *Food hydrocolloids*. Elsevier Ltd, 44, pp. 399–406.

Pérez-Ibarbia, L., Majdanski, T. C., Schubert, S., Windhab, N. and Schubert, U. S. (2016) 'Synthesis and characterization of colored EUDRAGIT as enteric coating material', *Journal of Polymer Science Part A: Polymer Chemistry*, 54(15), pp. 2386–2393.

Philip, A. K. and Philip, B. (2010) 'Colon targeted drug delivery systems: a review on primary and novel approaches.', *Oman medical journal*, 25(2), pp. 79–87.

Pikal, M. J. (2001) 'The role of electroosmotic flow in transdermal iontophoresis', *Advanced Drug Delivery Reviews*. Elsevier, 46(1–3), pp. 281–305.

Pirmoradi, F. N., Jackson, J. K., Burt, H. M. and Chiao, M. (2011) 'On-demand controlled release of docetaxel from a battery-less MEMS drug delivery device', *Lab on a Chip*, 11(16), p. 2744.

Pletcher, D. (1982) *Industrial electrochemistry*. Chapman and Hall.

Pletcher, D. (2009) *A first course in electrode processes*. Royal Society of Chemistry.

Plontke, S. K., Glien, A., Rahne, T., Mäder, K. and Salt, A. N. (2014) 'Controlled release dexamethasone implants in the round window niche for salvage treatment of idiopathic sudden sensorineural hearing loss', *Otology & neurotology : official publication of the American Otological Society, American Neurotology Society [and] European Academy of Otology and Neurotology*, 35(7), pp. 1168–1171.

Pole, S., Maurya, S., Hasnale, P., Rathod, N., Bendale, S. and Khutle, N. M. (2016) 'a Detail Understanding of Enteric Coated Tablet: Manufacturing and Evaluation', *European Journal of Pharmaceutical and Medical Research*, 3(4), pp. 135–144.

Ponnurangam, S., Connell, G. D. O., Hung, C. T. and Somasundaran, P. (2015) 'Colloids and Surfaces B : Biointerfaces Biocompatibility of polysebacic anhydride microparticles with chondrocytes in engineered cartilage'. Elsevier B.V., 136, pp. 207–213.

Prakash, S., Malhotra, M., Shao, W., Tomaro-Duchesneau, C. and Abbasi, S. (2011) 'Polymeric nanohybrids and functionalized carbon nanotubes as drug delivery carriers for cancer therapy.', *Advanced drug delivery reviews*, 63(14–15), pp. 1340–51.

Prausnitz, M. R. (2004) 'Microneedles for transdermal drug delivery', *Advanced Drug Delivery Reviews*, 56(5), pp. 581–587.

Prausnitz, M. R. and Langer, R. (2008) 'Transdermal drug delivery.', *Nature biotechnology*, 26(11), pp. 1261–1268.

Priya James, H., John, R., Alex, A. and Anoop, K. R. (2014) 'Smart polymers for the controlled delivery of drugs – a concise overview', *Acta Pharmaceutica Sinica B*, 4(2), pp. 120–127.

Qu, J., Li, X., Wang, J., Mi, W., Xie, K., Qiu, J. and al., et (2012) 'Inhalation of hydrogen gas attenuates cisplatin-induced ototoxicity via reducing oxidative stress.', *International journal of pediatric otorhinolaryngology*. Elsevier, 76(1), pp. 111–5.

Quinn, H. L., Bonham, L., Hughes, C. M. and Donnelly, R. F. (2015) 'Design of a Dissolving Microneedle Platform for Transdermal Delivery of a Fixed-Dose Combination of Cardiovascular Drugs', *Journal of Pharmaceutical Sciences*. Elsevier, 104(10), pp. 3490–3500.

Ramakrishna, S. U. B., Srinivasulu Reddy, D., Shiva Kumar, S. and Himabindu, V. (2016) 'Nitrogen doped CNTs supported Palladium electrocatalyst for hydrogen evolution reaction in PEM water electrolyser', *International Journal of Hydrogen Energy*, 41(45), pp. 20447–20454.

Rando, R. F., Obara, S., Osterling, M. C., Mankowski, M., Miller, S. R., Ferguson, M. L., Krebs, F. C., Wigdahl, B., Labib, M. and Kokubo, H. (2006) 'Critical design features of phenyl carboxylate-containing polymer microbicides', *Antimicrobial Agents and*

Chemotherapy.

Ren, L., Jiang, Q., Chen, Z., Chen, K., Xu, S., Gao, J. and Jiang, L. (2017) 'Flexible microneedle array electrode using magnetorheological drawing lithography for bio-signal monitoring', *Sensors and Actuators A: Physical*. Elsevier, 268, pp. 38–45.

Ren, Y., Xie, H., Liu, X., Bao, J., Yu, W. and Ma, X. (2016) 'International Journal of Biological Macromolecules Comparative investigation of the binding characteristics of poly- l -lysine and chitosan on alginate hydrogel', *International Journal of Biological Macromolecules*. Elsevier B.V., 84, pp. 135–141.

Richardson, R. T., Wise, A. K., Thompson, B. C., Flynn, B. O., Atkinson, P. J., Fretwell, N. J., Fallon, J. B., Wallace, G. G., Shepherd, R. K., Clark, G. M. and O'Leary, S. J. (2009) 'Polypyrrole-coated electrodes for the delivery of charge and neurotrophins to cochlear neurons.', *Biomaterials*, 30(13), pp. 2614–24.

Riggio, C., Ciofani, G., Raffa, V., Cuschieri, A. and Micera, S. (2009) 'Combination of polymer technology and carbon nanotube array for the development of an effective drug delivery system at cellular level', *Nanoscale Research Letters*, 4(7), pp. 668–673.

Rodríguez, J., Bravo-osuna, I., Herrero-vanrell, R., Teresa, I., Martínez, M. and Guzmán, M. (2016) 'European Journal of Pharmaceutical Sciences Optimising the controlled release of dexamethasone from a new generation of PLGA-based microspheres intended for intravitreal administration', *PHASCI*. Elsevier B.V., 92, pp. 287–297.

Rose, J. E., Herskovic, J. E., Trilling, Y. and Jarvik, M. E. (1985) 'Transdermal nicotine reduces cigarette craving and nicotine preference.', *Clinical pharmacology and therapeutics*, 38(4), pp. 450–6.

Ruggiero, F., Vecchione, R., Bhowmick, S., Coppola, G., Coppola, S., Esposito, E., Lettera, V., Ferraro, P. and Netti, P. A. (2018) 'Electro-drawn polymer microneedle arrays with controlled shape and dimension', *Sensors and Actuators B: Chemical*. Elsevier, 255, pp. 1553–1560.

Russell, L. M., Wiedersberg, S. and Delgado-Charro, M. B. (2008) 'The determination of stratum corneum thickness: an alternative approach.', *European journal of*

pharmaceutics and biopharmaceutics : official journal of Arbeitsgemeinschaft für Pharmazeutische Verfahrenstechnik e.V, 69(3), pp. 861–70.

Salvarezza, R. C. and Carro, P. (2017) 'The electrochemical stability of thiols on gold surfaces', *Journal of Electroanalytical Chemistry*. Elsevier, (October), pp. 0–1.

Santini, J. T., Cima, M. J. and Langer, R. (1999) 'A controlled-release microchip', *Nature*, 397(6717), pp. 335–338.

Santini, J. T., Cima, M. J. and Langer, R. (1999) 'A controlled-release microchip.', *Nature*, 397(6717), pp. 335–8.

Saraiya, N. V and Goldstein, D. A. (2011) 'Dexamethasone for ocular inflammation', *Expert Opinion on Pharmacotherapy*, 12(7), pp. 1127–1131.

Sattar, M., Sayed, O. M. and Lane, M. E. (2014) 'Oral transmucosal drug delivery--current status and future prospects.', *International journal of pharmaceutics*, 471(1–2), pp. 498–506.

Scaffaro, R., Botta, L., Maio, A. and Gallo, G. (2017) 'PLA graphene nanoplatelets nanocomposites : Physical properties and release kinetics of an antimicrobial agent', *Composites Part B*. Elsevier Ltd, 109, pp. 138–146.

Seitz, J.-M., Durisin, M., Goldman, J. and Drelich, J. W. (2015) 'Recent Advances in Biodegradable Metals for Medical Sutures: A Critical Review', *Advanced Healthcare Materials*, 4(13), pp. 1915–1936.

Shantha, K. L., Ravichandran, P. and Rao, K. P. (1995) 'Azo polymeric hydrogels for colon targeted drug delivery', *Biomaterials*, 16(17), pp. 1313–1318.

Sheybani, R., Gensler, H. and Meng, E. (2013) 'A MEMS electrochemical bellows actuator for fluid metering applications', *Biomedical Microdevices*, 15(1), pp. 37–48.

Shin, W., Lee, J. M., Nagarale, R. K., Shin, S. J. and Heller, A. (2011) 'A Miniature, nongassing electroosmotic pump operating at 0.5 v', *Journal of the American Chemical Society*, 133(8), pp. 2374–2377.

Silva, D., Pinto, L. F. V, Bozukova, D., Santos, L. F., Paula, A. and Saramago, B. (2016) 'Colloids and Surfaces B : Biointerfaces Chitosan / alginate based multilayers to

control drug release from ophthalmic lens', *Colloids and Surfaces B: Biointerfaces*. Elsevier B.V., 147, pp. 81–89.

Sokolowski, C. J., Giovannitti, J. A. and Boynes, S. G. (2010) 'Needle Phobia: Etiology, Adverse Consequences, and Patient Management', *Dental Clinics of North America*, 54(4), pp. 731–744.

Stanley, T. H. (2014) 'The fentanyl story.', *The journal of pain : official journal of the American Pain Society*, 15(12), pp. 1215–26.

Stauffer, W. R., Lau, P.-M., Bi, G.-Q. and Cui, X. T. (2011) 'Rapid modulation of local neural activity by controlled drug release from polymer-coated recording microelectrodes.', *Journal of neural engineering*, 8(4), p. 44001.

Stead, L. F., Perera, R., Bullen, C., Mant, D., Hartmann-Boyce, J., Cahill, K. and Lancaster, T. (2012) 'Nicotine replacement therapy for smoking cessation.', *The Cochrane database of systematic reviews*, 11, p. CD000146.

Streeter, I., Leventis, H., Wildgoose, G., Pandurangappa, M., Lawrence, N., Jiang, L., Jones, T. J. and Compton, R. (2004) 'A sensitive reagentless pH probe with a ca. 120mV/pH unit response', *Journal of Solid State Electrochemistry*. Springer-Verlag, 8(10), pp. 718–721.

Stubbe, B., Maris, B., Van den Mooter, G., De Smedt, S. C. and Demeester, J. (2001) 'The in vitro evaluation of "azo containing polysaccharide gels" for colon delivery', *Journal of Controlled Release*, 75(1–2), pp. 103–114.

Sun, S., Li, J., Li, X., Lan, B., Zhou, S., Meng, Y. and Cheng, L. (2016) 'Acta Biomaterialia Episcleral drug film for better-targeted ocular drug delivery and controlled release using multilayered poly- e -caprolactone (PCL)', *Acta Biomaterialia*. Acta Materialia Inc., 37, pp. 143–154.

Svagan, A. J., Benjamins, J., Al-ansari, Z., Bar, D., Müllertz, A., Wågberg, L. and Löbmann, K. (2016) 'Solid cellulose nano fi ber based foams – Towards facile design of sustained drug delivery systems', *Journal of Controlled Release*. Elsevier B.V., 244, pp. 74–82.

Svirskis, D., Travas-Sejdic, J., Rodgers, A. and Garg, S. (2010a) 'Electrochemically controlled drug delivery based on intrinsically conducting polymers', *Journal of Controlled Release*. Elsevier B.V., 146(1), pp. 6–15.

Svirskis, D., Travas-Sejdic, J., Rodgers, A. and Garg, S. (2010b) 'Electrochemically controlled drug delivery based on intrinsically conducting polymers', *Journal of Controlled Release*. Elsevier, 146(1), pp. 6–15.

Svirskis, D., Wright, B. E., Travas-Sejdic, J., Rodgers, A. and Garg, S. (2010) 'Evaluation of physical properties and performance over time of an actuating polypyrrole based drug delivery system', *Sensors and Actuators, B: Chemical*, 151(1), pp. 97–102.

Tang, H., Duan, X., Feng, X., Liu, L., Wang, S., Li, Y. and Zhu, D. (2009) 'Fluorescent DNA-poly(phenylenevinylene) hybrid hydrogels for monitoring drug release.', *Chemical communications (Cambridge, England)*. The Royal Society of Chemistry, (6), pp. 641–3.

Tarrants, M. L., Denarié, M. F., Castelli-Haley, J., Millard, J. and Zhang, D. (2010) 'Drug therapies for Parkinson's disease: A database analysis of patient compliance and persistence.', *The American journal of geriatric pharmacotherapy*, 8(4), pp. 374–83.

Tate, P. (2011) 'Seeley's Principles of Anatomy & Physiology'. McGraw-Hill.

Terukina, T., Saito, H., Tomita, Y., Hattori, Y. and Otsuka, M. (2017) 'Journal of Drug Delivery Science and Technology Development and effect of a sustainable and controllable simvastatin- releasing device based on PLGA microspheres / carbonate apatite cement composite : In vitro evaluation for use as a drug delivery system ', *Journal of Drug Delivery Science and Technology*. Elsevier Ltd, 37, pp. 74–80.

Thakur, R. R. S., Tekko, I. A., Al-Shammari, F., Ali, A. A., McCarthy, H. and Donnelly, R. F. (2016) 'Rapidly dissolving polymeric microneedles for minimally invasive intraocular drug delivery', *Drug Delivery and Translational Research*. Springer US, 6(6), pp. 800–815.

Thanki, K., Gangwal, R. P., Sangamwar, A. T. and Jain, S. (2013) 'Oral delivery of anticancer drugs: Challenges and opportunities', *Journal of Controlled Release*, 170(1), pp. 15–40.

Tharp, A. M., Winecker, R. E. and Winston, D. C. (2004) 'Fatal intravenous fentanyl abuse: four cases involving extraction of fentanyl from transdermal patches.', *The American journal of forensic medicine and pathology*, 25(2), pp. 178–81.

Ting, J. M., Porter, W. W., Mecca, J. M., Bates, F. S. and Reineke, T. M. (2018) 'Advances in Polymer Design for Enhancing Oral Drug Solubility and Delivery', *Bioconjugate Chemistry*. American Chemical Society, p. acs.bioconjchem.7b00646.

Tiwari, G., Tiwari, R., Sriwastawa, B., Bhati, L., Pandey, S., Pandey, P. and Bannerjee, S. K. (2012) 'Drug delivery systems: An updated review.', *International journal of pharmaceutical investigation*, 2(1), pp. 2–11.

TONG, S.-S., WANG, X.-J., LI, Q.-C. and HAN, X.-J. (2016) 'Progress on Electrocatalysts of Hydrogen Evolution Reaction Based on Carbon Fiber Materials', *Chinese Journal of Analytical Chemistry*. Changchun Institute of Applied Chemistry, Chinese Academy of Sciences, 44(9), pp. 1447–1457.

Tyler, B., Gullotti, D., Mangraviti, A., Utsuki, T. and Brem, H. (2016) 'Polylactic acid (PLA) controlled delivery carriers for biomedical applications ☆', *Advanced Drug Delivery Reviews*. Elsevier B.V., 107, pp. 163–175.

Valdés-Ramírez, G., Windmiller, J. R., Claussen, J. C., Martinez, A. G., Kuralay, F., Zhou, M., Zhou, N., Polsky, R., Miller, P. R., Narayan, R. and Wang, J. (2012) 'Multiplexed and switchable release of distinct fluids from microneedle platforms via conducting polymer nanoactuators for potential drug delivery', *Sensors and Actuators, B: Chemical*, 161(1), pp. 1018–1024.

Valdés-Ramírez, G., Windmiller, J. R., Claussen, J. C., Martinez, A. G., Kuralay, F., Zhou, M., Zhou, N., Polsky, R., Miller, P. R., Narayan, R. and Wang, J. (2012) 'Multiplexed and Switchable Release of Distinct Fluids from Microneedle Platforms via Conducting Polymer Nanoactuators for Potential Drug Delivery.', *Sensors and actuators. B, Chemical*, 161(1), pp. 1018–1024.

Valle, I., Tramalloni, D. and Bragazzi, N. L. (2015) 'Cancer prevention: state of the art and future prospects.', *Journal of preventive medicine and hygiene*. Pacini Editore, 56(1), pp. E21-7.

Vashist, S. K., Zheng, D., Pastorin, G., Al-Rubeaan, K., Luong, J. H. T. and Sheu, F.-S. (2011) 'Delivery of drugs and biomolecules using carbon nanotubes', *Carbon*, 49(13), pp. 4077–4097.

Venkatesan, J., Bhatnagar, I., Manivasagan, P., Kang, K.-H. and Kim, S.-K. (2014) 'Alginate composites for bone tissue engineering: A review.', *International journal of biological macromolecules*, 72C, pp. 269–281.

Vinayakumar, K. B., Hegde, G. M., Nayak, M. M., Dinesh, N. . and Rajanna, K. (2014) 'Fabrication and characterization of gold coated hollow silicon microneedle array for drug delivery', *Microelectronic Engineering*. Elsevier, 128, pp. 12–18.

Voicu, G., Geanaliu-nicolae, R. and Pîrvan, A. (2016) 'Synthesis , characterization and bioevaluation of drug-collagen hybrid materials for biomedical applications', *International Journal of Pharmaceutics*. Elsevier B.V., 510(2), pp. 474–484.

Wadhwa, R., Lagenaur, C. F. and Cui, X. T. (2006) 'Electrochemically controlled release of dexamethasone from conducting polymer polypyrrole coated electrode.', *Journal of controlled release : official journal of the Controlled Release Society*, 110(3), pp. 531–41.

Wang, X., Cheng, C., Wang, S. and Liu, S. (2009) 'Electroosmotic pumps and their applications in microfluidic systems.', *Microfluidics and nanofluidics*. NIH Public Access, 6(2), p. 145.

Wang, X., Gu, X., Yuan, C., Chen, S., Zhang, P., Zhang, T., Yao, J., Chen, F. and Chen, G. (2004) 'Evaluation of biocompatibility of polypyrrolein vitro andin vivo', *Journal of Biomedical Materials Research*. Wiley Subscription Services, Inc., A Wiley Company, 68A(3), pp. 411–422.

Wang, Y., Xu, S., Xiong, W., Pei, Y., Li, B. and Chen, Y. (2016) 'Colloids and Surfaces B : Biointerfaces Nanogels fabricated from bovine serum albumin and chitosan via self-assembly for delivery of anticancer drug', *Colloids and Surfaces B: Biointerfaces*. Elsevier B.V., 146, pp. 107–113.

Webber, M. J., Matson, J. B., Tamboli, V. K. and Stupp, S. I. (2012) 'Controlled release of dexamethasone from peptide nanofiber gels to modulate inflammatory response',

Biomaterials, 33(28), pp. 6823–6832.

Wildgoose, G. (2003) 'Anthraquinone-derivatised carbon powder: reagentless voltammetric pH electrodes', *Talanta*, 60(5), pp. 887–893.

Wildgoose, G. G., Lawrence, N. S., Leventis, H. C., Jiang, L., Jones, T. G. J. and Compton, R. G. (2005) 'X-Ray photoelectron spectroscopy studies of graphite powder and multiwalled carbon nanotubes covalently modified with Fast Black K: evidence for a chemical release mechanism via electrochemical reduction', *Journal of Materials Chemistry*. The Royal Society of Chemistry, 15(9), p. 953.

Wise, A. K. and Gillespie, L. N. (2012) 'Drug delivery to the inner ear.', *Journal of neural engineering*, 9(6), p. 65002.

Wong, C. Y., Martinez, J., Carnagarin, R. and Dass, C. R. (2017a) 'In-vitro evaluation of enteric coated insulin tablets containing absorption enhancer and enzyme inhibitor', *Journal of Pharmacy and Pharmacology*, 69(3), pp. 285–294.

Wong, C. Y., Martinez, J., Carnagarin, R. and Dass, C. R. (2017b) '*In-vitro* evaluation of enteric coated insulin tablets containing absorption enhancer and enzyme inhibitor', *Journal of Pharmacy and Pharmacology*, 69(3), pp. 285–294.

Woods, A., Patel, A., Spina, D., Riffo-vasquez, Y., Babin-morgan, A., Rosales, R. T. M. De, Sunassee, K., Clark, S., Collins, H., Bruce, K., Dailey, L. A. and Forbes, B. (2015) 'In vivo biocompatibility , clearance , and biodistribution of albumin vehicles for pulmonary drug delivery', *Journal of Controlled Release*. Elsevier B.V., 210, pp. 1–9.

Wu, X., Kubilay, N. Z., Ren, J., Allegranzi, B., Bischoff, P., Zayed, B., Pittet, D. and Li, J. (2017) 'Antimicrobial-coated sutures to decrease surgical site infections: a systematic review and meta-analysis', *European Journal of Clinical Microbiology & Infectious Diseases*. Springer Berlin Heidelberg, 36(1), pp. 19–32.

Xie, K., Yu, Y., Zhang, Z., Liu, W., Pei, Y., Xiong, L., Hou, L. and Wang, G. (2010) 'Hydrogen Gas Improves Survival Rate and Organ Damage in Zymosan-Induced Generalized Inflammation Model', *Shock*, 34(5), pp. 495–501.

Xie, S., Li, Z. and Yu, Z. (2015) 'Microneedles for transdermal delivery of insulin',

Journal of Drug Delivery Science and Technology. Elsevier Ltd, 28, pp. 11–17.

Xie, X., Pascual, C., Lieu, C., Oh, S., Wang, J., Zou, B., Xie, J., Li, Z., Xie, J., Yeomans, D. C., Wu, M. X. and Xie, X. S. (2017) 'Analgesic Microneedle Patch for Neuropathic Pain Therapy', *ACS Nano*, 11(1), pp. 395–406.

Yamaoka, T., Makita, Y., Sasatani, H., Kim, S.-I. and Kimura, Y. (2000) 'Linear type azo-containing polyurethane as drug-coating material for colon-specific delivery: its properties, degradation behavior, and utilization for drug formulation', *Journal of Controlled Release*, 66(2–3), pp. 187–197.

Yamashita, K., Takeno, S., Hoshino, S., Shiwaku, H., Aisu, N., Yoshida, Y., Tanimura, S. and Yamashita, Y. (2016) 'Triclosan sutures for surgical site infection in colorectal cancer', *Journal of Surgical Research*, 206(1), pp. 16–21.

Yan, X.-X., Liu, J.-Q., Jiang, S.-D., Yang, B. and Yang, C.-S. (2013) 'Fabrication and testing analysis of tapered silicon microneedles for drug delivery applications', *Microelectronic Engineering*. Elsevier, 111, pp. 33–38.

Yang, W.-W. and Pierstorff, E. (2012) 'Reservoir-based polymer drug delivery systems.', *Journal of laboratory automation*, 17(1), pp. 50–8.

Yang, Y., Shi, M., Goh, S. and Moochhala, S. M. (2003) 'P OE / PLGA composite microspheres : formation and in vitro behavior of double walled microspheres', 88, pp. 201–213.

Yasin, M. N., Svirskis, D., Seyfoddin, A. and Rupenthal, I. D. (2014) 'Implants for drug delivery to the posterior segment of the eye: A focus on stimuli-responsive and tunable release systems', *Journal of Controlled Release*. Elsevier B.V., 196, pp. 208–221.

Yassine, O., Zaher, A., Li, E. Q., Alfadhel, A., Perez, J. E., Kavaldzhiev, M., Contreras, M. F., Thoroddsen, S. T., Khashab, N. M. and Kosel, J. (2016) 'Highly Efficient Thermoresponsive Nanocomposite for Controlled Release Applications', *Scientific Reports*. Nature Publishing Group, 6(1), p. 28539.

Yin, J., Bao, F., Ma, R., Gao, J., Wang, G. and Yan, C. (2013) 'A lomefloxacin

hydrochloride-release system consisting of graphene oxide modified with polysebacic anhydride and polylactide', *Journal of Controlled Release*. Elsevier B.V., 172(1), pp. e29–e30.

Yoon, Y.-J., Li, K. H. H., Low, Y. Z., Yoon, J. and Ng, S. H. (2014) 'Microfluidics biosensor chip with integrated screen-printed electrodes for amperometric detection of nerve agent', *Sensors and Actuators B: Chemical*, 198, pp. 233–238.

Zhang, L., Chang, Q., Chen, H. and Shao, M. (2016a) 'Recent advances in palladium-based electrocatalysts for fuel cell reactions and hydrogen evolution reaction', *Nano Energy*. Elsevier, 29, pp. 198–219.

Zhang, L., Chang, Q., Chen, H. and Shao, M. (2016b) 'Recent advances in palladium-based electrocatalysts for fuel cell reactions and hydrogen evolution reaction', *Nano Energy*, 29, pp. 198–219.

Zhang, S., Liu, X., Wang, H., Peng, J. and Wong, K. K. Y. (2014) 'Silver nanoparticle-coated suture effectively reduces inflammation and improves mechanical strength at intestinal anastomosis in mice.', *Journal of pediatric surgery*. Elsevier, 49(4), pp. 606–13.

Zhang, Y., Jiang, G., Yu, W., Liu, D. and Xu, B. (2018) 'Microneedles fabricated from alginate and maltose for transdermal delivery of insulin on diabetic rats', *Materials Science and Engineering: C*. Elsevier, 85, pp. 18–26.

Zhang, Z., Shan, H., Chen, L., He, C., Zhuang, X. and Chen, X. (2013) 'Synthesis of pH-responsive starch nanoparticles grafted poly (L -glutamic acid) for insulin controlled release', *European Polymer Journal*. Elsevier Ltd, 49(8), pp. 2082–2091.

Zhuang, Z., Wang, F., Naidu, R. and Chen, Z. (2015) 'Biosynthesis of Pd–Au alloys on carbon fiber paper: Towards an eco-friendly solution for catalysts fabrication', *Journal of Power Sources*, 291, pp. 132–137.

Zilberman, M. (2005) 'Dexamethasone loaded bioresorbable films used in medical support devices: Structure, degradation, crystallinity and drug release', *Acta Biomaterialia*, 1(6), pp. 615–624.

Zubir, N. A., Yacou, C., Motuzas, J., Zhang, X. and Diniz Da Costa, J. C. (2014) 'Structural and functional investigation of graphene oxide-Fe 3 O 4 nanocomposites for the heterogeneous Fenton-like reaction', *Scientific Reports*, 4, pp. 1–8.

Publications Resulting from this Research Work

Book chapter release by Elsevier

Chapter 11. Design of Functionalised Materials for Use in Micro-Nanoscale Drug Delivery Devices and Smart Patches. Nanostructures for Drug Delivery, Nanostructures in Therapeutic Medicine Series. Editor(s): Grumezescu & Andronescu. Release date February 2017. Elsevier, ISBN 9780323461436.

In peer reviewed conferences

Anderson, A. & Davis, J., 2015. Next generation transdermal drug delivery – An electrochemical approach to pH manipulation for controlled release within smart patch technologies. IFMBE Proceedings: World Congress on Medical Physics and Biomedical Engineering, June 7-12, 2015, Toronto, Canada. 51, pp. 919-922.

In peer reviewed journals

Anderson, A., Phair, J., Benson, J., Meenan, B., and Davis, J., 2014. Investigating the use of endogenous quinoid moieties on carbon fibre as means of developing micro pH sensors. *Materials Science and Engineering C*. 43, pp.533-537.

Anderson, A. and Davis, J. (2015), Electrochemical Actuators: Controlled Drug Release Strategies for use in Micro Devices. Electroanalysis, 27: 872–878.

Anderson, A., McConville, A. & Davis, J., 2015. Electrochemical bubble rip: A new approach to controlled drug release. Electrochemistry Communications, 60, pp.88–91.

McLister, A., Lowry, N., **Anderson**, A., McHugh, J., & Davis, J. (2015). Novel pH sensing redox wire based on a polyamide homopolymer of L-tryptophan. Fibers and Polymers, 16(10), 2294–2297.

Morelli, F., **Anderson, A.,** McLister, A., Fearon, J.J., and Davis, J., 2017. Electrochemically driven reagent release from an electronic suture. Electrochemistry Communications, 81, pp.70-73.

Martin, A., McConville, A., **Anderson, A.**, McLister, A., and Davis, J., 2017 Microneedle Manufacture: Assessing Hazards and Control Measures. Safety 2017, 3, 25.